University of Strathclyde

Division of Pharmaceutical Sciences

Strathclyde Institute of Pharmacy and Biomedical Sciences

FORMULATION AND CHARACTERISATION OF THE LIPOGELS OF MAGNESIUM STEARATE AND LIQUID PARAFFIN

By

Khalid Ahmad Sheikh

A thesis presented in fulfilment of the requirements for the degree of Doctor of Philosophy

2010

Declaration of Author's Rights

Dedication

To my late parents, Mr. Nannay Khan and Mrs. Bismillah Begum

TABLE OF CONTENTS

Abstract

Lipogels were prepared by dispersing magnesium stearate (MgSt) in oil (either liquid paraffin, palm−olein or a combination of liquid paraffin and palm−olein (70:30 ratio respectively)). Hydrated and anhydrous forms of pure and mixed homologue magnesium stearate were prepared and used to investigate the influence of crystal state and homologue composition of MgSt on lipogel structure. Fluid or semisolid lipogels, were prepared using various concentrations of magnesium stearate (2.5%−20%) in the oil by heating to temperatures ranging from $110^{o}C–130^{o}C$ then cooling with different regimes. The lipogels were characterised by microscopy, DSC, TGA, FTIR, rheology and XRD. Franz diffusion cells, validated using Design of Experiment, were used to investigate drug (Ibuprofen) release from selected stable fluid and semisolid lipogels containing saturated oil concentrations of ibuprofen.

Lipogel structure was sensitive to the cooling procedures. Formulations containing mixed homologue magnesium stearate cooled slowly either with addition of 1-2% water (just below $100^{o}C$) or by homogenisation when the temperature reached $45^{o}C$ produced semisolid lipogels, whereas syneretic solids were obtained by slow cooling alone. In contrast, pure homologue magnesium stearate generally produced fluid lipogels. The exception was trihydrate pure homologue which produced semisolid lipogels, which reverted to liquids upon stirring implying pressure sensitivity. Semisolid lipogels only showed "Maltese cross" structures microscopically between crossed polars, suggesting presence of inverse lamellar phases. The XRD data showed that there was significantly more amorphous magnesium stearate in unstable solid lipogels compared to stable semisolid lipogels, which were mainly crystalline.

The incorporation of saturated oil concentrations of ibuprofen in semisolid liquid paraffin lipogel formulations produced structured fluids due to disruption of lamellar phases (confirmed microscopically). In Franz cell experiments the palm−olein fluid and semisolid lipogels showed significantly higher drug release than the liquid paraffin fluid lipogels. This was attributed to the presence of unsaturated fatty acids in the palm−olein which are known penetration enhancers and enhance drug release.

CHAPTER I

GENERAL INTRODUCTION AND AIMS OF THE STUDY

1.1 Topical drug delivery systems

An ideal topical drug delivery system should be "aesthetically elegant" and remain physically stable for an intended period of time in addition to "concentrating the drug at the target site" (Flynn, 1989; 1993; Megrab *et al*., 1995; Block, 2005). Semisolid oil–in–water (o/w) and water–in–oil (w/o) emulsions have long been used as vehicles for topical delivery of therapeutic and cosmetic agents (Tadros and Vincent, 1983; Barry and Eccleston, 1973; Rieger, 1988; Eccleston *et al*., 2000). The correlation between manufacturing variables, microstructure, rheology and stability of o/w emulsions has been well established (Davis, 1969; Barry 1974; Eccleston, 1977; Junginger *et al*., 1984; Lashmar, 1993). The evolution of gel network theory of emulsion stability led to the detailed structure elucidation of o/w systems stabilised by mixed emulsifiers (Eccleston, 1986, 2000). The effect of incorporation of drug on the microstructure and stability of o/w emulsions has also been investigated (Muller–Goymann, 2004; Al–Saidan 2004; Vintiloiu *et al*., 2007). However, little information is available on the structure elucidation of oily systems such as semisolid w/o emulsions (Bruggeller, 1982; Gasperlin *et al*., 1994) or lipogels, which may be useful for polysoluble drugs. Lipogels containing magnesium stearate dispersed in liquid paraffin described by Scric *et al*., (1985) may be suitable for dermatological delivery. This thesis investigates effect of different pseudopolymorphs (anhydrous, dihydrate and trihydrate) and homologue composition (mixed and pure) of magnesium stearate and preparation variables on the physical chemical properties of lipogels prepared with liquid paraffin and other oils (palm–olein and combination of liquid paraffin and palm–olein). In addition, ibuprofen was also incorporated into lipogels and drug release investigated using Franz diffusion cells.

The introduction will give a general view of topical vehicles for drug delivery systems such as creams, ointments, and gels followed by preparation and physical chemical properties (eg. microstructure) of magnesium stearate and the lipogels

prepared from it in liquid paraffin and other oils (palm−olein and combinations of liquid paraffin and palm−olein). The incorporation of ibuprofen into lipogels and its *in-vitro* release is studied using Franz diffusion cells.

1.2 Vehicles for topical drug delivery systems

Topical vehicles such as powders, liquids and semisolids have been used as carrier for the delivery of medicaments to and across the skin for a long time. Mobile topical dispersions include lotions and liniments and semisolid vehicles include creams, ointments and gels (Idson, 1988; Reilly, 2005). In the past, these traditional vehicles were considered as elegant frameworks for the transport of drugs to the skin. However, it is now well established that the colloidal properties of these vehicles significantly affect bioavailability of the drug in many ways *i.e.* drug–vehicle or vehicle–skin interactions (Barry, 1983; Barrett, 2004; Lang *et al*., 2005). Drug–vehicle interactions may affect solubility of the therapeutic or cosmetic agent in the vehicle, its diffusion from vehicle to the skin. In contrast, vehicle–skin interactions may lead to increase in therapeutic activity by interaction of vehicle components with the skin layers. Therefore, it is necessary to design a topical drug delivery system which not only possess good physical and chemical stability but also provide optimum environment to deliver the therapeutic agent to the intended site (Kinget *et al*., 1998; Ashford, 2002). In addition, investigation of the microstructure of various topical semisolid vehicles upon incorporation of the drug and other non-active ingredients provides essential information about the stability of the systems.

1.2.1 Emulsions

Emulsions are composed of two phases *i.e.* oil and water. They are thermodynamically unstable systems due to high interfacial energy. An attempt to obtain thermodynamic equilibrium causes breaking of emulsions in to individual components (*i.e.* oil and water) via flocculation or coalescence. Therefore, a third component, an emulsifier (surfactant or polymer) is used, which sits on the interface of water and oil to create an interfacial barrier between two phases to delay the separation process. Surfactants are also called amphiphiles due to their dual nature of having polar and non−polar components.

1.2.2 Creams

Creams are generally o/w semisolid emulsion and occasionally w/o systems. The difference between liquid and semisolid (cream) is that the droplets in creams are embedded in semisolid matrix to prevent flocculation and coalescence enhancing the shelf-life of the formulation.

1.2.2.1 O/W creams

In o/w creams, oil is dispersed in the continuous water phase. These creams due to high water content are mainly used for their moisturising effect on the skin. The hydration of skin has been linked to enhanced skin penetration of many drugs (Barry, 1987; Block, 2005). However, physical chemical properties and bioavailability of drugs from creams mainly depends on the structure of the system, therefore structure investigation is essential.

1.2.2.1a Microstructure of o/w creams

The rheological properties (*i.e.* semisolid nature) of creams prepared from fatty amphiphile/surfactant mixed emulsifiers, is due to the swelling properties of an α−crystalline lamellar gel network continuous phase, formed when the mixed emulsifier interacts with continuous phase water. The literature is confused because authors do not distinguish between such α−crystalline lamellar phase and smectic lamellar liquid crystals. Lamellar liquid crystals are fundamentally different that they do not swell significantly in excess water, but rather convert to micelles.

In the past, the stability of emulsions containing such mixed emulsifiers was described by the classical colloid theories of emulsification. Schulman and Cockbain, (1940) in their pioneering work on emulsion stability related the stability of emulsions to the formation of stable condensed interfacial film/s of fatty amphiphile/ionic surfactant at oil/water interface of high viscosity, leading to reduction in interfacial tension. However, it is now known that stable emulsions can also be prepared using fatty amphiphile and non−ionic emulsifier (Vold and Mittal, 1972).

Friberg *et al.*, (1969; 1990) proposed the existence of non−aqueous lamellar liquid crystals in systems containing n−hexadecane and lecithin. Various liquid crystalline phases (hexagonal, cubic and lamellar) that are produced in concentrated surfactant non-aqueous solutions are known. Fukasawa and Tsutsumi (1991) also described liquid formulations containing liquid crystals formed from long-chain dialkyl phosphate salt of aluminium in non−polar (n−hexadecane) system. The lamellar liquid crystalline structure may produce only two−dimensional systems showing little swelling and entrap the oil droplets forming liquid emulsions (Tadros *et al.*, 2005).

Eccleston attributed stability of o/w creams to the α−crystalline lamellar phases formed by specific mixed emulsifiers of fatty amphiphiles and ionic or non-ionic surfactants (work reviewed by Eccleston *et al.* 2000). These lamellar phases can extend from the droplet surface to the bulk liquid producing a three−dimensional semisolid gel network structure that prevents creaming or sedimentation. Over the years semisolid gel network theory of emulsion stability has evolved which is based on the models employed by classical theory of emulsification of oil droplet stabilisation (interfacial film) and the behaviour of mixed emulsifiers in the aqueous phase (Eccleston, 1997). The theory explains the manner in which mixed emulsifiers and the emulsifying waxes stabilise the oil droplets at the interface and control the rheological properties of the emulsions (semisolid) systems. According to this theory, the structure of semisolid emulsions is related to the swelling properties of a lamellar, α−crystalline gel network phase which is formed when emulsifier in excess to what is required to produce a monomolecular film at the oil droplet−water interface, interacts with continuous water phase (Eccleston *et al.*, 2000).

The structure of semisolid o/w creams can be explained in terms of following four phases (i) external free aqueous phase, (ii) α−crystalline gel phase with interlamellar fixed water, (iii) phase composed of crystalline hydrates of emulsifying wax and (iv) dispersed phase (Fig. 1.1). The lamellar α−crystalline gel phases can be identified microscopically between cross polars by the presence of distorted "Maltese crosses". The overall rheological properties of the semisolid emulsions are related to the swelling properties and concentration of the α-crystalline gel phase. The water

present between the crystalline hydrates and the gel phase is fixed or bound water which increases the volume ratio of the dispersed oil droplet to the free continuous water phase, causing increase in consistency of the system (Eccleston, 1986).
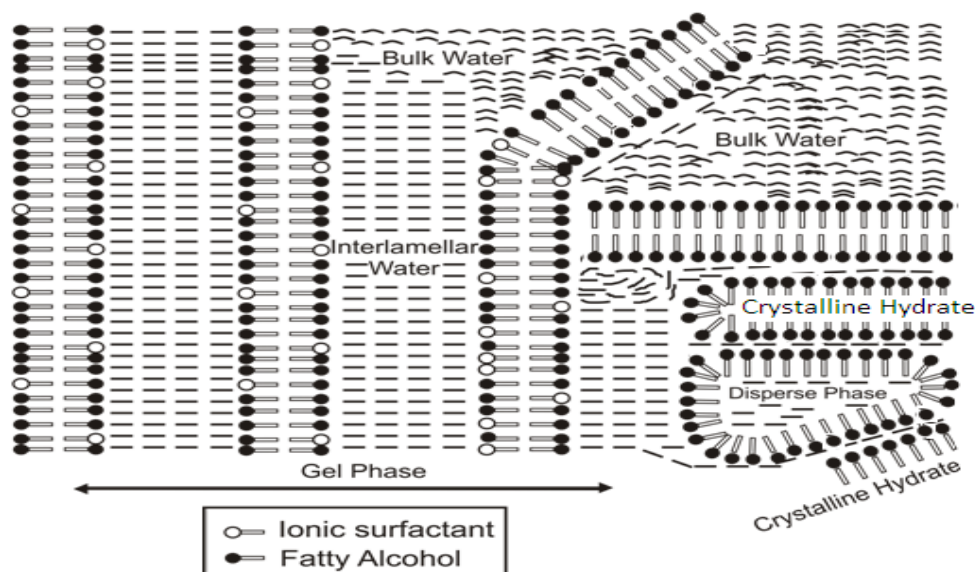
Figure 1.1: Schematic diagram showing microstructure of semisolid emulsions stabilised with α−crystalline gel structure showing various phases (Redrawn from Florence and Atwood, 2006).

However, the swelling properties of the lamellar α-crystalline gel phase depend on the type of emulsifier and the chain length of fatty alcohol used. Ionic emulsifying waxes showed significantly enhanced swelling in the presence of fatty alcohols compared to the non–ionic emulsifying waxes (Fig.1.2). The fatty alcohol chain length can also significantly affect the rheological properties of emulsions. Low chain length (C_{14} and C_{16}) produce semisolid emulsions immediately after preparation whereas fatty alcohol containing C_{18} chain length produces structured lotions which thickened with time especially in the first 48 hours (Eccleston, 1997).
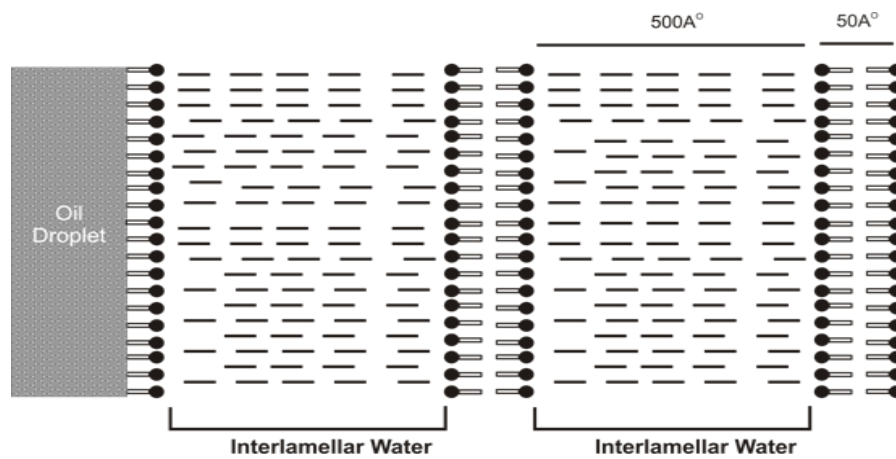
(a)
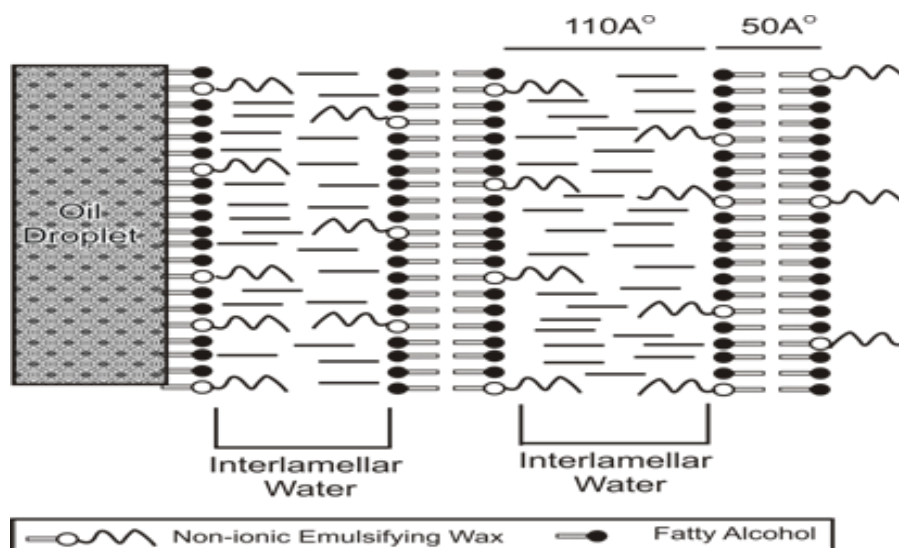
(b)

Figure 1.2: Schematic diagram showing effect of emulsifying waxes on the swelling properties of o/w creams (a) ionic and (b) non–ionic (Redrawn from Eccleston, 1997).

1.2.3 Oily Systems

1.2.3.1 W/O creams

W/O creams contain water and oil, in which water is present as dispersed droplet in the continuous oil phase. W/o creams are prepared, using weakly polar surfactants like fatty alcohols, sorbitan fatty acid esters and glyceryl monostearate (Mueller–

Goymann, 2004; Savic *et al*., 2005). Due to the presence of significantly high oil phase, they are better preserved than the o/w creams. Furthermore, these systems due to the high oil content offer better occlusive properties compared to o/w creams preventing skin dehydration which may help in enhanced skin permeation (Block, 2005). As discussed earlier, the structure of o/w semisolid creams is well established but molecular structure of w/o systems is yet to be identified.

Gasperlin *et al*., (1994) proposed freezing behaviour of water droplets in w/o semisolid emulsion systems containing silicone surfactants, white petrolatum and varying quantities of water (40−90%), attributed to the strong adsorption of surfactant at the water/oil interface and stearic affect due to surfactant's polymeric nature. The freezing behaviour is affected by several factors such as nature and concentration of surfactant and polydispersity of the dispersed phase droplets. They proposed existence of liquid crystals in the fluid systems. However, they were unable to resolve structure of semisolid systems and rather speculated presence of micellar aggregates.

1.2.3.2 Ointments

Ointments are topical vehicles containing a suitable ointment base used mainly for external application of medicaments to the skin or mucous membranes. There are four different types of ointment bases and include hydrocarbon, absorption, water–removable and water–soluble bases (Block, 2005). The ointments are categorised by their occlusive action in preventing skin dehydration and the occlusive effect of various ointments depends on the type of ointment base used (Table 1.1).

Table 1.1: Classification and properties of ointment bases

	Hydrocarbon bases	Absorption bases	Water–washable bases	Water-soluble bases
Example	White petrolatum	Lanolin USP	Hydrophilic ointment	Polyethylene glycol
Composition	Hydrocarbons	w/o emulsion	o/w emulsions	Water–soluble
Occlusiveness	Highest	Moderate to high	Low to moderate	Lowest

1.2.3.2a Ointment bases

1.2.3.2a(i) Hydrocarbon bases

These are also called oleaginous bases and are compatible with most active ingredients. They are either pure waxy hydrocarbons (petrolatum) or mixture of liquid petrolatum gelled with polyethylene. They show highest occlusive effect amongst all ointment bases and therefore increase water hydration by preventing the skin surface water loss (Block, 2005). These bases are used as emollients and skin moisturisers, which may lead to the increased drug permeation. However, the drug permeation from the waxy and gelled ointment bases has appeared to be different *i.e.* gelled bases showing faster drug release compared to the petrolatum and attributed to the quicker diffusion of drug from the less viscous gelled vehicle than through petrolatum (Eros *et al*., 1994). However, these bases owing to their high oil content leave a greasy appearance on the skin.

1.2.3.2a(ii) Absorption bases

Absorption bases include anhydrous or hydrous bases both of which have potential of absorbing more water. The anhydrous bases by absorbing water are changed to w/o emulsions whereas hydrous bases are w/o emulsions with the ability to absorb more water. Anhydrous bases may be used for the water sensitive active ingredients. However, absorption bases like hydrocarbon bases are greasy in nature and less preferred by the patients.

1.2.3.2a(iii) Water−removable bases

These bases are also called water-washable bases or emulsifying ointments, because on addition of water (with heat and homogenisation) they form the aqueous creams. They have some occlusivity, but can absorb large quantities of water.

1.2.3.2a(iv) Water soluble bases

Various polyethylene glycol (PEG) bases of varying consistency from liquids (PEG400), through semisolids (PEG1000) to hard waxy solids (PEG4000) depending on the molecular weights are used as water soluble bases. The number (400, 1000 *etc.*) represents the molecular weight of the respective PEG. They can be used alone but generally, they are used in combination to provide desired consistency of the vehicle. Although, most of the water soluble active ingredients can be easily dissolved in these bases but their high solubility does not ensure availability of the drug from these vehicles (Block, 2005; Ho, 2006). As hydrated skin is a major factor in the drug permeation, non-occlusive nature of these bases may actually retard drug permeation due to dehydration of stratum corneum.

1.2.3.2b Microstructure of ointments

Mueller–Goymann, (2004) reviewed microstructure of ointments such as hydrocarbon and emulsifying ointments. She suggested presence of crystalline and liquid crystalline networks, depending on the type of amphiphile and ointment bases. The hydrophilic ointments containing long−chain fatty alcohols such as cetyl and stearyl alcohol form crystalline networks at ambient temperature leading to irreversible deformation upon shear. However, crystallisation can be avoided by using appropriate amounts of mixed surfactants, producing liquid crystalline network at room temperature. In contrast, water soluble ointment bases form liquid crystalline lamellar structure. Various hydrophilic polymers *i.e.* Carbopols and hydroxyl propyl cellulose (HPC) have been used to prepare hydrophilic ointments where the particles of polymer disperse in ointment base, form crystalline gel network. The type and concentration of the hydrophilic polymers in addition to a small amount of water are

considered as the most important factors in modifying the crystalline structure and rheological properties of the ointments (Shigeyama *et al*., 2001).

1.2.4 Gels

Gels are formed by the dispersion of polymer in the liquid medium, forming a three dimensional physically aggregated semisolid swollen polymer network structure (Terech and Weiss, 1997). Gels offer many advantages over other vehicles such as ease of application, high degree of clarity, semisolid state, ease of removal and use, and good mucoadhesive properties due to their highly elastic nature. In addition, the gels often provide faster release of drugs, independent of the water solubility of the drug, as compared to ointments and creams (Crowley, 2005). Gels are usually white and opaque but may be translucent and in some cases they may appear transparent (Smith, 1947; Pena, 1990). On the basis of rheological properties gels are either weak or strong. Structured fluids are considered as weak gels whereas semisolid gels are strong gels (Terech, 2002).

Gels are generally divided into chemical and physical types depending on the mechanism of cross-linking of the polymer chains. The chemical gels result from the strong covalent bonds between the networks. In contrast, physical gels are formed, when the structure is held together by only molecular entanglements (Fig. 1.3) and/or secondary forces like hydrogen bonds, electrostatic and London-Van der Waals interactions (Terech, 2002). Gels are an example of lyophilic dispersion systems in which, polymer is readily dissolved in the liquid medium forming a three–dimensional aggregation network. When the vehicle is aqueous, gels are called hydrogels. In contrast, gels containing non-polar liquid have been referred to as organogels, oleogels, or lipogels depending on the type of vehicle used.
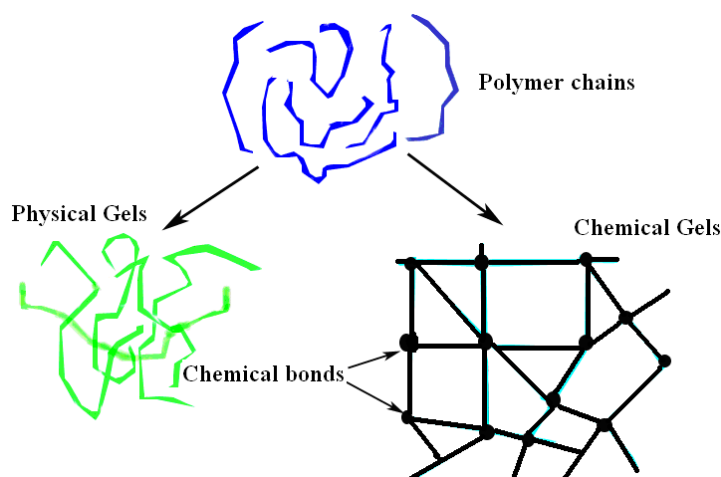
Figure 1.3: Molecular interactions in the preparation of physical and chemical gels (adapted from Terech, 2002).

1.2.4.1 Hydrogels

Hydrogels are aqueous monophasic systems formed by chemical or physical cross linking of the polymers. Hydrogels can be formed *in situ* by photopolymerisation induced by temperature using a simple phase change referred to as sol–gel phase transition temperature. The precise sol–gel transition temperature is important in designing drug delivery system as it determines the applicability of the delivery system. The sol–gel transition depends on the type, molecular weight and concentration also called critical gel concentration (CGC) of the polymer (Jeong *et al.*, 2002).

1.2.4.1a Polymers as gelling agents

Polymers are materials of high molecular weight made up of repeating units of monomers and are asymmetric. They are used in pharmaceutical drug delivery systems as emulsifying, flocculating and gelling agents. Their physicochemical properties such as solution rate depend mainly on molecular weight and asymmetric nature in addition to the chemistry and the way the monomers are clumped together. Polymers with high molecular weight possess stronger forces holding the chains together and therefore more energy is needed to keep the chains apart in the liquid. Their structure may show linear or branched chains, joined by cross–links. Various types of water soluble polymeric gelling agents have been used in hydrogels and

11

include natural gums and mucilages such as gelatin, alginates, bentonite, gum arabic and tragacanth, semi–synthetics like carboxymethylcellulose (CMC), and synthetic polymers containing carbomer microparticles or carbopol, methyl cellulose, polyethylene glycol (macrogols) and polyvinyl alcohol (Crowley, 2005). The polymer chains interact with the bulk solvent in a three dimensional cross–link fashion to yield gels. The gelling capacity of polymers is a function of concentration *i.e.* critical gelling concentration. Glycerin, acacia and methocel show low viscosity even at significantly high concentrations (~4%). In contrast, Gum Guar and carbopol show significantly higher viscosity in aqueous solution at lower concentrations (0.5–1%) whereas polymers like tragacanth show thickening similar to the carbopol but at higher concentration (~4%). Polymers rarely show perfect crystalline structure mainly due to the difficulty of arranging the monomer chains in regular fashion. This property is even prominent at higher molecular weights. Therefore, most of the polymers exist in various proportions of crystalline and amorphous forms. The gelling properties of the polymers depend on the crystallinity of the material as the permeability is a function of the volume fraction of the amorphous part. Therefore, the gelling agents with ordered crystalline structure show decreased solution rate compared to the amorphous materials. The crystalline regions of the solid polymer pose an impermeable barrier to the movement of the molecules leading to reduced dissolution (Jeong *et al*., 2002). Thus, greater the volume fraction of the crystalline material slower the movement of the molecules is. In addition, the interaction of polymer with solvents depends on the polymer structure and its affinity towards the solvent.

1.2.4.1b Mechanisms of hydrogel formation

The mechanism of aqueous gel formation depends on the type of polymer employed and involves conversion of polymer solutions in water (sol phase) into a gel phase on changing the temperature (thermogelation). Polymers are hydrophilic and may absorb significant amounts of water, showing intense swelling leading to markedly increased consistency upon change in temperature. The swollen structure is formed due to cross–linking of polymer chains.

Most natural polymers form gels upon lowering the temperature after high temperature mixing but certain cellulose–based polymers such as methyl and hydroxylpropyl cellulose show reverse thermogelation *i.e.* gelation at higher temperatures. However, some polymers such as poloxamers and combination of polyethylene oxide with propylene oxide form hydrogels at an intermediate temperature range, by dissolving equally well at high and low temperatures. The thermogelation mechanisms may include partial crystallisation, coil–to–helix transition (Fig. 1.4), hydrophobic associations and micelle formation, which serve as reversible physical cross–linking points to form hydrogel. However, the type of mechanism involved depends solely on the composition of the polymer (Bekturov and Bimendina, 1981).

Thermogelation with polymers involves development of double or triple helical conformation which causes crystal growth during gel formation. Formation and aggregation of helices leads to junction point (Fig. 1.4). Cellulose is water insoluble but its water solubility increases by incorporating hydrophilic moiety. In addition, cellulose with an appropriate balance of hydrophilic and hydrophobic components in contact with water undergoes sol–to–gel phase transition. Water upon heating becomes poor solvent for the polymer interaction and polymer–polymer interactions show dominance at elevated temperatures leading to gelification (Jeong *et al*., 2002).

Hydrogels of poloxamer show thermogelation at low temperatures and in combination with non–ionic surfactants (copolymers) show micelle formation in the system. Polyethylene oxide (PEG)/poly propylene oxide (PPO) block copolymers form micelles which equilibrate with poloxamer unimers at low temperature above the CMC. With an increase in the temperature the equilibrium shifts from unimers to spherical micelles, causing a reduction in the non-associated unimers in solution producing an increase in the micelle volume fraction leading to gel formation (Mortensen and Perdersen, 1993). At high temperatures, spherical micelles are converted to cylindrical micelles, releasing micelle–packing leading to reduced micelle volume fraction. In recent years, due to development of new organic gelling agents, many researchers have characterised non–aqueous gels (NAG) like organogels based on organic solvents and gelling agents (Kantaria *et al*., 1999).
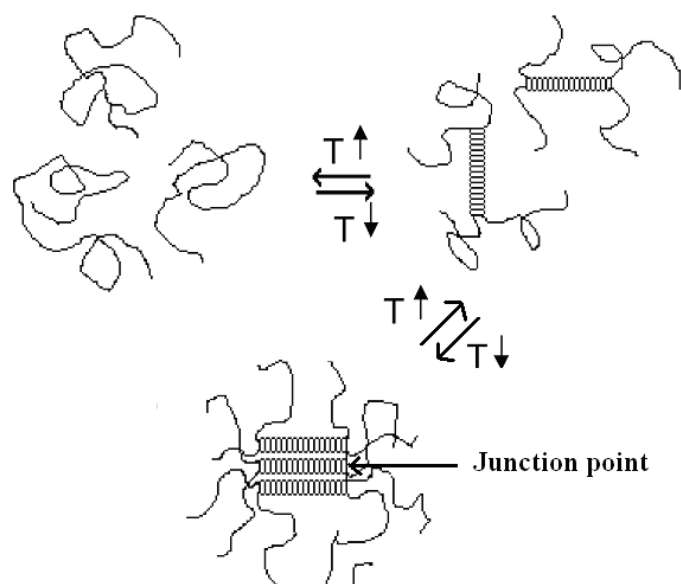
Figure 1.4: Temperature dependent hydrogel formation showing coil–to–helix phase transition (Redrawn from Murdan *et al*., 1999).

1.2.4.2 Non–aqueous gels

Gels containing gelling agents in non–aqueous vehicles are called non–aqueous gels (NAG). There are mainly several types of non-aqueous gel including organogels (Terech and Weiss, 1997; Vintiloiu and Leroux, 2008) and lipogels (Korbar-Smid & Bozic, 1978; Scric *et al*., 1985). The NAG containing solid sorbitan monopalmitate (Span 40) or sotbitan monostearate (Spans 60) as gelling agents and liquid Spans (Span 20, Span 80) or liquid Tweens (Tween 20, Tween 80) as oil phase are termed amphiphilogels (Jibry *et al*., 2004). In contrast, gels containing organic gelling agents (organogelators) and non–polar liquid phase are called organogels (Terech and Weiss, 1997; Murdan *et al*., 1999) or oleogels (Vintiloiu *et al*., 2007). However, gels containing metallic stearates (alkali and alkaline earth metals) as gelling agents in non–polar vehicles are called lipogels (Korbar-Smid and Bozic 1978; Bozic *et al.* 1980 and Scric *et al.* 1985). A mixture of stearate obtained from the combination of magnesium and aluminium salts have also been used to prepare stable slightly transparent gels of vegetable oil such as sweet almond oil (Uwe, *et al.* 1992).

Organogels, in the last decade, due to the development of new organogelators have attracted attention of many researchers (Terech *et al*., 1995; Murdan *et al*., 1999;

Terech, 2002) but rather limited emphasis is given to the lipogels. Lipogels are defined as the systems made up only of liquid lipophilic vehicles or containing small amount of water (~1−2%). Lipogels may be classified into isogels, where both liquid and solid are composed of hydrogen molecules or heterogels, where a hetero atom like metallic ion is present (Bozic *et al*., 1980). According to this definition, lipogels containing metallic soaps such as magnesium stearate (MgSt) are classified as heterogels. Various researchers have described formulation of lipogels of non-polar solvents using metallic soaps of sodium (Smith, 1947), aluminium (Friberg, 1965, 1966), zinc, magnesium, and calcium in non-polar solvents (Korbar-Smid and Bozic, 1978; Scric *et al*., 1985, 1988). The semisolid formulations containing stearates (stearate creams) are also described as acid-soaps in the literature (Cistola *et al*., 1986; Eccleston, 1997). The present work describes the lipogels of (MgSt) in liquid paraffin and palm−olein.

1.2.4.2a Organogels

Murdan *et al*., (1999) reviewed various types of organogels. Many organogelators such as sorbitan monostearate (Span 60), a hydrophobic non-ionic surfactant, gels a number of non-polar organic oils. Organogels are thermoreversible organic, opaque and semisolid systems. The gel formation involves a network of rod-like tubular aggregation of organogelator in the non-polar liquid dispersion medium (Fig. 1.5). The aggregates associate with each other with contact points also called junction points, producing a three-dimensional network immobilising the organic oil. Disruption of junction points with addition of a third component causes loss of gel network even in the presence of tubules.

Although the molecular structure shows presence of tubules after cooling to room temperature but during cooling, organogels show differences in microscopic structures. Upon cooling to gelling temperature, oil−surfactant affinity decreases, the polymer reassembles to form inverse toroidal vesicular structures which appear only at the gelling temperature and further cooling changes them to tubule form. The conversion of toroid to tubule may be due to its shrinkage or due to its splitting into one or more cylindrical tubules (Murdan *et al*., 1999).
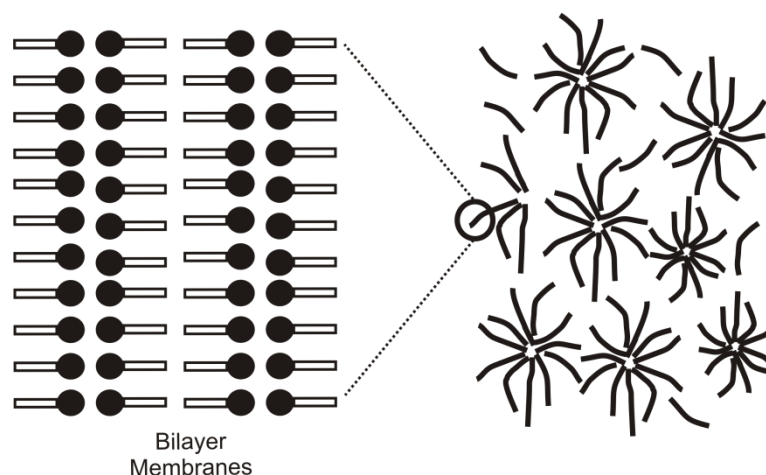
Figure 1.5: Precipitation of organogelator (Span 40) yielding organogels formed using Tween 20 as liquid phase showing tubule formation, made up of lamellar bilayers (modified from Murdan *et al*., 1999).

1.3 Lipogels

Lipogels belong to monophasic non-aqueous systems composed of a stearate-based gelling agent dispersed in oil. The lipogels are non-greasy and due to absence of water are self-preserving. In addition, skin permeation of lipophilic vehicles is believed to be higher than the hydrophilic vehicles due to lipophilic nature of the skin (Block, 2005). Therefore, lipogels can be regarded as ideal semisolid vehicle offering good aesthetic properties (non-greasy), reasonable ambient stability and enhanced drug delivery through skin.

Gelling agents for lipogels are mainly from the class of alkaline earth metals and include stearates of magnesium, calcium, zinc and aluminium. The stearate-based gelling agents have shown significantly varying physicochemical properties under the influence of temperature, moisture and stress, leading to formulations of varying stability (Bozic *et al*., 1980). Therefore, there is a need to investigate the influence of various factors on the properties of gelling agents.

1.3.1 Gelling agents for lipogels

Few metallic stearates have been used to prepare gels and include alkali metals (sodium stearates), alkaline earth metals (magnesium, calcium and zinc stearates) and some other metals like aluminium stearates (Nakagaki and Nishino, 1963).

Metallic stearates are compounds of long-chain fatty acids (C_{12}-C_{20}) with metals of varying valency. The molecules consist of two parts *a* fatty chain part and metal part (Fig.1.6). Depending on the metal, the stearate may contain 1–3 fatty chains. Stearates differ according to the type of fatty acid, length of the carbon chain and the alkali employed. Fatty acids with longer chains are insoluble in water (Garnier *et al*., 1988). The most important stearates, in terms of applications are the metallic stearates of calcium, zinc, magnesium and aluminium. These stearates are used for their lubricating, separating, water repellence and gelling properties and exist as fine powders with a large surface area, prills, flakes, pastilles or granules.

Pilpel (1963) in his review of the solutions of heavy metal soaps suggested that the solubility of the metallic soaps in non-polar solvents depends on the temperature, the metal base and on the solvent used. He also outlined the importance of the degree of unsaturation, fatty acid chain length and the nature of the acid. Metallic stearates of Zn and Mg show little solubility in organic solvents such as liquid paraffin at low temperature. In contrast, at high temperatures (around $110^{o}C$) there is a sudden and substantial increase in the solubility. He called this temperature, the critical solubility temperature (CST).
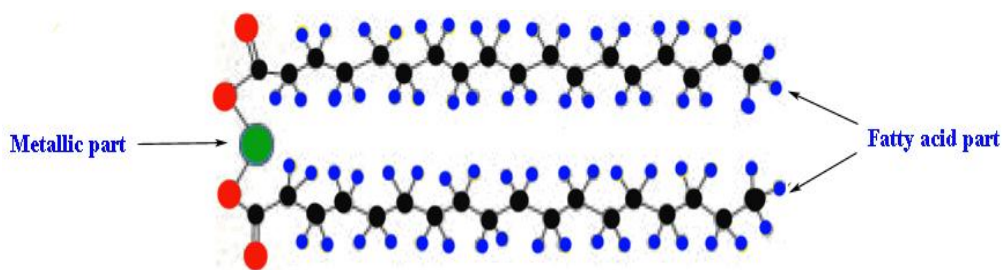
Figure 1.6: Schematic representation of structure of divalent metallic stearate showing the fatty and the metal moieties.

The properties of laurates are greatly influenced by the respective metal base due to the shorter chain length of the fatty acid. However, there is little reliable information available on the part played in the solubility by the metal portion of the molecule in the metallic stearate containing fatty acids of longer chain lengths. It is well established that solubility increases with unsaturation (Pilpel, 1971). Oleates show lower melting point and higher solubility than the stearates attributed to double bond.

Lubrication, release properties and water repellency are characteristics of all metallic stearates. These properties are determined by the cation, the chain length of the fatty acid and certain other properties of the respective metallic stearate *i.e.* the water of crystallisation content. The present work describes the use of alkaline earth metals in the preparation of lipogels. However, in line with the objectives of the present work only magnesium stearate will be investigated in detail.

1.3.1.1 Magnesium stearate

Magnesium stearate exists in different polymorphic forms, which affect its physicochemical properties. The changes in these properties have pronounced effects on the resultant formulation. In addition, method of stearate manufacture also affects their structure and properties (Miller et al., 1982; Rajala and Laine, 1995).

1.3.1.1a Physicochemical properties

Magnesium stearate (MgSt) is a white soft powder at room temperature insoluble in water. It is a low molecular weight (591.27) substance with the chemical formula $Mg(C_{18}H_{35}O_2)_2$ (Swaminathan & Kildsig, 2001). It is a salt containing two equivalents of stearate (the anion of stearic acid) and one magnesium cation (Mg^{2+}). The melting range of MgSt varies between 80^oC and 145^oC depending upon the source and composition of the fatty acid as it does not show a sharp melting point.

Preparation of some stable w/o cosmetic creams using MgSt is not possible without also incorporating magnesium oxide. The creams show significant instability (become fluid) in its absence (Eccleston, personal communications). Therefore, it is important to study the physicochemical properties of MgSt in greater detail to understand its effects on semisolid formulations.

MgSt is prepared from the commercial fatty acids derived from natural sources *i.e.* animal or vegetable, containing mostly mixtures of stearic and palmitic acids (Miller and York, 1985) and the physical and chemical properties of the material from both sources are found to be different. Furthermore, commercial stearate obtained from three different manufacturers presented very different XRD patterns *i.e.* one of the

samples showed amorphous nature and the other two were crystalline material with different hydration states (Moody *et al*., 1979; Marwaha and Rubinstein, 1988).

Although, MgSt is a hydrophobic material, TGA results have shown differences in the amount of water of crystallisation after treatment at varying relative humidities, leading to the formation of anhydrous, dihydrate or trihydrate forms (Fig. 1.7) suggesting that it can absorb moisture from the atmosphere (Rajala and Laine, 1995; Swaminathan and Kildsig, 2001).
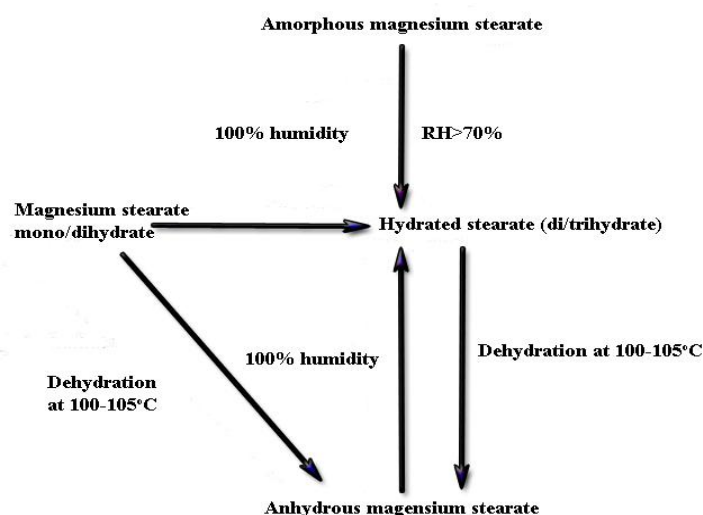
Figure 1.7: Schematic representation of interconversion of magnesium stearate pseudopolymorphic hydrates. (modified from Swaminathan and Kildsig, 2001).

In addition, MgSt is commercially available mainly in the monohydrate (MgSt-M) or dihydrate (MgSt-D) form or as a mixture of monohydrate and dihydrate forms (Wu, 2006; Okoye and Wu, 2007). Both hydrates appeared in the flakes form showing different particle size *i.e.* monohydrate showed smaller particle size (10.6μm) compared to bigger (14.3μm) dihydrate (Okoye and Wu 2007), suggesting the presence of different polymorphic forms. Depending on the amount of moisture present, pure grade MgSt can exist in four polymorphic forms; a needle-like trihydrate, a lamellar or plate-like dihydrate, a monohydrate and an amorphous form (Rajala and Laine, 1995). Each of the hydrate forms belong to a different crystal system and exhibits different crystal habits as evident from XRD patterns for monohydrate and dihydrate, which may affect their physicochemical properties

(Swaminathan and Kildsig, 2001; Rao *et al.,* 2005). DSC and TGA data of various hydrates also appear to be different. Water is loosely bound (free water) in the amorphous form whereas the presence of bound water in the crystalline form has been confirmed by a sharp change due to dehydration seen in TGA (Leinonen *et al.,* 1992). DSC thermograms of mono and dihydrate also showed differences. Although, both hydrates showed two endotherms each however, they peaked at different temperatures *i.e.* monohydrate showing endotherms peaking at 113 and 138°C whereas dihydrate showed endotherms peaking at 90 and 116°C (Fig.1.8).

Magnesium stearate (MgSt) is considered as the best lubricant in tablet manufacturing due to its hydrophobic nature. Commercial MgSt is obtained from stearic acid, which is a mixture of stearic (60–80%), palmitic (10–30%) and (4–5%) free fatty acids (Drozda, *et al.*, 1983; Wada and Matsuhara, 1994; Bracconi *et al.,* 2005). The fatty acids used in the manufacture of commercial magnesium stearate (cMgSt) are obtained mainly from two sources *i.e.* animal and vegetable (Swaminathan and Kildsig, 2001; Andres *et al.*, 2001; Okoye and Wu, 2007). The differences in the fatty acid composition, samples from two sources and different batches of magnesium stearate obtained from the same manufacturer have shown differences in their lubricating properties (Miller *et al.*, 1982; Ertel and Carstensen, 1988a; Britain, 1989).
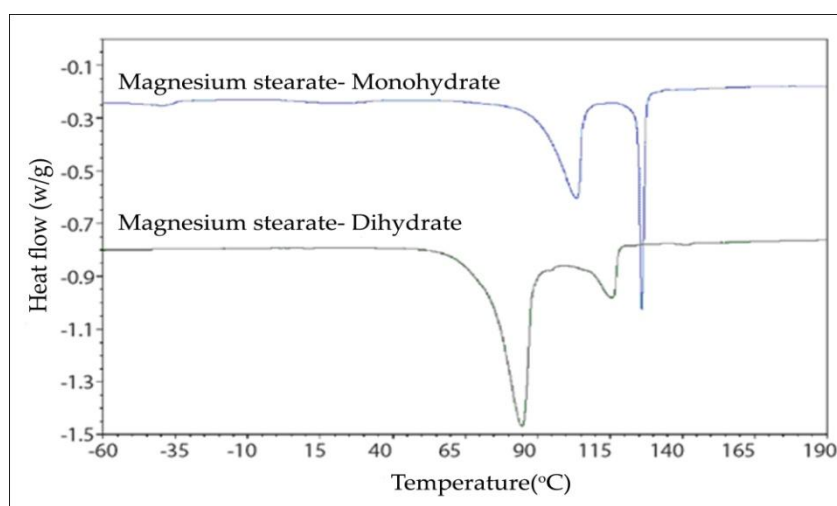
Figure 1.8: DSC thermograms of two hydrates of MgSt (redrawn from Okoye and Wu, 2007).

1.3.1.1b Polymorphism

The polymorphic state of an excipient or an active ingredient significantly influences its physicochemical properties. The temperature, stress or humidity-dependent structural modifications in pharmaceutical ingredients are common. Temperature or stress-related structural modifications are described as polymorphic changes. In contrast, structural or thermal changes brought about by variations in the moisture content are described as pseudopolymorphic modifications (Sharpe *et al*., 1997; Mueller–Goymann, 2004).

Long-chain saturated fatty acids such as stearic acid exhibit marked polymorphism (Gunstone, 1967). The polymorphs are described as A, B, C and E forms. The nomenclature of the polymorphs is based on the angle of tilt of the molecules towards the end group plane. The angle of tilt determines the stability of the polymorphs *i.e.* higher tilt represents stability of the polymorph. Polymorph A shows the smallest tilt whereas C form shows the highest. Therefore, Form C is the most stable and form A the most unstable (Sydow 1955a and 1955b; Garti *et al*., 1982; Lin *et al.*, 1994).

MgSt shows moisture–related structural modifications (Muller, 1976). Although, magnesium stearate is a hydrophobic material it has potential to absorb moisture when exposed to various relative humidities (Andres *et al.,* 2001; Swaminathan and Kildsig, 2001; Koivisto *et al.,* 2004). The samples treated at various relative humidities (RH) shows significantly different physicochemical properties, which may be attributed to the formation of different pseudopolymorphs (Rajala and Laine, 1995; Burnett *et al*., 2004). Drying of MgSt at higher temperature ($\sim100^{o}$C) and low relative humidity (RH) produces amorphous material whereas exposure of the same material to higher RH ($\sim70\%$) produces crystalline material, both of which show significantly different physicochemical properties.

In addition, polymorphic forms of stearic acid used for the manufacture of MgSt are sensitive to low pressures (private correspondence with Prof. Gillian Eccleston). Milling of the commercial sample has resulted in the smaller particle size, with large

surface area, showing varying lubricating properties compared to unmilled sample (Leinonen *et al.,* 1992).

Furthermore, the method of preparation of MgSt has also affected its physical properties *i.e.* alkaline and acidic precipitation methods have yielded MgSt having different particle size, surface area and crystal structure (Miller *et al.,* 1982; Ertel and Carstensen, 1988b). The large batch manufacture in acidic environment results in thin, regular, plate-like crystals, whereas alkaline conditions produce irregular plates or needle-like crystals depending on the batch size (Miller and York, 1985).

Commercial MgSt has been characterised by various researchers for its physicochemical properties including stearate–palmitate ratio, crystalinity, water content, particle size, shape and surface area using microscopy (Butcher and Jones, 1972; Miller and York, 1985), thermal analyses (Rajala and Laine, 1995; Swaminathan and Kildsig, 2001; Bracconi *et al.,* 2005; Okoye and Wu, 2007), FTIR (Ertel and Carstensen, 1988 a & b; Rajala and Laine, 1995) and XRD (Miller and York, 1985; Swaminathan and Kildsig, 2001; Okoye and Wu, 2007). Commercial MgSt has shown significant changes in the physicochemical properties even from the different batches from the same manufacturer, which are attributed to the fatty acid composition of stearic acid used for its manufacture and storage conditions, as revealed by the varying purity, crystal type and hydration state of the material (Andres *et al.,* 2001).

1.3.1.1c Manufacture

Magnesium stearate is prepared using three different methods; precipitation, direct reaction and fusion methods (Pilpel, 1963; Rajala and Laine, 1995). Sometimes combination of direct and fusion method is used to prepare high purity stearates. Nevertheless, each method imparts specific properties to the final product.

In the precipitation method, fatty acid is first treated with an equal molar concentration of the metal solution in large volume of hot water. The resultant stearate is soluble in water. A metal salt solution of Mg is added to the water-soluble stearate to obtain the desired water-insoluble metallic stearate (Fig.1.9a). The water

soluble bye-products like MgCl are removed by filtration and washing. Finally, the wet cake is dried and milled. The precipitation method produces fine powders with a large surface area and a platelet-like morphology (Rajala and Laine, 1995).

In contrast, the direct method involves mixing of stearic acid with metal oxide or hydroxide at elevated temperatures in excess water at either atmospheric conditions or under pressure (Fig.1.9b). The advantage of this method is that no by–products are produced. Fine powder of high purity with different particle size can be obtained by this method by varying the water content. The particle size is affected by the interaction between fatty acid and water *i.e.* higher the amount of water, smaller the particle size and large surface area. The powder form obtained by this method has higher bulk density compared to the product obtained by precipitation method.

The fusion method utilises heating of stearic acid and the metal oxide/hydroxide under pressure at temperatures higher than the melting point of the metallic stearate with continuous stirring. Most of the metallic stearates have melting point higher than $100^{o}C$, therefore, water produced as a by–product can be separated as steam in a separate container (Fig.1.9c). Henceforth, drying of the final product is not needed. Various forms of the stearates (flakes, prills and powder) can be produced depending on the melting point of the stearates.

Although, all of the above mentioned methods can be used to prepare alkaline earth metals and their preparation appeared to be quite simple but processing variables like pH of the system, batch size and the quality and composition of the fatty acid used have significantly affected the appearance and properties of the final product (Miller and York, 1985) as well as the appearance and stability of the resultant lipogels prepared using them (Bozic *et al*., 1980). Therefore, MgSt should be stored in well closed containers at appropriate temperature and humidity prior to their use in the preparation of the lipogels.

$$2C_{17}H_{35}COOH \ + \ NaOH \longrightarrow \ 2C_{17}H_{35}COO^{-}Na^{+} \ + \ H_2O$$

Step I

$$2C_{17}H_{35}COO^{-}Na^{+} \ + \ M^{2+} +2X^{-} \longrightarrow \ (C_{17}H_{35}COO^{-})_2M \ + \ 2Na^{+}X^{-}$$

Step II

(a)

$$2C_{17}H_{35}COOH \ + \ Ca(OH)_2 \longrightarrow \ (C_{17}H_{35}COO)_2Ca. \, H_2O \ + \ H_2O$$

(b)

$$2C_{17}H_{35}COOH \ + \ MgO \longrightarrow \ (C_{17}H_{35}COO)_2Mg. \, H_2O \ + \ H_2O$$
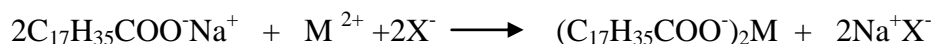
(c)

Figure 1.9: Various methods for the preparation of metallic stearates (a) Precipitation method, (b) direct reaction and (c) fusion method.

1.3.2 Oils used in lipogels

Oil for topical formulations should be compatible with the active and non-active ingredients. In addition, it should be resistant to the adverse effects of environmental factors such as pH, temperature, stress and relative humidity. Furthermore, solvent for lipophilic semisolids should ideally be hydrophobic and non–polar in nature (Young *et al*., 1968). Various natural and synthetic solvents such as paraffins, ointment bases and some liquid surfactants are considered safe, problem-free (Ho, 2006) and have successfully been used in the preparation of lipophilic topical drug delivery systems. Liquid paraffin is considered as non-reactive, safe, cheap solvent which is stable at various environmental conditions and has been used in the preparation of ointments (Ho, 2006), w/o creams in addition to the lipogels (Bozic *et al*., 1980; Scric *et al*., 1985).

In contrast, natural vegetable oils such as olive, palm, jojoba and sweet almond oil are normally used as edible oils and their use in pharmaceutical preparations is limited, mainly due to their complex structure and instability upon storage at varying environmental conditions. For example, the liquid fraction of palm oil *i.e.* palm-olein is known to solidify upon storage at lower temperatures (Swe, *et al*., 1994; Siew *et*

al., 1995). The temperature-dependent changes have been associated to the polymorphic modifications in the oil (Siew and Ng, 1995, 2000; Mamat *et al.*, 2005). However, stable polymorphs have been obtained by creating a balance in the saturated and unsaturated fatty acids in the oil (Mahmoud *et al.*, 1996; Nor Aini *et al.*, 1996; Yusuf *et al.*, 2000). Therefore, enhanced stability of the vegetable oils has lead to their increased use in gel formulations (Genova *et al.*, 1997). In recent years, vegetable oils have increasingly been used in topical semisolids (Almeida and Bahia, 2006). Olive oil and jojoba oil are used in pharmaceutical creams and gels respectively whereas palm oil has mainly been used in cosmetics for the preparation of creams and lipsticks. Palm stearin was first used in the topical pharmaceuticals for the formulation of suppositories and ointments (Ooi, 1980). However, recent use of palm–olein in topical formulations is in emulsions (Ayesha, 1998) and o/w creams for wound healing (Baie and Sheikh, 1999).

Fatty acids are known to enhance skin permeation from the semisolid vehicles. Therefore, palm oil due to its unique fatty acid composition is expected to enhance drug release from lipogels. Henceforth, the present work explores the influence of liquid paraffin and palm–olein on the preparation, stability and structure of the lipogels of magnesium stearate in addition to the investigation into drug permeation profile of ibuprofen from the same.

1.3.3 Preparation of lipogels

Organogels and amphiphilogels have been studied by various researchers in detail but little is known about lipogels. Some work was undertaken decades ago (Smith 1947; Friberg 1965; 1966) on chemical lubricating greases, which form the basis of lipogels, using sodium stearate in various hydrocarbon bases such as hexane and benzene. Bozic *et al.*, 1980; Bozic and Korbar–Smid 1980 and Scric *et al.* 1985; 1988, first time reported preparation of stable solid lipogels of magnesium and calcium stearate and semisolid lipogels of zinc and aluminium stearates in liquid paraffin. Scric *et al.* (1985) after studying various factors prepared solid lipogels of magnesium stearate and liquid paraffin using the following method: Magnesium stearate in different concentrations was mixed with liquid paraffin to obtain a

homogenous white dispersion. The dispersion was heated in an oil-bath to 120–130°C. Upon complete dissolution of magnesium stearate a clear solution of oil was produced. The solution was cooled naturally to room temperature in the oil-bath, which produced solid lipogel.

1.3.4 Structure of lipogels

The detailed structure of the lipogels is not known. However, some researchers have studied the structure using SEM and polarised light microscopy (Scric *et al.* 1988). They showed very small anisotropic particles in the stable lipogels. In contrast, isotropic structures were observed in the unstable lipogels. They explained the structure of lipogels on the basis of micellar theory and electron transfer dependent-aggregation of the stearate molecule in the non-polar solvent.

According to the first theory, the formed micelles are of reverse or inverted type with a core of hydrated or non-hydrated polar groups surrounded by polar hydrocarbon chains forming inverted bilayer vesicles in the lipogels. They also suggested presence of water molecules in between the metal atoms, which provides stability to the lipogels against syneresis (Fig. 1.10).

The second theory suggested aggregate formation, which involves polar interactions between the metal cation and the anion of the carboxylic group. However, the exact structure of the lipogels is far from understood.

Figure 1.10: Proposed molecular structure of the lipogels containing magnesium stearate and the liquid paraffin (redrawn from Scric *et al.*, 1988).

1.3.5 Stability of lipogels

Korbar-Smid and Bozic (1978) and Bozic *et al.,* (1980) studied the effect of process variables such as quality and composition of stearic acid, addition of a stabiliser such as cetostearyl alcohol, moisture content, stirring upon heating and cooling, heating time and cooling rate on the appearance and stability of resultant lipogels of various stearates. They suggested that stirring and cooling rate did not show any significant effect on the stability of the lipogels. However, the quality of the stearate and the moisture content significantly affected the appearance and stability of the lipogels.

Scric *et al*. (1985) demonstrated the effect of water and free fatty acids in metallic soap on the stability of the lipogels. They claimed that the gel formation is not achieved until a certain amount of water and free fatty acids are present in the system. As reported earlier MgSt occurs as various pseudopolymorphic forms depending on the solvate/hydrate that forms upon exposure to various humidity levels (Muller, 1977; Barra and Somma, 1996; Bracconi *et al*., 2005; Okoye and Wu, 2007) and these affect its physical properties. Anhydrous (amorphous) form of stearate results in syneretic, crumbly, solid lipogels. In contrast, the hydrated (crystalline) form of the stearate produces elastic, solid, lipogels that synerese. A stabiliser/emulsifier such as lanolin or cetostearyl alcohol reduced syneresis in these solid lipogels (Bozic *et al*., 1980).

Magnesium stearate (MgSt) used for the preparation of lipogels is obtained from a reaction of stearic acid with an alkali (Pilpel, 1963). The commercially available stearic acid is not pure, but available as a triple pressed mixture containing 55% palmitic acid (C_{16}) and 45% stearic acid (C_{18}) with small amounts of other unsaturated and saturated free fatty acids (Eccleston, 1997). The triple pressing removes the fatty acid unsaturation, with significant removal of oleic acid. Bozic *et al*., (1980) reported that pure stearic acid provided unstable lipogels *i.e.* significant amount of syneresis was observed. In contrast, some free fatty acids in addition to the homologue composition of stearic acid (mixture of palmitic and stearic acid) produced rather stable solid lipogels.

The nature of the solvent and moisture content in addition to the processing variables such as cooling rate, stirring rate and time in addition to the temperature cause changes in the physicochemical properties of stearate-based o/w creams which was related to polymorphism/pseudopolymorphism in the stearate (Timmins *et al*., 1990; Lin *et al*., 1994; Eccleston, 1997). Slow cooling (5−10°C/min), resulted in a stable polymorph whereas supercooling (40°C/min) provided a metastable form, which in turn significantly affected the stability of an anhydrous ointment containing fatty alcohol propylene glycol (FAPG) and stearic acid (Lin *et al*., 1994). However, their results showed insignificant effect of stirring time on the stability of the ointments. Eccleston (1997) described that the stability of o/w stearate creams is affected by the temperature in addition to the process variables such as cooling rate and stress. She showed that in some systems swollen crystalline gel phase (necessary for the stability of semisolid creams) appeared to be metastable, and under pressure, changed into non-swollen unstable structures. In addition, she also described the effect of stirring time on the appearance of the creams *i.e.* stiff creams were obtained when stirring was stopped upon cooling. In contrast, continued stirring upon cooling produced rather soft creams emphasising the effect of stress on the formulation.

With Lipogels, Bozic *et al*., (1980) showed insignificant effect of the same process variables *i.e.* cooling rate and stirring speed on the stability of lipogels of MgSt and liquid paraffin but in later work, they described that heating for longer period of times (90 minutes) than usual (60 minutes) at high temperatures resulted in unstable lipogels (Scric *et al*., 1985), suggesting that temperature had an effect on the stability. In addition, they showed that lipogels of MgSt and liquid paraffin appeared to be solid in consistency. They reported preparation of lipogels by heating the dispersion of MgSt and the non-polar solvent to high temperatures (130°C) and reported a range for CST from 110–125°C. Identification of specific CST rather than range is very important for the stability of these temperature-sensitive systems. Therefore, heating and cooling variables in the lipogel preparation needs to be closely monitored to obtain non−syneretic, stable semisolid systems.

The previous work does explain preparation of stable lipogels with MgSt but they appeared to be solid and the effect of process variables such as heating and cooling

showed no effect on the appearance of resultant lipogels (Bozic *et al*., 1980). Therefore, the present work describes an investigation into the influence of various processing variables such as source of stearate, effect of stirring, heating and cooling variables, addition of water before/after heating and storage conditions in addition to the hydration states of the MgSt on the formulation and stability of the semisolid lipogels. On the basis of previous knowledge of the lipogels and results of preliminary work in the present study we find significant importance of the above said variables with reference to the stability of the lipogels. The thermodynamic properties and the phase behaviour of these systems are not well understood.

1.3.6 Applications of lipogels

Lipogels form the basis of the structure of w/o emulsions and therefore, their applications are also rather similar to w/o emulsions. Lipogels are studied for their water binding capacity in order to establish their use in emulsion formulation (Bozic *et al.* 1980). Due to the absence of water, lipogels are self-preserved as ointments. However, unlike ointments, lipogels are silky and non-greasy and can be a good replacement for ointment bases. The high lipid content produces optimal reduction of skin roughness, produces occlusive effect, preventing skin dehydration and can be used in hand, cracked foot skin and lip care products (Lautenschlager, 2004). Furthermore, lipogels due to their high occlusive effects can significantly enhance the drug permeation through skin. Therefore, it is necessary to investigate the drug release from the lipogels.

1.3.7 Incorporation of drugs into semisolids

The incorporation of a drug into a semisolid vehicle may affect its rheological properties leading to variation in the consistency. The apparent viscosity of the vehicle is inversely proportional to the drug release from the drug delivery system (Al–Saidan, 2004). Certain drugs due to their surfactant nature may extract lipids form the vehicle, causing crystallisation, disrupting the originally formed liquid crystalline lamellar gel network showing instability of the emulsion system. Furthermore, the thermodynamic activity of the drug in the vehicle depends on its saturated solubility in addition to the partition coefficient of the drug between the

vehicle and the skin (Lien and Tong, 1973; Sarveiya *et al*., 2004). Drug showing high partition coefficient (solubility) in a hydrophilic vehicle would show limited drug release as it requires more time to leave the vehicle and get partitioned into the skin. On the other hand, increased solubilisation of the drug in the hydrophilic vehicle may concentrate the drug at the release site which may lead to enhanced release. In contrast, a lipophilic drug may show enhanced drug permeation from a lipophilic vehicle due to increased solubilisation in the vehicle in addition to the lipophilic nature of the skin.

Most of the drugs used in the topical drug delivery systems are of low molecular weight, lipophilic and effective at low doses. However, many active ingredients are weak acids or bases and ionize under normal physiological pH. In addition, charged drugs show decreased permeation compared to uncharged drugs (Sarveiya *et al*., 2004). Therefore, drugs for topical drug delivery systems should be carefully selected.

1.3.8 Evaluation of drug permeation from the lipogels

The biological activity of the topical medicament depends on its permeation through skin. Therefore, it is essential to evaluate the penetration of the drug from the vehicle into the skin. The drug permeation can be evaluated either by the *in vivo* or the *in vitro* tests (Pellet *et al*., 1977; Sriwirayanont, 2001).

1.3.8.1 Skin as a model for *in vivo* drug permeation

The skin is the largest of the body organs, occupying a significantly large surface area *i.e.* ~10% of the body mass. An average adult's skin has a surface area of ~$2m^2$. Anatomically, the human skin is described as stratified organ with three distinct viable tissue layers *i.e.* epidermis (outer layer), the dermis (middle layer) and the subcutaneous (innermost) fat layer (Fig. 1.11).
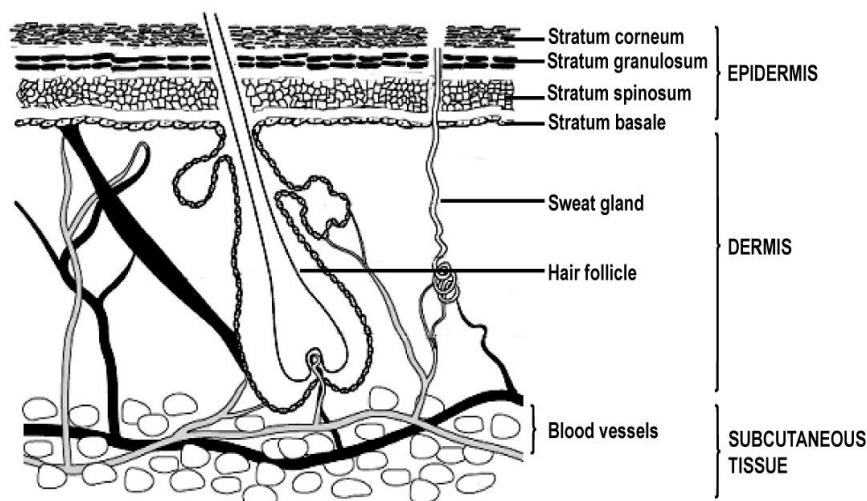
Figure 1.11: A schematic diagram of cross-section through human skin (redrawn from Williams, 2003).

The skin provides an effective and selective barrier to the permeation of noxious substances *i.e.* chemicals or microorganisms and at the same time helps in the regulation of heat and water loss from the body (Roberts, 1997; Hadgraft, 2001). The unique characteristics such as high surface area and the presence of several permeation pathways makes skin a preferred portal for the delivery of topical medicaments.

The drug molecules at the skin surface come in contact with the microorganisms, cellular debris and appendages, which offer negligible help in the permeation (Barry, 2001). It is now generally accepted that the SC is the only barrier to the drug permeation (Moghimi *et al*., 1996; Williams, 2003). To overcome this biological barrier, an understanding of routes and mechanisms of drug permeation across skin is essential.

1.3.8.1a Routes of skin permeation

The route and mechanism of permeation of drugs through skin have been a topic of debate for a long time. In 1970s, it was postulated that drug mainly permeate through transcellular route (Scheuplein and Blank, 1971; Roberts *et al*., 1977). Scheuplein and Blank (1971) in the pioneering work on the shunt routes reported permeation of drugs through appendages *i.e.* follicular route. However, it is now generally accepted

that drug can permeate through the skin by three routes *i.e.* intercellular, intracellular and the appendages (Fig. 1.12) the sweat glands and the hair follicles (Liu *et al.*, 1993).
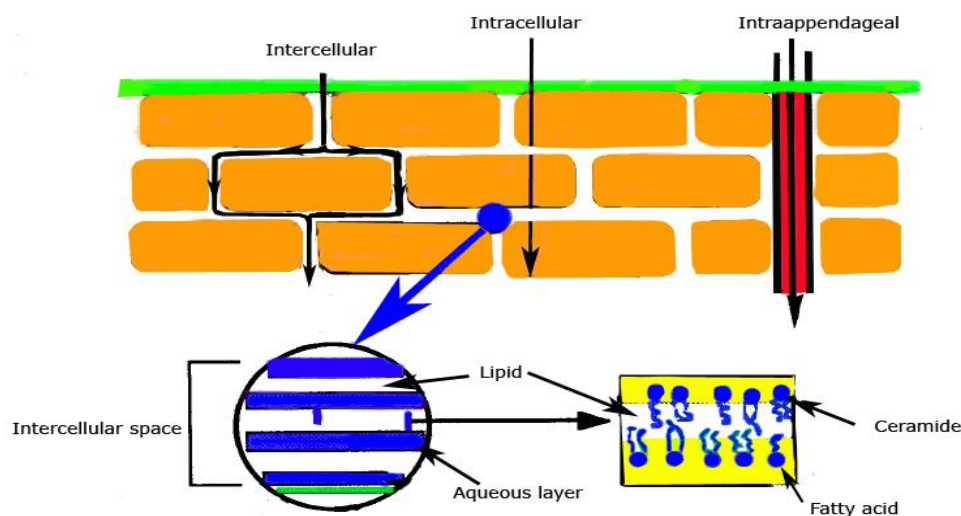
Figure 1.12: Routes of drug permeation through skin (redrawn from Roberts and Walters, 1998).

The use of XRD, polarised microscopy and FTIR for the assessment of drug permeation across skin has revealed that the main pathway for the drug permeation through the skin is intercellular route via lipid bilayers (McIntosh, 2003). The large surface area of SC makes this route the preferred pathway. However, modifications in the geometry, composition and mesomorphic phases of lipid bilayer may limit the diffusion from this pathway. The diffusion of the polar and non-polar solutes across skin has been reported to be different (Roberts *et al.*, 1978) and is attributed to the barrier composition.

Although, the penetration through appendages bypasses the SC but the overall penetration from these routes is rather little owing to the small area (less than 0.1%) available for diffusion (Pugh *et al.*, 1996). In addition, absorption through the shunt routes is actually against the flow of the secretions from these glands, making permeation difficult. However, development of novel technologies *i.e.* iontophoresis and ultrasound have made this route of drug administration main area of research for the transdermal delivery of ionic molecules (Barry, 2001). In addition, these routes

account for half of the total ions transported through skin by iontophoresis (Roberts, 1997).

The intercellular diffusion involves penetration of drug through lipid bilayers whereas the drugs opting for intracellular route requires penetration through the mortar of intercellular lipid bilayers in addition to the proteinaceous part of the corneocytes (Abraham, 1993, 1995). The corneocyte envelop is impermeable to most of the chemicals and therefore, diffusion of the drug from the intercellular lipid bilayers back into the corneocytes is not possible making this route of negligible importance (Roberts, 1997; Barry, 2002). Therefore, it is generally accepted that most of the small and non-ionic dugs penetrate the skin through intercellular route. In contrast, permeation of ionic molecules is expected through shunt routes. After knowing various routes of drug permeation across skin, it is important to understand how drug behaves when it comes in contact with the SC. As discussed earllier, the SC is highly impermeable and only selective hydrophobic drug substances of MW<500 Da can permeate through it. The percutaneous absorption of drug invovles transport from the vehicle to the stratum corneum by partioning, transport from SC to the lower layers of epidermis through intercellular route of diffusion and through the dermis into the blood stream. In contrast, drug permeation is related to transport across the SC only. Therefore, dermal concentration of the drug from topical drug delivery vehicles involves drug permeation rather than percutaneous absorption.

The stratum corneum is composed of dead corneocytes and no active transport of the drugs is possible (Roberts *et al*., 1977). The diffusion of drug through the skin is a purely physical, passive process and no energy is required (Pugh *et al*., 1998). The delivery of drugs across SC takes place in two steps *i.e.* transport of the drug from vehicle to the surface of SC by partitioning between vehicle and the SC and then transport across it (Pugh *et al*., 1996).

However, it is now well established that skin is the most important and the only rate-limiting factor affecting topical drug permeation (Roberts *et al*., 1977; Hadgraft *et al*., 1986; Zettersten *et al*., 1997; Barry, 2001; Al-Saidan, 2004; Cilurzo *et al*., 2007; Sangkil *et a*l., 2007). Highly impermeable human skin limits the accurate delivery of

drugs from the topical route. Furthermore, human skin penetration is highly variable and large differences exist between different body sites (Scheuplein and Blank, 1971; Cornwell and Barry, 1995) and even at the same site in the same individual (Southwell *et al.*, 1984). Therefore, other options such as *in vitro* drug release should be explored.

1.3.8.2 *In vitro* drug release

The *in vivo* testing of topical dosage forms is very complex, expensive, and highly variable and requires lengthy procedures. Therefore, the *in vitro* testing offers a cheaper option where the results can be obtained in relatively short span of time and used for the quality control purpose (Shah *et al.*, 1989). The *in vitro* diffusion cells have extensively been used to investigate the drug release profile of newly developed topical dosage forms (Franz, 1975, Cooper *et al.*, 2004; Huang *et al.*, 2005). In addition, in late nineties the FDA released SUPAC-SS guidelines, which involves *in-vitro* diffusion cell testing of non-sterile semisolid dosage (NSSSD) forms when manufacturing or material changes have been made to an approved dosage form (FDA-SUPAC-SS, 1997). Furthermore, the i*n vitro* diffusion experiments can also be used to obtain useful information relevant to various interactions in a drug delivery system such as drug-excipient, drug-vehicle, drug-skin and vehicle-skin interactions (Aungst *et al.*, 1986, 1990; Walters, 1989; Walter *et al.*, 1998; Cho and Choi, 1998; Brown *et al.*, 2000; Anuer and Valenta, 2004; Adami *et al.*, 2006). Furthermore, *in vitro* analyses of drug performance are used mainly for quality control and bioequivalence studies of the drug in two formulations rather than simulation of drug performance *in vivo*.

1.3.8.2a Franz diffusion cells as a model for *In vitro* drug release

Diffusion cells have been used extensively in the investigation of drug release from the topical and transdermal formulations for the past few decades (Franz, 1975; Addicks *et al.*, 1987; Chilcott *et al.*, 2005; Hauck, *et al.*, 2007) Franz diffusion cells, the most popular type of diffusion cells, due to their simple construction (Fig. 1.13) are available in various forms such as static, flow-through, side by side, and modified Franz cells (Sriwirayanont, 2001). Both types of cells have two major components

i.e. a donor and a receiver. The donor is shorter in length and is used as the reservoir for the drug. In contrast, receiver is much longer and contains diffusion medium. The receiver has one to two sampling arms at the side depending on the type of Franz diffusion cell. Franz diffusion cells are available commercially with the proper heating systems to maintain the desired temperature throughout the period of study with very low inter-cell variability in the dimensions.

Both static and flow-through cells have extensively been used in the *in vitro* drug release experiments (Franz, 1975; Addicks *et al*., 1987; Pellett *et al*., 1997; Gallagher *et al*., 2003). In the static cells a specified amount of sample is removed at regular intervals whereas in the flow-through cells entire receptor solution is replaced with the fresh one at frequent intervals to simulate the blood flow beneath the skin where there is a constant flow of blood, which washes away the permeated drug, maintaining the sink condition (zero% drug) just below the skin (Barry, 1983; Ng, 2007). However, many researchers have reported rather similar drug flux using either type of cell (Addicks *et al*., 1987; Clowes *et al*., 1994; Liebenberg *et al*., 2004).

However, the use of Franz diffusion cells is associated with great variability in the results which question their reliability. The use of tailor-made and commercially available Franz cells has shown differences in the drug release (Ng, 2007).

| (a) | (b) |
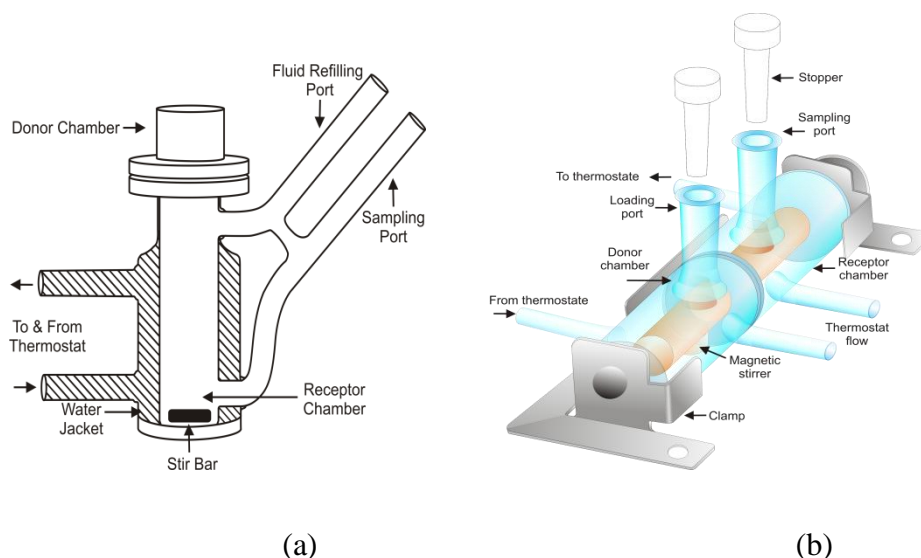
Figure 1.13: Types of commercial Franz diffusion cells (a) vertical and (b) side-by-side

In addition, inter and intra laboratory differences have also been reported with the use of Franz diffusion cells having similar dimensions and obtained from the same manufacturer (Chilcott *et al*., 2005; Khan *et al*., 2005)**.** Furthermore, same unit of the Franz cell, with similar methodologies, used in two different laboratories have also shown significant variance in the results (Hauck *et al*., 2007). In an ideal situation human skin should be used in the experiments. However, ethical issues have limited their use, which leads to the use of other biological membranes such as pig skin, which is thought to be most closely related to the human skin as far as lipid content is concerned. However, biological membranes vary significantly in their composition mainly the lipid content and therefore considered the leading contributing factor causing the significant variance in the permeation of drug (Costa and Lobo, 2001; Khan *et al*., 2005; Cilurzo *et al*., 2007). In recent years, the use of synthetic membrane has increased tremendously. Although, the use of synthetic membranes have reduced the errors but the level of variance is still significant. The membranes should be used only as a support rather than to limit the drug permeation. In addition, studies have shown that the experiments carried out with or without membrane did not affect the drug release but still gave high variance in the results (Hauck *et al*., 2007). This shows that the membrane is not the only contributing factor in results variations and there must be other factors such as the operator and the factors related to the diffusion cell.

Due to such variability in the use of diffusion cells, various researchers have studied the effect of validation of the Franz cells on the drug release (Smith and Haigh, 1992; Cordoba-Diaz *et al*., 2000; Thakker and Chern, 2003; Siewert *et al.*, 2003). However, most of these studies were focused on the validity of the experimental design for a specific drug and the effect of validation of diffusion cell on the reproducibility of results has grossly been ignored. Therefore, a recent work (Ng, 2007) using custom made Franz cells has proven that the proper validation of the Franz cells in the drug release studies is extremely important because improper validation resulted in significantly high % coefficient of variance (%CVs). Henceforth, the use of Franz cells in drug delivery studies requires proper validation, which should include the investigation of the factors related to the formulation as well as the Franz cell. The Franz cell related factors may include dimension of the equipment, heating and

stirring variations in addition to the membrane type. Although, commercially available Franz cells show a little variation in the dimensions but custom made Franz cell have shown variations in the effective diffusion area leading to significant variation in the results (Ng, 2007). Furthermore, temperature, stirring and type of membrane have also shown considerable variations in the permeation of Betamethasone (Smith and Haigh, 1992).

1.3.8.2b Factors affecting Franz diffusion cell studies

Franz diffusion cell studies over the years have become powerful tool to evaluate the performance of topical vehicles. However, due to significant variations in the results of different laboratories and even within the laboratory, reproducibility of Franz cell (FC) studies has become main concern and therefore greater emphasis is given to the validation process instead (Shah *et al*., 1989; Shah and Polli, 1996; Chilcott *et al*., 2005; Hauck *et al*., 2007; Ng *et al*., 2005a). However, most of the validation studies focus on the formulation related factors and grossly ignore the factors related to the Franz cell such as available diffusion area, temperature changes during experiment and factors related to stirring (Ng, 2007). Henceforth, it results in the significant variability in the results.

Recently, Ng *et al*., (2005b) in their pioneer work on the detailed validation of Franz cell, studied various factors related to Franz cells and concluded that the factors such as Franz cell dimensions, stirring and temperature variables, types, characteristics and cleaning of membranes significantly affect the drug flux and cause great variation in the results in addition to the operator. Nevertheless, validated Franz cell significantly reduces the variability leading to reproducible results (Ng *et al*., 2005a). However, their validation experiments were based on one factor at a time approach (OFAT), which provides information about the effect of individual factor but does not reveal the interactions (if any) between different factors and requires enormous amount of experimentation due to inclusion of only one factor at a time to investigate its effect on the overall performance. In contrast, computer-aided Design of Experiment (DoE) approach reveals critical factors, their interactions and suggests the best combinations of the factors for optimised outputs with lesser number of

experiments (Lewis *et al.* 1999; Rowe, 1993; Rowe, 1997; Anderson and Whitcomb, 2005). Thus, OFAT approach surrenders in favour of DoE. Although, its use in the optimisation of formulations development is well established but its use in the drug permeation experiments has yet to be explored. Therefore, this study aims to explore the critical Franz cell related factors employing DoE approach using a commercial 5% Ibuprofen gel.

1.4 Aims of the study

Although, the presence of moisture has been related to the structure of lipogels (Scric *et al.* 1988), its role in the preparation and stability of the lipogels has not been fully understood. It is also known that the stearic acid used to prepare magnesium stearate is rather sensitive to applied shear such as stirring rate and time (Eccleston, 1997).

Although, magnesium stearate is a hydrophobic material it has shown marked polymorphism upon slight changes in the moisture content and the applied stress. The moisture treatment of magnesium stearate at various relative humidity levels have shown to cause changes in the hydration state, which changes the crystalline structure of the material. Anhydrous material has shown amorphous nature whereas hydrated sample represents various crystalline forms depending on the moisture content, showing different physicochemical properties. Magnesium stearate has also shown changes in the physicochemical properties with the stirring (Lin *et al*., 1994; Eccleston, 1997). Cooling of stearate-based o/w creams with or without stirring showed different consistency, which are attributed to the polymorphic modifications of the stearic acid leading to the conversion of stable form to a metastable polymorph. Therefore, similar changes can be expected in the lipogels of magnesium stearate due to stress and need to be investigated to understand their structure and stability.

The overall objectives of the study are to prepare stable, semisolid lipogels and to evaluate their structure. The overall aims are to investigate the:

i. preparation of reproducible stable semisolid, lipogels of MgSt in liquid paraffin and palm−olein.

ii. influence of homologue composition of magnesium stearate on the lipogels.

iii. effect of pseudopolymorphism of magnesium stearate on appearance of lipogels.

iii. influence of vehicle on the consistency of the resultant lipogels.

iv. effect of various process variables such as heating, cooling and changes in the environmental conditions such as relative humidity on the appearance of the lipogels

v. storage stability of the lipogels at ambient temperature

vi. influence of addition of ibuprofen drug on the rheological properties of the lipogels.

vii. influence of unique combination of saturated and unsaturated fatty acids of palm−olein on the drug penetration enhancement.

viii. drug release characteristics from various lipogels.

CHAPTER II

MATERIALS AND METHODS

This chapter encompasses all materials and methods used in this work. In addition, this chapter also contains comprehensive details of the methods and theoretical background of all the analytical techniques used in this research.

2.1 Materials

2.1.1 Chemicals, gases and membranes

Liquid paraffin BP was purchased from JM Loveridge Plc, Southampton, England. Palm olein, palm stearin and crude palm oil were a gift from Lam Soon Edible Sdn. Bhd. Kuala Lumpur, Malaysia. The following three batches of magnesium stearate were bought and used as such:

Batch 1: GPR grade, loss on drying 4%, batch no. 298464C, BDH chemicals (England).

Batch 2: GPR grade, loss on drying 6%, batch no. 29846, BDH chemicals (England). Batch 3: (60:40– stearic and palmitic acid homologues respectively), batch no. 41505–7 (Dorset, UK).

Anhydrous potassium bromide (KBr), stearic acid, magnesium oxide, potassium sulfate (K_2SO_4), sodium hydroxide pellets, mannitol, sodium metal and potassium permanganate were purchased from Merck (Germany). Ibuprofen BP powder was provided by IOL Chemical and Pharmaceuticals (India). Phosphate buffer solution (pH 4.2 and 9.21) were purchased from Mettler Toledo, Switzerland. GC grades dichloromethane, hexane, glacial acetic acid, chloroform, HPLC grade methanol and boron trifluoride (BF_3) were obtained from BDH chemicals, England. Decon 90 was purchased from Decon Laboratory Ltd. Deionised double distilled water was used throughout. Sodium methoxide was prepared using sodium metal and HPLC grade methanol. Nitrogen, oxygen, helium, hydrogen and purified air were purchased from MOX Gas, Sdn. Bhd. Malaysia.

Cellulose acetate membranes, pore size 0.22μm and 0.45μm were purchased from Sterltech (USA) while regenerated cellulose (Visking tubings) of molecular weight cut off point (MWCO 12,000–14,000) were purchased from VWR International Ltd (Lutterworth, UK). Ibuprofen 5% gel was obtained from Mentholatum, Glasgow, UK. Aluminium crucibles for DSC (40μL capacity) and TGA (70μL capacity) were purchased from Mettler Toledo, Switzerland.

2.2. Analytical Methods

2.2.1 Gas chromatography

Chromatography is an analytical technique, which depends on the separation of components from the sample between two phases *i.e.* stationary and mobile phase. When the mobile phase is liquid it is called liquid chromatography. In contrast, when a gas is used as a mobile phase it is called gas chromatography (GC). The separation of materials depends on two principles *i.e.* adsorption or partition and named accordingly depending on the principle.

Adsorption chromatography utilises a mobile liquid or gas that is adsorbed on the surface of a stationary solid phase. Components of the sample are adsorbed at active sites of stationary phase and are eluted at different times based on the attractive force between stationary phase and each of the individual components. It is also called gas solid chromatography (GSC). In contrast, partition chromatography is based on the formation of a thin film on the surface of a solid support by a liquid stationary phase. In this type of GC, components are separated on the basis of difference in the partition ability through the stationary phase layer. Components with better partition ability elutes before the components of poor partition ability for the same stationary phase and is also called gas liquid chromatography (GLC).

2.2.1.1 Gas chromatography components

GC components include a carrier gas supply system, injector, column, oven, detector and data handling system.

The carrier gas system consists of the gas cylinder, pressure regulator, tubing and fitting and purifier traps that includes moisture, hydrocarbon and oxygen traps (Fig. 2.1). Commonly used gases for GC are hydrogen, helium and nitrogen. The choice of gas depends on the type of detector used and the speed of analysis.
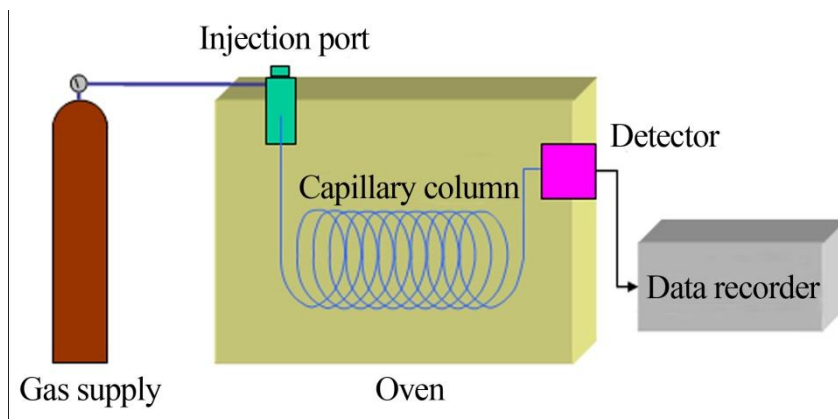
Figure 2.1: Schematic diagram of GC components (redrawn from Perkin Elmer GC user manual).

Injector is an area in which sample is introduced, where it is evaporated instantaneously and carried by the gas to the column with a minimum of band spreading. The injector consists of a septum and a glass liner and is heated using a thermal source. Injectors are designed based on three parameters *i.e.* sample size, temperature and gas flow. In this context, two main types of injectors are available *i.e.* conventional and programmed split/splitless (PSS) injectors.

The GC columns are made up of glass or metal, packed with long chain length hydrocarbons and serve as the stationary phase of the system. Columns of various lengths ranging from eighteen (18) to hundred (100) meters are available and length of the column depends on the hydrocarbon chain length. There is a general consensus that the column performance increases with an increase in the column length. However, at most times there is slight increase in the efficiency even with doubling up the column length. Two main types of columns are used in GC *i.e.* packed and capillary columns.

Packed columns are based on the outer diameter and are classified into micro (1/16") and macro (1/8" and 1/4") columns with 2–4mm internal diameter (ID). In contrast,

capillary columns are classified on the basis of internal diameter and include columns with small (0.1–0.53mm ID) and wide (0.75–1.0mm ID) bore size. Detectors for GC are mainly of two types *i.e.* destructive and non–destructive. Destructive detectors such as flame ionisation detector (FID) degrade the sample producing only one type of data. In contrast, non–destructive detectors such as electron capture detector (ECD) do not affect the sample and many different types of detectors can be used in a row to obtain significant information based on each detector principle.

2.2.1.2 Experimental methodology for GC

Sample preparation for GC involves conventional liquid–liquid and solid phase extraction methods, head space, thermal desorption and purge and trap methods. Extraction methods are commonly used and depend on the polarity of the compounds and the solvent used. The solvent must be non–reactive to the compound and should dissolve the maximum amount of the compound.

Analysis of any compound by GC starts with the selection of appropriate mobile and stationary phases in addition to the detector. Clarus® 500 (PerkinElmer, Inc. USA) GC has been used in this study. The data is handled by TotalChrom® software, starting from method development to data analysis.

A method is developed by providing the relevant information about carrier gas system, column and detector type in addition to temperature of the injector, column and detector. A small amount (0.5−1μL) of sample is carefully drawn into a glass syringe and loaded into the injector either manually or using an autosampler. The sample is separated on the column into various components based on their affinity to the liquid phase and identified by the detector. GC was used in the present study to investigate the fatty acid composition of the magnesium stearate (Chapter III). Fatty acids are non–volatile and therefore, converted into their corresponding volatile methyl esters prior to GC studies.

2.2.2 Microscopy

2.2.2.1 Polarised light microscopy

Electromagnetic radiations such as ordinary light vibrate in all possible directions. When a polariser is placed in the path of the electromagnetic radiation, the radiations parallel to the polariser are allowed to transmit producing plane polarised light and the radiations perpendicular to the axis are blocked. A second polariser (also called analyser) is placed after the first polariser, parallel to the first one (Fig. 2.2) and the radiations passing from the first one transmits through the analyser as well. Nevertheless, when the analyser is rotated at the right angle to the polariser, no radiations are transmitted. In addition, when the analyser is placed perpendicular to the polariser, they are termed cross–polars (Chaudhary *et al*., 2005; Ng, 2007).
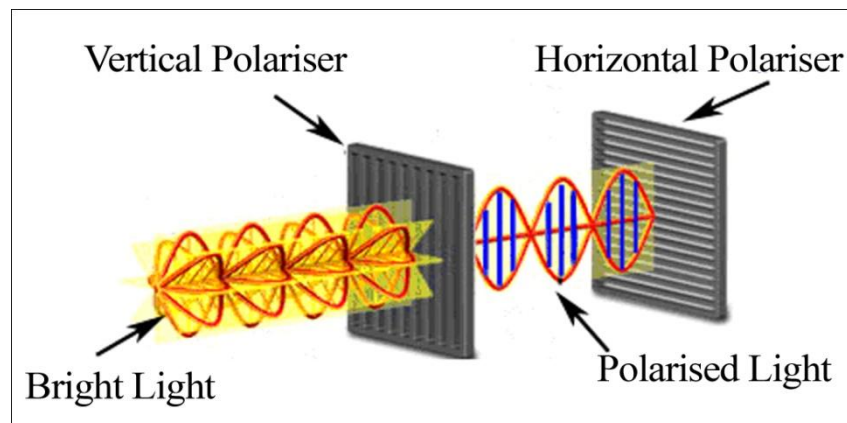
Figure 2.2: A schematic diagram of polarised light microscopy (redrawn from Chaudhary *et al*., 2005).

The speed of light plays a key role in the refraction of light in any material and the refractive index determines the entry and exit of the light. The materials having similar refractive indices in all directions are called isotropic whereas the materials with varying refractive indices in different directions are called anisotropic. Polarised light microscopy helps differentiate the isotropic materials from the anisotropic ones *i.e.* the isotropic materials allow transmission of plane polarised light when the two polarisers are parallel to each other. However, under cross polars, isotropic materials show no transmittance and the microscopic view appears dark. In contrast, the anisotropic materials when placed in the path of light, they rotate the plane polarised

light, showing characteristic white crystalline structures against dark background (McIntosh, 2003). Some highly ordered crystalline materials can divide the plane polarised light into two components *i.e.* ordinary and extraordinary light, which travel at different velocities at right angles, as the light radiations are considered as two separate vector components. These rays recombine after passing trough the analyser. The materials exhibiting such properties are known as birefringent (Chaudhary *et al.*, 2005).

Polarised light microscopy was used to analyse the microstructure of magnesium stearate and various lipogels prepared from it together with liquid paraffin and palm–olein. A small amount of each sample was placed in the centre of polished, clean microscope slides (76 x 26mm) using a clean, wooden stick. Slides were covered with rectangular glass cover–slips (22 x 22mm), and viewed under polarised light at appropriate magnifications (x 5, x 10, x 20 and x 40) using either Leica DMLS (Histocentre, Malaysia) or Reichert–Jung Polyvar (Ansberg, Germany) compound microscopes. Digital photographs of samples were taken using the Image Pro Express software for Leica and the Leutron computer software for Polyvar microscopes respectively. Some of the samples' images were poorly reflected on the computer monitor compared to the clear structure observed under microscope and therefore necessary changes were made using the software to enhance brightness and contrast to view photomicrographs clearly. No other changes were made using the software. A manual SLR film camera was attached to the Polyvar microscope and photomicrographs taken of various raw materials in addition to the lipogels prepared using various amounts of MgSt.

2.2.2.2 Hot stage microscopy

Hot stage microscopy is one of the thermal analyses tools, which provides information about phase changes with the temperature variation at the microscopic level. It provides a means to perform programmed and controlled phase studies with desired temperature ramping. The system consists of a highly temperature resistant stage for holding the sample and the hating/cooling device (Fig. 2.3). The body size of the stage is 160 x 80 x 24 mm. The extreme sub–ambient temperatures are

regulated either by the use of liquid nitrogen or a digital intracooler. This allows investigation of the real–time phase behaviour of a material at ambient, sub–ambient and at extremely high temperatures. The stage is then placed on a suitable microscope equipped with the polarised light in addition to the bright light. The principle is same as that of the polarised light microscopy. The only difference being in the sample preparation *i.e.* the sample is sandwiched between two circular cover slips instead of placing on a glass slide.
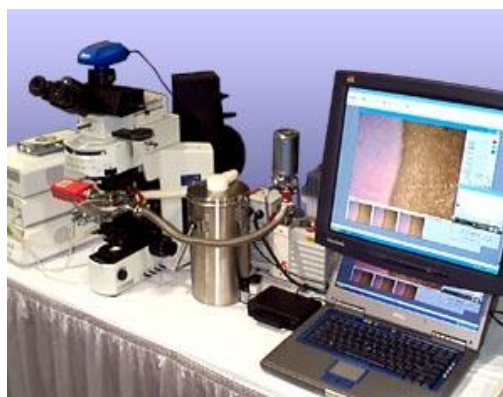
(a)   (b)

Figure 2.3: The hot stage microscopic analyses (a) Stage with the automated pumps and (b) complete set up of the hot stage microscopy (adapted from the User Manual, Linkam Scientific Instruments, UK).

A thin smear of sample is sandwiched between two 16 mm circular glass cover–slips on the stage, which is then placed on the rectangular stage of the microscope with the objective working distances of 0.1–4.9mm and condenser working distances of minimum 12.7mm respectively. The heating and cooling cycle is selected and the sample studied under bright as well as polarised light to investigate the phase changes with increase or decrease in the temperature. The phase transition temperature range is recorded as the temperature between which the sample starts to flow and the temperature at which the structure completely disappears. Thermal changes at various temperatures are recorded and photographed using digital or manual film camera attached to the microscope.

In the present study a TMS 91 hot stage (Linkam Scientific Instruments, UK) attached to the Polyvar microscope was used to determine the melting point of the raw materials in addition to investigate the phase transition temperatures of various lipogels.

2.2.2.3 Scanning electron microscopy (SEM)

The analysis of materials using SEM involves the bombardment of the specific area of the specimen with an electron beam also called primary electrons, emitted from an electron gun, which is fitted with a tungsten filament cathode. Tungsten is commonly used in the electron guns because of its highest melting point amongst all metals, therefore allowing its use as to be heated for electron emission.

The electron beam is bombarded on the sample surface with an energy ranging between a few hundred electron volts (eV) to forty (40) kilo electron volt (keV) and an electron spot is formed by the objective and condenser lenses. A deflection coil system scans the focused electron beam in a raster fashion across the sample surface. The electrons interact with the sample surface, and extends deep into the specimen up to a certain depth, which is also known as the interaction volume, which varies between few hundred nm to 5μm. Upon contact with the sample surface, the primary electrons may experience one or all of the following interactions: the electrons may pass through the sample without interaction, the electrons may be elastically reflected without energy loss, they may be absorbed by the sample emitting low–energy secondary electrons in addition to X–rays, they may be absorbed and emit photons of visible light and they may give rise to electric current within the sample. All these emitted radiations can be used to produce image and can be detected by specific detectors. However, most commonly, image formation involves the low–energy secondary electrons.

The secondary electrons are selectively attracted to a grid held at low (50V) positive potential with reference to the specimen. In addition, there is a disc behind the grid, which is held at high (10KV) positive potential with reference to the sample. The disc consists of scintillant, coated with a thin layer of aluminium. The secondary electrons emitted from the specimen pass through the grid and strike the disk, which

results in the production of light from the scintillant. The light is transmitted through the light pipe to the photomultiplier tube where photons of light are converted to voltage signal. The voltage signals are generated pixel by pixel. The voltage signal is fed out of the microscope column to an electronic device where it is amplified to generate image. The image is built up by scanning the electron beam across the whole surface of the sample in the exact synchronised way with the electron beam from a separate cathode–ray tube scanned over the screen. The intensity of the cathode–ray tube is modulated by the voltage signal to form image of the surface. The image can be captured digitally and displayed on a computer monitor (Fig. 2.4).

The samples for SEM should be of an appropriate size to fit on a specimen holder called specimen stub. In addition, specimen must be a conductor of electricity or at least show conductivity at the surface. In this context, metallic specimens require little preparation for SEM. Contrary to this, nonconductors of electricity, upon interaction with the secondary electrons, are charged leading to scanning problems in addition to the accumulation of the static electric charge on the specimen. Therefore, nonconductors are usually coated with an ultra–fine coating of an electric conductor such as gold and platinum to avoid these problems and are deposited on the sample either by low or high vacuum coating. In contrast, non–conducting specimens may be studied uncoated in a relatively high pressure chamber where the working distance is short and the vacuum is kept low at the electron gun using a cold plate. The high pressure region around the sample in the SEM neutralises charge production on the surface of the sample and provides an amplification of the secondary electron signal (Dorset, 1985).
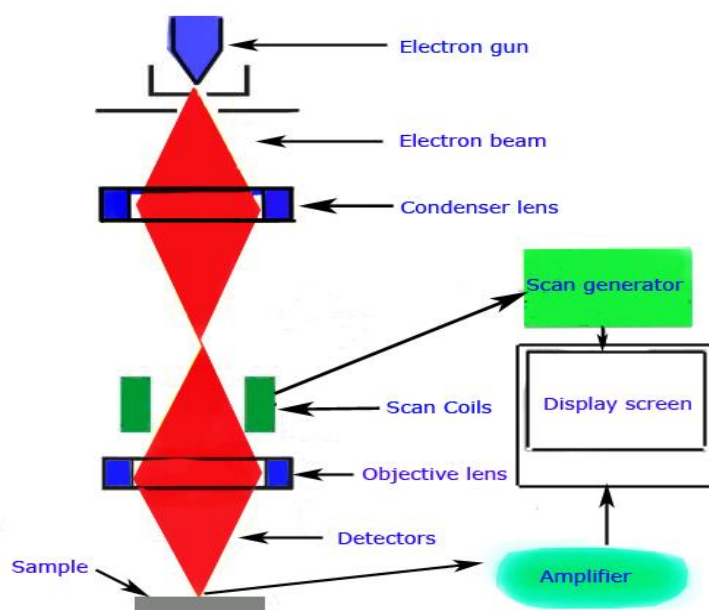
Figure 2.4: A simplified schematic diagram of the image generation using scanning electron microscope (adapted from LEO 1400 Series Scanning Electron Microscopes– Operator User Manual).

In the present work, SEM was used to characterise magnesium stearate in addition to the lipogels obtained from the magnesium stearate and the liquid paraffin. A LEO 1450VP SEM (Oxford Instruments, UK) equipped with Gatan C1002 cold stage and Oxford ITC 1502 temperature controller was used. A small sample of each powder of magnesium stearate was coated with gold for 2–3 minutes, placed on the stub of the microscope and studied under high vacuum. In contrast, the lipogels were studied directly without gold coating, by placing a small sample on the stub using the cold plate under low vacuum. Each sample was studied at powers between x 15 and x 5000 and was photographed at appropriate magnifications.

2.2.3 Thermal analyses

Thermal characterisation determines the physical properties of a substance as a function of controlled increase in the temperature. The variation in the temperature may lead to the changes in the mass of the sample in addition to phase changes such as melting or crystallisation. Most thermodynamic events involve loss of heat or addition of energy (changes in enthalpy). The weight changes can be studied using

thermogravimetric analysis (TGA). In contrast, phase changes may be studied either by differential thermal analysis (DTA) or by differential scanning calorimetry (DSC).

The DSC provides accurate information about the amount of heat absorbed or released by the sample at the phase transition as the area under the curve is directly proportional to the heat transfer to the system. In contrast, the DTA determines only the temperature of the phase transition instead as the area of the curve is not directly proportional to the heat absorbed by the system.

2.2.3.1 Differential scanning calorimetry (DSC)

DSC is used to study phase behaviour of the materials as a function of controlled temperature changes. In a DSC experiment, the sample is heated or cooled between two selected temperatures at a specific heating or cooling rate. The heating or cooling may lead to the thermodynamic changes in the sample, which are reflected in the DSC thermogram as an endotherm or exotherm depending on the absorption or loss of heat.

2.2.3.1a Types of DSC

There are mainly two types of DSC systems in use *i.e.* the heat flux and power–compensation DSC (Fig. 2.5). In heat flux DSC both sample and the reference materials are heated by one furnace. The sample and the reference pans are placed on the separate platforms, which are located at one single metal disc heated by the furnace. In contrast, power compensation DSC utilises the use of individual heater for the sample and the reference. However, the sample and the reference in both cases are heated at the same rate. In the present study, the heat flux DSC822^e (Mettler Toledo, UK) was used. The DSC was connected to the TS0801 RO sample robot and controlled by the Star^e software v 8.10). The DSC was used to study the melting point of various raw materials (Chapter III) in addition to the phase behaviour of the lipogels (Chapters IV and V).

2.2.3.1b DSC Instrumentation

The important components of DSC include a heating and cooling device, furnace, sample holders, heat sensors, gas flow systems and recording device. An electric heater is used for the heating and the heat flow is monitored by thermocouples, which vary in number from 8–128 depending upon the model of the DSC in use. An increase in the number of thermocouples increases the monitoring efficiency of the heat exchange in the DSC. Inert gases *i.e.* dry nitrogen, are commonly used to keep the DSC environment constant. Furthermore, the use of reactive gases *i.e.* oxygen is also common to study the chemical reactions such as oxidation.
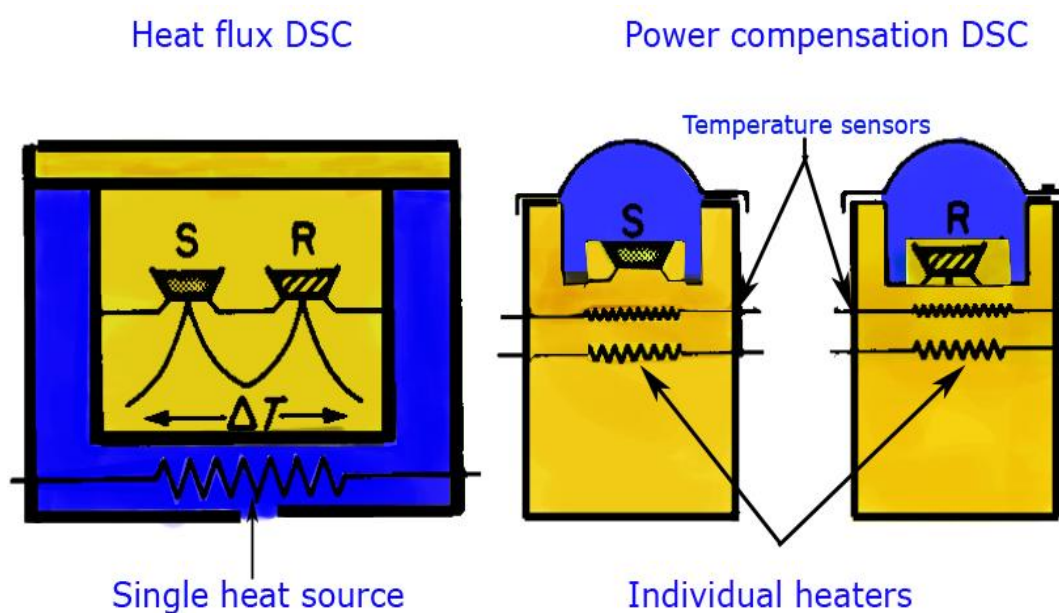
Figure 2.5: A schematic diagram of heat flux and power compensation DSC (adapted from Mettler Toledo DSC 851[e] user guide).

2.2.3.1c Principle of DSC

The basic principle of DSC involves heating or cooling the sample and an inert reference material at a controlled rate to identical temperatures and measuring the energy necessary to establish a zero temperature difference between the two materials. The material to be examined is carefully weighed in the aluminium crucibles (available in various sizes) and placed in the furnace just above the heat sensors. An empty pan, which serves as the reference, is also placed next to the

sample pan and both pans are heated by the thermocouples at a similar rate. The crucibles are normally covered with a lid and hermetically sealed to avoid contact with the environment. Upon temperature variation, when a thermal event takes place in the sample, the heat changes (absorption or evolution) cause a difference in the temperature of the sample and the reference material. Therefore, extra or less energy will need to flow to the sample to maintain a zero temperature difference between the two pans. For example, upon heating, a solid melts, by absorbing energy from the environment at its melting temperature, showing an endotherm and therefore, more energy will flow to the sample to keep its temperature same as that of the reference. In contrast, when a liquid is cooled, it crystallises at a specific temperature by releasing heat and an exothermic peak is observed. DSC is also commonly used to study the glass transition temperatures of the polymers. The glass transition is a temperature where a crystalline material, normally in a glass state is changed to an amorphous liquid–like rubbery state (Skoog *et al.*, 1998). A typical DSC thermogram is shown in Figure 2.6.

2.2.3.1d Interpretation of the DSC results

At the completion of the DSC experiment various thermal events may be observed in the form of endotherms or exotherms depending on the heat supplied to the system. Therefore, the heat flow or enthalpy changes in the sample can be determined directly from the area under the curve of the thermal event by the following relationship:

$$\Delta H = KA \qquad \text{(Equation 2.1)}$$

Where ΔH is the enthalpy of transition, K is the calorimetric constant, and A is the area under the curve. The calorimetric constant varies from instrument to instrument. The enthalpy is expressed in joules per gram (Jg^{-1}).

Furthermore, the onset, peak and endset temperatures in addition to the peak areas of the endotherms or exotherms are also studied to ascertain any discernible patterns related to the specific thermal event. The DSC results can also be used to determine the nature of the material *i.e.* crystalline or amorphous state.
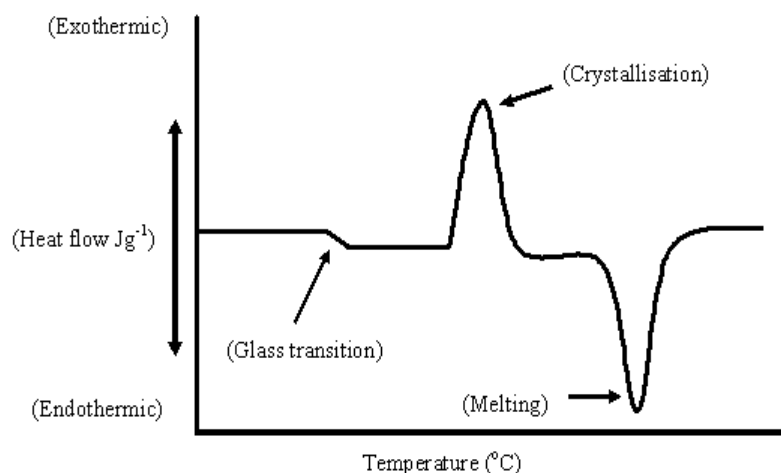
Figure 2.6: A typical DSC spectrum showing various phase transitions.

2.2.3.1e Calibration of DSC

The DSC sensors are very sensitive and minor variations in the system can lead to significant variations in the enthalpy of thermal events during the experiment. Therefore, it is important to calibrate the DSC. Organic compounds and metals such as zinc and indium are used to calibrate the heat flux DSC. The most important calibrations include tau–lag, heat flow and temperature calibration. Tau–lag calibration involves the time taken to attain the temperature equilibration between the sample and the reference. It is important to perform this calibration as the temperatures of sample and the furnace may change when different heating rates are employed. The calibration is based on the determination of the onset temperature of the peak using different heating rates.

Heat flow calibration measures the required amount of heat for the melting of a standard with specific weight and heat flow. It reflects the sensitivity of the DSC sensors. In contrast, the temperature calibration determines the sensitivity of the thermocouples, which records the temperature related to the melting of the standard.

The heat flow and onset temperature calibrations were performed using indium of known weight. The calibration was performed in triplicates and the mean values used

to compare the experimental data with the manufacturer's recommendations *i.e.* onset temperature (156.6±0.3) and heat flow (28.45±0.6). Figure 2.7 shows the DSC thermogram of indium calibration for heat flow and temperature.

Exo

Integral normalised -28.05 J/g
Onset: 156.78 C
Limit: -27.85 ...... -29.01J/g
156.3.......156.9 C

mW

120   130   140   150   160   170   180
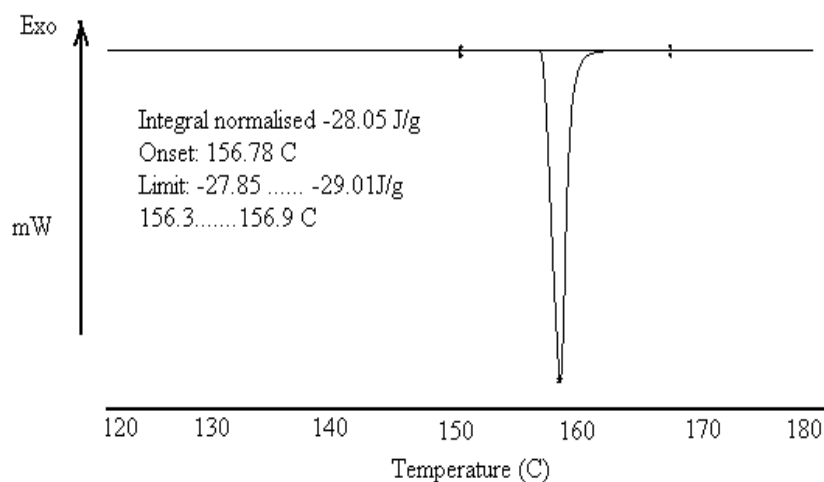
Temperature (C)

Figure 2.7: Calibration of DSC using indium showing melting onset temperature and the enthalpy.

2.2.3.2 Thermogravimetric analysis (TGA)

TGA provides supplementary information to the DSC results. It measures the amount and rate of change in the mass of a sample as a function of temperature or time in a controlled atmosphere (Chaudhary *et al*., 2005). The major components of TGA include an electronic microbalance, furnace for heating, temperature sensors and a recording device to monitor weight and temperature changes (Fig. 2.8). The sample is placed in a 70μL aluminum crucible, which is suspended on the extremely sensitive microbalance over a furnace with controlled temperature. The experiments are conducted in an inert atmosphere with the use of nitrogen gas. The weight of sample is recorded as a function of increasing or decreasing temperature. The temperature calibration of TGA is important and done using the Curie point method. The Curie point method involves determination of the loss of magnetism of a ferromagnetic metal such as iron and nickel upon heating.

The metal is loaded in the aluminium crucible and a permanent magnet is placed under the crucible, which pulls the crucible down and an increase in the weight is

shown on the microbalance (Chaudhary *et al*., 2005; Ng, 2007). The crucible is then heated at a specified rate and the temperature where iron looses its magnetism is recorded and compared with the manufacturer's recommendations.

In the present study, TGA/SDTA 851^e was used to analyse the weight loss from various raw materials such as magnesium stearate, liquid paraffin, palm–olein in addition to the lipogels. The TGA was connected to the same TS0801 RO sample robot, which was linked to the DSC and controlled by the Star^e software v 8.10).
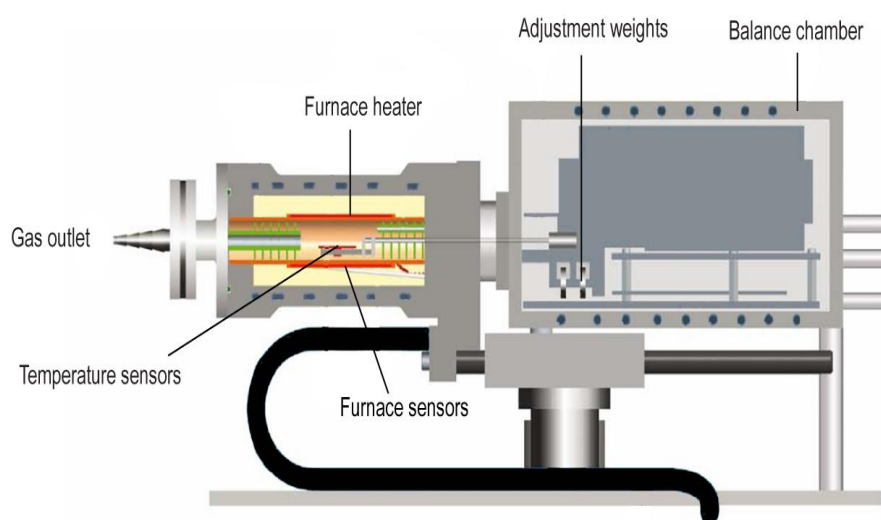
Figure 2.8: Schematic diagram of the thermogravimetric analyser (Redrawn from the Mettler Toledo TGA/SDTA 851^e user guide).

2.2.4 Rheology

Rheology deals with deformation and flow of matter and plays an important role in the development, stability and use of the pharmaceutical products. In particular, rheology has been used widely in semisolid formulations as a method of quality control during and after manufacturing processes as well as to understand the structure of the phases present in addition to determine the effect of various components of a formulation (Davis, 1969).

The rheological properties of materials are governed by two fundamental laws of physics *i.e.* Hook's law of elasticity and Newton's law of flow (Equations 2.3 and 2.4 respectively). "When a shear stress is applied to a material, the resistance to

deformation of a solid or the flow of a liquid, is described by the modulus of elasticity for an elastic material and by the coefficient of viscosity (η) for a liquid or viscous material"

$$G = \sigma/\gamma \qquad \text{(Equation 2.3)}$$

$$\eta = \sigma/\dot{\gamma} \qquad \text{(Equation 2.4)}$$

Here, γ is the elastic deformation, σ is applied shear stress and $\dot{\gamma}$ is the shear rate and G = modulus of elasticity. These concepts can be explained with the help of a hypothetical example of Newtonian model of laminar flow as follows:

Imagine a liquid which is contained in a box between two large, parallel plates one being moving and the other one stationary, and being separated by various thin plates in between sliding on each other like a deck of cards (Fig. 2.9). When the shear stress is applied on the moving plate, with a constant force (F) per unit area (A) with certain separation height (x) at a velocity of V, then the top plate which is adhered to the moving plate also moves with the same velocity. The second layer beneath it is dragged along by friction but its velocity is reduced by the resistance of the layers beneath it. Each layer is pulled by the layer above it but held by the layer beneath it. However, the bottom layer adheres to the stationary plate and hence has zero velocity. Therefore, the velocity of the layer reduces with an increase in the distance from the top moving plate. The shear stress is the force per unit area ($\sigma = F/A$) whereas shear rate is the velocity gradient or change in velocity with the distance ($\dot{\gamma} = dV/dx$). The shear rate indicates how fast the liquid flows when shear is applied and according to the Newton's law shear stress is proportional to the shear rate whereas the proportionality constant is viscosity (η).
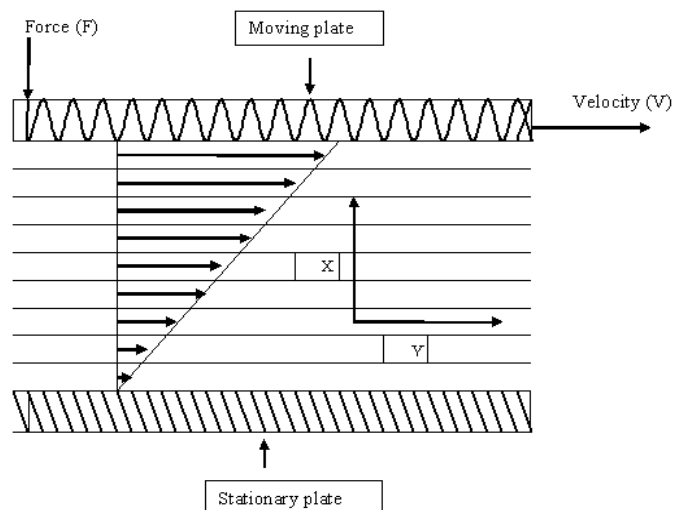
Figure 2.9: Newton's model of laminar flow showing movement of various layers of a liquid under stress (redrawn from Schnaare *et al.*, 2005).

For elastic material, instantaneous deformation takes place when stress is applied and upon removal of stress, the material returns to its original shape at time = 0. On the other hand, liquids flow when stress is applied with a velocity gradient and upon removal of stress may not return to their original position. The materials showing pure elastic nature are known as Hookean solids. In contrast, the materials showing pure liquid or viscous nature are called Newtonian liquids.

Pharmaceutical dosage forms such as structured liquids and semisolid dosage forms such as creams, ointment and gels possess viscous as well as elastic characteristics and also called viscoelastic materials. Either destructive or non–destructive tests are commonly used to investigate rheology of formulations.

Destructive tests such as flow curves are used to study apparent viscosity changes in the formulations using continuous shear rheology. The "apparent viscosity" is investigated because it changes with applied stress instead of "absolute viscosity" which is a relative term and does not change. As their name suggests, these tests cause destruction of the sample due to high shear stress. The shear rate vs. shear stress flow curve determines the effect of increasing shear on the viscosity. Only Newtonian fluids show no change in viscosity upon increasing the shear. Materials showing change in the viscosity (Shear stress / shear rate) with increasing shear rate

are known as non–Newtonian fluids. Materials showing an increase in the viscosity during the course of experiment are described as shear thickening or dilatant materials. In contrast, the materials showing decrease in viscosity (shear thinning) are called plastic or pseudoplastic materials. Plastic materials behave as elastic bodies until a certain shear is applied, the yield value, after which they flow. However, pseudoplastic materials show a constant decrease in viscosity with an increasing shear rate (Fig. 2.10). Most of the semisolid pharmaceutical formulations such as creams and gels show either plastic or pseudoplastic behaviour.

Flow curves provide invaluable information about the flow behaviour of the formulations however it does not provide information about the complex rheological behaviours such as viscoelasticity. Therefore, non–destructive tests like oscillation and creep recovery are used to study the viscoelastic properties.
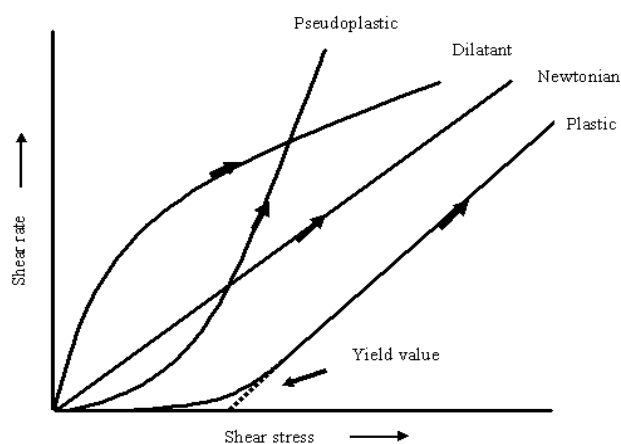
Figure 2.10: Shear rate vs. shear stress flow curves showing Newtonian and non–Newtonian flow behaviour.

Oscillation experiments provide information about viscoelastic behaviour of a material at very low strains. The oscillation strain sweep is used to find the range of strain at which the sample is independent of the strain applied. Two types of experiments *i.e.* amplitude sweep and frequency sweep are carried out.

The amplitude strain sweep is used to determine the linear viscoelastic region of material response, which is used for the frequency sweep testing. The maximum strain at which storage modulus (G′) remains constant is known as the critical strain

and defines the limits of the linear viscoelastic region and is a fundamental yield value, unlike the yield value derived from flow curves, which is dependent on the experimental conditions. Once the maximum linear amplitude is determined, a frequency sweep is performed. In the frequency sweep, the amplitude strain is maintained at a level less than the critical strain and frequency is varied normally between 0.01 and 100Hz.

To explain oscillatory shear measurements, a sinusoidal stress (or strain), smaller than the critical strain is applied on the material and the corresponding resultant sinusoidal strain (or stress) is measured. Typical stress−strain sinusoidal waves are shown in Figure 2.11. The sample responds to this type of stress or strain by elastic energy storage and viscous energy dissipation and these energy responses can be represented by storage modulus (G′), which represents the energy stored per unit volume and loss modulus (G′′), energy dissipated per unit volume.
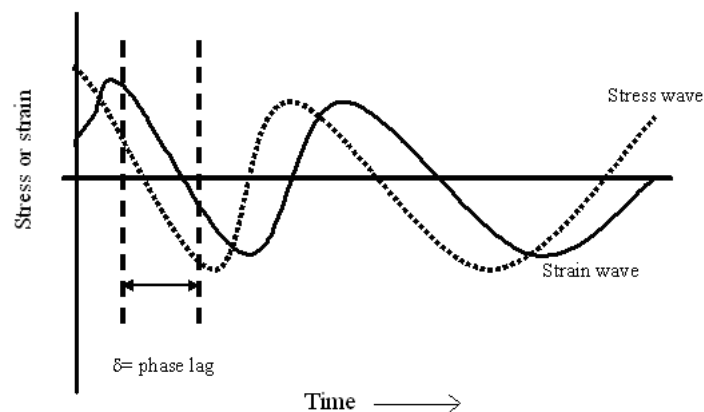
Figure 2.11: Typical sinusoidal wave showing stress and strain wave during oscillation (Redrawn from Marriot, 2002).

During an experiment, the system looses energy due to its viscoelastic nature therefore the amplitude of the stress wave is less than the strain wave. The stress wave also lags behind the strain wave and the difference between two waves is known as lag (δ), which helps in the determination of G′ and G′′ which can be calculated using equations 2.5 and 2.6 respectively (Marriot, 2007). Low phase angle represents elastic nature whereas high values are associated with the viscous behaviour.

$$G' = (\sigma/\gamma) \cos \delta \qquad \text{(Equation 2.5)}$$

$$G'' = (\sigma/\gamma) \sin \delta \qquad \text{(Equation 2.6)}$$

Flow curves of various lipogels in this study were conducted using a Carri–Med cone and plate rheometer (Crawley, UK) using continuous shear by increasing shear rate to a predefined value, and then decreasing the shear rate back to zero, which resulted in flow curves. In contrast, the viscoelastic properties were studied at fixed, low strain to determine G′ and G″ in addition to the phase angle.

Cone and plate geometry consists of an inverted cone in close contact with the platen. The sample is placed in the narrow gap between the cone and the platen. Due to specific cone angle, the material thickness in contact with the cone varies, however for a material undergoing laminar flow, the shear rate is uniform throughout the gap because the shear rate is the ratio of the velocity difference across the material to the distance over which shearing occurs. Nevertheless, flat cones with zero angles (*i.e.* parallel plates) are also available and their use has increased in the recent past.

2.2.5 Texture analysis

A semisolid formulation needs to fulfill certain desirable attributes, which contribute to the ultimate patient acceptability and clinical efficacy of the product and include optimized mechanical properties such as ease of removal from the container, ease of application to the skin (good spreadability), good retention to the site of application, after feel effects and good drug release after absorption (Jones *et al*., 1997). Upon application of the formulation to the skin, it experiences shear forces like rubbing, which are oscillatory in nature and may affect the rheology, clinical efficacy and mechanical properties of the product.

Texture profile analysis (TPA) is one of the analytical techniques used for the investigation of mechanical and textural properties such as hardness, index of viscosity, compressibility, cohesiveness and adhesiveness of the topical semisolids and the information obtained are correlated to the *in–vivo* textural properties of the formulation such as removal from the container and application characteristics of the

product and therefore directly related to the development of the semisolid formulations (Jones *et al.*, 1996).

The technique utilises depression of an analytical probe of known size and diameter into the semisolid formulation to a specified distance at a known speed for specified period of time. Figure 2.12 shows the typical texture analysis trace. Various parameters (positive force, negative force, positive and negative area under the curve are used to determine the mechanical properties of the formulation.
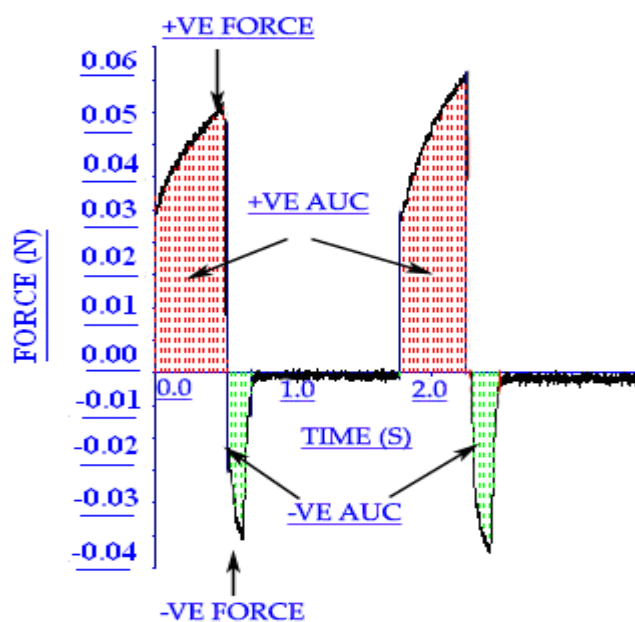
Figure 2.12: Typical TPA showing various parameters used to study the mechanical properties of a semisolid formulation.

The positive force required for a probe to compress the formulation to a specified distance, causing a deformation and is associated with the hardness of the formulation and compressibility describes the work needed to spread the formulation through a fixed distance whereas cohesiveness is calculated by the positive area under curve (AUC), which represents the work needed for the penetration of the probe through the specified distance and involve weakening of the cohesive forces holding the structure together. In contrast, the negative force required to detach the probe from the sample determines the consistency of the formulation and negative AUC is related to the adhesiveness of the formulation, which represents the work needed to overcome the attractive forces between the formulation surface and the

surface of the probe. In the present study the textural properties of various lipogels were investigated using a texture analyser (Model TA–XT2, Stable Micro Systems, UK) at ambient temperature.

2.2.6 X–ray diffraction (XRD)

When a specific type of electromagnetic radiations such as X–ray, impinge on a crystalline material such as an inorganic salt, which is composed of atoms arranged in a specific order, the radiations are scattered in many different directions by the scatterers such as electrons or the nucleus of the atom as shown in Figure. 2.13.

The visible light has very long wavelength (5500 Å), possessing very low energy and is unable to produce significant scattering. In contrast, X–rays, electrons and neutrons which are considered as waves of electromagnetic radiations, possess extremely high energy and penetration power with relatively medium wavelength (0.1–100 Å). The analytical techniques using X–rays, electrons and neutrons as electromagnetic waves are called X–ray diffraction (XRD), electron diffraction crystal analysis (EDCA) and small angle neutron scattering (SANS) respectively.

The X–rays upon striking the atom produce secondary spherical waves emerging from the electron cloud, causing electrons to move and to reflect the X–rays in a different direction. This phenomenon is known as scattering. The scattered overlapping X–rays interfere with each other either constructively by adding together to produce stronger peaks or destructively by subtracting each other producing a diffraction pattern on the detector. Therefore, the interference pattern forms the basis of the diffraction analysis. Most of the scattered waves are of the destructive type and fewer are of the constructive type. The emission of constructive waves is governed by the Bragg's Law of diffraction (Equation 2.7) and schematically represented in Figure. 2.14.

$$2d \sin \theta = n\lambda \qquad \text{(Equation 2.7)}$$

Where d is the inter–planer distance between two atoms, θ is the angle of diffraction between incident ray and the scattering planes, λ is the wavelength of incident and

scattered rays whereas n is the order of the diffraction and its values range between 1 and 5 (Chaudhary *et al*., 2005).
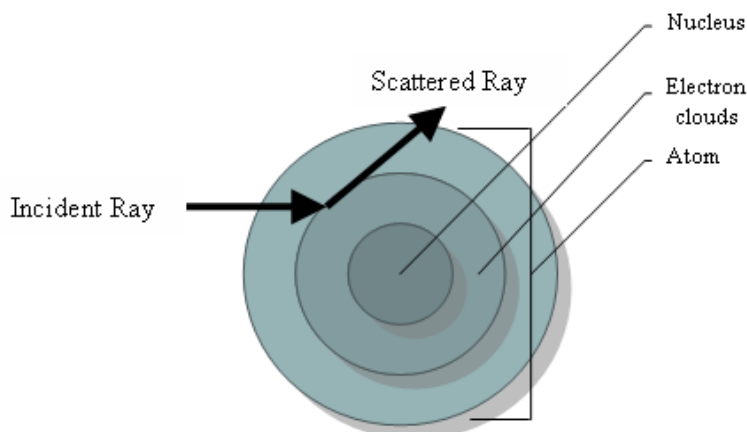
Figure 2.13: A schematic representation of scattering of the incident electromagnetic rays by the electron clouds of the atoms

According to Bragg's Law, the incoming X–ray causes production of small spherical waves after interacting with the electron. When the scatterers are arranged symmetrically with a separation *d*, the path length between the two beams is equal to 2d sin θ. The spherical waves add constructively only when the path difference is equal to the whole number of the wavelength (λ) and part of the incoming beam is deflected by an angle 2θ producing a reflection spot in the diffraction pattern (Bragg and Bragg, 1913). In addition, the incident rays after striking the electron may be scattered in either of the two ways *i.e.* elastic scattering or inelastic scattering.

In the elastic scattering, diffraction occurs due to the interaction of the incident rays and the electrons, therefore, the planes are separated by an inter–planar spacing of atoms, which is also called d spacing. The diffracted peak is representative of the d spacing of the equivalent set of the three Miller planes, also called Miller indices, represented by hkl. The Miller indices determine the electron densities, which are used to identify peak positions of atoms in the crystal. The peak intensity is the function of the atoms that make up the crystal and their scattering is a function of the electron density surrounding the atoms in addition to their location in the crystal. Therefore, diffraction pattern, which is different for each material provides

information about the packing and the unit cell content yielding a unique fingerprint for each crystal form (Chaudhary *et al*., 2005).

The X–ray diffractometer also called Bragg Brentano geometry consists of an X–ray source normally called X–ray tube, sample holder called Goniometer and the detector (Fig. 2.15). In a typical powder XRD experiment, a thin film of sample is placed on the Goniometer and is scanned at a specific step using known range of diffraction angle (normally between 2.5^{o}–70°) with fixed wavelength of X–rays and the diffracted waves are recorded at the detector to generate a diffractogram, presenting 2θ on the x–axis and peak intensity on the y–axis.

Different elements are used as the source of X–ray generators like chromium, iron, cobalt, and copper but a copper X–radiation source is commonly used as it produces highly energetic monochromatic $K\alpha_1$ radiation *i.e.* radiation of similar wavelength ($1.54056cm^{-1}$). The other radiations produced by these X–ray generators include $K\alpha_2$, $K\beta_1$ and $K\beta2$, which are less energetic and normally filtered using a Ni $K\beta$ filter. The difference in the intensity ratio of various rays *i.e.* $K\alpha1$, $K\alpha2$ and $K\beta$ is in the order of 10:5:1 respectively.

In the present study a powder X–ray diffractometer (Bruker 8 Advances, Germany) was used to analyse magnesium stearate (Chapter III) in addition to various lipogels prepared from these stearates (Chapters V and VII).
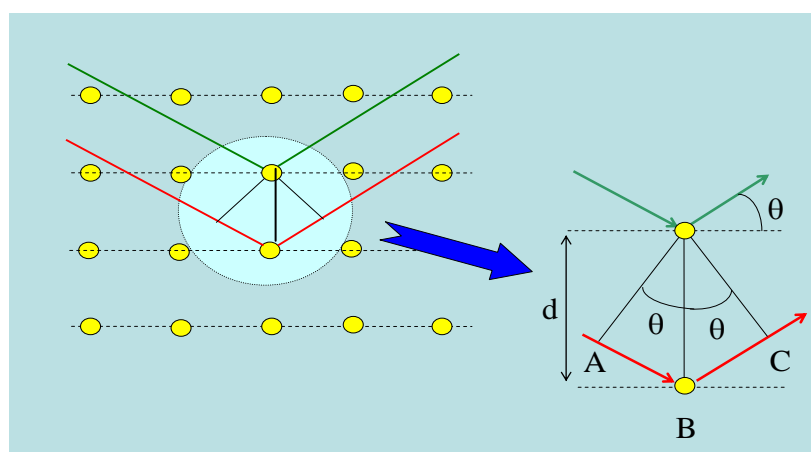
Figure 2.14: Schematic representation of the Bragg's Law of diffraction showing incident and diffracted rays.
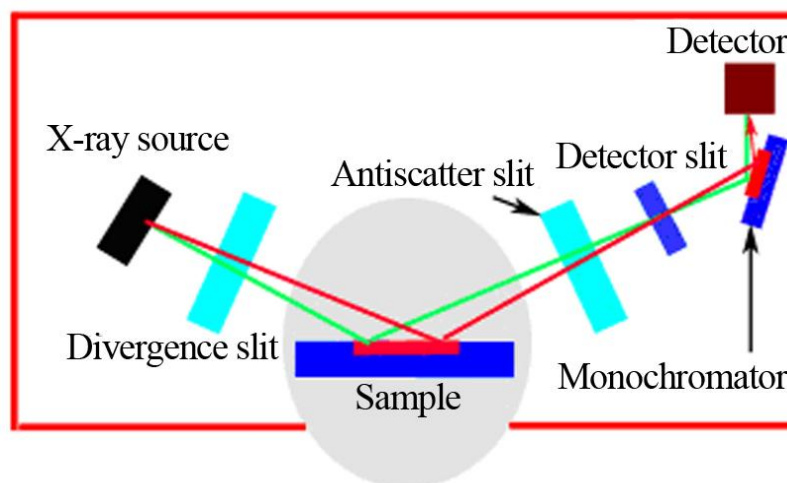
Figure 2.15: A schematic diagram of the powder X–ray diffractometer showing X–ray source, sample holder, various slits and the detector (redrawn from Chaudhary *et al*., 2005).

2.2.7 Fourier transform infrared (FTIR) spectroscopic analyses

The spectrum of visible light consists of various wavelengths of varying frequencies. The highest frequency is observed just beyond the red colour and therefore this part of the electromagnetic spectrum is known as infrared and can be expressed in terms of energy, wavelength, or frequency. Infrared have wavelengths longer than the visible light and shorter than the microwaves and ranges between 5 and 14000cm^{-1}. These frequencies are further subdivided into three portions depending on the frequency range *i.e.* near infrared ($4000–14000 \text{cm}^{-1}$), mid infrared ($500–4000 \text{cm}^{-1}$) and far infrared ($5–500 \text{cm}^{-1}$).

The infrared spectrum is formed due to the absorption of electromagnetic radiation at certain frequencies which are associated with the vibration of the atoms and specific chemical bonds in a molecule (Coates, 2000). The vibrations may be symmetric and asymmetric stretching or bending in nature depending on the change in dipole moment. The symmetric vibrations have zero dipole moment and therefore called IR non–reactive. In contrast, asymmetric stretching and bending vibrations have certain dipole moment and hence called IR reactive. Generally, the frequencies of the IR reactive vibrations are taken in to account for the elucidation of the structure (Chapman, 1957). However, knowledge of the IR non–reactive vibrations can help in

rapid identification. IR spectrum provides information about the strength of the covalent bond between two atoms (intensity), the mass of the interacting atoms and the position of the functional groups. Therefore, IR spectrum serves as the fingerprint of the entire molecule.

FTIR analyses use Michelson interferometer, which consists of a fixed mirror, a moving mirror and a beam splitter. Two mirrors are placed at 90° to each other and separated by a beam splitter located at 45° (Fig. 2.16).

The infrared beam generated from the source impinges on a beam splitter, half of which is transmitted to a moving mirror and remaining half to a fixed mirror. A change in the optical path difference, which is also called retardation (δ) is obtained by the movement of the moving mirror at a constant velocity over a fixed distance to scan the sample. Upon travelling the fixed distance, the mirror quickly returns to the start position to begin the next scan. In addition, while the moving mirror travels, each wavelength of the collected radiation is recorded at a unique frequency as a function of the wavelength of the radiation and the velocity of the moving mirror. Upon reflection from the mirrors, the rays interfere constructively or destructively at the beam splitter, depending on the wavelength or frequency and the optical path difference, giving a signal at the detector.
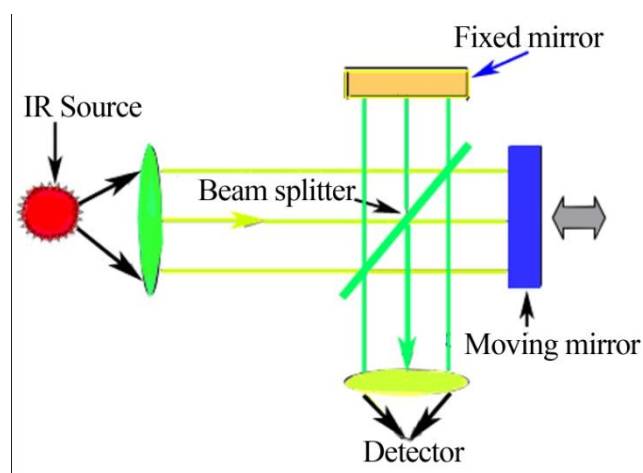
Figure 2.16: A schematic diagram of interferometer used for the FTIR analyses, showing static and moving mirrors and the beam splitter (Adapted from Coates, 2000).

Upon entrance of multiple wavelengths from the infrared source, the combination of different frequencies and the intensities as a function of retardation, forming cosine waves produces an interferogram. The interferogram represents a series of data points between retardation and intensity, collected during the movement of the mirror and all the retardation data points are necessary to obtain the IR spectrum. The availability of "Fourier transformation" technology, which utilises microcomputer to detect all vibrations as they take place using mathematical equations, has made continuous data collection much easier. The microcomputer is able to decode 'Fourier Transform' all the individual cosine waves by converting all the retardation data points into intensity contributing to the interferogram, producing a plot of intensity vs frequency. The computational efficiency of FTIR and the accuracy of its laser reference system contribute in the addition and averaging of individual spectra also called scans to produce spectra linked with rapid data collection times (10 ms). Therefore, a few seconds exposure of sample to IR is sufficient to collect data.

The KBr disk method is commonly used for the preparation of solid samples, where KBr is mixed with the solid sample in specific proportion and compressed to a thin transparent pellet. However, liquid and semisolid material cannot be analysed using this method. Therefore, liquids are analysed using the liquid glass made up of NaCl. The limitation of this method is that only non–hydrophilic materials can be analysed.

Total reflectance measurements (TRM) have become the preferred choice to analyse samples as it does not require sample pretreatment. TRM include diffuse and specular reflectance, transflectance and attenuated total reflectance (ATR). Diffuse and specular reflectance both are difficult to handle as they cause distortion of the bands. ATR is the simplest to handle and allows analysis of all kinds of samples from solids through liquids to semisolids. However, its main limitation is that it shows increased intensity of the band with an increase in the wavelength, which is reduced by the wavelength correction using the software.

In the present study FTIR–8400S (Shimadzu, Kyoto, Japan) was used for the analysis of magnesium stearate (Chapter III) and the lipogels prepared from these stearates (Chapter IV). KBr disc method was used for the sample preparation of

magnesium stearate whereas lipogels were analysed using ATR. FTIR spectra of various samples were analysed using IR Solution software.

2.3 Drug release studies

The biological activity of the medicament in a semisolid formulation can be assessed by either of the two methods *i.e. in–vivo or in–vitro*. The former evaluates the activity of the drug inside the living body whereas the later utilises diffusion cells for the simulation of the activity of the drug upon application to the skin. Franz cell is one of the most common diffusion cell used for these *in–vitro* studies.

2.3.1 Franz diffusion cell studies

Various types of Franz diffusion cells have been used for the investigation of drug release from the topical formulations and are categorised mainly into two types *i.e.* static and flow–through cells. Both types are composed of two major components *i.e.* a donor and a receiver. The donor is shorter in length and is used as the reservoir for the drug. In contrast, receiver is much longer than donor. The receiver may have one to two sampling arms at the side with varying degree of angles depending on the type of Franz cell. Static cells normally have one arm whereas flow–through cells have two arms. The sampling arm of the commercial static cells normally has a calibration mark to which the receiver fluid should be filled. The Franz cells are available commercially with the proper heating systems to maintain desired temperature throughout the period of study with very low inter–cell variability in the dimensions. Furthermore, Franz cells can be custom–made using the glass blowers.

The main difference between the two types of cells is the mode of handling the receiver fluid. In case of static cells, the measured volume of fluid is kept in the receiver for the entire period of experimental time and samples withdrawn and replenished at intervals. In contrast, in the flow–through cells, the receiver fluid is constantly replaced with the fresh one at frequent intervals (2–3minuts), simulating the flow of blood underneath the skin which is in continuous motion that sweeps away the drug absorbed through the skin. Therefore, flow–through cells offer more realistic situation compared to static cells. However, they are difficult to manage as

huge volumes of the receptor fluid are required for a single experiment. In contrast, static cells are used for the qualitative analyses of the drug absorbed.

2.3.2 Experimental methodology

The Franz diffusion cell is set up by placing the receiver in a stirring block, a membrane placed on top of the receiver, the donor placed on the membrane and clamped. The receiver fluid is transferred to the receiver and the drug is loaded at the membrane in the donor. The Franz cell is then heated normally at $33^{o}C$ (skin temperature) using either dry or wet heating approach. In dry heating approach, the block containing receiver is heated using digital heater whereas wet heating approach involves heating of the Franz cell using a circulating water bath, linked through latex tubing to the block containing receiver (surrounded by water jacket). Generally, the experiments are conducted at $33^{o}C$ and conducted in 3–6 replicates.

The samples are withdrawn at regular intervals for a specified period of time (usually 7 hours) and the cumulative drug release (Equation 2.8), permeability coefficients and drug flux (Equation 2.9) in addition to the percent coefficient of variation (Equation 2.10) are calculated.

$$Q= (C_nV+ \Sigma_{i=1}C_iS)/A \qquad \text{(Equation 2.8)}$$

Where Q is the cumulative drug release, C_n the concentration of drug at nth interval, V is the volume of receiver, $\Sigma_{i=1}$ is the sum of concentration of the drug at sampling interval 1 through n–1, S represents the amount of sample withdrawn and A is the area of the receiver.

$$Kp= J/Cv \qquad and \qquad J=Kp/Cv \qquad \text{(Equation 2.9)}$$

Where J represents drug flux, Kp is for permeability coefficient and CV is the coefficient of variance.

$$\%CV= (standard\ deviation/Mean) \times 100 \qquad \text{(Equation 2.10)}$$

In the present study PermeGear (Bethlehem, USA) static Franz diffusion cells with temperature regulating circulating water bath (Fig. 2.17) were used for the investigation of ibuprofen release from various lipogels of magnesium stearate (Chapter VIII).

Figure 2.17: Franz cell experiment set up showing receiver, donor, stirring and heating glass blocks in addition to the circulating water bath.

2.4. Design of Experiment (DoE)

The traditional approach to drug–design experimentation requires that only one factor at a time (OFAT) is changed while keeping all the other factors constant. The OFAT approach has many major disadvantages, *i.e.* it is costly, requires lengthy experimentation, and does not analyse interactions between experimental factors (Rowe and Roberts, 1990; Anderson, 2008). In contrast, statistical Design of Experiment (DoE), a matrix–based multifactor method, is cost effective, quick and does provide information about interactions between factors (Anderson and Whitcomb, 2005). Therefore, DoE is recognised as an important tool for the rapid pharmaceutical product development (Bolton and Bon, 2004).

The process begins with the researcher identifying the factors which may affect the overall experiment, for example stirring speed, temperature etc. The experimental factor may have discrete levels (where the number of levels is the number of

variables considered in each factor). If two levels are selected for each experimental factor and the factor selected is stirring speed, a two level experiment might consider stirring on and stirring off or alternatively stirring speed low and stirring speed high.

It is extremely difficult to visualize all the factors affecting any experiment, however experience and the literature related to the experiments in question may help to shortlist important experimental factors. The validation of Franz diffusion cell experiments was carried out using DoE in this study (Chapter VIII) and the selection of the experimental factors to be investigated was largely based on Ng's (2007) recent work in our laboratory in addition to recognizing the differences in the two types of Franz diffusion cells used in the two studies.

Franz diffusion cells are frequently used in drug release experiments for quality control purposes. Nevertheless, large variation occurs in the Franz cell experimental results. Recently, there has been an increased awareness about the validation of Franz diffusion cell prior to drug release studies. However, most of the researchers focus on experimental factors such as membrane type and less attention is given to the factors related to the Franz cell apparatus. Therefore, Ng (2007) undertook a detailed study of validation of Franz cell experiment focusing on the apparatus related factors. She identified diffusion cell dimensions, stirring speed, choice of stirring bar dimension and temperature regulation as the critical experimental factors producing large CVs. The CVs were significantly reduced from 26% to 4% by performing simple validation steps such as physical measurement, visual observations and temperature regulation. She also compared performance of synthetic membranes. Nevertheless, all these studies were performed using OFAT approach involving enormous amount of resources and time and did not reveal any interactions between the factors.

Franz cells used in the present drug release studies (PermGear) were different from the tailor made Franz cells used by Ng. (2007). Therefore, additional factors such as sampling site and the need for premixing of the dissolution medium (Chapter VIII) were also investigated in addition to the factors studied by Ng. (2007) to capture effect of each factors. Furthermore, present study was carried out using DoE to

reduce cost, save time and to investigate interactions between factors (if any).

Once the number of experimental factors and their levels are selected, the researcher needs to choose an appropriate experimental design. Different statistical models include factorial design, the Taguchi model, the Box Behenken design (BBD) or the central composite design (CCD). The number of variables determines the selection of model. The Taguchi model, the BBD and the CCD are used to investigate one factor with multiple levels. The factorial design model is used to investigate more than one factor at multiple levels.

In the present work validation of Franz cell experiments (Chapter VIII) is conducted by DoE using more than one experimental factor (six), each with two levels and the factorial design model was used. For this reason the factorial design is discussed here in detail with an example of three experimental factors (A, B and C) each with two levels (represented by minus (-) and plus (+) signs respectively). The factors and levels are entered into the DoE software (Table 2.1).

Table 2.1: Factorial design consisting of three experimental factors (A, B, and C) at two discrete levels (represented by signs plus (+) and minus (-) respectively).

Factor	Level 1	Level 2
A	-	+
B	-	+
C	-	+

On the basis of the data entered, DoE first identifies all possible factors and the interactions between the factors using the formula 2^K (basis for the OFAT approach), where 2 (base) is the number of levels and K (power) is the number of factors. Therefore, the formula for the above example containing 3 factors at 2 levels will be 2^3 or (2x2x2) = 8 experiments (Table 2.2).

Table 2.2: A typical example of number of experiments to be performed using one factor at a time approach on the basis of 3 factors (A, B and C) each at 2 levels.

	Factors A	Factors B	Factors C
Experiment 1	A-	B-	C-
Experiment 2	A-	B-	C+
Experiment 3	A-	B+	C+
Experiment 4	A-	B+	C-
Experiment 5	A+	B-	C+
Experiment 6	A+	B+	C-
Experiment 7	A+	B-	C-
Experiment 8	A+	B+	C+

Next, DoE generates a matrix of minimum number of experiments (Table 2.3) needed to obtain the same information as that of OFAT approach in addition to studying the interactions between the factors by significantly reducing the experimentation time.

Table 2.3: A typical matrix of experiments generated by the DoE on the basis of 3 factors (A, B and C) each at 2 levels to study the influence of each factor and the interactions between the factors.

	Factor A	Factor B	Factor C
Experiment 1	A+	B+	C+
Experiment 2	A-	B-	C-
Experiment 3	A+	B+	C-
Experiment 4	A-	B-	C+

The real experiments are then performed according to the matrix generated by the DoE. In this case, using Factorial design with minimum experimental runs resolution 5 (Minimum Run Res 5) without centre points and the results are analysed by the software using appropriate statistical model (ANOVA), selected by the DoE based on the significance level determined by probability (p) value <0.05. Based on the

significance level of p value (<0.05) in analysis of variance (ANOVA) the DoE also categorises factors into significant and non-significant. The non-significant factors are excluded by backward elimination keeping alpha (smallest possible significant effect produced by a factor either alone or in combination with other factors) to a minimum value (0.1). After backward elimination, the model is re–fitted with only significant factors and appropriateness of the model is verified based on the goodness–of–fit statistical criteria using Box Cox Plot (Fig. 2.18), which determines the pattern of data distribution. The lambda (λ- a transformation parameter) is plotted on the X-axis against the residual sum of square (correlation coefficient) on the Y-axis. When the λ value is equal or closer to the best λ value predicted by the DoE (1.5 in the above example) at the corresponding lowest residual sum of square values (-1.15 in the above example) then the data is considered as normally distributed and shows a strong power of the model. The model passes goodness-of-fit criteria and no power transformation is required. However, an increase in the residual sum of square may cause a change in the λ value leading to abnormal distribution and the data needs to be transformed to obtain normal distribution (Box *et al.,* 1978; Khuri and Cornell, 1987; Derringer, 1994; Vaughn, 2007).
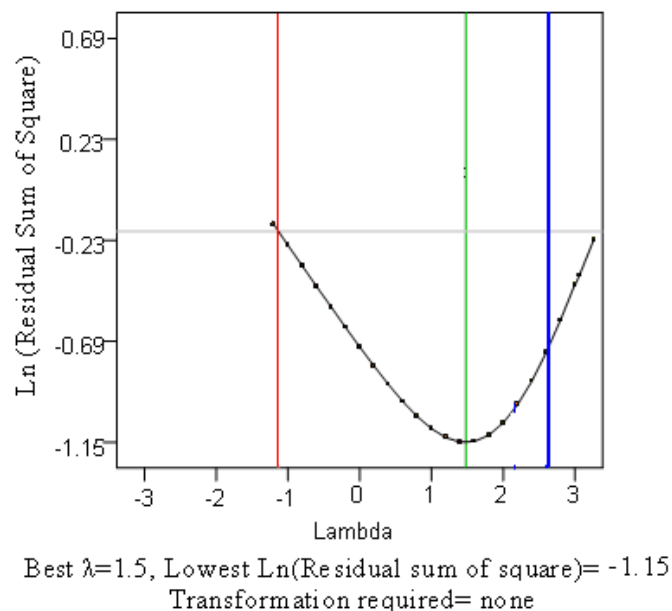
Figure 2.18: A typical Box-Cox Plot evaluating power of the model by comparing Lambda (parameter for transformation) with residual sum of square.

Next, the Pareto chart (Fig. 2.19) explains influence of each factor on the experimental outcome (t-value of effect). The factors may have a positive, negative, combinational or no effect on overall results and are distinguished by colour *i.e.* orange and blue colours representing positive and negative effects respectively (Fig. 2.19). The factors showing t-value above the Bonferroni limit (red horizontal line-7.2456) (Significance level $P<0.001$) are considered as critical factors.
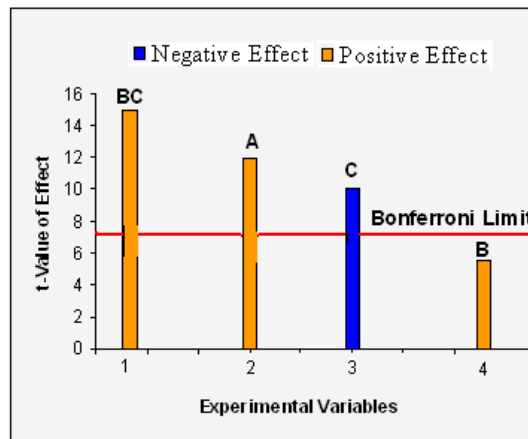
Figure 2.19: A typical Pareto chart showing influence of the experimental factors and their combinations on the t-value of effects.

Finally, the 3-Dimensional cube plot (Fig. 2.20) reveals influence of each factor and the interactions between factors on the overall outcome. The DoE predicts expected outcome using critical factors, generating a typical set of experiment. This set of experiment employing critical factors is then performed to confirm the predicted outcome.
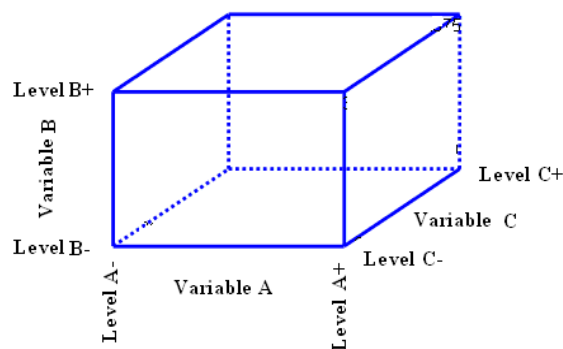
Figure 2.20: Typical 3-dimensional Cube plot template showing interactions of variables A, B and C each at two levels (+) and (-).

CHAPTER III

PREPARATION AND ANALYSES OF MAGNESIUM STEARATE AND ITS HYDRATES

3.1 Introduction

As discussed earlier (Chapter I), commercial magnesium stearate is a homologous mixture of palmitic and stearic acid and depending on the moisture content, available as either pseudopolymorphic crystalline solvate *i.e.* mixture of mono– and dihydrate, or di– and trihydrate (rarely as a single phase hydrate) or as an anhydrate. The formation of various pseudopolymorphic forms cause changes in physicochemical properties, which have been shown to affect the properties of solid formulations prepared with magnesium stearate (MgSt) and may also affect the appearance and stability of lipogels. Therefore, this chapter explores the preparation of pure homologue MgSt and also investigates conversion of commercial and prepared (pure homologue) MgSt to various hydrates by exposing them to various relative humidity levels at ambient temperature.

3.2 Aims of the chapter

The present work describes the preparation of anhydrous pure homologue (C_{18}) magnesium stearate ($pMgSt_A$) from stearic acid (nominal purity 95% C_{18}) and magnesium oxide and the preparation of various hydrates of $pMgSt_A$ by moisture treatment. In addition, anhydrous commercial magnesium stearate (of unknown homologue composition) was obtained by drying the Batch 3 at high temperature. The overall objectives include:

1. preparation of anhydrous magnesium stearate from "pure" stearic acid (nominally 95% pure C_{18}) and magnesium oxide using a fusion method,

2. To form anhydrous commercial magnesium stearate ($cMgSt_A$) by drying commercial MgSt as received (cMgSt) at elevated temperatures and 0% humidity,

3. Investigation of the homologue composition of both the prepared pure MgSt and commercial MgSt using gas chromatography,

4. to investigate the polymorphism of the different magnesium stearates (prepared and commercial), including preparation of pseudopolymorphs (hydrates) by exposing them to various relative humidities *i.e.* 70%, 95% and 100%, using either saturated salt solutions or a stability chamber.

5. characterisation of the polymorphs and hydrates of prepared and commercial magnesium stearate using polarised light microscopy, electron microscopy, hot stage microscopy, DSC, TGA, FTIR, GC and XRD.

3.3 Methods

3.3.1 Gas Chromatography

A Clarus® 500 (PerkinElmer, Inc. USA) gas chromatograph was used to analyse fatty acid composition of the anhydrous prepared magnesium stearate, $pMgSt_A$ (of nominal 95% C_{18} Purity) and the commercial magnesium stearate (cMgSt) of unknown homologue composition. A 25m x 0.32mm, SE–52 column was used. Helium was purged at a flow rate of 1.4mL/min, using 1/50 split. The temperature of the injector and detector was 280^oC. In contrast, the oven temperature was 210^oC.

Samples were prepared by dissolving 25mg of MgSt in 40mL of glacial acetic acid in a conical flask, stored at 55^oC in a hot air oven overnight. 50mL of distilled water was then added, and the mixture extracted with 20mL of chloroform in a separating funnel.

3.3.2 Preparation of anhydrous pure homologue magnesium stearate

Anhydrous pure homologue magnesium stearate (100 g) was prepared using two (2) moles of pure homologue (nominal purity 95% C_{18}) stearic acid (93.5g) and one mole of magnesium oxide (6.5g). The ingredients were weighed separately in the weighing boats and transferred to 500mL round bottom flask. The flask was fixed to a rotary evaporator (IKARV05 Basic, Germany) connected to the vacuum and stirrer.

The flask was then immersed into the oil bath of 130ºC and stirred at a rate of 70rpm/min for four (4) hours. After heating, the preparation was left to cool inside the oil bath naturally (~0.1°C–0.2°C/min) to room temperature under vacuum. After cooling, the vacuum was removed and the flask taken out from the rotary evaporator, the pure homologue MgSt anhydrous (pMgSt$_A$), removed and immediately ground in the mortar, passed through a series of sieves of seven different mesh sizes (ranging from 0.5mm to 2mm) to obtain particle size of ~5µm. It was then transferred to a 100g screw capped container, flushed with nitrogen for 10 minutes at a rate of 200mL/min, container capped and stored in the desiccator containing silica gel under vacuum.

3.3.3 Moisture treatment of magnesium stearate

3.3.3.1 Preparation of anhydrous commercial magnesium stearate

Anhydrous commercial magnesium stearate (cMgSt$_A$) was prepared by heating the commercial magnesium stearate (cMgSt) of unknown homologue composition under vacuum. The cMgSt was weighed (93.5g) in a 500mL round bottom flask, and heated using the same method as in the section 3.3.2, except that the sample was heated at 110°C overnight instead of 4 hours. After cooling, the flask was removed from the oil bath, the sample removed (cMgSt$_A$), ground in a mortar and stored in the desiccator containing silica gel under vacuum.

3.3.3.2 Preparation of hydrates of magnesium stearate

cMgSt, cMgSt$_A$, and pMgSt$_A$ were treated at different relative humidities to obtain various hydrates as shown in Fig.3.1 using (i) saturated salt solutions/distilled water and (ii) a stability chamber.

(i). preparation of hydrates using a saturated solution/water

A saturated salt solution of potassium sulfate (K$_2$SO$_4$) in distilled water was used to achieve a relative humidity of 95% at ambient temperature (30°C) using the method described by Nyqvist (1983). Potassium sulfate (200mg) was weighed and

transferred to a 250mL conical flask containing 200mL distilled water which was preheated to 60°C. The conical flask was then transferred to a shaker, and agitated at ambient temperature (~28°C) for 24 hours. The solution was then filtered through a 0.22μm disc filter. The filtrate (saturated salt solution) was collected and stored in the desiccator prior to use. The saturated salt solutions of K_2SO_4 produced 95% relative humidity (RH) at 28°C.

$cMgSt_A$, $cMgSt$ and $pMgSt_A$ were spread thinly in the glass Petri dishes, which were placed in the desiccators containing saturated salt solutions of K_2SO_4 (95% RH) to obtain hydrated mixed $cMgSt_{AH}$, $cMgSt_H$ and pure homologues $pMgSt_H$ respectively. The desiccators were covered with the lids and left undisturbed for at least 6 weeks.

To achieve 100% RH, a separate experiment was performed using desiccators containing distilled water instead of saturated salt solutions as described by Nyqvist (1983). The Petri dishes containing $cMgSt$, $cMgSt_A$ and $pMgSt_A$ were placed in the desiccators containing distilled water and left for at least 6 weeks to allow maximum moisture sorption and labelled as $cMgSt_H$, $cMgSt_{AH}$ and $pMgSt_H$ at 100% RH.
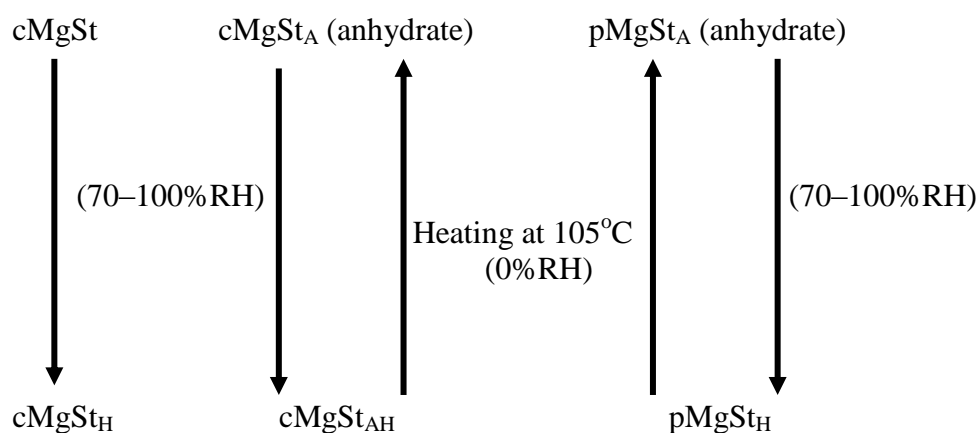
Figure 3.1: Schematic diagram showing effect of varying the relative humidity and temperature on the hydration state of magnesium stearate.

(ii) Preparation of hydrates of magnesium stearate using a stability chamber

A Stability Chamber (Fischer Scientific, Germany) was used to obtain 70% and 95% RH. $cMgSt_A$, $cMgSt$ and $pMgSt_A$ were spread thinly on the metal trays and placed in the stability chamber to obtain $_CMgSt_{AH}$, $_CMgSt_H$ and $pMgSt_H$ respectively. Using

the key–board on the chamber door, the RH and temperature were selected to be either 70% or 95% and 30°C respectively and samples left undisturbed for 6 weeks. A maximum of 95% RH can be achieved using the stability chamber.

3.3.4 Characterisation of magnesium stearate

3.3.4.1 Appearance

All hydrates prepared using either the Stability chamber or saturated salt solutions at either 95% or 100% RH appeared similar as white powders and showed no differences in texture. Therefore, $pMgSt_H$, $cMgSt_{AH}$ and $cMgSt_H$, hydrated at 100% RH using saturated salt solutions were chosen to be used for further work (*c.f.* results 3.6.3.2).

3.3.4.2 Polarised light microscopy

A Leica DMLS compound microscope (Histocentre, Malaysia) was used to study the microstructure of anhydrates and various hydrates of MgSt between crossed polars *i.e.* cMgSt, $cMgSt_A$, $cMgSt_{AH,}$ $cMgSt_H$, $pMgSt_A$ and $pMgSt_H$ and liquid paraffin. The same method of sample preparation and analysis was used as described in section 2.2.2.1. Slides were placed between crossed polars and studied at various magnifications (x 5, x 10, x 20 and x 40). Digital photomicrographs were taken using the Image Pro Express software.

3.3.4.3 Hot stage microscopy

A TMS 91 hot stage (Linkam Scientific Instruments, UK) attached to the Polyvar microscope was also used to determine the melting point of the commercial magnesium stearate (cMgSt). A thin smear of sample was sandwiched between two 16 mm circular glass cover–slips. The stage was heated slowly from 25°C to 170°C at a rate of 5°C/minute and changes in the microstructure were observed at appropriate magnification (x 20). The melting point was recorded as the temperature between which the sample started to flow and the temperature at which the structure completely disappeared. Thermal changes at various temperatures were recorded and photographed at 30°C, 90°C, 120°C and 150°C using the Leutron computer software.

However, only photographs below and above melting points are presented in the results.

In addition, SMP1 melting point apparatus (Stuart Scientific, UK) was also used to investigate the melting points of pure homologue stearic acid, magnesium oxide, cMgSt, cMgSt$_A$, cMgSt$_H$, pMgSt$_A$ and pMgSt$_H$.

3.3.4.4 Scanning Electron Microscopy (SEM)

A Leo 1450VP electron Microscope (Oxford Instruments, UK) was used to study the structures of cMgSt$_H$ and pMgSt$_H$. A small sample of each powder of magnesium stearate was coated with gold for 2−3 minutes, placed on the stub of the microscope and studied under high vacuum. Each sample was studied at powers between x 15 and x 5000 and photographed at appropriate magnifications.

3.3.4.5 Differential Scanning Calorimetry (DSC)

A DSC 822^e (Mettler Toledo, Leicester, UK) with the sample robot, was used for the analysis of samples at the University of Strathclyde and a DSC 823^e (Mettler Toledo, Switzerland) with single sample holder (no robot) was used at the IMU. The materials used in the preparation of MgSt namely stearic acid (pure homologue-C$_{18}$) and magnesium oxide were examined (DSC 823e), as was liquid paraffin (DSC 822e) which is used to prepare lipogels (Chapter IV). The three batches (B1, B2, B3, Section 2.1.1) of commercial magnesium stearate (cMgSt$_{B1,B2,B3}$) were examined (DSC 822e) in addition to various hydrates of batch 3 magnesium stearate (cMgSt$_H$, cMgSt$_{AH}$ and pMgSt$_H$) and anhydrous materials (cMgSt$_A$ and pMgSt$_A$) were characterised (DSC 823e). Approximately 1.5−10mg of each sample was carefully weighed by difference in 40µL aluminium DSC pans, the pans were sealed and placed in the machine. A standard heating cycle of 25°C−150°C at a rate of 10°C/min was chosen to observe thermal changes in the samples. The results were plotted together after normalisation to eliminate weight bias due to the weight differences of the samples.

Additional experiments were performed with commercial magnesium stearate (cMgSt) using open DSC pans to dry the samples before the actual DSC run (DSC 822) as follows:

Drying the samples in situ by heating the pans without lids under nitrogen environment (i) to $105^{o}C$ @ $2^{o}C$, holding for an hour at $105^{o}C$ cooling to $25^{o}C$ @ $5^{o}C$ and (ii) heating pans without lids at $40^{o}C$, holding for 2 hours at $40^{o}C$, cooling to $25^{o}C$. The DSC runs were then performed after this drying procedure using a heating cycle of $25^{o}C–140^{o}C$ at a rate of $10^{o}C/min$.

Sealed pans were subjected to the same procedure as the open pans (annealed as a control), and then DSC data obtained using a heating cycle of $25^{o}C–200^{o}C$ at a rate of $10^{o}C/min$ (the higher temperature to capture any thermal events above $140\,^{o}C$).

3.3.4.6 Thermogravimetric analysis (TGA)

A TGA/SDTA851[e] (Mettler Toledo, Leicester, UK Switzerland) with sample robot was used at the University of Strathclyde to examine weight loss from the three batches of mixed homologues of MgSt ($MgSt_{B1,B2,B3}$). In addition, the same machine (Mettler Toledo, Switzerland) with single sample holder was used at SIRIM, Malaysia for the analysis of $cMgSt_A$, $cMgSt_H$, $pMgSt_A$ and $pMgSt_H$. The 70µL aluminium crucibles were placed in the machine and an approximately 25−45mg of each sample was carefully weighed prior to heating. A standard heating cycle of $30^{o}C–150^{o}C$ at a rate of $10^{o}C/min$ was selected to achieve optimal weight loss. The experiments were conducted under dry nitrogen. The results were plotted together after normalisation to eliminate weight bias due to the weight differences of the samples.

3.3.4.7 Fourier Transformed Infra−red (FTIR) spectroscopy

The FTIR−8400S (Shimadzu, France) was used to obtain the infra−red spectra of the materials used in the preparation of MgSt namely stearic acid and magnesium oxide. In addition, the three batches of mixed homologues of MgSt ($cMgSt_{B1,B2,B3}$), $cMgSt_H$, and $pMgSt_A$ were also examined. The method of sample preparation and

analytical parameters for all samples was adopted from Coates (2000) as follows: Each sample was ground with dry potassium bromide (KBr) in a small mortar, and compressed to a transparent disc, using a hand press for 10 minutes. A (16:1) ratio of KBr and magnesium stearate was used to achieve best resolution and maximum transmission. Samples were scanned for three (3) minutes from 4000–600 cm^{-1}. FTIR data were analysed using IR Solution software.

3.3.4.8 X–ray diffraction (XRD)

A powder X–ray diffractometer (Bruker 8 Advances, Germany) was used for the analysis of cMgSt$_H$, cMgSt$_A$, cMgSt$_{AH}$, pMgSt$_A$ and pMgSt$_H$. The method was adopted from Koivisto et $al.$ (2004). The samples were irradiated with X–rays from a copper target using the following conditions and parameters: Filter Ni, Generator 40kV, voltage 40kV, current 20mA, λ 0.15410nm using a Soller slit. The samples were continuously scanned from 2.3^o–40° at a rate of 2.5^o/sec with a step of 0.025s^{-1}. The XRD spectra were analysed using Diffract Plus software. CuK$_{\alpha 1}$ values were used for the analysis of each peak.

3.5 Statistical analysis

Pearson's correlation coefficient test was employed using Statistics Package for Social Sciences (SPSS) to assess the correlation between the DSC (integration) and TGA (weight loss) data of various samples. A p value <0.05 was considered as significant. Interactions between DSC and TGA data were evaluated using design of experiment (DX 7.1®).

3.6. Results

3.6.1 Gas Chromatography (GC)

Figure 3.2 shows the GC chromatograms of commercial (batch 3) and the prepared MgSt. Both samples showed two peaks each at 13.335 and 14.703 seconds of varying area under the curve (AUC). The AUC for the peaks of (cMgSt$_A$) appeared to be rather similar (Fig. 3.2a). In contrast, pure homologue (pMgSt$_A$) showed

significantly different AUC for each peak (Fig. 3.2b). When compared with the standard fatty acids, the first and the second peaks appeared to be due to the palmitic (C16:0) and stearic acids (C18:0) respectively. The commercial magnesium stearate was composed of mixed homologue, showing approximately similar concentrations of both fatty acids (50% each) whereas the prepared magnesium stearate confirmed the manufacturer's composition *i.e.* that stearic acid represented the major homologue (95%) and with less than(5%) palmitic acid.
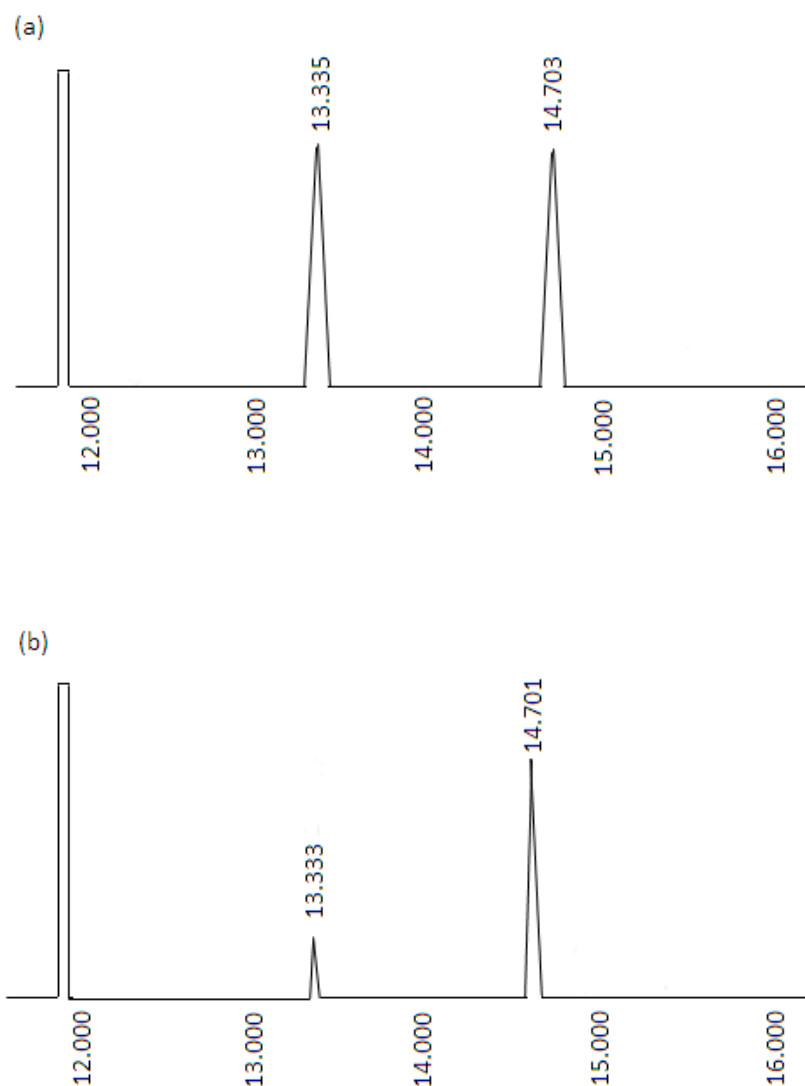
Figure 3.2: GC chromatograms of (a) anhydrous commercial magnesium stearate (cMgSt$_A$) and (b) anhydrous magnesium stearate prepared from stearic acid and magnesium oxide (pMgSt$_A$).

3.6.2 Visual appearance of anhydrous pure homologue magnesium stearate

Anhydrous pure homologue MgSt (pMgSt$_A$) was prepared by heating magnesium oxide and stearic acid (pure homologue) under vacuum. Upon cooling, the clear solution slowly changed to solid (off white in colour), at a temperature range between 80–90°C. The solid was a fine white powder (pMgSt$_A$) after grinding in the mortar at room temperature.

3.6.3 Visual appearance of moisture treated magnesium stearate

3.6.3.1 Visual appearance of anhydrous commercial mixed homologue magnesium stearate

Anhydrous mixed homologue magnesium stearate (cMgSt$_A$) was obtained by heating cMgSt at 110°C overnight and cooling naturally at (~0.1^{o}C–0.2^{o}C/min) to room temperature with continuous stirring under vacuum. This resulted in a total weight loss of 6g (assumed to be water). A fine white powder of anhydrous mixed homologue (cMgSt$_A$) was produced by grinding.

3.6.3.2 Visual appearance of hydrates of magnesium stearate

cMgSt$_A$, cMgSt and pMgSt$_A$ were exposed to 70%, 95% and 100% RH for 6 weeks either using saturated salt solutions or a stability chamber to obtain hydrates of mixed homologues (cMgSt$_{AH}$ and cMgSt$_H$) and pure homologue (pMgSt$_H$).

The hydrates prepared from a specific homologue (for example cMgSt) using either the Stability chamber or saturated salt solutions at a specific RH (either 70% or 95%) appeared similar as white powder and showed no change in colour or texture.

However, hydrate of pure homologue (pMgSt$_H$) obtained using saturated salt solutions at 100% RH appeared to be wet compared to the cMgSt$_H$ when touched with the glass rod. Therefore, pMgSt$_H$, cMgSt$_{AH}$ and cMgSt$_H$ obtained using saturated salt solutions at 100% RH were used for characterisation or magnesium stearate.

3.6.4 Characterisation of magnesium stearate

3.6.4.1 Appearance

All samples of magnesium stearate (pure and mixed homologue) whether anhydrous or hydrates appeared as white powders and showed no differences in texture.

3.6.4.2 Polarised light microscopy

Figure 3.3 shows the photomicrographs of the $cMgSt_A$, $cMgSt_H$, $pMgSt_A$ and $pMgSt_H$. All samples showed characteristic anisotropic structures with clusters of small irregular shaped crystals against the dark background under polarised light. There was generally more structure in the hydrated samples compared to the anhydrous ones. In addition, there was more structure in the hydrate of pure homologue ($pMgSt_H$) compared to the mixed homologue ($cMgSt_H$) at the same hydration state. $pMgSt_A$ also showed more structure than $cMgSt_A$ (Fig. 3.3 a & 3.3c). All samples showed two different types of crystals *i.e.* large plate–like crystals and small acicular structures. However, the crystals of $pMgSt_H$ appeared to be bigger compared to the crystals of $cMgSt_H$ (Fig. 3.3 c & 3.3d).

3.6.4.3 Hot stage microscopy

The melting of magnesium stearate was determined by the hot stage microscopy and melting point apparatus. Figure 3.4 shows typical photomicrographs of magnesium stearate below the melting point (Fig. 3.4a) and above the melting point (Fig.3.4b). There were no obvious thermal changes in the crystals of magnesium stearate until $135^{o}C$ (Fig. 3.4a). The irregular small crystals started melting at $140^{o}C$ and completed at $150^{o}C$ (Fig. 3.4b).

Melting of all samples in the melting point apparatus showed different melting behaviours. Stearic acid and the $pMgSt_A$ showed sharp melting points at $70^{o}C$ and $85^{o}C$ respectively. In contrast, $cMgSt_A$, $cMgSt_{AH}$ and $cMgSt_H$ showed a similar range of melting point between $120–170^{o}C$. The first few crystals in the material started melting at $\sim120^{o}C$ but no additional change was observed up to $145^{o}C$. Most of the

crystals melted between 145–160°C. However, the complete melting was observed at ~170°C. Magnesium oxide, a raw material in the preparation of magnesium stearate did not show melting up to 350°C (the maximum limit of the thermometer used in the malting point apparatus).
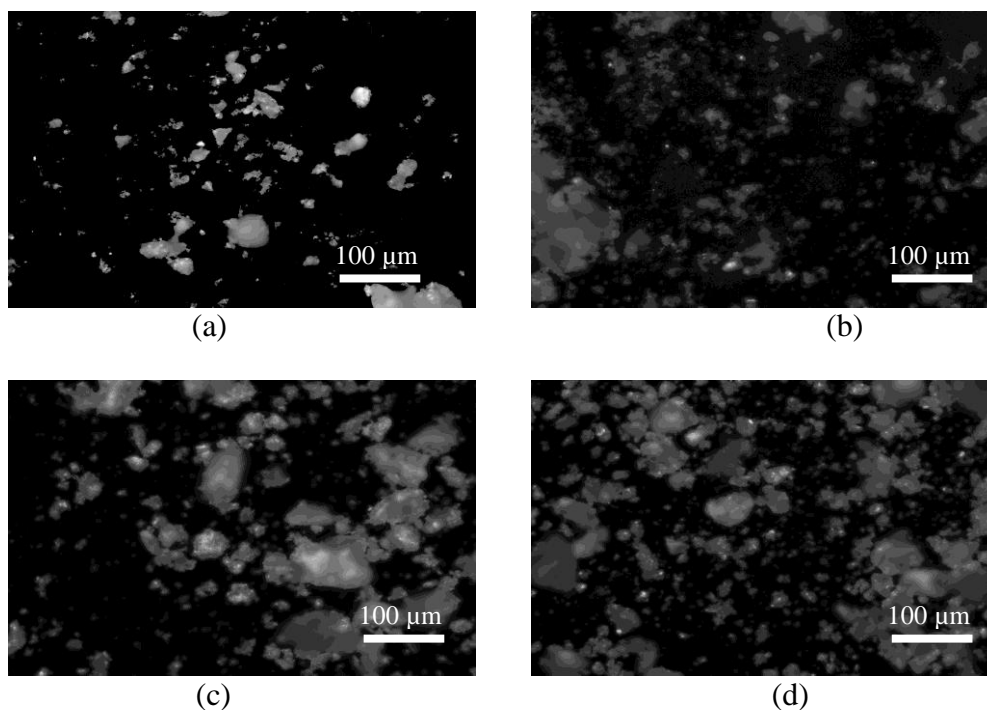
Figure 3.3: Photomicrographs of magnesium stearate (a) anhydrous mixed homologue (cMgSt$_A$) (b) hydrated mixed homologue (cMgSt$_H$) (c) anhydrous pure homologue (pMgSt$_A$), and (d) hydrated pure homologue (pMgSt$_H$). (Scale: 1cm= 100µm).
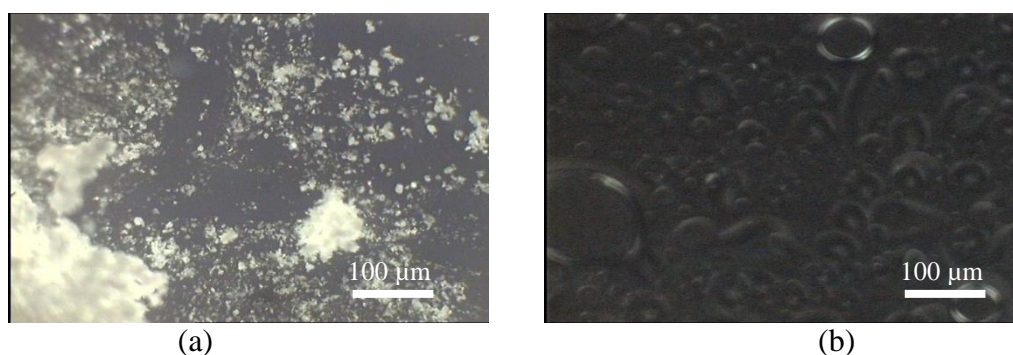
Figure 3.4: Typical hot stage photomicrographs of the mixed homologue cMgSt (a) below melting point (135°C) and (b) above the melting point (150°C). (Scale: 1cm= 100µm).

3.6.4.4 Scanning Electron Microscopy (SEM) of MgSt hydrates

Figure 3.5 shows the electron photomicrographs of hydrates of mixed and pure homologues of MgSt. cMgSt$_H$ showed only one type of large plate like crystals (Fig. 3.5a). The crystals appeared in the form of scattered clusters. In contrast, pMgSt$_H$ showed two different types of crystals *i.e.* small acicular crystals in addition to the very large plate like crystals similar to the one observed in the mixed homologue samples (Fig. 3.5b). The plate–like crystals observed in the pMgSt$_H$ were much larger than the crystals of mixed homologue and appeared in the form of compact clusters. Furthermore, small particles also called "kinks" were observed on the top of large plate like crystals only in the pMgSt$_H$.

(a)   (b)
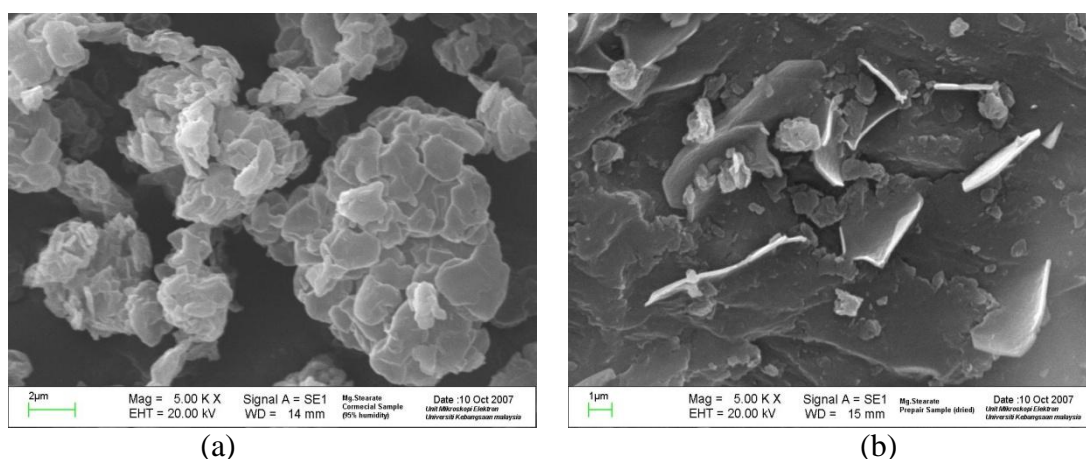
Figure 3.5: Electron photomicrographs of hydrates of (a) mixed homologue and (b) pure homologue. Both photomicrographs were taken at magnification x 5000.

3.6.4.5 Differential Scanning Calorimetry (DSC)

The raw materials, stearic acid (DSC 823^e) and liquid paraffin (DSC 822^e) were examined using standard heating cycle of 25–150°C at a rate of 10°C/min. Figure 3.6 shows the DSC thermogram of stearic acid (pure homologue). A broad endotherm was observed peaking at ~72°C with high enthalpy value of -224.7J/g (Table 3.1). No other thermal event was observed. In contrast, liquid paraffin showed a straight line as no thermal event occurred (Fig. 3.7).
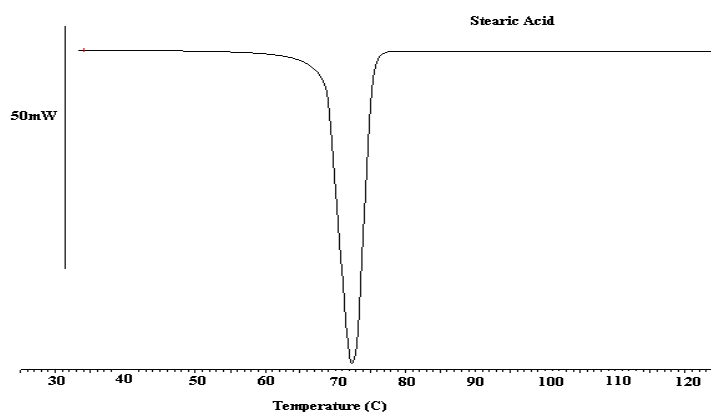
Figure 3.6: DSC (823^e) Thermogram of stearic acid (pure homologue) obtained using a heating cycle of 25–150°C@10°C/min.
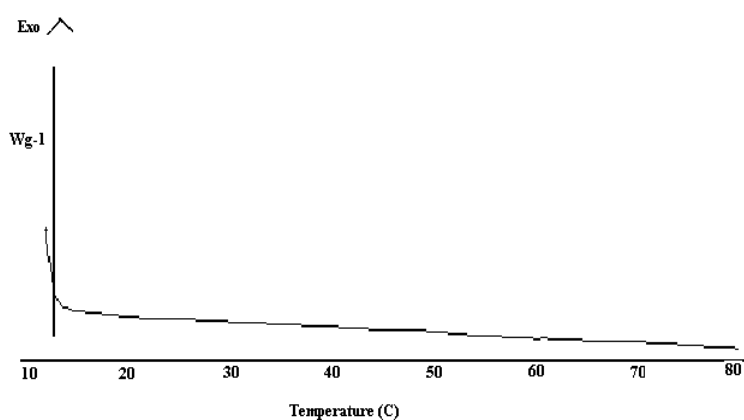
Figure 3.7: DSC (822^e) Thermogram of the liquid paraffin obtained using a heating cycle of 25–150°C@10°C/min.

Table 3.1: Thermal properties (peak temperatures (T^{o}C) and enthalpy changes (ΔH)) of various samples determined by DSC.

Sample Type	T1 (^{o}C)	ΔH1 (J/g)	T2 (^{o}C)	ΔH2 (J/g)
MgSt Batch 1	89.8	-16.0	119.3	-102.9
MgSt Batch 2	63.9	-10.5	116.0	-88.2
cMgSt	104.3	-26.2	121.4	-114.8
cMgSt$_A$	120.0	-9.8	130.0	-48.1
cMgSt$_H$	74.9	-47.7	115.1	-243.5
cMgSt$_{AH}$	66.7	-40.6	96.7	-891.9
pMgSt$_A$	66.5	-1.2	84.3	-136.5
pMgSt$_H$	66.9	-12.8	91.5	-206.9
Stearic acid	72.0	-224.7		

Figure 3.8 shows the DSC spectra of the three batches of magnesium stearate. The thermograms of the three batches were different from each other, each showing more than one endotherm peaking at different temperatures (Fig. 3.8).

Mixed homologue batch 3 (cMgSt$_{B3}$) showed two distinct, high temperature broad endotherms peaking at 104.3^{o}C (enthalpy -26.2J/g) and 121.4^{o}C (-114.8J/g) (Fig. 3.8) and a small thermal event just before the first endotherm. In contrast, batches 1 (cMgSt$_{B1}$) and 2 (cMgSt$_{B2}$) showed several endotherms each of significantly different enthalpy values (Table 3.1). Batch 2 showed three broad endotherms peaking at 63.9^{o}C, 100°C and 116°C (Fig. 3.8). The low temperature, very broad endotherm (63.9^{o}C) was not seen in any other batch. The second endotherm was a broad shoulder on the third extremely broad endotherm.

The third endotherm may or may not be the same as the distinct second endotherm of the batch 3. In contrast, batch 1 showed two broad endotherms peaking at 89.8^{o}C and 119.3^{o}C (Fig. 3.8). The low temperature, broad endotherm with a shoulder at 82°C was not seen in any other batch. There was an extremely broad, high temperature endotherm peaking at 119.3^{o}C, which may or may not be the same as the high temperature endotherms seen in batches 2 and 3.
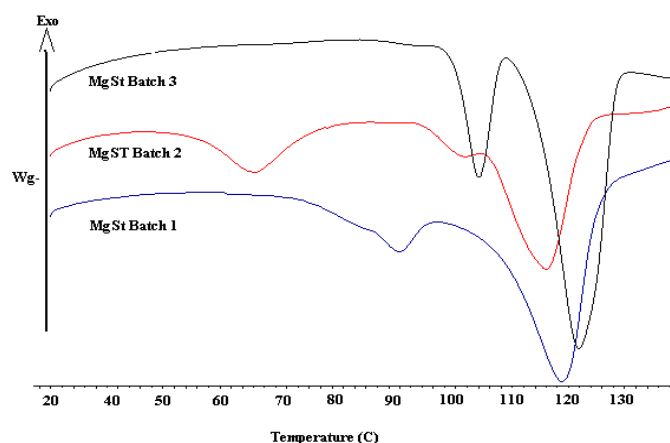
Figure 3.8: DSC (822^e) Thermograms of the three batches of mixed homologues of magnesium stearate using a heating cycle of 25−140°C at a rate of 10°C/min.

cMgSt samples were dried *in situ* on the DSC with open pans over nitrogen at different temperatures before testing showed different DSC data from undried

cMgSt, and also from each other (Fig. 3.9).

Mixed homologue MgSt dried at 105°C for an hour in an open pan (cMgSt$_A$) showed two high temperature broad endotherms (Fig. 3.9). The first small endotherm peaked at 122°C whereas the 2nd broad endotherm peaked at 131°C. There was no water peak. In contrast, cMgSt dried at 40°C for 2 hours showed four peaks (Fig 3.9). The 1st small endotherm peaked at 83°C. The 2nd extremely broad endotherm, due to water loss peaked at 100°C. The 3rd and 4th endotherms were similar to the ones seen in the sample dried at 105°C (122 and 131°C) but peaked at slightly lower temperatures $i.e.$ 120°C and 128°C respectively (Fig. 3.9).

Figure 3.10 shows DSC data for a control after annealing in sealed pan heated to the higher temperature of 200°C (rather than the usual 140°C), to confirm that there were no further thermal events. The sample analysed in the sealed pans using a heating cycle of 20°C–200°C at a rate of 10°C/min showed a very small high temperature endotherm at 150°C which may be related to the melting of cMgSt in addition to the two endotherms similar to the one seen in cMgSt, peaking at 100°C (due to water loss) and 122°C respectively (Fig. 3.10).
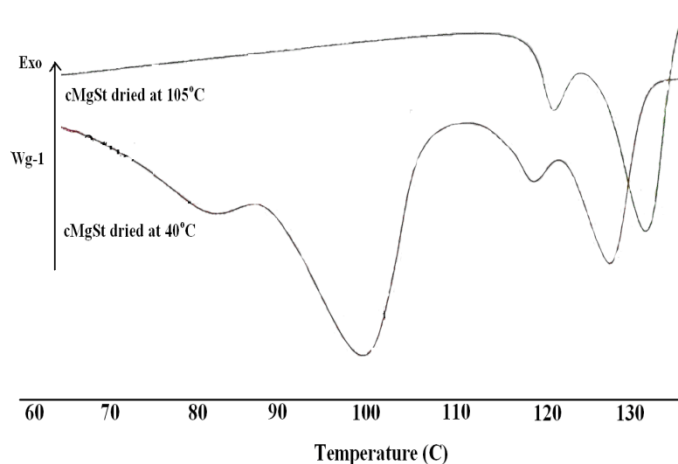
Figure 3.9: DSC (822^e) Thermograms of mixed homologues of MgSt dried at 105°C or 40°C in open pans, and cooled prior to DSC studies using a standard heating cycle of 25–140°C @10°C/min.
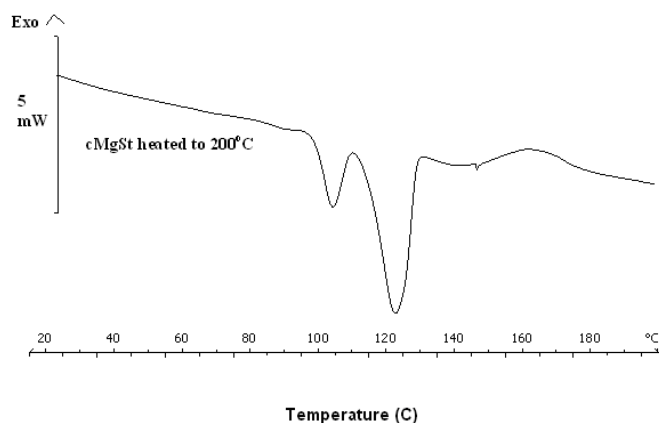
Figure 3.10: DSC (822^e) Thermogram of cMgSt investigated after annealing for its melting point using a heating cycle of 20–200°C@10°C/min.

Various hydrates of mixed homologue (cMgSt$_{AH}$, cMgSt$_H$) and pure homologue (pMgSt$_H$) in addition to the anhydrates of mixed and pure homologues (cMgSt$_A$ and pMgSt$_{A,}$) were also analysed (DSC 823^e) using a standard heating cycle of 25–150°C@10°C/min. Figure 3.11 shows the DSC spectra of the mixed and pure homologue magnesium stearate. The thermograms of all the samples were different from each other, each showing more than one endotherm peaking at different temperatures.

The pure homologue samples (pMgSt$_A$ and pMgSt$_H$) showed two distinct, broad endotherms peaking at relatively similar temperatures between 64.2^{o}C and 91.4^{o}C (Fig. 3.11a). pMgSt$_A$ showed a very small, low temperature endotherm peaking at 66.5^{o}C of negligible enthalpy (-1.2J/g). The second extremely broad endotherm was a doublet, peaking at 84.3^{o}C and 90.0^{o}C respectively with significantly high enthalpy (-136.5J/g). In contrast, pMgSt$_H$ showed a low temperature, relatively sharp endotherm peaking at ~66.9^{o}C (-12.8J/g) and an extremely broad endotherm (doublet) peaking at 84°C and 91.5^{o}C respectively with a shoulder at 105°C (Fig. 3.11a). There appeared to be a right shift of the second endotherm of pMgSt$_H$ with significantly higher enthalpy (-206.9J/g).

All mixed homologue samples (cMgSt$_A$, cMgSt$_{AH}$ and cMgSt$_H$) showed two distinct, broad endotherms peaking at different temperatures between 66.7^{o}C and 118.9^{o}C (Fig. 3.11b). cMgSt$_A$ showed two distinct, high temperature endotherms peaking

92

between 120°C and 130°C (Fig. 3.9). The first broad endotherm peaked at 120°C (-9.8J/g) whereas the second extremely broad endotherm peaked at 130.0°C (-48.1J/g). In contrast, cMgSt$_{AH}$ showed two distinct, extremely broad low temperature endotherms peaking at 66.7°C (-40.6J/g) and 96.7°C (-891.9J/g).

The pure and mixed homologue samples after moisture treatment showed an increase in the heat energy (enthalpy) with an increase in the moisture level (Table 3.1). However, increase in the enthalpy values of commercial samples varied with the samples. The commercial sample dried and then rehydrated at 100% RH (cMgSt$_{AH}$) showed marked increase in the total integration of the two endotherms (-931.9J/g) compared to the cMgSt$_H$ (-87.8J/g). These results suggest that the moisture treatment of the pure and mixed homologue MgSt produced hydrates, significantly different from each other with respect to their thermal behaviour.

(a)   (b)
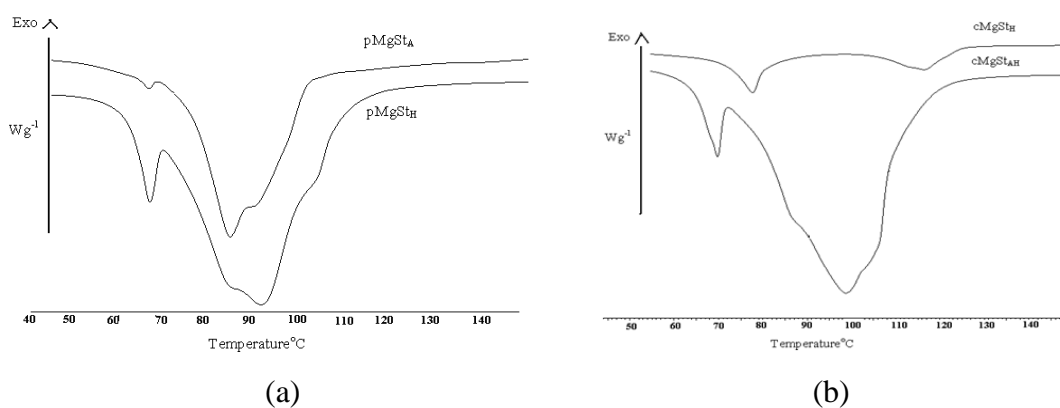
Figure 3.11: DSC (823^e) Thermograms of magnesium stearate obtained using a heating cycle of 25−150°C@10°C/min (a) anhydrous and hydrated pure homologue MgSt (pMgSt$_A$ and pMgSt$_H$) and (b) hydrates of mixed homologues (cMgSt$_{AH}$ and cMgSt$_H$).

3.6.4.6 Thermogravimetric analysis (TGA)

Commercial and prepared samples of magnesium stearate treated at various humidity levels were investigated by TGA for their weight loss.

Figures 3.12 and 3.13 show the TGA plots of the pure (pMgSt$_H$) and mixed homologue (cMgSt$_A$ and cMgSt$_H$) samples respectively. All samples showed varying amounts of weight loss ranging from 1.56%−6.69%, except pMgSt$_A$ which did not

show any weight loss as a straight line was observed (Fig. 3.12). Maximum weight loss (-6.69%) was observed in the pMgSt$_H$. In contrast, minimum weight (1.56%) was lost from the cMgSt$_A$ (Table 3.2).

The weight loss from each sample varied as the hydrate of pure homologue (pMgSt$_H$) showed a single step weight loss (Fig. 3.12) compared to the three step weight loss from the hydrate of mixed homologue (cMgSt$_H$) (Fig. 3.13b). In contrast, cMgSt$_A$ showed single step weight loss (Fig. 3.13a).
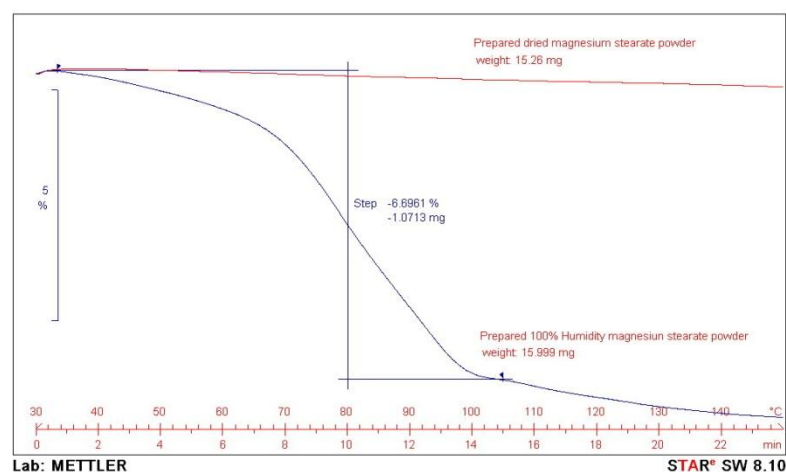
Figure 3.12: TGA plots of anhydrous and hydrated pure homologue magnesium stearate using a heating cycle of 30–150°C@10°C/min.

Table 3.2: TGA data showing weight loss from various samples of commercial and prepared MgSt using a heating cycle of 30–150°C@10°C/min.

Sample Type	Weight loss (mg)	Weight loss (%)
pMgSt$_A$	0.0	0.0
pMgSt$_H$	-1.0713	6.69
cMgSt$_A$	-0.0071	1.56
cMgSt$_H$	-0.5550	4.75
cMgSt$_{B1}$	-0.5995	4.54
cMgSt$_{B2}$	-0.4629	4.86
cMgSt$_{B3}$	-0.4278	4.14
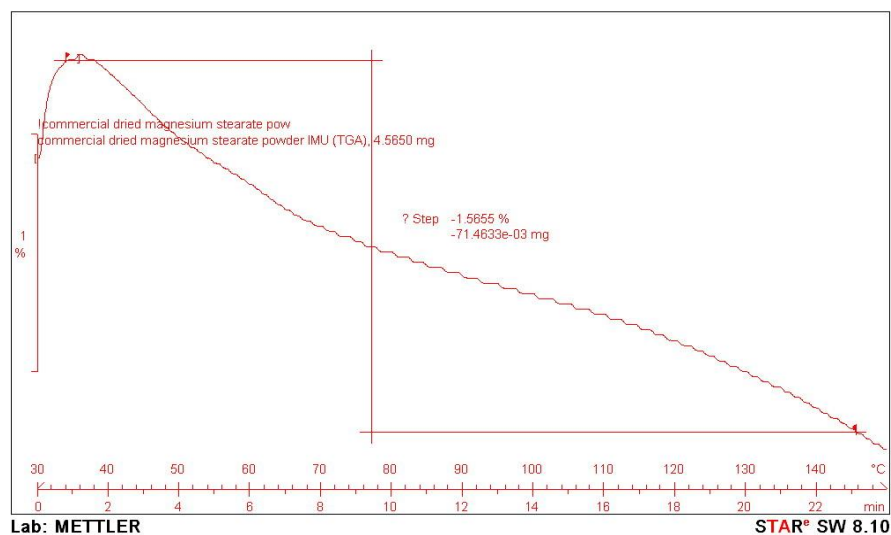
(a)
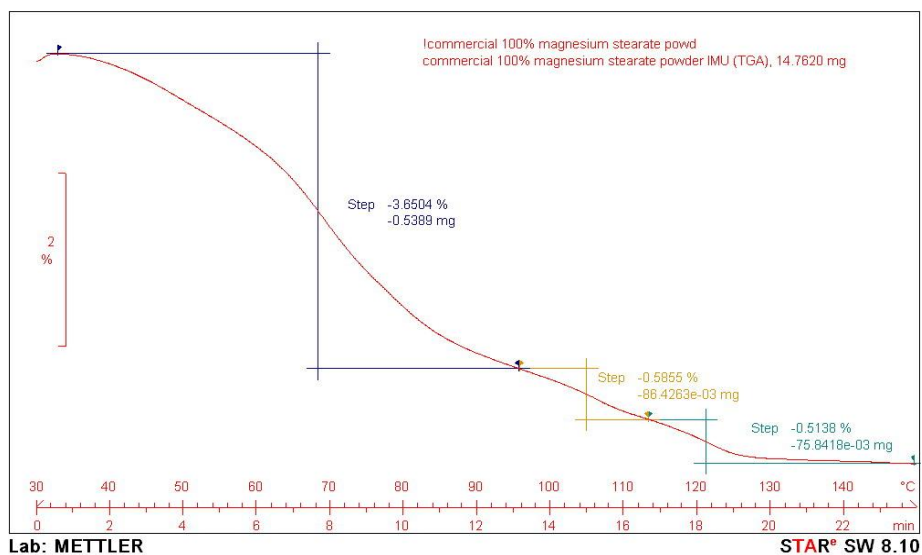
(b)

Figure 3.13: TGA plots of mixed homologue magnesium stearate (a) anhydrous (cMgSt$_A$) and (b) hydrated (cMgSt$_H$) using a heating cycle of 30–150°C@10°C/min.

Figure 3.14 shows the TGA plots of the three batches of mixed homologue magnesium stearate (cMgSt$_{B1, B2, B3}$). The three batches showed rather similar weight loss *i.e.* 4.54%, 4.86% and 4.14% respectively. In contrast, the liquid paraffin showed no weight loss.
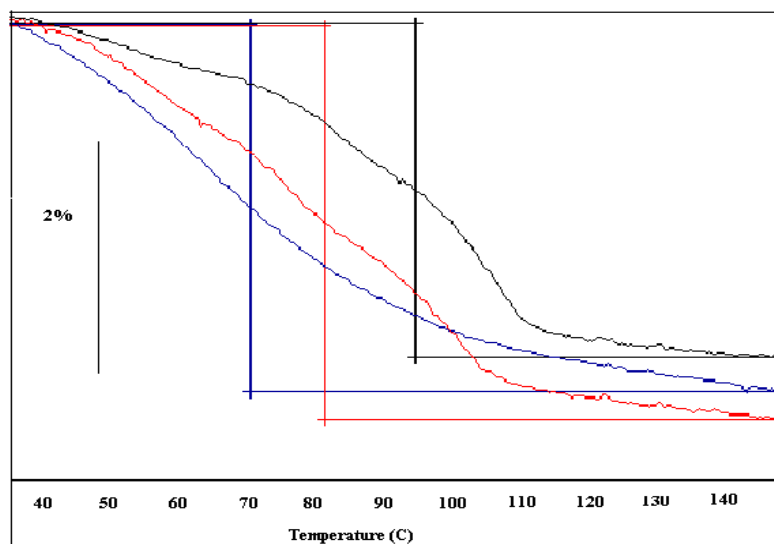
Figure 3.14: TGA plots of the three batches of mixed homologue magnesium stearate (cMgSt$_{B1,B2,B3}$) using a heating cycle of 30–150°C@10°C/min.

3.6.4.7 Fourier transform Infrared (FTIR) spectroscopy

Figure 3.15 shows the FTIR spectra of magnesium oxide, stearic acid and various samples of magnesium stearate. Magnesium oxide and stearic acid showed numerous peaks, each peak showing varying correlated intensity and appearing at different frequency (Fig.3.15a). In contrast, anhydrous and hydrated samples of mixed and pure homologues showed rather similar spectra with numerous peaks appearing at similar frequencies (Fig. 3.15b).

The main differences were observed at the absorption band in the region of 1600–1700 cm^{-1} (carbonyl end of the molecule). Both magnesium oxide and stearic acid showed a peak of high correlated intensity at 1639 cm^{-1} and 1705 cm^{-1} respectively (Fig. 3.15a). In contrast, all samples of magnesium stearate (pMgSt and cMgSt$_A$ and cMgSt$_H$) did not show peak in this region (Fig. 3.15b). In addition, magnesium stearate showed a peak at 1562 cm^{-1}, which was not observed in either magnesium oxide or stearic acid.

There were also changes observed in the aliphatic portion of the samples. Magnesium stearate showed various peaks in the region of 891–1411 cm^{-1}. In contrast, stearic acid did not show any peak in this region. Magnesium stearate

96

showed a doublet between 688 cm-[1] and 721 cm-[1]. In contrast, stearic acid showed a singlet at 721 cm-[1]. Furthermore, there were changes observed in the region of 3100–3600 cm-[1]. The anhydrous samples of pure and mixed homologue magnesium stearate did not show peak in this region (Fig. 3.15b). In contrast, magnesium oxide, stearic acid and hydrated samples of magnesium stearate showed peak at 3433 cm-[1] and 3410 cm-[1] respectively (Fig. 3.15a).
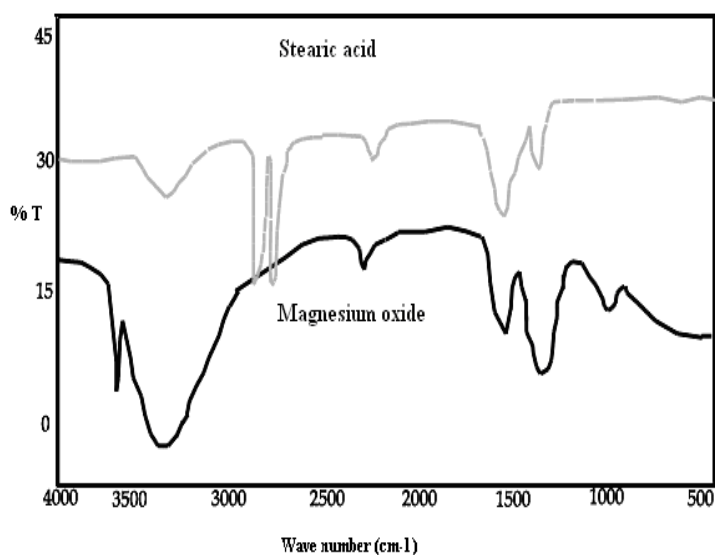
(a)
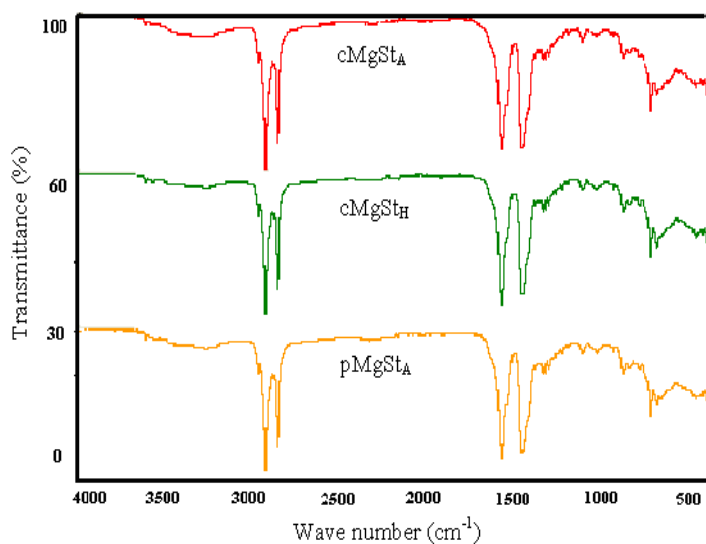
(b)

Figure 3.15: FTIR spectra of various raw materials (a) Magnesium oxide and stearic acid and (b) samples of pure and mixed homologue.

3.6.4.8 X–ray diffraction (XRD)

Powder XRD was used to investigate the XRD spectra of magnesium stearate. Figure 3.16 shows the XRD spectra of the pure and mixed homologues of magnesium stearate. All anhydrous and hydrated samples showed numerous distinct peaks in the range of $2\theta= 3.5^{o}$–30°. All samples showed numerous sharp peaks between 3.5^{o} and 10° in addition to one to three broad to sharp peaks at 2θ between 20° and 22°.

(a)

(b)
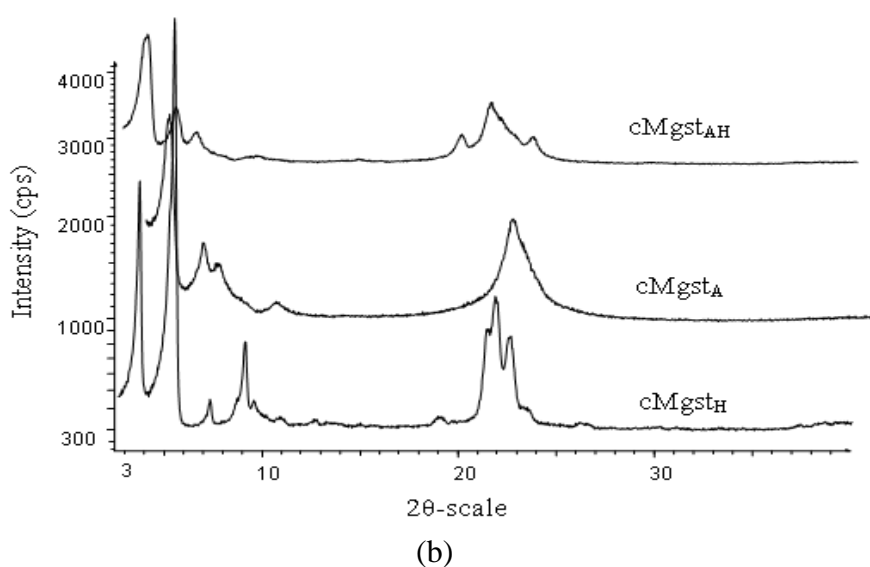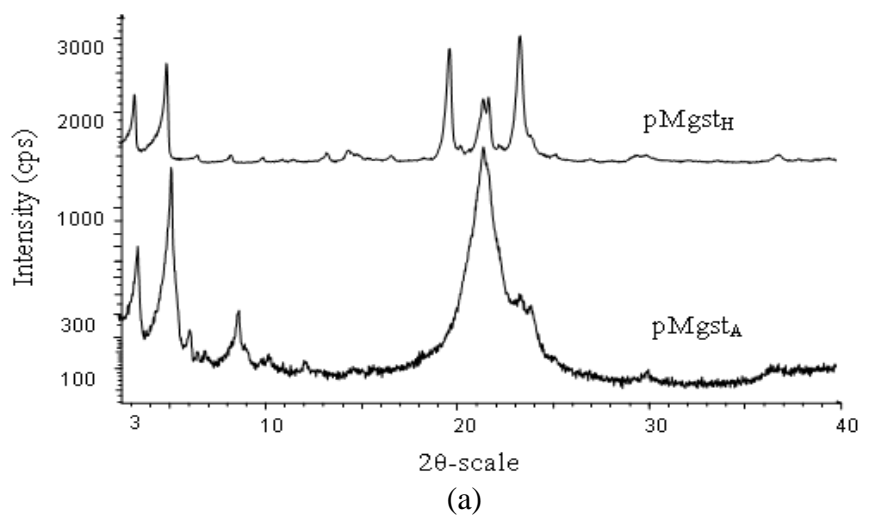
Figure 3.16: XRD diffractograms of magnesium stearate (a) pure homologue and (b) mixed homologues.

Figure 3.16a shows diffractograms of anhydrous and hydrated pure homologues of magnesium stearate. Hydrated sample (pMgSt$_H$) showed two sharp peaks between 3° and 5°. In addition, three sharp peaks were observed between 2θ= 22° and 24° representing trihydrate state of the material. In contrast, anhydrous sample (pMgSt$_A$) showed additional peaks at 2θ between 6° and 10° in addition to the two sharp peaks similar to the hydrated sample at 2θ between 3° and 5°. In addition, a single broad peak was observed at 2θ= 22° with two small shoulders between 23° and 24° representing mixture of amorphous and crystalline nature of the material *i.e.* broad peak representing amorphous state whereas small shoulders representing traces of crystalline material.

Figure 3.16b shows the diffractograms of the anhydrous and hydrated mixed homologue of magnesium stearate. All samples showed numerous sharp peaks at 2θ= 3.5^o and 10°. However, all samples showed one to three peaks at 2θ= 20°–22° *i.e.* anhydrous sample showing a very broad (halo) peak representing amorphous nature, cMgSt$_H$ showed two sharp peaks at 2θ= 20°–22° representative of dihydrate. In contrast, cMgSt$_{AH}$ showed three peaks of low intensity in the same region (2θ= 20°– 22°) also representing trihydrate state (Fig.3.16b).

The XRD spectra of all the mixed homologues did not match with the reference spectra of pure (C$_{18}$) magnesium stearate in the reference library. In contrast, most of the major peaks of the pure homologue (pMgSt$_H$) containing mainly C$_{18}$ matched with the reference XRD spectra of the pure magnesium stearate in the reference library.

The hydrates of pure and mixed homologues (cMgSt$_H$ and pMgSt$_H$) although showed three peaks in the region 2θ= 20°–22° suggesting trihydrate form. However, both samples showed significantly different intensities *i.e.* 1148cps for pure homologue and 325cps for mixed homologue of the three sharp peaks at 2θ= 20°–22°. There also appeared to be an increase in the sharpness of the peaks in this region with an increase in the moisture content with the peaks shifting slightly to the left. In contrast, anhydrous pure and mixed homologue samples (cMgSt$_A$ and pMgSt$_A$) showed a single broad peak also called halo in the same region. However, both broad

peaks were also different *i.e.* pure homologue showing two shoulders on the broad peak whereas mixed homologue showed characteristic halo shape, suggesting differences in the structures. Therefore, drying of both pure and mixed homologues produced amorphous forms represented by broad peak whereas rehydration of anhydrates by exposing to 100% humidity produced trihydrate represented by the three sharp peaks.

3.7 Discussion

Anhydrous magnesium stearate (MgSt) was prepared from pure homologue of (C_{18}) stearic acid and magnesium oxide in the solid state using fusion method. Various hydrates of mixed and pure homologues were also obtained by storing anhydrate materials at 100% relative humidity. The hydrated and anhydrate samples were then characterised using polarised light microscopy, GC, DSC, TGA, FTIR and XRD.

The heating of stearic acid (pure homologue) and magnesium oxide at $105^{o}C$ under vacuum produced white anhydrous pure homologue of MgSt powder. The prepared anhydrous magnesium stearate ($pMgSt_A$) was identified and differentiated from stearic acid by the differences in the melting point, FTIR, XRD, and DSC data.

The preparation of $pMgSt_A$ was confirmed by the differences in the FTIR spectra of the pure anhydrous MgSt and the stearic acid *i.e.* the presence of absorption band at $\sim1562cm^{-1}$ in $_PMgSt_A$ which was not present in the stearic acid spectrum. In addition, an absorption band at $1705cm^{-1}$, typical of C=O bond of the carboxylic acid was observed only in the stearic acid. According to Ertel and Carstensen (1988a), preparation of stearate from the stearic acid involves stretching of the C=O bond of the carbonyl group from 1705 cm^{-1} to 1562 cm^{-1}, converting it from an unionised to ionised form. Therefore, the presence of the absorption band at $1562cm^{-1}$ in the prepared material confirms the presence of MgSt. This point of view was further supported by the XRD results as most of the peaks in the diffractogram of the anhydrous prepared MgSt matched with the peaks of the material assigned to the pure MgSt in the reference library.

Anhydrous nature of the $_P$MgSt$_A$ was confirmed by the FTIR spectrum in the absorption band at 721cm^{-1}. A singlet in the absorption band of $_P$MgSt$_A$ at ~721cm^{-1} represents anhydrous nature which is consistent with the findings of Ertel and Carstensen 1988a. This point of view was further supported by the XRD results where a broad (halo) peak was observed at $2\theta=20–22^o$ in the XRD diffractogram of the pMgSt$_A$ representing amorphous nature. This may be due to the loss of moisture from the pure homologue upon heating causing disruption of the three-dimensional ordered crystalline structure resulting in a disordered amorphous material. Koivisto *et al.,* (2004) dried commercial MgSt at 105°C and observed identical peak (halo) at $2\theta=20–22^o$ and assigned it to the anhydrous state of MgSt. Furthermore, TGA results showed no moisture loss from pMgSt$_A$ further suggesting anhydrous nature of the material.

The melting points of stearic acid and the pMgSt$_A$ were observed to be 70°C and 85°C respectively. It has been reported that commercial MgSt melts between 80°C and 145°C depending on the homologue composition of the stearic acid in MgSt (Miller and York, 1985). Therefore, as the anhydrous material was prepared from the pure stearic acid and differentiated from mixed homologue MgSt on the basis of differences in the GC spectra (Fig.3.2). Mixed homologue showed presence of equal amounts of C_{16} and C_{18} whereas prepared (pure) homologue of MgSt showed almost 95% C_{18} and 5% C_{16}, suggesting that prepared MgSt contains pure homologue of fatty acid and the commercial sample represents mixed homologue composition.

This view was supported by the DSC data. Stearic acid showed only one melting endotherm peaking at ~72°C with an enthalpy of -223.74J/g whereas anhydrous pure homologue MgSt showed one very broad melting endotherm peaking at 84°C (-136.5J/g), which is consistent with the melting point data. In addition, a very small low temperature endotherm peaking at 66.5^{o}C (-1.61 J/g) was also observed which is assigned to the traces of adsorbed moisture. The assignment of the endotherms to the adsorbed water and melting was confirmed by comparing the DSC of the pMgSt$_A$ and pMgSt$_H$. The pMgSt$_H$ showed an increase in the enthalpy (-12.8J/g) of the first endotherm at 66.9^{o}C due to moisture uptake whereas the second endotherm associated with melting shifted to right (91.3^{o}C) with a significant increase in the

enthalpy (from -136.5J/g to -206.9J/g) suggesting that $pMgSt_A$ and $pMgSt_H$ are two different pseudopolymorphs of different hydration states *i.e.* $pMgSt_A$ representing anhydrous form and $pMgSt_H$ belonging to the trihydrate state.

$cMgSt_A$, cMgSt and $pMgSt_A$ were treated at 100% RH to investigate the formation of various hydrates. $cMgSt_A$ and $pMgSt_A$ treated at 100% RH produced $cMgSt_{AH}$ and $pMgSt_H$ showed significant increase in the moisture content (5.0% and 6.7% respectively) (Table 3.2). According to Koivisto *et al.*, (2004) one mole of monohydrate magnesium stearate contains 2.75% moisture. Therefore, dihydrate and trihydrate should possess 5.5% and 7.5% moisture respectively. TGA results of $pMgSt_H$ showed slightly lower weight loss of 6.7% than the 7.5% moisture expected for trihydrate, nevertheless XRD results clearly showed presence of the three sharp peaks of high intensity at $2\theta=20\text{--}22^o$ (Fig. 3.16a), suggesting formation of a trihydrate. Similarly, $cMgSt_{AH}$ although showed only 5% moisture loss but exhibited the three distinct peaks in the same region ($2\theta=20\text{--}22^o$) of low intensity, suggesting existence of certain amount of trihydrate form. This point of view was confirmed by the work of Swaminathan and Kildsig (2001) and Koivisto *et al.* (2004) that commercial anhydrous MgSt treated at 98% RH for six weeks showed three distinct peaks in the XRD region of $2\theta=20\text{--}22^o$, confirming existence of trihydrate state of MgSt. In contrast, cMgSt treated at 100% RH produced $cMgSt_H$ showed a fractional increase (4.1% to 4.7%) in the moisture content (Table 3.2). XRD spectra of both (cMgSt and $cMgSt_H$) showed two distinct peaks of high intensity at $2\theta=20\text{--}22^o$ suggesting the existence of dihydrate form. This point of view was supported by the results of Koivisto *et al.*, (2004) that showed similar XRD spectrum for commercial MgSt and associated it to the dihydrate state. This observation suggests that moisture treatment of cMgSt and $cMgSt_A$ at 100% RH produces di– and trihydrate respectively. However, type of pseudopolymorph representing di- and trihydrate could not be identified due to the limitation of the software for not resolving "miller indices".

The differences in the moisture contents of cMgSt, $cMgSt_A$ and $cMgSt_H$ affected their physical properties such as thermal behaviour evident from the significant differences in the DSC spectra of all samples. cMgSt showed two high temperature

endotherms peaking at 104.3^{o}C (-26.2J/g) and 121.4^{o}C (-114.8J/g), which were similar to the endotherms observed by Miller and York (1985) and Koivisto *et al*., (2004). They assigned the two endotherms (104°C and 120°C) to the water of crystallisation and melting respectively. In the present study, similar observations were recorded for both endotherms *i.e.* cMgSt dried at 105°C at 0% RH to form cMgSt$_A$, did not show the first endotherm (104.3^{o}C), which confirms that this endotherm is related to the water of crystallisation. The second endotherm (120°C) in the cMgSt was related to the melting. However, cMgSt$_A$ showed two endotherms between 120°C and 130°C suggesting that drying causes change in the physical properties of MgSt producing a new polymorph (*identification of specific polymorph is not possible due to lack of "miller indices"*). cMgSt and cMgSt$_H$ showed very different DSC. cMgSt$_H$ showed a left shift of the melting endotherm from 121.4^{o}C to 115°C, with a significant increase in the enthalpy (-291.2J/g). These results suggest that the moisture treatment of the cMgSt caused a significant change in the physical properties (changes in the thermal behaviour) of the sample producing a different solvate (pseudopolymorph) without affecting its hydration state (dihydrate). This point of view is consistent with the findings of Miller and York, 1985; Rajala and Laine, 1995; Barra and Somma, 1996; Swaminathan and Kildsig, 2001 and Bracconi, 2003, who suggested that slight variation in the moisture content, brought about by changes in RH at room temperature, is sufficient to produce a different pseudopolymorph of MgSt, showing significantly different physicochemical properties such as melting behaviours which are attributed to the moisture–related modifications in the crystal structure. In contrast, trihydrate of cMgSt$_{AH}$ showed two endotherms peaking at 66.7^{o}C (-40.6J/g) and 85.9^{o}C (-891.8J/g) suggesting that dihydrate (cMgSt, cMgSt$_H$) and trihydrate (cMgSt$_{AH}$) possess different crystalline structures, which further confirms that depending on the hydration state MgSt can exist in different pseudopolymorphic states.

The pure and mixed homologue (anhydrous) samples used in the present study were different from each other and also from the MgSt described in the literature. Electron microscopy showed differences in the two (pure and mixed homologue anhydrate samples). Although, both samples appeared as flakes but the crystals of pMgSt$_A$ appeared significantly larger in size than the cMgSt$_A$. Furthermore, pMgSt$_A$ showed

small particles (kinks) on top of the large flakes (Fig. 3.5b). Leinonen et al., (1992) assigned presence of kinks to the amorphous state. Therefore, pMgSt$_A$ prepared in the present study shows amorphous nature. The XRD and GC results for both types of stearate were also different.

XRD results showed different phases in the diffractograms of the pMgSt$_A$ and cMgSt$_A$. Most of the peaks in the diffractogram of the pMgSt$_A$ matched with the spectrum of the pure MgSt in the reference library. In contrast, cMgSt$_A$ did not match with any compound in the reference library. Therefore, the structural diversity observed in the DSC, GC and XRD results in the investigated samples of cMgSt$_A$ and pMgSt$_A$ can also be explained in terms of the fatty acid homologue composition, the method of manufacture in addition to the differences in the hydration state.

Mixed homologue MgSt was rather similar to the MgSt studied by Koivisto et $al.,$ (2004) as both samples showed similar DSC spectra and weight loss (4.11%), suggesting similar polymorphic structures. However, all samples of mixed homologue MgSt $i.e.$ cMgSt, cMgSt$_A$ and cMgSt$_H$ were different from the MgSt investigated by Ertel and Carstensen (1988a). In addition, pMgSt$_A$ was also different from the MgSt investigated by the Ertel and Carstensen (1988a) as well as Koivisto et $al.,$ (2004) which was confirmed by the DSC and XRD results. These differences can be explained on the basis of the homologue composition of MgSt.

The homologue composition of fatty acid in the MgSt can affect the physical properties of the material. It is well known that the commercial magnesium stearate is a mixture of magnesium salt of different fatty acids, mainly stearic and palmitic acid (Bozic et al., 1980; Miller and York, 1985; Wada and Matsuhara, 1994; Bracconi et al., 2003). However, magnesium stearate in the present study was prepared using pure stearic acid (~95% purity) to investigate the significance of pure stearic acid and the mixed homolog composition of the stearic acid on the physicochemical properties of the MgSt such as moisture content and the thermal behaviour. There appeared to be an increase in the enthalpy values with an increase in the moisture content for both pure and mixed homologue samples (Table 3.1), which is consistent with the findings of Bracconi et al., (2005) who demonstrated

enhanced enthalpies in the moisture treated MgSt compared to the anhydrous MgSt. However, the enthalpy of the pure hydrated sample (pMgSt$_H$) was significantly lower than the mixed homologue hydrated sample (cMgSt$_H$), suggesting that moisture content alone is not responsible for the sample's significantly enhanced thermal activity and may be attributed to the fatty acid homologue composition of the stearate. This point of view was supported by the results of gas chromatography where the chromatograms for both samples appeared to contain varying ratio of the two fatty acids. The mixed homologue (anhydrous) cMgSt$_A$ showed equal ratio of stearic and palmitic acids whereas pure (anhydrous) homologue pMgSt$_A$ possessed approximately 95% stearic acid and traces of palmitic acid. The enhanced enthalpy of the mixed homologue samples therefore can be attributed to the mixed homologue composition of the stearic acid in addition to the moisture content.

The preparation method can also affect the physical properties of the resultant MgSt. Pure magnesium stearate can be prepared by fusion or precipitation methods. The fusion method uses the heating of materials in the solid state to produce anhydrate MgSt. Therefore, stable solvates can be obtained by the moisture treatment of the anhydrate at room temperature without affecting the structure. In contrast, in the precipitation method ingredients are mixed in the liquid state and various hydrates *i.e.* monohydrate, dihydrate and trihydrate can be obtained by this method. However, the final hydration state depends on the pH of the precipitation medium and the cooling rate (Miller *et al.,* 1982; Rajala and Laine, 1995), which may sometimes depending on the pH variation lead to the formation of mixture of hydrates rather than pure hydrate and therefore require strict pH control during precipitation. Therefore, MgSt in the present study was prepared using fusion method to avoid pH dependency.

3.8 Conclusions

1. Anhydrous magnesium stearate was prepared from pure homologue stearic acid (~95% C$_{18}$) and magnesium oxide using a fusion method which involved heating of two moles of stearic acid with one mole of magnesium oxide at 130°C with continued stirring for four hours under vacuum.

2. GC results indicated that the homologue composition of the anhydrous magnesium stearate prepared from 1 above was mainly C_{18} (~95%) whereas a commercial batch of magnesium stearate (batch 3) used in subsequent work to prepare lipogels was of mixed homologue composition (50:50 ratio of C_{16} and C_{18}).

3. The anhydrous pure homologue magnesium stearate (pMgSt$_A$) was amorphous in nature. The XRD diffractogram shows a broad (halo) peak at $2\theta=20$–22° confirming presence of amorphous state. DSC results showed a significant decrease in the enthalpy values of the anhydrous form (-137.7J/g) than the hydrated (pMgSt$_H$) crystalline state (-219.7J/g) confirming that anhydrous material lost the three-dimensional crystalline network producing a less stable amorphous material.

4. The commercial Mg stearate (mixed homologue–cMgSt) was the di-hydrate pseudopolymorph. In contrast, the anhydrous form of the mixed homologue MgSt (formed by drying mixed homologue MgSt (batch 3) at 110^oC for four hours under vacuum) was amorphous in nature. The dihydrate nature of the cMgSt was confirmed by the TGA and XRD results. TGA showed 4.14% water loss and XRD showed two sharp peaks at $2\theta=20$–22° confirming dihydrate state. In contrast, anhydrous mixed homologue showed a broad (halo) peak at $2\theta=20$–22° in the XRD diffractogram suggesting presence of amorphous state as in (3) above for pMgSt$_A$. DSC of cMgSt$_A$ also showed decreased enthalpy (-58.9J/g) compared to the cMgSt (-141J/g) suggesting that anhydrous material has lost the three-dimensional crystalline structure producing a less stable amorphous material.

5. Various hydrates of the pure C_{18} homologue anhydrous magnesium stearate (*c.f.* 1 above) and mixed commercial (di-hydrate and anhydrous) magnesium stearate containing mixed homologue fatty acids were prepared by exposing the magnesium stearate to various relative humidities (70–100%) at room temperature for six weeks using either saturated salt solutions of potassium sulfate or a stability chamber.

6. The pure homologue magnesium stearate changed from anhydrate (amorphous state) to the trihydrate by treatment at 100% RH. In contrast, the mixed homologue (dihydrate) did not show change and remained as the dihydrate, confirmed by the

XRD diffractogram. However, it showed a slight increase in the moisture content (from 4.14% to 4.75%) which caused significant changes in the thermal behaviour of the material. The enthalpy values increased from -141J/g (cMgSt) to -291.2J/g for cMgSt$_H$ suggesting production of a new pseudopolymorph without an increase in the hydration state. However, type of crystalline form could not be resolved due to lack of "miller indices".

7. Mixed homologue dried at 110°C overnight under vacuum produced amorphous form evident from broad halo peak in the XRD diffractogram. In contrast, exposure of dried sample to 100% RH at room temperature showed a significant increase in the moisture uptake and converted it to trihydrate form evident from the three small peaks in the XRD spectrum of cMgSt$_{AH}$.

8. All mixed homologue samples *i.e.* cMgSt$_A$, cMgSt and cMgSt$_H$ showed similar chemical composition but different crystalline phases, confirmed by XRD spectra. However, their physical properties were significantly different from each other exhibited by changes in the moisture content and the DSC spectra suggesting that they belong to different pseudopolymorphic states.

9. The physicochemical properties of MgSt are affected by the homologue composition of the fatty acid, hydration state, and the method of its manufacture, exhibited by the differences in the fatty acid composition of cMgSt$_A$ and pMgSt$_A$ by GC, production of di- and trihydrate obtained after moisture treatment at 100% relative humidity and the manufacture of MgSt using fusion method respectively.

CHAPTER IV

INFLUENCE OF DIFFERENT PSEUDOPOLYMORPHIC FORMS OF MIXED AND PURE HOMOLOGUE MAGNESIUM STEARATE ON THE PROPERTIES OF LIPOGELS

4.1 Introduction

Scric *et al*., (1985) prepared stable lipogels using 12.5% MgSt in liquid paraffin using a standard method of heating and cooling. The heating of MgSt in liquid paraffin to a specific temperature caused intense foaming, which they stated was due to the release of water causing an increase in the solubility of MgSt. This temperature is called critical solubility temperature (CST). However, we were unable to obtain stable lipogels (opaque to translucent solid lipogels showed little syneresis) using 12.5% of the three different batches of mixed homologue MgSt (chapter III) using Scric's method. It was thought that moisture content and amount of MgSt in addition to the heating (temperature and duration) may affect the appearance and stability of lipogels. Therefore, the present chapter investigates the CST, the influence of concentration, batch type and various hydrates of pure and mixed homologue MgSt (chapter III), on the appearance and stability of the lipogels. The effect of heating (temperature and duration) on the appearance of lipogels was also investigated by micropreparation of lipogels in the hermetically sealed DSC pans using controlled heating and cooling cycles.

4.1.1 Aims of the chapter

The present chapter investigates the influence of various hydrates in addition to the amount and batch of MgSt on the preparation and stability of the lipogels and overall aims include:

1. To investigate critical solubility temperature (CST)

2. To investigate the effect of concentration of magnesium stearate on the appearance of lipogels,

3. To study the influence of batch of magnesium stearate on the appearance of the lipogels,

4. To investigate the influence of various hydrates (anhydrate, dihydrate and trihydrate (chapter III)) of magnesium stearate on the appearance and stability of the lipogels.

5. To investigate the effect of heating and cooling on the appearance of lipogels using micropreparation of lipogels in DSC pans with subsequently controlled heating and cooling cycles

4.2 Methods

4.2.1 Investigation into critical solubility temperature (CST)

The CST was determined by dispersing 12.5% MgSt in liquid paraffin in a glass beaker using glass rod. The systems were heated without stirring at a rate of ~5–10°C/minute to a maximum of 90°C, 100°C, 105°C, 110°C, 115°C or 120°C and held at the maximum temperature for up to 3 hours in an oil–bath. The effect of stirring on the CST was also investigated by agitating the dispersions at regular intervals using an overhead stirrer (IKA–Werk–RW–16B, Germany) at 200rpm.

4.2.2 Preparation of lipogels using various concentrations of commercial magnesium stearate

Various amounts (2.5–20%w/v) of mixed homologue MgSt (dihydrate, batch 3) (chapter III) were incorporated into the liquid paraffin (Table 4.1) and lipogels prepared using the Scric's method which involves preparation of a dispersion of MgSt and the liquid paraffin in a beaker by mixing with a glass rod, heating the dispersion (5–10°C/min) in an oil−bath to 130°C, holding the dispersion at 130°C for an hour, removing the dispersion from the oil−bath and leaving on the bench allowing it to cool naturally (~2°C/min) to ambient temperature (28±3°C). This type of cooling is referred to as "fast cooling".

4.2.3 Preparation of lipogels using three batches of commercial magnesium stearate

A fixed amount (12.5%) of the three different batches of mixed homologue dihydrate (batch 1, batch 2 and batch 3 MgSt, chapter III) was used to prepare lipogels using Scric's method as described above.

Table 4.1: Formulae of various preparations of liquid paraffin and MgSt. Values in superscript represent percentage of MgSt, and L=lipogel.

Formulation type	% liquid paraffin (w/w)	% MgSt (w/w)
$L^{2.5}$	97.5	2.5
L^{5}	95.0	5.0
$L^{7.5}$	92.5	7.5
L^{10}	90.0	10.0
$L^{12.5}$	87.5	12.5
L^{15}	85.0	15.0
L^{20}	80.0	20.0

4.2.4 Preparation of lipogels using pure and mixed homologue anhydrate and hydrated magnesium stearate

The anhydrates of pure and mixed homologue ($pMgSt_A$ and $cMgSt_A$) in addition to the dihydrate of mixed homologue ($cMgSt_H$) and trihydrate of pure homologue ($pMgSt_H$) magnesium stearate (chapter III) were used to prepare lipogels using the Scric's method as described above in 4.2.2.

4.2.5 Micropreparation of lipogels using DSC

In the above experiments, using Scric's method of heating and cooling unstable (syneresis of oil) lipogels of varying appearance were obtained. Therefore, lipogels were prepared using 12.5% MgSt (bath 3) with various programmed heating and cooling cycles in the DSC pans as follows:

The dispersion was prepared using the glass rod in a beaker (Scric's method). Small quantities of the dispersion (5–10mg) were weighed and placed in the DSC pans, which were then hermetically sealed. The DSC was programmed to provide various heating/cooling cycles (Table 4.2). After the DSC cycles, the lids were removed from the pans, the samples examined visually, photographed and stored at ambient temperature (20 ± 2^oC) for six months.

Table 4.2: The DSC heating/cooling cycles to create the controlled environment for the preparation of lipogels. *Left in the DSC pans to cool naturally.

No.	Heating cycle	Heating rate (per minute)	Hold time	Cooling cycle	Cooling rate (per minute)
1.	Normal heating	5^oC	1 hour	normal cooling	5^oC
2.	Slow heating	2^oC	1 hour	slow cooling	2^oC
3.	Slow heating	2^oC/quench cool	1 hour	shock cooling	quench
4.	Fast heating	10^oC	1 hour	slow cooling	2^oC
5.	Fast heating	10^oC	1 hour	shock cooling	quench
6.	Short isotherm (1 hour)	10^oC	1 hour	*No programmed cooling	
7.	Long isotherm (4 hours)	10^oC	1 hour	*No programmed cooling	
8.	Normal heating and hold at high temperature (140^oC)	10^oC	1 hour	normal cooling	5^oC
9.	Normal heating and hold at low temperature (120^oC)	10^oC	1 hour	normal cooling	5^oC
10.	Normal heating	5^oC	No hold	normal cooling	5^oC

4.2.6 Characterisation of lipogels

4.2.6.1 Polarised light microscopy

The lipogels containing various amounts of MgSt (5−20%) in liquid paraffin in addition to the lipogels of the three different batches of MgSt were studied using polarised light microscopy.

4.2.6.2 Hot stage microscopy

Hot stage microscopy was used to investigate the lipogels prepared from various amounts of MgSt (5–20%) in liquid paraffin between 25 and 150°C at 10°C/min. The melting behaviour of the lipogels prepared using two different batches of MgSt (batch 1 and 2) were also investigated.

4.2.6.3 Differential scanning Calorimetry (DSC)

The lipogels prepared using varying amounts of MgSt (5–20%) and liquid paraffin, lipogels of the three different batches of MgSt and various hydrates of MgSt were analysed using a standard heating cycle of 25°C–150°C at a rate of 10°C/min to observe thermal changes.

4.2.6.4 Thermogravimetric analysis (TGA)

The TGA/SDTA851^{e} (Mettler Toledo, Leicester, UK) was used for the analysis of the liquid paraffin lipogels prepared using various amounts of magnesium stearate (5−15%). Additional experiments were performed on the lipogels prepared using the three different batches of MgSt and hydrates of pure and mixed homologue MgSt.

4.2.6.5 Fourier Transform Infrared (FTIR) spectroscopy

The FTIR−8400S (Shimadzu, Germany) was used to obtain the infra−red spectra of the lipogels of the hydrates of MgSt (pure and mixed homologue) using attenuated total reflectance (ATR). The samples were scanned for three (3) minutes from 4000–600 cm^{-1}. FTIR data were analysed using IR Solution software.

4.2.6.6 X–ray diffraction (XRD)

A powder X–ray diffractometer (Bruker 8 Advances, Germany) was used for the analysis of the lipogels prepared using different hydrates of pure and mixed homologue MgSt (chapter III) using the same method as described in chapter III (section 3.3.4.8).

4.2.6.7 Texture profile analyses

Texture profile analyses (TPA) were performed on the lipogels prepared using various concentrations (5−15%) of magnesium stearate and the liquid paraffin after homogenisation. The mechanical properties (hardness, cohesiveness, consistency and index of viscosity) of each lipogel were evaluated using a texture analyser (Model TA–XT2, Stable Micro Systems, UK) at ambient temperature ($23 \pm 5^{\circ}$ C).

The experiments were performed on the samples packed into a 60mm plastic bottle to a fixed height (approximately 30mm). A 2mm stainless steel probe was allowed to move slowly into the sample at right angles to a fixed depth (distance) at a preset test speed (1mm/sec). The pre and post test speeds (5mm/sec) did not affect the test and were used to attach/detach the probe to/from the sample respectively. All experiments were performed in triplicate on day 8. Data collection and calculation were performed using the Texture Exponent software package of the instrument.

Various parameters (positive force, negative force, positive area under the curve (AUC), negative AUC and the time between two bites) were used to determine the mechanical properties of each lipogel. The positive force required for a probe to compress the formulation to a specified (5mm) distance gave an indication of the hardness of the formulation. Cohesiveness was determined by calculating the positive AUC. The negative force required to detach the probe from the sample determined the consistency of the formulation and negative AUC provided the index of viscosity.

4.3 Results

4.3.1 Critical solubility temperature (CST)

The CST was investigated by heating the dispersions of MgSt and liquid paraffin up to 90°C, 100°C, 105°C, 110°C, 115°C and 120°C for a maximum of 3 hours.

Upon heating, all samples showed foam production at each temperature. However, each temperature required different holding time for the complete disappearance of the foam, producing the clear solution *i.e.* longest holding time was required for the lowest temperature and vice versa (Table 4.3).

Table 4.3: Effect of temperature and heating time on the Critical Solubility Temperature (clearance of foam).

Temperature (^{o}C)	Clearance of foam at				
	Zero hr	**0.5 hr**	**1 hr**	**2 hrs**	**3 hrs**
90	0	0	0	0	0
100	0	0	0	0	1
105	0	0	0	0	1
110	1	1	2	3	
115	1	3			
120	2	3			
130	2	3			

0: foam; 1: little foam cleared; 2: Most foam cleared; 3: No foam

In dispersions heated for 3 hours at 90, 100 and 105°C the foam did not disappear. In contrast, the dispersion heated to 110°C and held for 2 hours showed complete foam disappearance, leaving clear solution. In contrast, the dispersions heated to 115°C and 120°C required only 30 minutes for the complete foam disappearance, producing clear solutions. However, stirring upon heating showed significant reduction in the holding time and therefore the effect of stirring type was also explored on the CST as follows:

The dispersions were continuously stirred using an overhead stirrer at 200rpm. The overall holding time at each temperature was significantly reduced with the use of stirring. The dispersions heated to 90°C–105°C and stirred using overhead stirrer

showed very little foam reduction. The dispersions did not change to clear solution when held at the same temperature for 3 hours. However, holding times with overhead stirrer at 110°C, 115°C and 120°C required only 45 minutes, 20 minutes and 5 minutes respectively for the corresponding temperatures.

4.3.2 Appearance of lipogels prepared using various concentrations of magnesium stearate

Various amounts of magnesium stearate (2.5–20%) were used to prepare lipogels using Scric's method. All lipogels showed foam production upon heating. However, the amount of foam produced was dependent on the amount of MgSt *i.e.* minimum foam was observed in the lipogel containing 2.5% MgSt and maximum foam in the lipogel containing 20% MgSt. It was extremely difficult to contain the foam in the lipogels container having more than 12.5% MgSt. Therefore, continuous stirring was required while heating the dispersions containing 15 and 20% MgSt. However, all dispersions changed to clear dispersions after holding at 130°C for an hour.

Upon cooling, all clear dispersions changed into opaque solids* (Table 4.4). Upon storage at ambient temperature, all lipogels showed varying amounts of syneresis with the lipogel having maximum amount of MgSt showing least syneresis and vice versa (Fig. 4.1).

Table 4.4: Visual characterisation of various formulations of liquid paraffin and MgSt.

Visual characteristics	Lipogels (2.5–20% MgSt)
Consistency	Solids*
Appearance/colour	Opaque
Physical stability	Unstable (crumbly and syneretic)

Solids*- These systems are not exactly solids like tablet. The systems are extremely viscous (consistency is like that of suppository or shoe polish). However, gentle poking causes syneresis of oil.
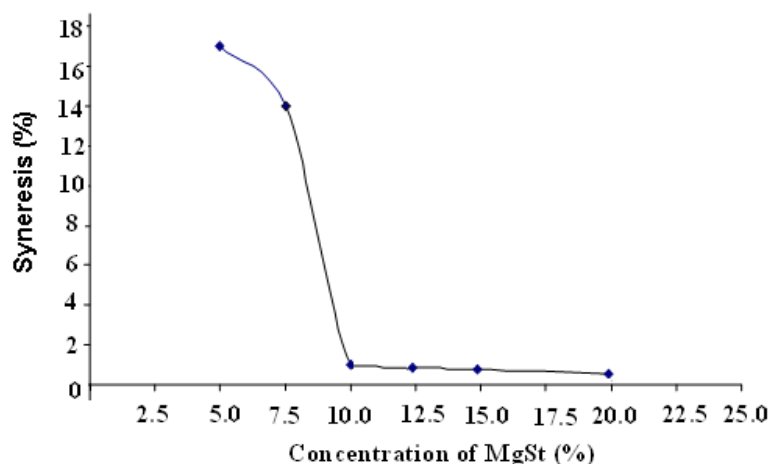
Figure 4.1: Syneresis observed in the lipogels containing various concentrations of MgSt (5–20%) on day 28.

4.3.3 Appearance of lipogels prepared with the various batches of magnesium stearate

The lipogels were prepared using 12.5% of the three different batches of MgSt. Lipogels of all three batches showed similar events upon heating producing clear dispersions as described in section 4.3.1.

Upon cooling to room temperature, the clear dispersions changed to solids of varying appearance. The solid lipogel of batch 1 appeared to be opaque while the lipogels of batches 2 and 3 were clear. However, all lipogels crumbled to the touch.

Upon storage for two days, the solid, clear lipogels prepared using batches 2 and 3 changed to opaque solid lipogels. All three lipogels showed significant syneresis after two days and visual observation showed increase in syneresis upon further storage for seven days.

4.3.4 Appearance of lipogels prepared using various pseudopolymorphs of magnesium stearate

Various pseudopolymorphs of pure ($pMgSt_A$ and $pMgSt_H$) and mixed homologues ($cMgSt_A$ and $cMgSt_H$) were used to prepare lipogels.

All pseudopolymorphs produced lipogels of varying consistency including mobile liquids, soft and stiff semisolid lipogels. In addition, significantly different observations were recorded upon heating and cooling.

Upon heating, the dispersions of the anhydrous pure and mixed homologues ($cMgSt_A$, $pMgSt_A$) showed little foam production as the anhydrate samples easily dissolved in the liquid paraffin. In contrast, the dispersions containing trihydrate of pure ($pMgSt_H$) and dihydrate of mixed homologue ($cMgSt_H$) produced intense foam.

Upon cooling to 70^oC, all clear dispersions showed little change in their appearances. Upon further cooling to $55–60^oC$, the lipogels of mixed homologues, both anhydrous and dihydrate ($cMgSt_A$ and $cMgSt_H$) changed to opaque solid lipogels, which showed no further changes upon cooling to room temperature. In contrast, dispersions of pure homologue anhydrate ($pMgSt_A$) and trihydrate ($pMgSt_H$) showed no change until 45^oC. However, at temperatures between $35–40^oC$ the clear dispersions of both pure homologues quickly changed to white dispersions. This behaviour of sudden change in the colour (from clear to white) at low temperature was not observed in any other formulation. Further cooling to ambient temperature ($\sim28^oC$) changed the formulation of trihydrate pure homologue ($pMgSt_H$) to a soft semisolid lipogel. However, the formulation of anhydrous pure homologue ($pMgSt_A$) remained as a white homogenous dispersion.

The semisolid lipogels of pure homologue trihydrate ($pMgSt_H$) were significantly sensitive to stirring. The semisolids changed to white fluids when stirred with glass rod even for few seconds and remained the same for 2–3 weeks. However, white dispersions changed back to stiff semisolid lipogels after storage for one month at room temperature. Furthermore, no syneresis is observed to date (more than two year's of storage).

Upon storage for two weeks, significant changes were observed in the white dispersions of $pMgSt_A$ samples, which changed to a soft semisolid lipogel with no syneresis. No further changes were observed in both lipogels to date upon storage for two years.

Figure 4.2 summarises the effect of various pure (anhydrate and trihydrate) and mixed homologue (anhydrate and dihydrate) hydrates on the appearance and stability of the lipogels.
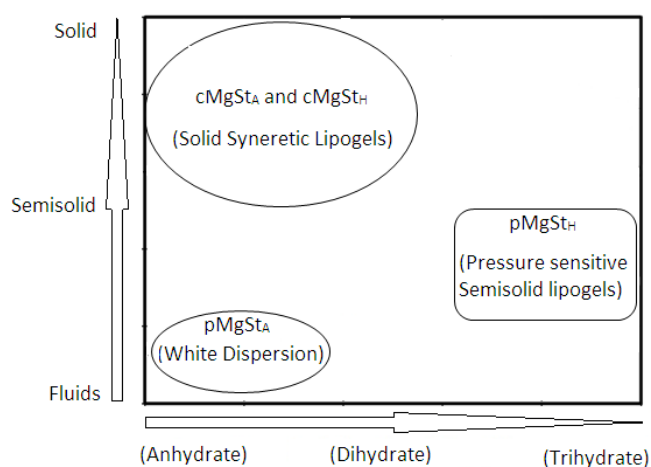
Figure 4.2: Effect of various hydrates of pure and mixed homologue MgSt on the appearance and stability of lipogels.

4.3.5 Appearance of lipogels prepared using DSC pans

All of the heating/cooling cycles used for the micropreparation of the lipogels using the batch 1 of magnesium stearate produced clear, solid lipogels in the DSC pans. The DSC pans with lid removed were left on the bench and all lipogels remained clear and did not show syneresis upon storage for at least five months.

4.3.6 Characterisation of lipogels

4.3.6.1 Polarised light microscopy

The lipogels containing various amounts of MgSt in liquid paraffin in addition to the lipogels prepared using various hydrates were studied using polarised light microscopy. All lipogels showed significantly different anisotropic structures with many crystals and clusters against dark or glowing background under cross polars. Figure 4.3 shows photomicrographs of the selected lipogels containing minimum (5%) and maximum amount (20%) of MgSt. All lipogels showed few crystals and clusters with background glow except lipogels containing 12.5% (not shown) and

118

20% magnesium stearate which showed crystals against dark background. Very few Maltese crosses were observed in the lipogels containing (12.5–20% MgSt). However, no Maltese crosses were seen in the lipogels containing 5–10% MgSt.

(a)   (b)
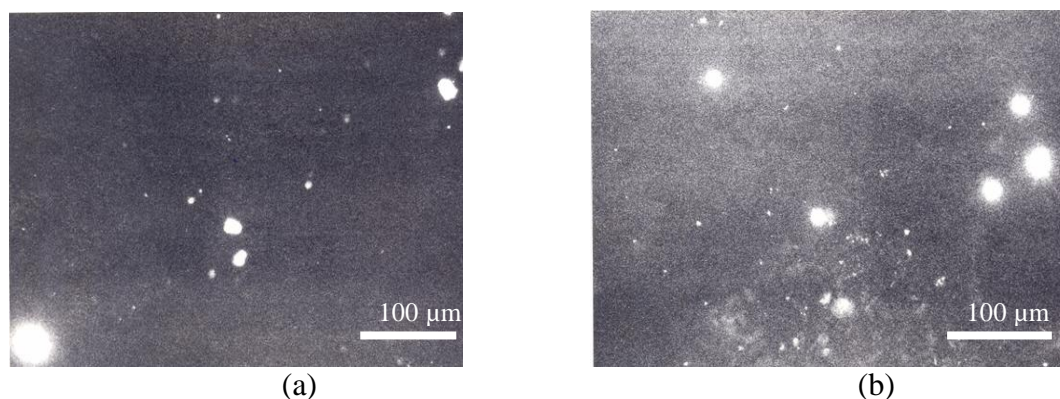
Figure 4.3: Photomicrographs of the lipogels prepared using liquid paraffin and various amounts of MgSt (a) 5% (b) 20% (1cm=100 µm).

Batch variation of the MgSt also showed significant influence on the structure of the lipogels. Figure 4.4 shows photomicrographs of lipogels prepared using different batches of magnesium stearate immediately after preparation. All lipogels showed anisotropic structures with many crystals against dark or glowing background. Occasional Maltese crosses were seen in all lipogels (not seen in the figures).

(a)   (b)
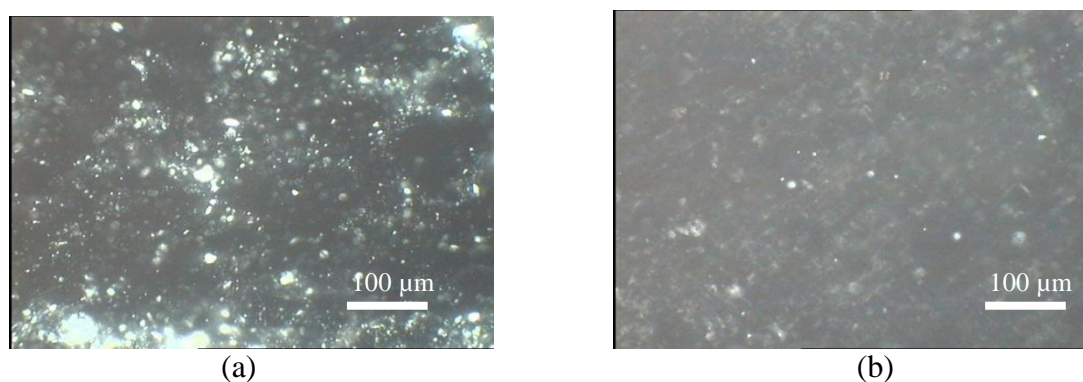
Figure 4.4: Photomicrographs of the lipogels prepared using liquid paraffin and the two different batches of 12.5% MgSt (a) Batch 1 and (b) Batch 2 (1cm=100 µm).

Figure 4.5 shows photomicrographs of the lipogels prepared using pure MgSt (anhydrous and trihydrate). The fluid system containing pure anhydrous MgSt showed numerous anisotropic crystals against dark background (Fig. 4.5a). No Maltese crosses were seen in these systems. In contrast, unstable semisolid lipogel

containing pure homologue MgSt trihydrate (_PMgSt_H) prior to stirring showed numerous Maltese crosses (not shown). However, upon gentle stirring semisolid lipogels changed to structured fluids, showing presence of numerous plate−like crystals and anisotropic clusters of crystals (Fig. 4.5b). No Maltese crosses were seen after stirring.

<div align="center">(a)   (b)</div>
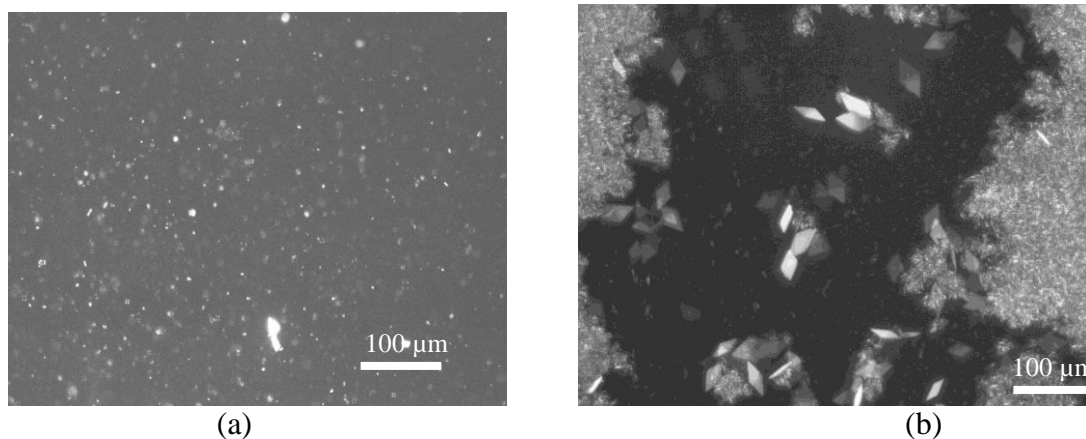
Figure 4.5: photomicrographs of the lipogels prepared using pure homologue MgSt (a) anhydrous and (b) trihydrate (1cm=100 μm).

4.3.6.2 Hot stage microscopy

All lipogels showed melting of anisotropic crystals, plate−like crystals and Maltese crosses at distinct temperatures. The clusters of crystals disappeared between 70 and 90°C. In contrast, Maltese crosses in the unstable semisolids melted around 120°C whereas plate−like crystals of unstable semisolids after stirring disappeared between 70 and 90°C (not shown).

4.3.6.3 Differential Scanning Calorimetry (DSC)

Lipogels were analysed using a standard heating cycle of 25°C–150°C at a rate of 10°C/min to observe thermal changes in the samples.

Figure 4.6 shows the thermograms of the lipogels prepared using liquid paraffin and various amounts (5−20%) of MgSt. The thermograms of lipogels were different, each showing one endotherm except lipogels containing 20% MgSt, which showed two endotherms peaking at different temperatures. However, enthalpy values of all

lipogels were rather similar (Table 4.5). There appeared to be a general trend of endotherm shift to the left with an increase in the MgSt concentration in the lipogels (Fig. 4.6).

The lipogels containing 5–15% MgSt showed one broad endotherm each peaking between 86°C and 100°C. Lipogels with 10% MgSt showed a broad endotherm peaking at 88°C with a shoulder at 86°C. There appeared to be a small thermal event at 80°C with no specified peak. Lipogel containing 12.5% MgSt showed a broad endotherm peaking at 86°C. Lipogel containing 15% MgSt showed a high temperature extremely broad endotherm peaking at 91°C with a shoulder at 84°C (Fig. 4.6). Lipogel containing 20% MgSt showed two broad endotherms peaking at 78°C and 86°C.

Figure 4.7 shows the DSC thermograms of the lipogels prepared using the three different batches (1–3) of MgSt. All lipogels showed rather similar thermal events occurring at similar temperatures *i.e.* broad doublets peaked between 85 and 100°C. However, all lipogels showed changes in the thermal events with storage (data not shown).

Table 4.5: DSC data showing peak temperatures and enthalpy values for various lipogels.

Sample Type	Peak temperature (T^{o}C)	Enthalpy (J/g)
L^{5}	99.0	-2.0
L$^{7.5}$	89.4	-2.5
L^{10}	88.1	-2.5
L$^{12.5}$	86.0	-5.0
L^{15}	91.0	-3.7
L^{20}	78.0, 85.9	-4.8 (total)
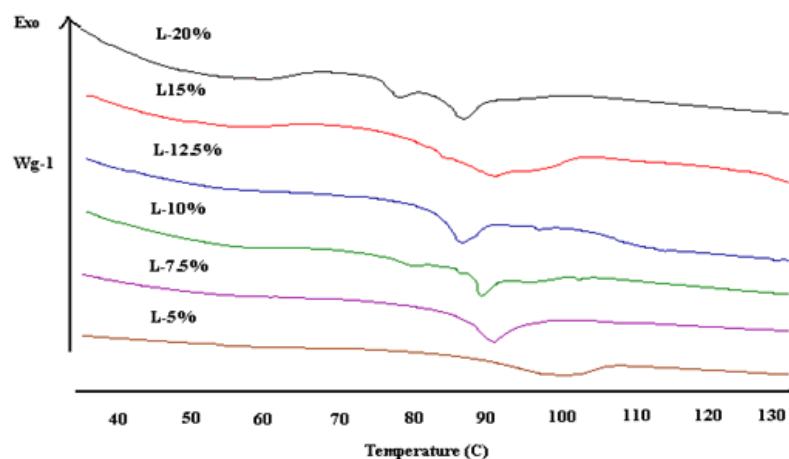
Figure 4.6: DSC (822^e) thermograms of the lipogels of liquid paraffin and various amounts (5−20%) of MgSt on day 1.
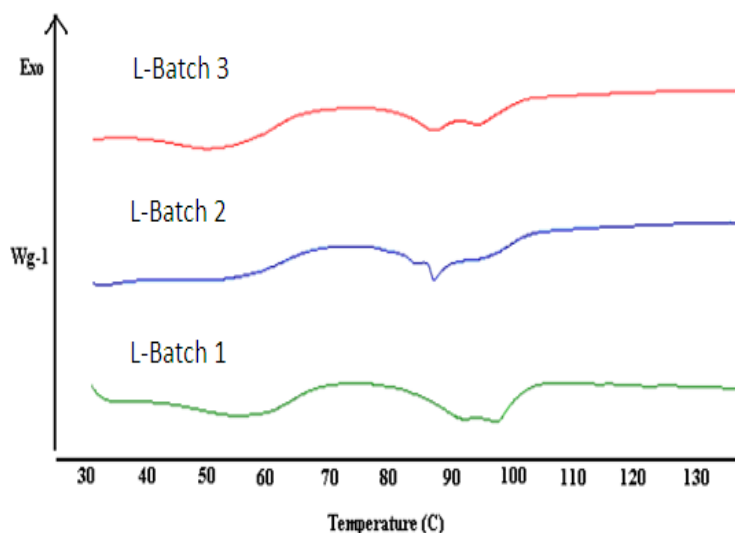
Figure 4.7: DSC (822^e) thermograms of the lipogels prepared using liquid paraffin and the three different batches of MgSt on day 1.

Batch 1 showed a doublet, peaking at 90 and 94°C respectively on day 1. The endotherm on day 2 also showed a doublet peaking at a bit lower temperature (86 and 92°C respectively). A broad endotherm was observed on day 3 peaking at a bit lower temperature (86°C) than day 1 and day 2. On day 4, a very broad endotherm was observed peaking at 95°C with a shoulder at 99°C.

The thermal events for the lipogels prepared using batch 2 of magnesium stearate were quite similar to those observed in the lipogels of batch 1 (Fig. 4.7). The lipogels showed a broad endotherm on each day peaking between 86°C and 90°C. There was a very broad endotherm on day 1 peaking at 90°C. A doublet on day 2 looked very similar to the corresponding endotherm of the lipogels of batch 1 peaking between 86°C and 92°C (not shown). The lipogels on day 3 showed a broad endotherm peaking at 90°C with a shoulder at 95°C. On day 4, there was a very broad endotherm peaking at 92°C with a shoulder at 85°C.

Batch 3 also showed only one broad endotherm on each day, as did the lipogels of other batches, peaking between 90°C and 96°C (Fig. 4.7). The lipogel on day 1 showed a broad doublet peaking between 92°C and 97°C. The doublet looked similar to the endotherm seen on day 2 of the lipogels of both batches 1 and 2.

Figure 4.8 shows the DSC thermograms of the lipogels prepared using various hydrates of magnesium stearate. All lipogels of various hydrates were very different from each other, each showing one to two distinct, small to extremely broad endotherms peaking between 87°C and 115°C depending on the hydrate used. In addition, at least one lipogel also showed endotherm with high temperature shoulder.

The lipogel obtained from anhydrate of pure homologue (pMgSt$_A$) showed an extremely broad endotherm peaking at ~87.5^{o}C with a broad shoulder at ~100°C. In contrast, the lipogel obtained from the trihydrate pure homologue (pMgSt$_H$) showed an extremely broad endotherm peaking at ~92.5^{o}C and did not show any shoulder (Fig. 4.8a). The enthalpy values of the lipogels obtained form pMgSt$_H$ were slightly higher than the lipogels of pMgSt$_A$ (not shown).

The lipogels obtained from pseudopolymorphs of mixed homologue (cMgSt) were also different from each other. The lipogel of dihydrate mixed homologue (cMgSt) showed two endotherms peaking between 95.2^{o}C and 115.9^{o}C (Fig.4.8b). The first endotherm was very small with low enthalpy. The second distinct, high temperature extremely broad endotherm (115.9^{o}C) was not seen in any other lipogel. In contrast, the lipogel of anhydrate (cMgSt$_A$) showed one distinct, very broad endotherm peaking at ~97.4^{o}C (Fig. 4.8b). Furthermore, the lipogels obtained from hydrated

mixed homologues (cMgSt$_H$, cMgSt$_{AH}$) showed very small endotherms of very low enthalpy peaking between 80 and 90°C (Fig. 4.8b). The lipogels of mixed homologue pseudopolymorphs did not show any discernible pattern in the enthalpy values.
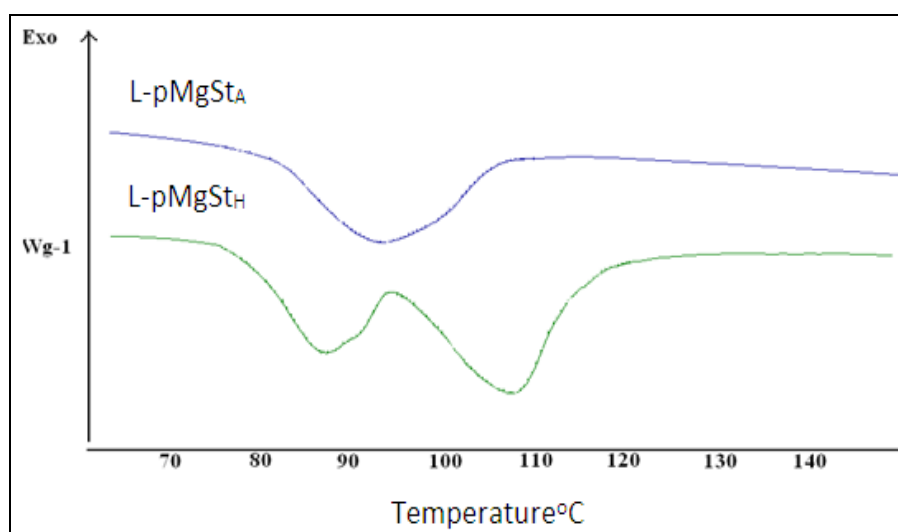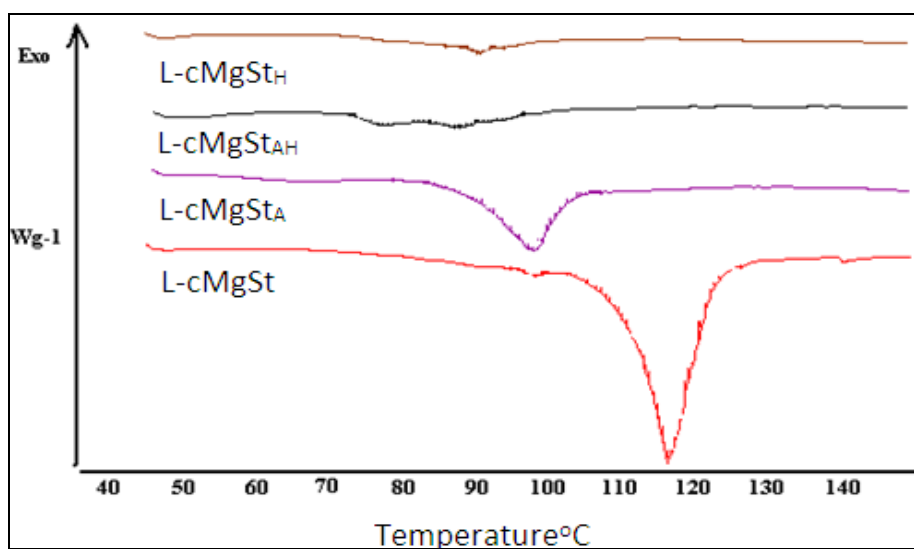
(a)

(b)

Figure 4.8: DSC (823^e) thermograms of the lipogels prepared using various pseudopolymorphs of magnesium stearate (a) pure homologue and (b) mixed homologue.

4.3.6.4 Thermogravimetric analysis (TGA)

TGA was used for the analysis of the weight loss in the lipogels prepared using various hydrates of MgSt and variation in the batch of MgSt.

All lipogels showed very small amount of weight loss from 0.002–1.2% (Table 4.6). However, there was a significant difference in the weight loss amongst various lipogels.

The lipogels prepared using liquid paraffin and various amounts of magnesium stearate showed very little weight loss (between 0.002% and 0.38%) compared to raw material (magnesium stearate– 4.1451%) and no discernible pattern was observed with an increase in MgSt concentration (Table 4.6). Lipogel containing 7.5% MgSt showed 0.33% weight loss compared to 0.38% weight loss observed in the lipogel containing 15% MgSt. In contrast, lipogel containing 12.5% MgSt showed negligible weight loss *i.e.* 0.002% (Table 4.6).

The lipogels prepared using the three different batches of MgSt appeared to be similar in appearance after TGA experiment. Although, lipogel of batch 1 showed significantly higher weight loss compared to the lipogels of other two batches however, the three lipogels showed very little weight loss compared to magnesium stearate (Table 4.6).

Table 4.6: TGA data showing weight loss from various lipogels.

Type of sample	Weight loss (%)	Type of sample	Weight loss (%)
L^5	Not calculated	$L–cMgSt_{B2}$	0.005
$L^{7.5}$	0.330	$L–cMgSt_{B3}$	0.006
L^{10}	Not calculated	$L–pMgSt_A$	0.620
$L^{12.5}$	0.002	$L–pMgSt_H$	0.871
L^{15}	0.380	$L–cMgSt_A$	0.529
$L–cMgSt_{B1}$	0.087	$L–cMgSt_H$	1.233

Figure 4.9 shows the TGA plots of the lipogels prepared using anhydrate and dihydrate of mixed homologue MgSt (cMgSt$_A$ and cMgSt$_H$). All lipogels showed varying amounts of weight loss. Furthermore, the weight loss appeared to occur only in one step. The lipogels also showed weight loss starting at different temperatures. Generally there was an increase in the weight loss from the lipogels with an increase in the moisture content of the MgSt used (Table 4.6). In addition, the lipogels prepared using dihydrate of mixed homologue (cMgSt$_H$) showed higher weight loss than the lipogels of trihydrate pure homologue (pMgSt$_H$). The lipogels prepared using anhydrates (pMgSt$_A$ and cMgSt$_A$) showed weight loss only after 100°C (Fig. 4.9a). In contrast, the lipogels containing di (cMgSt$_H$) and trihydrate (pMgSt$_H$) showed weight loss starting at ~75–80°C (Fig. 4.9b).
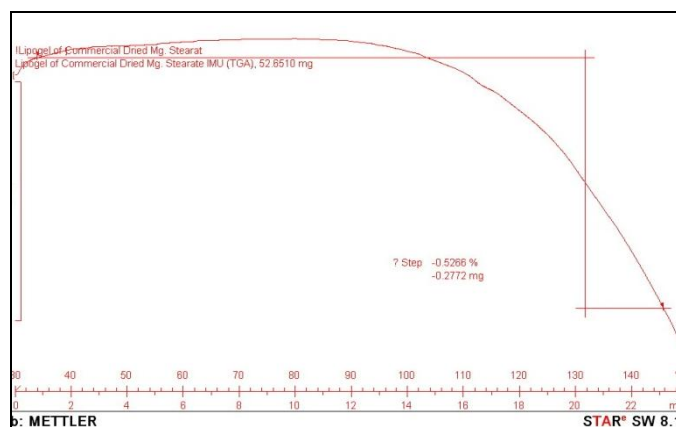
(a)
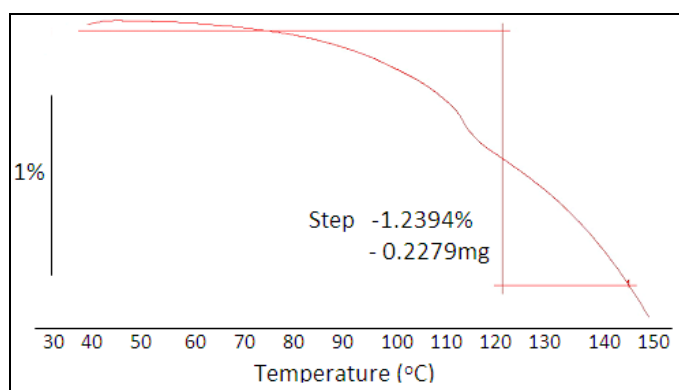
(b)

Figure 4.9: TGA plots of the lipogels of mixed homologue magnesium stearate (a) anhydrate (cMgSt$_A$) and (b) dihydrate (cMgSt$_H$) using a heating cycle of 30–150°C@10°C/min.

4.3.6.5 Fourier transform Infrared (FTIR) spectroscopy

Figure 4.10 shows the FTIR spectra of the lipogels prepared using various hydrates of pure and mixed homologue MgSt. All samples showed numerous peaks appearing at various frequencies. No changes were observed in the FTIR spectra of the lipogels except at the 1590cm^{-1}. $cMgSt_A$ and $cMgSt_H$ showed a distinct sharp peak of varying intensity at 1590cm^{-1}. The peak in the lipogels of cMgSt showed higher intensity compared to the lipogels of $cMgSt_A$ or $cMgSt_H$ (Fig. 4.10b). This peak was not seen in the lipogels of pure homologue MgSt ($pMgSt_A$ and $pMgSt_H$). No other differences were observed and all lipogels showed similar peaks at 2900cm^{-1}, 1450cm^{-1}, 1390cm^{-1} and 700cm^{-1} (Fig. 4.10a and b).
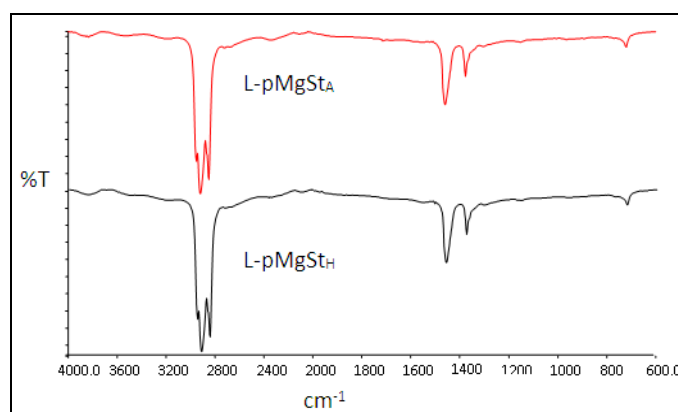
(a)
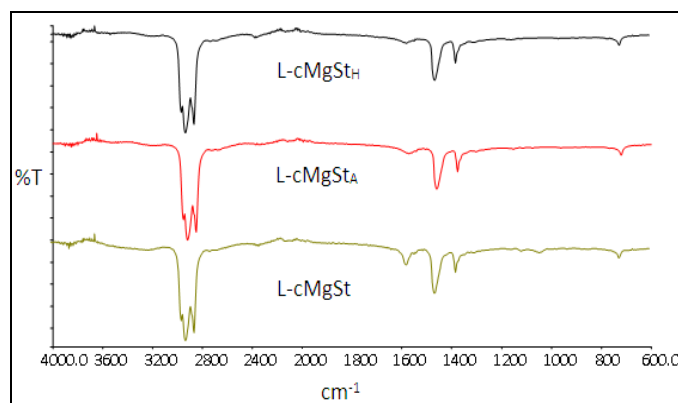
(b)

Figure 4.10: FTIR spectra of the lipogels prepared using various pseudopolymorphs of magnesium stearate (a) pure homologue and (b) mixed homologue.

4.**3.6.6 X–ray diffraction (XRD)**

Figure 4.11 shows the XRD diffractograms of the lipogels prepared using various hydrates of pure and mixed homologue MgSt. All lipogels appeared to be different from each other, each showing numerous peaks between 3° and 25°.

There appeared to be a discernible pattern of increase in the intensity and sharpness of the peaks at $21–24^o$ with an increase in the moisture content of mixed homologue MgSt *i.e.* the lipogel of dihydrate ($cMgSt_H$) showed sharp peaks of high intensities compared to the lipogel of anhydrate ($cMgSt_A$), which showed a broad doublet. Furthermore, both lipogels showed similar peak at $2\theta=5^o$. The lipogel prepared using trihydrate pure homologue ($pMgSt_H$) showed a broad doublet at $2\theta=21^o$ in addition to sharp peaks at $2\theta=5^o$.
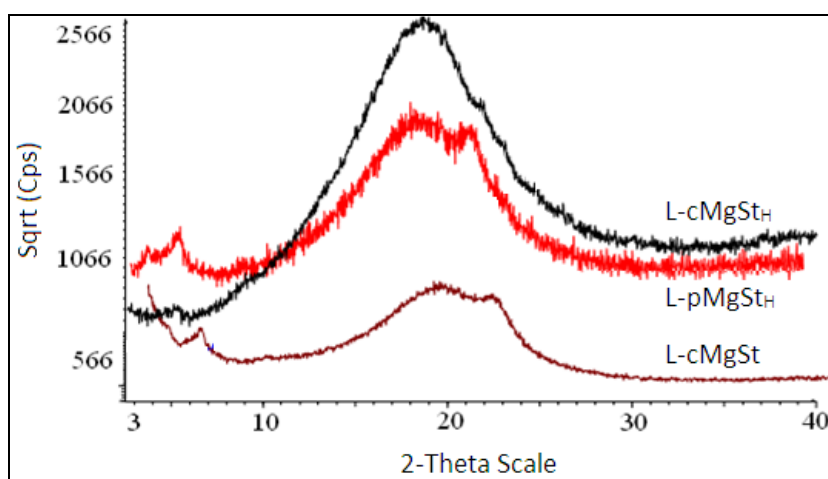
Figure 4.11: XRD diffractograms of the lipogels prepared using liquid paraffin and various hydrates of mixed and pure homologue MgSt.

4.3.6.7 Texture profile analyses

Texture analyses were performed to evaluate the mechanical properties of the homogenised lipogels prepared using various amounts of magnesium stearate (5–15%) and the liquid paraffin.

Figure 4.12 shows the mechanical properties such as hardness, cohesiveness, consistency and index of viscosity of lipogels. There was an increase in the

mechanical properties of homogenised lipogels with increasing MgSt concentration (Fig. 4.12).
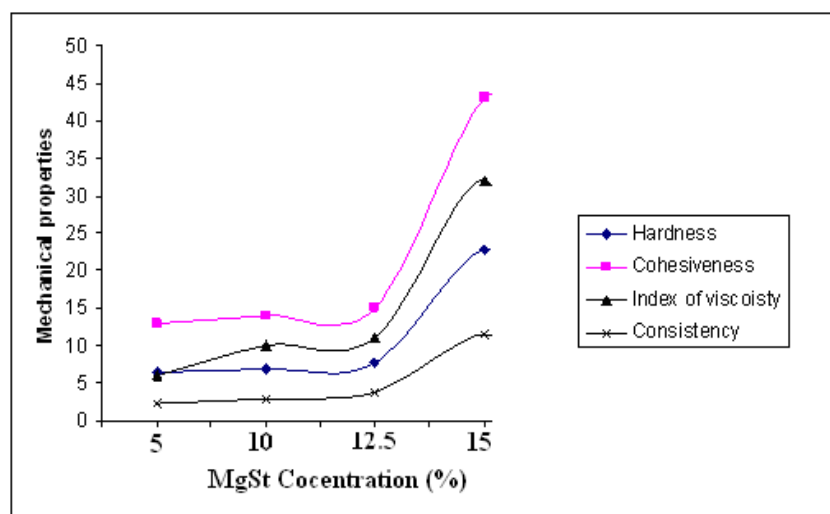
Figure 4.12: Mechanical properties of the lipogels of liquid paraffin and various amounts of MgSt (5−15%) homogenised.

4.4 Discussion

Solid lipogels were prepared using 12.5% of commercial (mixed homologue dihydrate) magnesium stearate in liquid paraffin using Scric's method. Scric's method involves dispersing the magnesium stearate in the liquid paraffin in a glass beaker using glass rod, heating to a preset (130°C) temperature, holding for 30−60 minutes and cooling the dispersion at 5−10°C/min to room temperature. In addition, the influence of various concentrations (2.5−20%) of commercial (mixed homologue dihydrate) MgSt, batch type and the effect of various pseudopolymorphic forms of mixed (anhydrate and dihydrate) and pure homologue (anhydrate and trihydrate) MgSt on the stability of the lipogels was also investigated.

All lipogels prepared either by Scric's method or using the three different batches of commercial MgSt, various concentrations of MgSt (2.5−20%), anhydrate and hydrate of mixed homologue MgSt appeared to be unstable opaque solids showing varying degree of syneresis and crumbled to touch except lipogels of pure homologue MgSt (anhydrate and trihydrate) which appeared to be stable semisolids.

All concentrations (2.5−20%) of MgSt resulted in opaque solids with syneresis. However, maximum syneresis was seen at low concentration and vice versa. Furthermore, concentration above 10% showed much less syneresis. This observation was supported by microscopy and DSC results. Lipogels containing 12.5−20% MgSt showed presence of Maltese crosses, which have been related to the existence of α−crystalline lamellar gel structure (Eccleston, 1986). Therefore, reduction in syneresis with an increase in concentration of MgSt may be due to the presence of lamellar phases in the lipogels. However, microscopy does not explain the solid nature of the lipogels. The DSC results also showed a slight shift to the left in the endotherm temperature with an increase in the MgSt concentration. The low temperature, high enthalpy endotherms have been related to the stable formulations (Lindenbaum *et al*., 1985; Lin *et al*., 1994)**.** However, we observed no differences in the enthalpy values of the lipogels. These results suggest that MgSt concentration plays a role in reducing syneresis but does not affect the solid nature of the lipogels. Therefore, 12.5% concentration was selected as optimum concentration for further work on lipogels (chapter V) as it produced least syneretic, slightly elastic solid lipogels.

The solid nature of lipogels can be attributed to the mainly amorphous state of MgSt as explained by XRD results. The solid lipogels showed a broad peak at $2\theta=21–24^{o}$ as no sharp peak was observed, suggesting very little swelling of the lipogels. The broad peaks are related to the amorphous nature and sharp peaks to the crystalline (Gunstone, 1967). Therefore, it is suggested that hydrated MgSt in the dispersion upon heating to high temperature may have been converted to amorphous form giving the formulation solid appearance. Amorphous materials are easy to disintegrate and penetration of the solvent is rather easier due to lack of any ordered structure compared to the crystalline materials (Garti *et al*., 1982; Leinonen *et al*., 1992). The lipogel structure was brittle, fragile and crumbled to touch. Due to lack of water, lamellar structure was not fully developed and the lipogels showed syneresis as a consequence.

The three different batches of commercial mixed homologue dihydrate MgSt were also used to investigate influence of batch type on the stability of lipogels. The

lipogel of batch 1 was opaque solid on preparation day. In contrast, batches 2 and 3 produced transparent solid lipogels. However, both lipogels (batch 2 and 3) also changed to opaque solids after two days. The differences in appearance on preparation day may be due to the moisture content of the lipogels as the lipogel of batch 1 showed significantly higher moisture content compared to lipogels of batches 2 and 3.

Our observations of the lipogels after TGA experiments support this view that differences in moisture content can affect the structure of the lipogels. TGA experiments are conducted in open pans and the weight loss, which may be due to moisture, is expected.

We observed differences in the visual appearance of the lipogels (in the TGA crucibles) at the end of the TGA experiments. The solid, opaque lipogels prepared using the batch 1 of magnesium stearate became solid, clear (transparent) lipogels. The lipogels using batch 1 of magnesium stearate also showed more weight loss compared to the clear lipogels prepared using batches 2 and 3 of magnesium stearate. This supports the view that the loss of moisture changes the structure of the lipogels by changing them from opaque to clear.

The influence of absorption of moisture from the environment on the properties of lipogels was also investigated by preparing lipogels in the DSC pans using various heating and cooling cycles under nitrogen. All lipogels appeared to be clear solids, suggesting that controlled environment irrespective of heating or cooling cycle produce clear lipogels. The opaque lipogels obtained from the batch 1 of MgSt then can be related to the absorption of moisture from the environment upon cooling. This supports the view that the lipogels' appearance *i.e.* clear or opaque is affected by the environmental conditions such as absorption of moisture from the surroundings.

Therefore, any of the three batches of MgSt studied can be used and we selected batch 3 of MgSt for further work on lipogels (chapter V) as batches 1 and 2 were not enough for further work.

After knowing the effect of absorption of moisture on the appearance of lipogels, we investigated the influence of various hydrates of pure homologue (anhydrate and trihydrate) and mixed homologue (anhydrate and dihydrate) MgSt prepared in chapter III by moisture treatment on the properties of lipogels.

The anhydrate of mixed homologue MgSt produced syneretic opaque solid lipogel. In contrast, the anhydrate of pure homologue MgSt produced white fluid dispersion (Fig. 4.2), which slowly thickened to a soft semisolid lipogel upon storage for two weeks at ambient temperature, suggesting differences in the structure of the lipogels although both prepared using anhydrates.

The hydrated samples of pure and mixed homologue MgSt also produced lipogels of different consistency. The dihydrate of mixed homologue MgSt produced syneretic opaque solid lipogel whereas trihydrate of pure homologue MgSt produced stress sensitive semisolid lipogels.

Surprisingly, the lipogels prepared using both anhydrate and dihydrate of mixed homologue MgSt were similar in appearance (showing opaque syneretic solids). These results suggest that hydration state of mixed homologue MgSt have no influence on the properties of the resultant lipogels. In contrast, hydrated sample of pure homologue MgSt produced unstable semisolid lipogels. The semisolid lipogels changed to fluids upon gentle stirring showing plate−like crystals, implying pressure sensitivity. Eccleston, (1986) showed existence of plate−like crystals in the unstable aqueous semisolids containing stearic acid, suggesting disruption of α−crystalline lamellar structure. Same analogy can be used to explain the pressure sensitivity of the unstable semisolid lipogels.

It has been suggested that the moisture treatment of MgSt produces different pseudopolymorphic form affecting its physical properties (Miller and York, 1985; Rajala and Laine, 1995; Swaminathan and Kildsig, 2001; Okoye and Wu, 2007) and the formation of different pseudopolymorphs is attributed to the changes in the moisture content (Ertel and Carstensen, 1988a and b; Rajala and Laine, 1995; Bracconi *et al*., 2005). The commercial MgSt is available as monohydrate and exposure to 100% humidity slightly increases the moisture content but does not

change the hydration level *i.e.* remains as monohydrate (Okoye and Wu, 2007). However, increase in the moisture content significantly affects the properties of the MgSt as different pseudopolymorph is formed with increased moisture content.

We obtained similar results with pure homologue MgSt upon moisture treatment *i.e.* hydrated sample was different pseudopolymorph than the anhydrous material producing stable semisolid lipogel on the day of preparation. It is suggested that the white dispersion of anhydrous pure homologue MgSt may have absorbed moisture from the atmosphere hydrating the anhydrous form of MgSt to produce soft semisolid lipogel as a consequence. However, although moisture treatment of commercial MgSt produced different pseudopolymorphs of varying hydration level but they showed no effect on the properties of lipogels *i.e.* all produced syneretic solids.

Scric *et al*., (1988), produced stable lipogels using MgSt with higher moisture content. Our results on the lipogels of pure homologue trihydrate agreed to the Scric's results. However, the differences in the stability of our lipogels prepared with commercial mixed homologue MgSt from Scric's lipogels may be due to different batch of MgSt rather than moisture content. Therefore, fine tuning of the Scric's method is needed to prepare stable semisolid lipogels using commercial mixed homologue MgSt.

4.5 Conclusions

1. Solid systems (syneresis) of MgSt and liquid paraffin were obtained using Scric's standard heating and cooling method using various concentrations (2.5−20%) of MgSt. However, increase in MgSt concentration reduced syneresis up to 10% MgSt after which there was no reduction in the syneresis with an increase in the MgSt concentration. However, 12.5% concentration was selected as optimum concentration as slightly elastic systems were obtained at this concentration and will be used for further work in chapter V.

2. The solid nature of the lipogels may be related to the conversion of crystalline form of MgSt to the mainly amorphous form upon heating to high temperature. At

high temperature, crystalline material changes to amorphous form loosing its ordered structure causing syneresis upon cooling.

3. The three different batches of mixed homologue dihydrate MgSt produced syneretic opaque to transparent solid lipogels. The appearance of lipogels depended on the amount of moisture absorbed from the atmosphere upon cooling. The lipogels with more moisture appeared opaque and the lipogels with low moisture showing transparent appearance.

4. The hydrates of pure homologue (anhydrate and trihydrate) and mixed homologue (anhydrate and dihydrate) MgSt influenced lipogels differently. The pure anhydrate homologue produced white fluid dispersions, which changed to soft semisolid upon storage. The pure trihydrate homologue produced unstable semisolid lipogels, which changed to fluids upon gentle stirring, implying pressure sensitivity. In contrast, both (anhydrate and dihydrate) mixed homologue MgSt produced syneretic solid lipogels.

5. All lipogels prepared in the DSC pans using various programmed heating and cooling cycles produced transparent solid lipogels, suggesting that the appearance of the lipogels is affected by the absorption of moisture from the atmosphere instead of heating or cooling cycles.

CHAPTER V

PREPARATION OF LIPOGELS: INFLUENCE OF PREPARATION VARIABLES

5.1 Introduction

In the previous chapter it was shown that the lipogels prepared using 12.5% mixed homologue dihydrate magnesium stearate produced little syneresis but were crumbly solids. In contrast, Scric found that 12.5% MgSt produced stable semisolid lipogels. The difference may be due to different batch of MgSt and thus Scric's method may need to be fine tuned. Therefore, the aim of this chapter was to explore the influence of heating, cooling and homogenisation on the quality of lipogels using Scric's method. From this data an improved method (with variation in the Scric's method) was developed and the influence of water, homogenisation and phosphate buffer solution (PBS) on lipogels prepared by the new method was investigated.

5.1.1 Aims of the chapter

The present chapter explores the influence of various process variables on the preparation of lipogels. The overall aims include:

1. To investigate influence of various processing variables such as dispersion technique and heating and cooling, using Scric's method as a template, on the quality of the lipogels.

2. To develop an improved method from Scric's method for the preparation of stable lipogels using mixed homologue MgSt (dihydrate) and liquid paraffin.

5.2 Methods

5.2.1 Preparation of lipogels using variations in the Scric's method

The influence of dispersion technique, heating and cooling (systematically) was investigated on the quality of lipogels prepared using variations of Scric's method (chapter IV, section 4.2.2) as follows:

5.2.1.1 Variation in the dispersion technique

MgSt was dispersed in liquid paraffin using a mortar and pestle instead of the glass rod and beaker. The dispersion was then heated and cooled using the Scric's method as described in chapter IV (section 4.2.2).

5.2.1.2 Variation in the heating method

Heating variables were investigated on dispersions of 12.5% MgSt in liquid paraffin prepared by Scric's method. After heating all samples were cooled using Scric's cooling method (fast cooling). The heating variables include the following:

i. The oil–bath was heated to 130^oC, and then the dispersion placed in the oil–bath and heated at 130^oC for 60 minutes.

ii. The dispersion was placed in the oil−bath and heated to 130^oC for 90 minutes instead of 60 minutes.

iii. The liquid paraffin was heated in the oil–bath to 130^oC, and then MgSt stirred in.

iv. The dispersion was stored at room temperature for one week, and then heated in the oil-bath to 130^oC for 60 minutes.

v. The dispersion was stored at room temperature for one month, and then heated using the same method as above in iv.

vi. The dispersion was stored at ambient temperature (28 ± 3^oC) for a month and not heated at all.

5.2.1.3 Variation in the cooling method

The influence of varying types of cooling was investigated on the quality of lipogels using dispersions prepared and heated by Scric's method as described in chapter IV (section 4.2.2) as follows:

i. Slow cooling– The dispersion was left in the oil–bath to cool naturally (~0.1–0.2^{o}C/min) to room temperature.

ii. Shock cooling– The dispersion was removed from the oil–bath at 120°C, and placed in an ice box (beaker filled with ice) to cool.

iii. Cooling under controlled humidity– At 120°C, the dispersions were transferred to the desiccators maintained at various humidity levels *i.e.* 100% humidity, 50% humidity and 0 % humidity, and then allowed to cool to room temperature.

iv. Cooling under stirring– The dispersion was heated and cooled with continuous stirring using an overhead stirrer at a speed between 200–500rpm.

5.2.2 Preparation of lipogels by improved methods

The fixed amount (12.5g) of pure (anhydrate and trihydrate) and mixed (anhydrate and dihydrate) homologue MgSt was weighed and dispersed in 87.5g of liquid paraffin in a 250mL glass beaker by stirring with a glass rod, to obtain 100g dispersion. The dispersion was heated in an oil–bath (IKA–Werk–HB4, Germany) at a rate of ~5–10°C/min to 110°C, and then held at 110°C for 1–2 hours with continuous stirring using an overhead stirrer (IKA–Werk–RW–16B, Germany) at 200rpm. The dispersion was then left in the oil–bath and allowed to cool naturally (slow cooling) to ambient temperature (28±3°C) under stirring.

Dispersions containing mixed homologue MgSt (anhydrate and dihydrate) were treated using either of the two following methods *i.e.* by adding water to the cooling dispersions or by homogenisation of the cooled dispersions. The use of these two different methods upon cooling produced good results. Therefore, both of them can be used as the standard methods.

i. Addition of water upon cooling (method 1)

The heating of dispersion was carried out as described above. Upon cooling at 90$^{\text{o}}$C, 1–4% distilled water was stirred in the cooling dispersions, and then allowed to cool naturally in the oil–bath to room temperature with continuous stirring.

Upon cooling to room temperature, the formulations were stored in screw–capped plastic bottles and the effect of storage time was investigated on the day of preparation, after a week, a month and after three (3) months.

ii. Homogenisation upon cooling (method 2)

The heating of dispersion was carried out as described above. Upon cooling to 45$^{\text{o}}$C, the dispersions were homogenised using Ultra Torrax Homogeniser, UK at 8000 rpm/min for 15–20 minutes.

5.2.3 Polarised light microscopy

The controls prepared using slow and fast cooling (Scric's method) in addition to the lipogels prepared by method 1 (1−4% water) were studied by polarised light microscopy using a Polyvar microscope. The same method of sample preparation and visualisation under microscope was used as described in the section 2.2.2.1. The photomicrographs were taken using digital and manual SLR film cameras attached to the microscope.

5.2.4 Hot stage microscopy

A TMS 91 hot stage (Linkam Scientific Instruments, UK) attached to the Polyvar microscope was used to investigate the lipogels prepared by homogenisation (method 2) and solid lipogels cooled without adding water or homogenisation (Scric's method). The same method of sample preparation and visualisation under microscope was used as described in the section 2.2.2.2 using a standard method of heating from 25$^{\text{o}}$C to 140$^{\text{o}}$C at a rate of 5$^{\text{o}}$C/min. Thermal changes at various temperatures were recorded and photographed using digital and manual SLR film camera attached to the microscope.

5.2.5 Scanning electron microscopy (SEM)

A Leo 1450VP electron Microscope (Oxford Instruments, UK) was used to study the structure of the lipogels prepared by homogenisation (method 2) and Scric's method (unhomogenised). The lipogels were studied directly without gold coating, by placing a small sample on the stub using cold plate under low vacuum. Each sample was studied at powers between x 15 and x 5000, and photographed at appropriate magnifications.

5.2.6 Differential Scanning Calorimetry (DSC)

A DSC 822^e (Mettler Toledo, Leicester, UK) was used for the analysis of fast and slow cooled controls using a standard heating cycle of $25^oC–150^oC$ at a rate of $10^oC/min$. A DSC 823^e was also used to study thermal changes in the lipogels prepared under controlled humidity environment, and the lipogels prepared by methods 1 and 2 in addition to the dispersions prepared using two different methods (not heated). The results were plotted together after normalisation to eliminate the weight bias due to the weight differences of the samples.

5.2.7 Thermogravimetric analysis (TGA)

The TGA/SDTA851^e (Mettler Toledo, Leicester, UK) was used for the analysis of slow and fast cooled (Scric's method) controls.

Approximately 25–45mg of each sample was carefully weighed in 70µL aluminum crucibles and placed in the machine. A standard heating cycle of $30^oC – 150^oC$ at a rate of $5^oC/min$ was selected to achieve optimal weight loss. The experiments were conducted under dry nitrogen. The results were plotted together after normalisation to eliminate weight bias due to the weight differences of the samples.

5.2.8 Rheology

A cone and plate Physica MCR 301, air–bearing Pelletier rheometer (Anton Paar, Germany) was used to investigate the flow curves of the lipogels prepared by methods 1 and 2.

The dimension of the measuring plate was 50 mm and the zero gap was fixed to be 1mm. All experiments were conducted at room temperature (~28°C).

Flow curves were obtained using shear rate vs shear stress experiments to investigate the zero shear and apparent viscosities of the lipogels. Flow curves were obtained using up and down curves with minimum shear rate of 10^{-3} (s^{-1}) and maximum of 10^{2} (s^{-1}).

5.2.9 X-ray diffraction (XRD)

A powder X–ray diffractometer (Bruker 8 Advances, Germany) was used for the analysis of the lipogels prepared by method 1 (1−4% water) using the same method as described in chapter III (section 3.3.4.8).

5.2.10 Accelerated stability centrifuge test

A LumiFuge LF111 stability analyser (L.U.M. GmbH, Berlin, Germany) was used for the accelerated stability analyses of the lipogels containing liquid paraffin and MgSt prepared by method 1 (1−4% water). Approximately 0.5ml of each sample was filled into rectangular 2.1mm polycarbonate cells. The experiments were conducted at two different speeds i.e. 1500rpm (328xg) and 4000rpm (2300xg) for 2 and 15 hours respectively. The measurements were recorded every 30 and 211 sec respectively. All measurements were conducted at 25°C.

5.3 Results

5.3.1 Visual appearance of lipogels using variations in the Scric's method

5.3.1.1 Appearance of lipogels prepared using variation in the dispersion preparation technique

The dispersions were prepared using mortar and pestle instead of the glass rod and beaker. The lipogels were similar in the appearance to the one prepared using glass rod (Scric's method). Furthermore, the dispersions prepared by two different methods and analysed by DSC prior to heating also showed similar thermal events

(*c.f.* DSC results Fig. 5.5) suggesting that dispersion preparation technique does not influence the quality of the lipogels.

5.3.1.2 Appearance of lipogels prepared using variation in the heating method

Different types of heating methods were used to investigate the influence of heating type on the appearance and consistency of the lipogels. Upon heating, all lipogels were cooled using Scric's cooling method (5−10°C/min):

i. The oil–bath was heated to 130°C, dispersion placed in the oil–bath and maintained at 130°C for 60 minutes. Intense foam was produced in couple of minutes and therefore significantly less time was required to obtain foam–free solution using this method. However, this type of heating resulted in the solid, opaque lipogels upon cooling and showed some syneresis.

ii. The same heating method was used as above but the dispersion was held at 130°C for 90 minutes instead of 60 minutes. The solid, clear lipogels prepared were similar to the lipogels prepared using the method (i). However, the lipogels of method (ii) showed more syneresis (visual observation) than lipogels prepared using method (i).

iii. The liquid paraffin was heated in the oil–bath to 130°C, and then MgSt stirred in. MgSt dissolved in the liquid paraffin quickly producing foam in the same fashion as observed in method (i) and produced lipogels of similar consistency (solid syneretic lipogels).

iv. The dispersion was stored at room temperature for one week. The dispersion separated into two distinct phases *i.e.* lower solid phase like lump of powder and upper liquid phase. However, little agitation of the two phases produced a homogenous dispersion, which upon heating and cooling produced syneretic solid lipogels.

v. The dispersion was stored at room temperature for one month, and then heated using the standard method. The dispersion separated into two phases like in (iv). However, the lower layer appeared like a thick cream instead of a lump of solid powder. Upon agitation of two phases, the bottom creamy layer started detaching

from the base of the container slowly and dispersed in the liquid phase to form homogenous dispersion. However, upon heating and cooling similar observations were recorded as described for the other heating methods producing syneretic and solid lipogels.

vi. The dispersion was stored at room temperature and not heated at all. Upon storage, the dispersion separated into two phases as described in the above method producing semisolid bottom layer and top liquid phase. After one month storage, the top liquid layer was decanted to a separate beaker and the bottom phase clearly observed to be a nice semisolid elastic gel.

5.3.1.3 Appearance of lipogels prepared using variation in the cooling method

The dispersions after heating to 130^oC and holding for 60 minutes were cooled in different ways to investigate the effect of cooling type on the appearance, consistency and physical stability (syneresis) of the lipogels as follows:

i. Slow cooling

Upon cooling, the dispersion was left untreated in the oil–bath to cool naturally ($\sim$0.1–0.2^oC/min) to room temperature. Upon cooling to room temperature, clear, solid, slightly elastic, non–syneretic lipogels were formed. However, upon storage for four months slight syneresis was observed.

Although, lipogels obtained from slow and fast cooling methods appeared similar (solid) but their thermal behaviour and microscopic appearance were very different (*c.f.* results microscopy (Fig. 5.1) and DSC (Fig. 5.6)).

ii. Shock cooling

The dispersion was removed from the oil–bath at 120^oC, and placed in an ice box (beaker filled with ice) to cool. The dispersion became solid and opaque immediately after placing in the ice box. Upon storage for one day, the lipogel showed significant syneresis and did not change with time.

iii. Cooling under controlled humidity

The lipogels were cooled in the controlled humidity (100%, 50% and zero%) to room temperature. The lipogels appeared to be solid and crumbled to touch. However, the solid lipogel cooled at 100% humidity when triturated using glass rod produced thick structured fluid, which changed to semisolid lipogel after three (3) months of storage time. Nevertheless, these lipogels did not show syneresis upon storage. In contrast, the dispersions cooled under zero% or 50% humidity produced solid, syneretic lipogels.

iv. Cooling with stirring

The lipogels were prepared by continuous stirring using an overhead stirrer at 200rpm. Upon cooling to 70°C, the formulations showed sign of thickening and the speed was increased to 500rpm. Upon further cooling to 50°C, the formulation became more viscous and it was difficult to stir the resultant soft solid lipogel. Therefore, the stirring was stopped and the soft solid lipogel was allowed to cool naturally to room temperature in the oil–bath.

The resultant dispersions appeared to be soft solid lipogel, different from other solid lipogels in consistency. Upon storage for two days, the soft solid lipogel showed significant syneresis. However, further storage at room temperature, showed little changes with time.

5.3.2 Visual appearance of lipogels prepared by methods 1 and 2

The lipogels were prepared using 12.5% pure homologue (anhydrate and trihydrate) and mixed homologue (anhydrate and dihydrate) MgSt in liquid paraffin. Heating of dispersions to 110°C and holding for 1–2 hrs produced foam–free translucent dispersions.

Upon cooling, opaque dispersions of pure homologue MgSt (trihydrate) produced significantly stress sensitive semisolid lipogels *i.e.* which changed to fluids upon gentle stirring. However, after storage for 3 days at ambient temperature structured fluids changed back to the semisolid lipogels. In contrast, pure homologue

(anhydrate) upon cooling produced structured fluids. However, structured fluids after storage for one month at ambient temperature changed to semisolid lipogels. No syneresis is observed in the lipogels of both pseudopolymorphs (anhydrate and trihydrate) to date after two years.

In contrast, semisolid lipogels of mixed homologue MgSt (anhydrate and dihydrate) were prepared by either adding 1−4% water (method 1) or by homogenisation (method 2).

(i) Visual appearance of lipogels prepared by method 1

The dispersions contained 1–4% water, added at 90°C during cooling cycle with continuous stirring, which produced lipogels of varying consistency from structured fluids to semisolid lipogels. Upon cooling to 65°C, opaque solution changed to white dispersion. Further cooling to 45°C with continuous stirring, produced either structured fluid or semisolid lipogel depending on the amount of water. The water (1–2%) produced white, semisolid, non−syneretic, elastic lipogels. In contrast, 3% and 4% water produced white structured fluid. Further cooling to room temperature did not show any changes in the formulations. Upon storage for three days at ambient temperature, all lipogels showed sign of significant thickening. Further storage for three months changed the structured fluids containing 3% and 4% water to semisolid lipogels. All lipogels showed no syneresis to date (two years storage time) at ambient temperature (~28°C).

(ii) Visual appearance of lipogels prepared by method 2

The dispersion cooled to 45°C was homogenised using a homogeniser, which produced semisolid, non−syneretic lipogel. Upon storage, no changes were observed in the consistency of the lipogels and all lipogels remained physically stable for at least 2 year (to date) as no syneresis was observed.

5.3.3 Polarised light microscopy

The lipogels prepared using different cooling methods (fast and slow) in addition to the lipogels prepared using method 1 (1−4% water) were studied by polarised light

microscopy. All lipogels showed significantly different anisotropic structures with many crystals and clusters against dark or glowing background between cross polars. Some lipogels showed Maltese crosses.

Figure 5.1 shows the lipogels prepared with two different types of cooling *i.e.* fast and slow cooled respectively. Both lipogels showed many crystals with background glow. Numerous Maltese crosses were seen in both lipogels. However, the lipogel prepared using fast cooling showed fewer Maltese crosses (Fig. 5.1a). In contrast, the lipogel prepared using slow cooling showed numerous Maltese crosses (Fig. 5.1b).

(a)   (b)
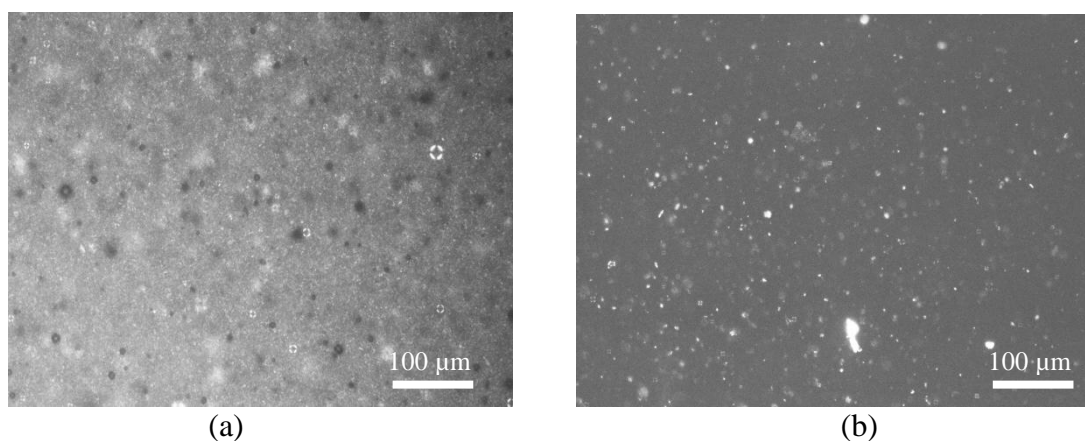
Figure 5.1: Photomicrographs of the lipogels prepared using liquid paraffin and 12.5% MgSt using different cooling methods (a) Fast cooled (b) Slow cooled (1cm=100 μm).

Figure 5.2 shows selected photomicrographs of the lipogels prepared by methods 1 (2% water) and 2 (homogenisation). All lipogels showed different types of anisotropic structures against the dark and glowing background. The stable semisolid lipogels prepared by method 1 (~1−2% water) showed existence of numerous Maltese crosses in addition to the anisotropic crystals (Fig. 5.2a). In contrast, systems containing 3−4% water showed few Maltese crosses in addition to the numerous clusters of anisotropic crystals (not shown). The lipogel prepared by method 2 (homogenisation) showed microstructure similar to the method 1 (1−2% water) having numerous Maltese crosses (Fig. 5.2b).
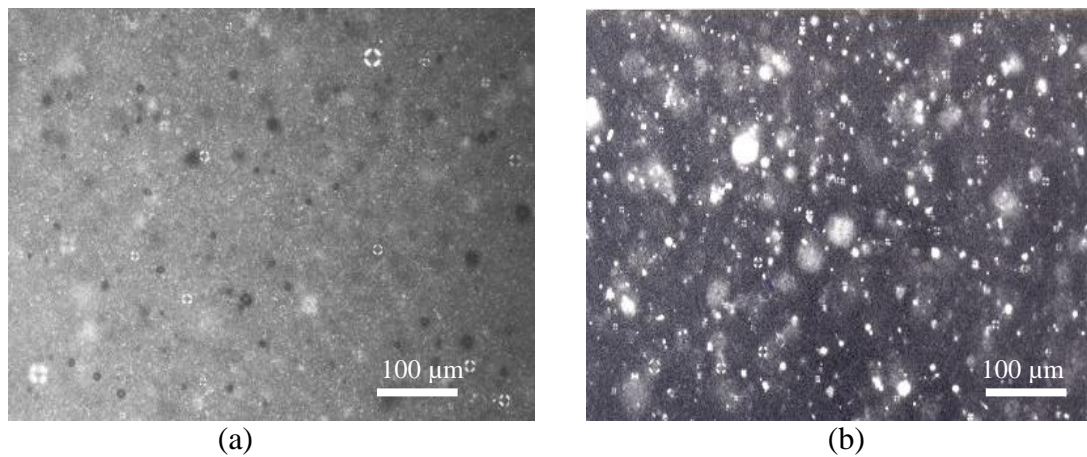
Figure 5.2: Photomicrographs of the lipogels containing MgSt (12.5%) prepared by (a) method 1 (2% water) and (b) method 2 (homogenisation) (1cm=100 μm).

5.3.4 Hot stage microscopy

Hot stage microscopy was used to investigate the lipogels prepared by methods 1 and 2 in addition to the slow and fast cooling controls.

Figure 5.3 shows the photomicrographs of the lipogels prepared by method 1 (2% water). Small crystalline masses were observed with numerous Maltese crosses. The Maltese crosses melted around 120°C. In contrast, small crystals disappeared between 80 and 100°C. However, the complete melt was seen at 120°C (Fig. 5.3b)
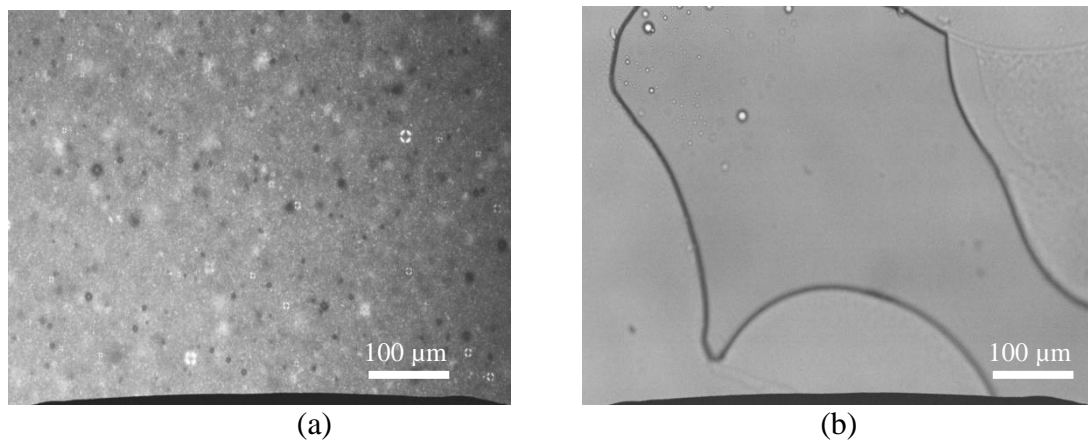
Figure 5.3: Hot stage photomicrographs of the lipogels prepared using improved method with homogenisation (a) at 30°C and (b) 120°C (1cm=100 μm).

146

The lipogels containing liquid paraffin and 12.5% MgSt prepared using fast and slow cooling methods showed numerous crystals with background glow with varying number of Maltese crosses. The small crystals in both lipogels started disappearing around 100°C and 110°C whereas Maltese crosses melted at ~120°C (not shown).

5.3.5 Scanning electron microscopy

Figure 5.4 shows the electron photomicrographs of the lipogels prepared using mixed homologue (dihydrate) MgSt by Scric's method and the lipogels prepared by method 2 (homogenisation). The photomicrographs of both lipogels were different from each other. Generally, there was more structure in the homogenised lipogels (Fig. 5.4a) compared to the unhomogenised (Scric's method) lipogels. Homogenised lipogels showed continuous, ordered mesh–like structure at 500x (Fig. 5.4a). In contrast, unhomogenised lipogel showed rather cloudy, unclear and fractured structure even at 2000X (Fig. 5.4b).

| (a) | (b) |
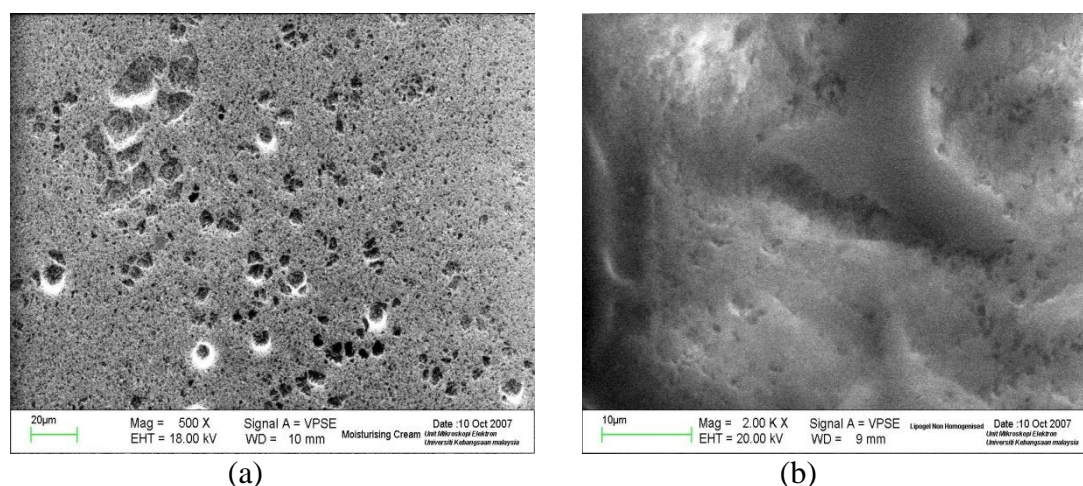
Figure 5.4: Electron photomicrographs of lipogels containing 12.5% mixed homologue dihydrate MgSt prepared by (a) method 2 (homogenisation) and (b) Scric's method.

5.3.6 Differential Scanning Calorimetry (DSC)

The lipogels prepared using various processing variables including method of preparation of dispersion, slow and fast cooled controls, cooling under controlled humidity in addition to the lipogels prepared by methods 1 and 2 were investigated using a standard heating cycle of 25°C–150°C at a rate of 10°C/min to observe

thermal changes in the samples. The thermal properties of all systems are summarised in the Table 5.1.

Table 5.1: DSC data showing peak temperatures and enthalpy values for various lipogels.

Type of Lipogels	T (^{o}C)	ΔH (J/g)
L$^{12.5}$ 60 minutes heating	96.2	-8.1
L$^{12.5}$ 90 minutes heating	110.1	-2.1
L–1% water	85.1	-22.2 (Total)
	111.2	
L–2% water	87.0	-21.6 (Total)
	111.6	
L–3% water	87.6	-25.1 (Total)
	110.6	
L–4% water	89.2	-22.4 (Total)
	111.7	
L-homogenised	86.5,	-34.3
	116.0	
L–cooled at 100% RH	80.2	-6.83 (Total)
	100.2	
	110.4	

Figure 5.5 shows the DSC spectra of the two dispersions prepared using two different techniques of mixing *i.e.* using glass rod (Scric's method) and the mortar and pestle prior to heating. Both dispersions showed two similar endotherms each, peaking between 95 and 115°C. The first small endotherm peaked at 97°C whereas the second high temperature extremely broad endotherm peaked at 111°C suggesting that the two dispersion preparation techniques have similar effect on the thermodynamic activity of the dispersions.

Figure 5.6 shows the DSC spectra of fast (Scric's method) and slow cooled lipogels prepared using liquid paraffin and magnesium stearate. The thermograms of both samples were different from each other. Fast cooled sample showed one endotherm and slow cooled sample showed two endotherms peaking at different temperatures. Both samples showed a high temperature extremely broad endotherm peaking at 98°C. In addition, slow cooled lipogel showed a distinct, low temperature very broad endotherm peaking at 83°C, which was not seen in the fast cooled lipogel. In

addition, the enthalpy values of both lipogels were very different from each other.
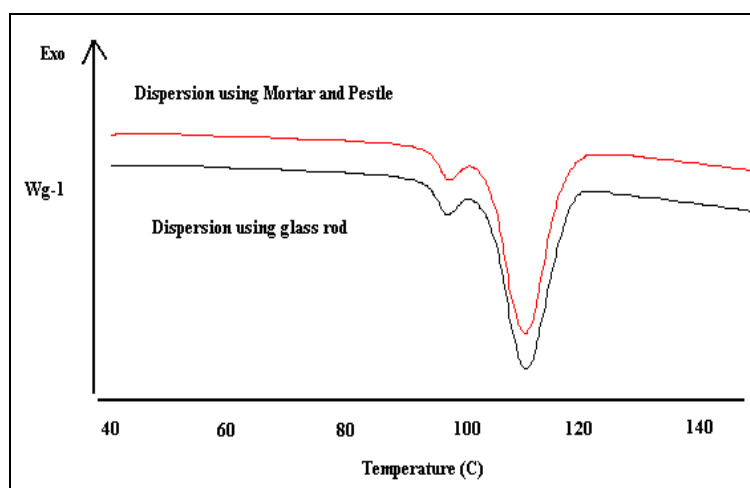
Figure 5.5: DSC (823^e) thermograms of the two dispersions of liquid paraffin and MgSt obtained using mixing either by glass rod (Scric's method) or using a mortar and pestle.
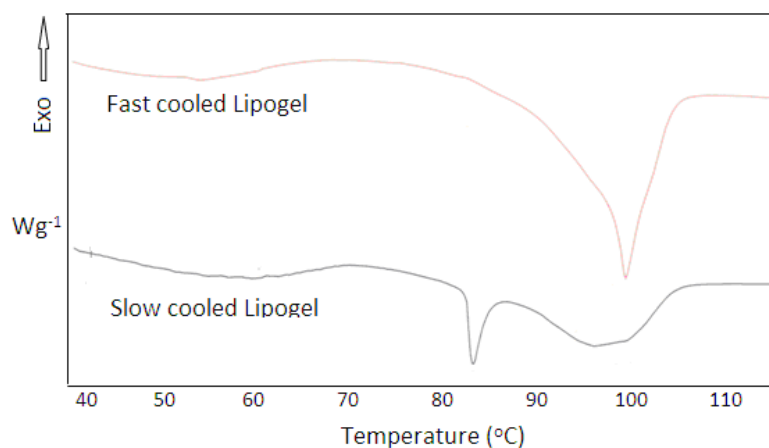
Figure 5.6: DSC (822^e) thermograms of fast (Scric's method) and slow cooled lipogels prepared using dihydrate mixed homologue magnesium stearate using a heating cycle of 25–130°C at a rate of 10°C/min.

Figure 5.7 Shows the DSC spectra of the lipogels prepared by methods 1 (1–4% water) and 2 (homogenisation). Each lipogel containing water showed two endotherms peaking between 85°C and 120°C (Fig. 5.7a). The first small endotherm peaked between 86°C and 90°C. There appeared to be a slight shift to the right in the first small endotherm with an increase in the amount of water. In contrast, the second extremely broad high temperature endotherm peaked at 120°C in all lipogels.

149

Furthermore, enthalpy values of all lipogels were also not very different (Table 5.1). The lipogel prepared by method 2 also showed similar thermal events (Fig. 5.7b) but with significantly high enthalpy values compared to the lipogels containing water (Table 5.1).
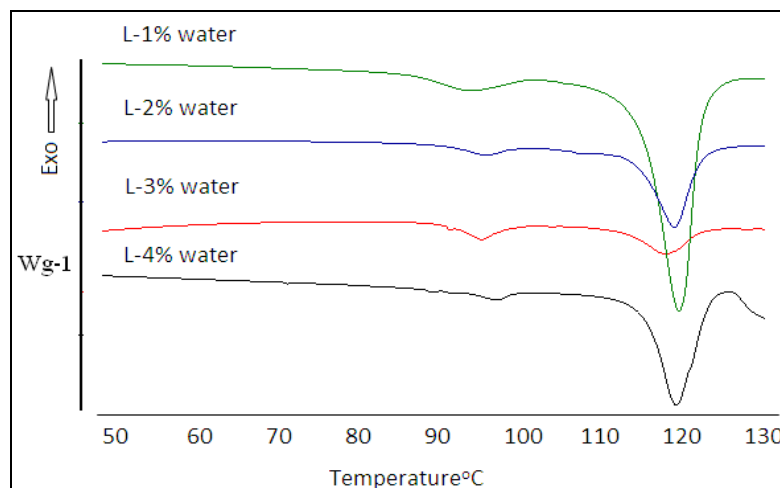
(a)

(b)
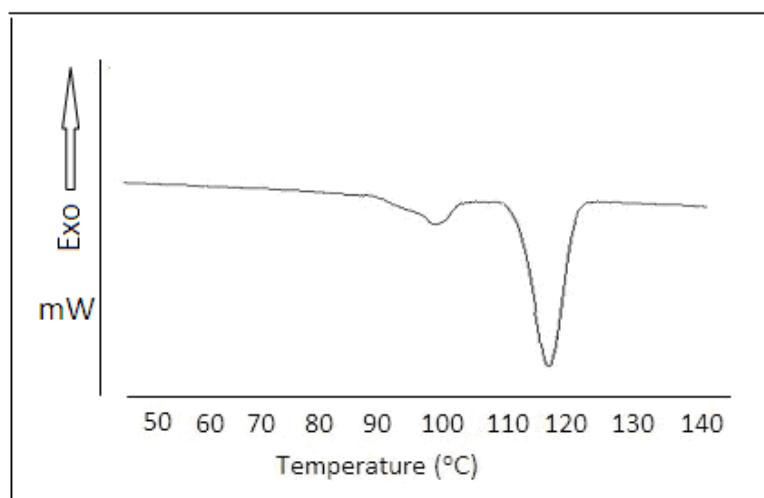
Figure 5.7: DSC (823^e) thermograms of the lipogels prepared using improved method (a) with the addition of various amounts (1–4%) of water upon cooling and (b) homogenised.

Figure 5.8 shows the DSC thermogram of the lipogel prepared by cooling at 100% RH. The lipogel showed two extremely broad high temperature endotherms peaking between 100 and 111°C. There appeared to be another small thermal event at ~82°C. The high temperature endotherm (110.4°C) was similar to all lipogels prepared by adding various amounts of water. However, endotherm at 100°C was not observed in any other lipogel. Furthermore, total enthalpy of the endotherms was significantly lower than the lipogels containing various amounts of water. However, its enthalpy was comparable to the solid, crumbly lipogels obtained after heating for 60 (Scric's method) or 90 minutes (Table 5.1).
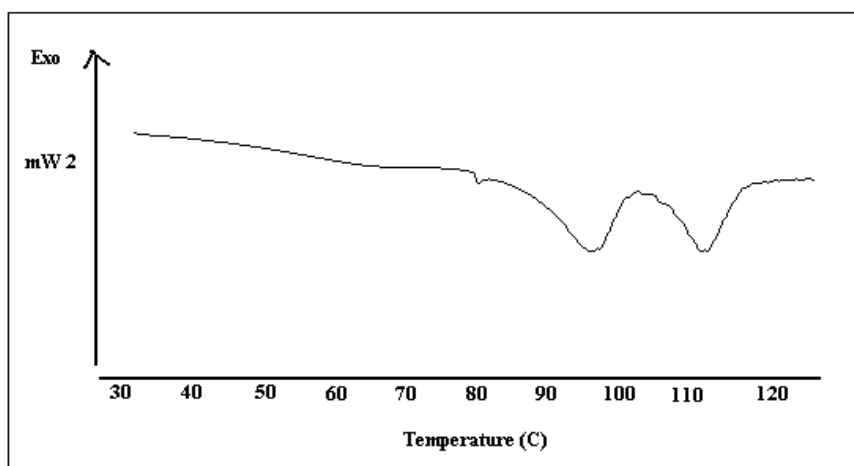
Figure 5.8: DSC (823^e) spectra of the lipogel cooled under controlled (100%) humidity.

5.3.7 Thermogravimetric analysis (TGA)

TGA was used for the analysis of the lipogels prepared using variation in the cooling methods *i.e.* slow and fast cooled controls. The lipogels showed negligible amount of water compared to the raw material MgSt (Chapter III). However, the slow cooled lipogel showed 15 fold higher weight loss (0.3%) compared to 0.002% weight loss of the fast cooled (Scric's method) lipogel.

5.3.8 Rheology

Figure 5.9 shows the flow curves of the selected lipogels prepared by method 1 (1−4% water) on day 1 and after 3 months. All lipogels showed complex rheograms,

each showing varying degree of anti clock wise hysteresis loop and yield values. There appeared to be a decrease in the apparent viscosity of the lipogels with an increase in the amount of water from 1–4% (Table 5.2). The lipogel containing 1% water showed maximum viscosity. In contrast, lipogel containing 4% water showed least viscosity. However, upon ageing for 3 months, all lipogels showed varying degree of increase in the apparent viscosity. The lipogel containing 1% water showed least increase and the lipogel containing 4% water showed the maximum increase in the viscosity (Table. 5.2). The lipogel prepared by method 2 showed highest viscosity on day of preparation (Table 5.2) and did not change upon storage (not shown).
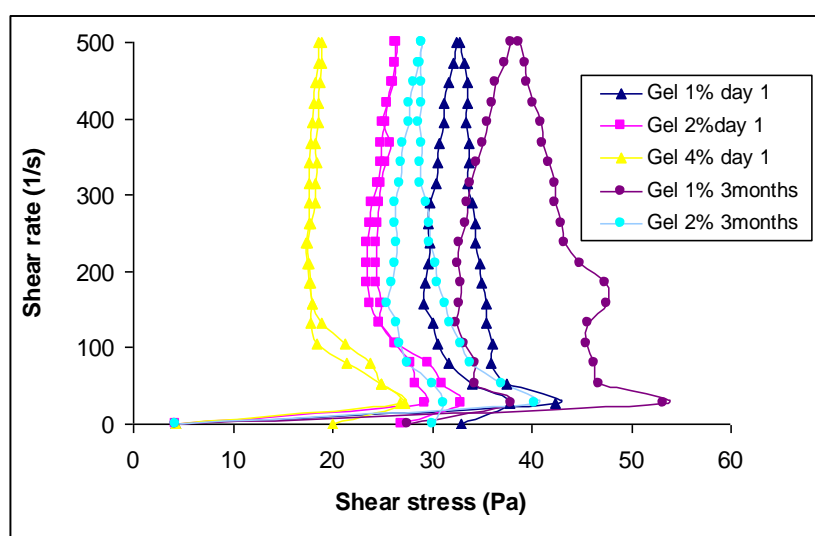
Figure 5.9: Flow curves of the lipogels prepared using improved method (containing various amounts of water) on day1 and after 3 months.

Table 5.2: Apparent viscosity of various lipogels on day 1 and after ageing for 3 months.

Type of Lipogel	ηApp on day 1 (Pa.s)	ηApp after 3 months (Pa.s)
L–1% water	0.65	0.76
L–2% water	0.53	0.58
L–4% water	0.37	0.70
L–Homogenised	0.75	0.76

5.3.9 X–ray diffraction (XRD)

Figure 5.10 shows the XRD diffractograms of the dispersion (unheated), unhomogenised (Scric's method) and methods 1 and 2. The XRD diffractograms of all preparations were different from each other, showing sharp to broad peaks. The spectrum of unheated dispersion (Fig. 5.10a) appeared to be similar to the dihydrate mixed homologue MgSt (Chapter III) and was very different from all other lipogels.

The XRD spectrum of unhomogenised lipogels (Scric's method) was different from the homogenised ones showing differences in the intensity of the peaks at $21-24^o$ (Fig. 5.10b). Homogenised lipogels showed three sharp peaks between $2\theta=21-24^o$. In contrast, unhomogenised lipogels showed a broad doublet peak in the same region.

The lipogels prepared by method 1 (1–4% water) showed different XRD spectra (Fig. 5.10c). There appeared to be a decrease in the number of sharp peaks at $2\theta=21-24^o$ with an increase in the water content $i.e.$ three sharp peaks with 1% water and 2 sharp peaks with both lipogels containing 2 and 4% water. However, the three sharp peaks of lipogel containing 1% water between $2\theta=21-24^o$, were similar to the three sharp peaks of homogenised lipogels.

(a)

153

(b)

(c)
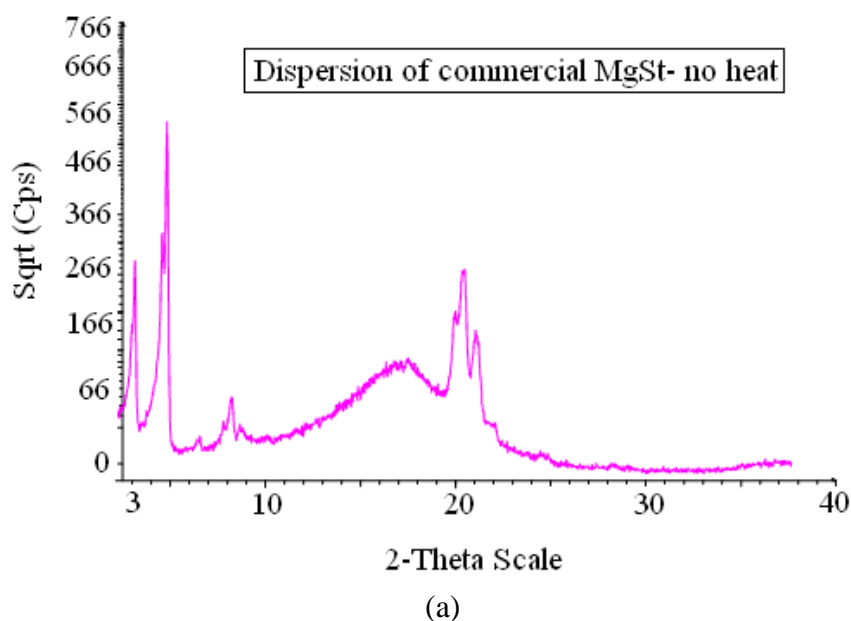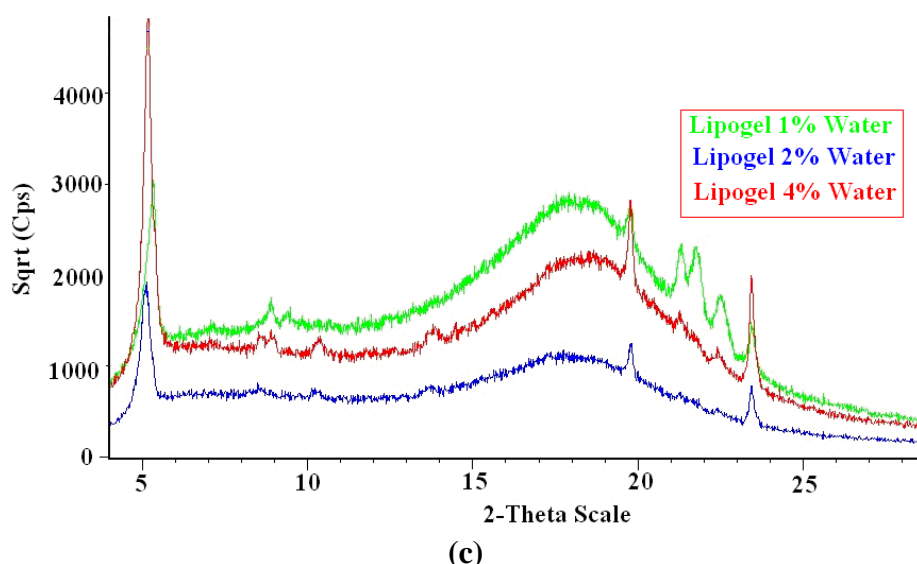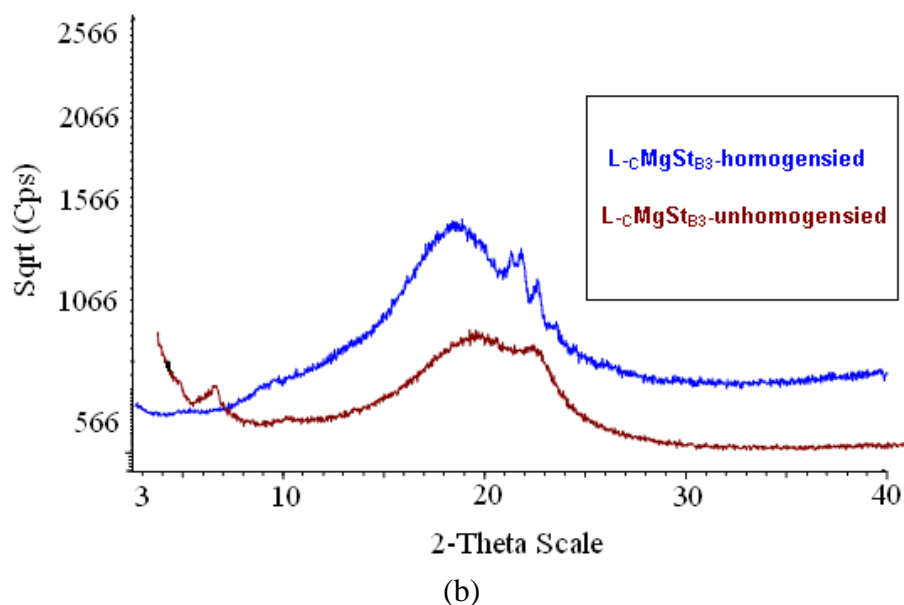
Figure 5.10: XRD diffractograms of the lipogels prepared using liquid paraffin and magnesium stearate (a) Dispersion not heated (b) unhomogenised lipogel (Scric's method) and lipogels prepared by method 2 (homogenised) and (c) lipogels containing 1–4% water (method 1).

5.3.10 Accelerated stability centrifuge test

The LumiFuge stability analyser was used to investigate the accelerated stability of the lipogels containing MgSt (12.5%) prepared by method 1 (1–4% water). Figures 5.11−5.12 show the accelerated stability of the lipogels as a function of centrifuge speed and time. The behaviour and movement of separated oil under high shear was investigated. In addition, the slope of time (s) versus oil separated (mm) was also

calculated. The lowest slope is related to the greatest stability and vice versa. The lipogels showed a discernible pattern of increase in slope with an increase in the amount of water in the lipogels (Fig. 5.12), showing instability of the system at higher shear rates with an increase in water. However, all lipogels irrespective of the amount of water showed reasonably good stability at ground state. Furthermore, the separation was due to sedimentation where clear phase was formed near meniscus. In general, the lipogel containing 1% water was most stable whereas rest of the lipogels showed similar separation kinetics.

Figure 5.11 shows the effect of injection speed on the % integral transmission of each lipogel. The lipogels were either injected slowly (A) or fast (B) into the sample vial. Each lipogel showed slight change in the % transmission at different injection speed, suggesting pressure sensitivity of the lipogels.

Figure 5.12 shows the separation kinetics of the lipogels containing 1–4% water as a function of slope. There was a discernible pattern of increase in slope with an increase in the amount of water from 1–4%. The slopes of the lipogel containing 1% and 4% water were 0.0576 and 0.4664 μm/s respectively at 4000rpm (Table 5.3). However, the slopes of all lipogels were much lower at 1500rpm (0.0041 and 0.0250 respectively) than at 4000rpm.

Table 5.3: Accelerated stability testing: Effect of increasing water concentration in the lipogels on the slope values.

Lipogel Type	Slope (μm/sec)	
	1500 rpm	4000 rpm
L-1% water	0.0041	0.0576
L-2% water	0.0193	0.3470
L-3% water	0.0199	0.4525
L-4% water	0.0250	0.4664
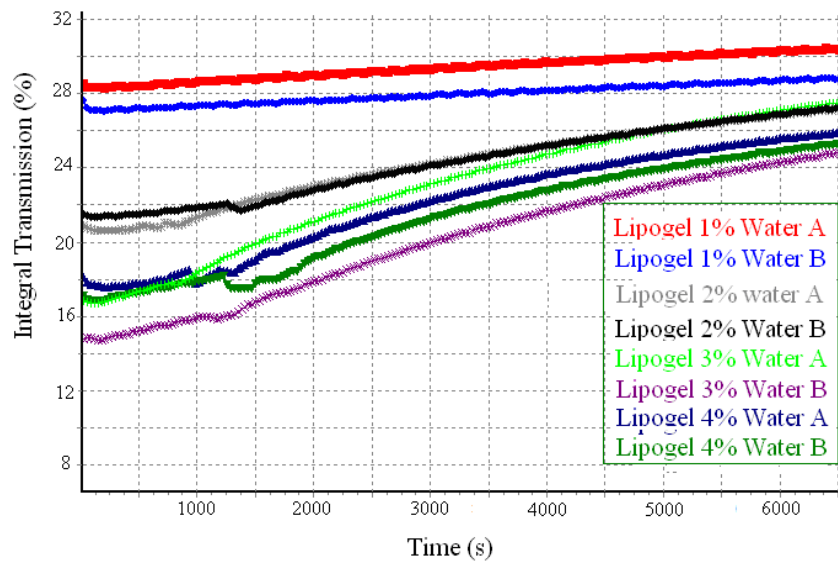
Figure 5.11: Accelerated stability centrifuge testing at 4000rpm: Effect of injection speed (stress) on the stability of the lipogels prepared by method 1 (1–4% water). Each lipogel was filled in the sample container at two different speeds (A) low speed and (B) high speed.
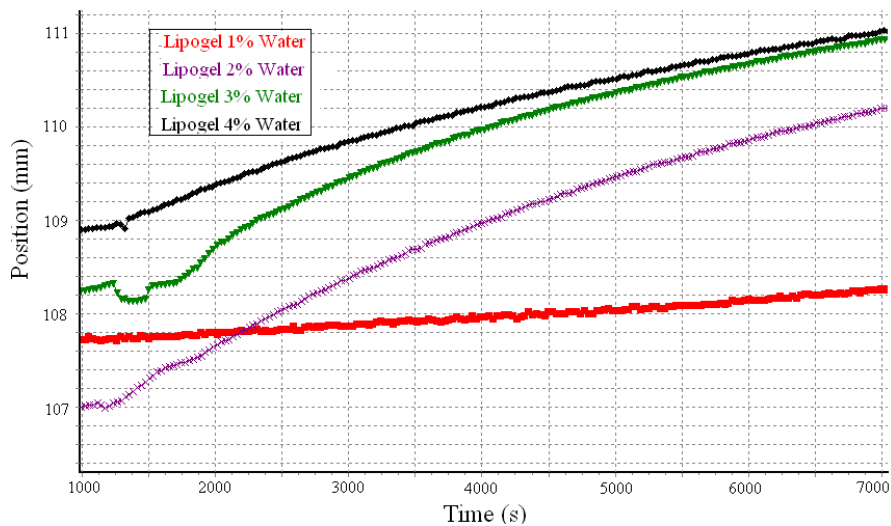
Figure 5.12: Accelerated stability centrifuge testing at 4000rpm: The separation kinetics of oil from the lipogels prepared by method 1 (1–4% water) for a time period between 1000 and 7000 seconds.

5.4. Discussion

The semisolid lipogels were prepared with magnesium stearate (12.5%) in liquid paraffin using a standard method. The standard method of preparation involves dispersing the magnesium stearate in the liquid paraffin using a glass rod in a beaker,

156

heating to a preset (110°C) temperature, holding for 30−60 minutes and upon cooling either by adding water to the dispersion at 90°C (method 1) or by homogenisation (method 2) during cooling cycle.

The lipogels prepared by methods 1 and 2 were rather similar and appeared as white stable semisolids showing similar microscopic, thermal and XRD behaviour. The lipogels prepared by method 2 showed relatively higher viscosities and changed little with time. In contrast, the lipogels obtained by method 1 showed significant increase in viscosity upon ageing.

The structure of the semisolid lipogels prepared using homogenisation and with addition of water can be explained in terms of microscopic, DSC and XRD data. All lipogels showed Maltese crosses. The presence of Maltese crosses in the aqueous semisolid formulations has been related to the swollen α−crystalline lamellar structures (Eccleston, 1986). Therefore, the semisolid lipogels showing Maltese crosses are structured by an inverse swollen α−crystalline lamellar phase formed from the physical aggregation of long−chain fatty acid with the liquid paraffin. Lipogels prepared by methods 1 (1−2%water) and 2 showed numerous Maltese crosses whereas lipogels prepared by method 1 (3−4%water) showed fewer Maltese crosses, suggesting that the lipogels containing different amount of water possess different structure. However, thickness of lamellar α−crystalline gel structure of various lipogels depended on the polymorphic nature of MgSt (amorphous or crystalline) and caused significant changes in the gel structure. In the characterisation of various anhydrates and hydrated samples of pure and mixed homologue MgSt (Chapter III) it was observed that increase in hydration level caused an increase in the intensity of the peaks at $2\theta=21-24^{o}$ producing crystalline ordered structures and removal of water from the crystals produced mainly amorphous material.

Figure 5.13 shows influence of pseudopolymorphic modification of MgSt on the physicochemical properties of the lipogels. It is postulated that conversion of predominantly amorphous state of MgSt to crystalline state due to addition of water (1−2%), produces lamellar α−crystalline gel structure converting solids to semisolids. Further addition of water (3−4%) produces predominantly amorphous

157

content disrupting the lamellar α−crystalline gel structure reducing viscosity, producing structured fluids.
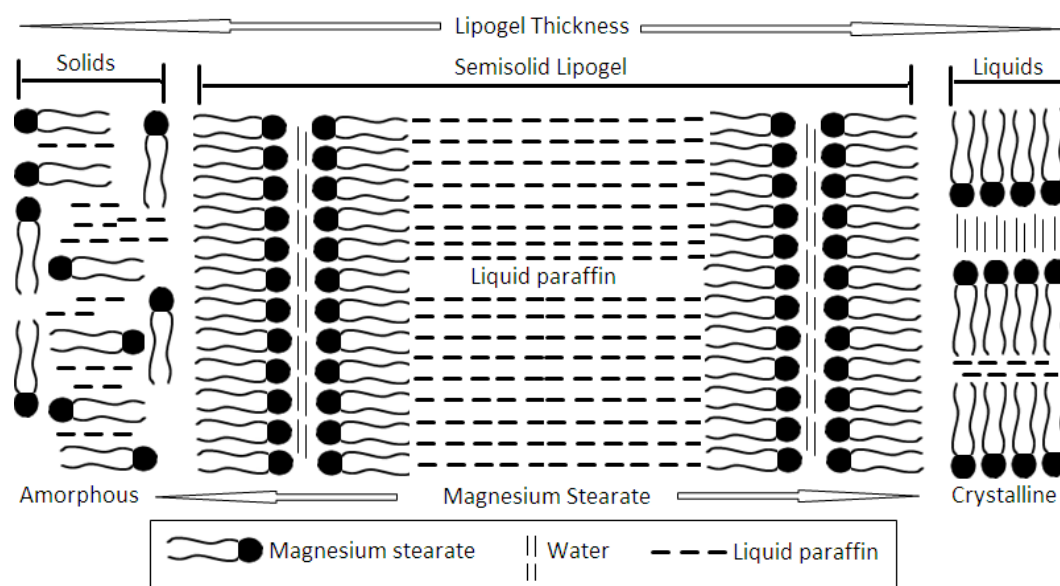
Figure 5.13: Schematic diagram showing proposed lipogel structure based on the pseudopolymorphic changes in the magnesium stearate in the presence or absence of water.

This view was supported by the XRD spectra where white, semisolid lipogels prepared either by methods 1 (1−2% water) or 2 showed sharp peaks of high intensity at $2\theta = 21-24^{o,}$ suggesting marked swelling of the lipogels and is attributed to the increase in crystalline component of MgSt (Fig. 5.10). Maximum swelling was observed at the least amount of water (1%) and swelling decreased with an increase in the amount of water, which was confirmed by the maximum sharpness of the peaks in the lipogels containing 3−4% water. This was consistent with an increase in crystalline content of MgSt observed at $2\theta = 21-24^{o}$ with an increase in the amount of water.

Polarised microscopy and DSC further support this view. The lipogels with increasing amount of water showed decrease in number of Maltese crosses, suggesting disruption of lamellar α−crystalline gel structure. DSC also showed changes in the endotherm attributed to the hydration level of MgSt, peaking at 120°C. This endotherm was linked with the Maltese crosses. Therefore, reduction in the sharpness of the endotherm with an increase in water also suggests reduction in

Maltese crosses and an increase in the amorphous state. Increase in amorphous component has also been linked to the reduction in viscosity. We also observed reduction in viscosity of the lipogels with an increase in water and hence increase in amorphous component of MgSt.

Various researchers have reported significant effect of process variables such as stirring, temperature and solvent on the appearance and stability of the formulations containing stearic acid (Timmins *et al*., 1990; Lin *et al*., 1994; Eccleston, 1997; Wellner *et al*., 2006). Therefore, various preparation variables were investigated for their effect on the resultant lipogels and included variation in the preparation of dispersion, variations in the heating methods, effect of controlled environment and variations in the cooling methods.

The lipogels prepared with or without heating showed significant differences in appearance. The dispersions heated to 130°C produced solid lipogels whereas the dispersion left on the bench without heating separated into two phases. The heating time also affected the appearance of the lipogels. The formulations prepared by heating at 130°C for 60 minutes were less syneretic compared to the lipogels heated at the same temperature for 90 minutes. This observation was consistent with the results of Scric *et al*., (1988) who showed that longer heating time (90 minutes) produced significantly unstable lipogels with lots of syneresis. This view was further supported by the DSC results. The formulation heated for 60 minutes showed endotherm peaking at lower temperature (96.2^{o}C) with higher enthalpy compared to the formulation heated for 90 minutes (Table 5.1). Generally, the lower melting form would be a more energetic species, resulting in faster dissolution and increased stability (Lindenbaum *et al*., 1985). Lin *et al*., (1994), also showed increased stearic acid solubility in the fatty alcohol propylene glycol (FAPG) ointment base with polymorph showing low temperature, high enthalpy endotherm compared to the metastable polymorph showing high temperature endotherm of low heat of fusion. Therefore, same analogy can be used to explain the amount of syneresis observed in two lipogels. Therefore, the low temperature endotherm in the formulation heated for 60 minutes may be related to the relatively stable polymorph of MgSt whereas longer

heating time may result in the high temperature unstable polymorph causing significant syneresis.

The effect of pressure on the lipogels of MgSt was observed in the experiment on cooling with and without stirring, accelerated centrifuge stability test using two different injection speeds as well as homogenisation of the lipogels upon cooling. The formulations prepared using cooling with continued stirring produced relatively softer lipogels compared to the unstirred formulations. It is reported that polymorphic modifications in the stearate systems are affected by the changes in the stirring rate (Garti *et al*., 1982; Lin *et al*., 1994). Milling of magnesium stearate has also shown to affect its particle size and surface area causing changes in the lubrication properties and may be related to the polymorphic modifications upon milling (Leinonen *et al*., 1992). Therefore, same analogy can be used to explain the differences in the lipogels prepared with or without stirring. The lipogels filled in the centrifuge vial at slow or fast speed representing varying degree of applied pressure showed slight change in the slope of the stability curve (Fig. 5.11), confirming changes in the lipogel structure with pressure which can be attributed to the polymorphic modifications.

Homogenised lipogels were semisolid elastic and lost more moisture compared to the unhomogenised lipogels. The enthalpy and mechanical properties of the homogenised lipogels appeared to be higher than unhomogenised ones, suggesting sensitivity of the lipogels to the applied stress in the form of homogenisation, which may have an influence on the structure of the lipogels. XRD results also supported this view because homogenised lipogels showed sharp peaks at $2\theta=21^{o}$ whereas unhomogenised lipogels showed broad peak (Fig. 5.10a), suggesting higher degree of lamellar crystalline structure. This observation suggests that homogenisation resulted in the marked polymorphism in these lipogels causing changes in the structure of the lipogels. Eccleston (1997) showed that stearate creams are markedly affected by the mixing. She described that continued mixing until cool resulted in the softer creams compared to the much stiffer creams obtained when mixing was stopped at setting temperatures and attributed these differences to the marked polymorphism in the stearate creams. She also described the effect of stress on the swollen crystalline

structures. It was shown that in some systems, the swollen lamellar structures appeared to be metastable and changed to non–swollen structures under pressure.

In our work, the polarised microscopy also supported this view by showing differences in the structure of both lipogels *i.e.* homogenised lipogels showed more anisotropic crystalline structure with numerous Maltese crosses compared to the unhomogenised lipogels. The increase in the anisotropic structure may be related to the new crystalline phases appearing at ($2\theta=21^{o}$) in the homogenised lipogels. It is also reported that the long–chain saturated fatty acids such as stearic acid exhibit marked polymorphism (Gunstone, 1967) and described as A, B, C and E forms. Form C is the most stable and form A the most unstable (Sydow 1955a; Lin *et al.*, 1994). In this context, the physical stability of the homogenised formulations can be attributed to the presence of the stable polymorphic form C of the stearic acid whereas syneresis in the unhomogenised lipogels may be attributed to either polymorph A, B or E or mixtures of these polymorphs.

The effect of the composition of the MgSt was observed on the lipogels prepared using MgSt composed of either pure stearic acid (pMgSt) or containing a homologue composition of palmitic and stearic acid (cMgSt). We observed lipogels of mobile to semisolid nature on the preparation day using pMgSt and cMgSt respectively. Furthermore, the lipogels prepared using pMgSt thickened with time. These observations were consistent with the work conducted by Eccleston (1977) almost three decades ago on the stearate creams (ternary systems). Eccleston described preparation of mobile structured fluids to semisolid ternary systems containing stearic acid, water and fatty alcohol of different chain lengths. She described that mobile fluids thickened to semisolid creams with time and attributed the thickening of the ternary systems with time to the length of the fatty alcohols present *i.e.* long chain fatty alcohol (stearyl alcohol) needed more time to produce semisolid systems. In our work, the thickening of the lipogels may also be attributed to the chain length of the fatty acids instead *i.e.* the homologue composition of fatty acids (cMgSt) produced semisolids upon cooling whereas the formulations containing pure stearic acid (pMgSt) thickened at ambient temperature upon ageing.

Cooling methods have also shown an effect on the appearance and stability of the lipogels. Slow cooled lipogels appeared to be solid, slightly elastic and non–syneretic. In contrast, fast cooling resulted in the solid, crumbly, syneretic lipogels. This observation was consistent with the results of Lin *et al*., (1994) who showed significant effect of cooling type on the resulting stearate–based ointments. Lin *et al*., (1994) showed that super cooled (equivalent to fast cooling in our work) ointments have less stable polymorph B of stearic acid. In contrast, slow cooling produced the more stable form C. Therefore, stability of slow cooled lipogels can be attributed to the presence of the stable polymorphic form C whereas less stable form B is produced upon fast cooling. This view is supported by the DSC, TGA and microscopy results. The slow cooled lipogel showed a low temperature endotherm in addition to a high temperature endotherm with higher enthalpies (Fig. 5.6) compared to the fast cooled lipogel, which showed relatively high temperature endotherm only with low enthalpy values. In addition, the slow cooled lipogel showed significantly high moisture loss and numerous Maltese crosses. Fewer Maltese crosses were observed in the fast cooled lipogel.

5.5 Conclusions

1. Semisolid, non–syneretic, elastic lipogels of MgSt and liquid paraffin can be prepared using a standard heating and cooling method by addition of 1–2% water or PBS upon cooling just below 100°C or homogenisation after cooling to room temperature.

2. The semisolid consistency of lipogels is due to the presence of liquid crystalline gel network produced by aggregation of MgSt upon cooling and attributed to the optimum balance of amorphous and crystalline component of MgSt. A perfect amorphous MgSt produced syneretic, solid lipogels. In contrast, perfect crystalline component produced structured fluids.

The lipogels also showed sensitivity to mechanical stress, attributed to the polymorphic modification in the MgSt upon homogenisation. Amorphous component of MgSt produced by heating to high temperature may have been reduced by homogenisation yielding more crystalline component, converting solid lipogels into

semisolids.

3. All heating variables produced syneretic solid lipogels. The syneresis may be attributed to the formation of metastable perfect amorphous form of MgSt.

4. Variation in the cooling methods also affected the appearance of the lipogels. The fast cooling produced syneretic, crumbly solid lipogels, attributed to amorphous state. In contrast, slow cooled lipogels were non–syneretic, slightly elastic and solid showing numerous Maltese crosses suggestive of lamellar structure of the lipogels, attributed to the decrease in amorphous component.

CHAPTER VI

PREPARATION AND EVALUATION OF LIPOGELS OF PALM–OLEIN

6.1 Introduction

In chapter V, the preparation of stable, semisolid lipogels of MgSt dispersed in liquid paraffin was described. The literature method (Scric *et al*., 1985) was adapted to develop two methods which were identical except that method 1 involved addition of 1−4% water, and method 2 involved homogenisation of system upon cooling without water.

Malaysia is amongst the largest exporters of crude and refined Palm–olein, which has been used successfully as a vehicle for cosmetics and ointments. Palm–olein contains saturated and polyunsaturated fatty acids of varying chain lengths. In contrast, liquid paraffin is composed of long chain saturated hydrocarbons.

Preliminary experiments using Scric's original method on palm–olein alone or mixtures of liquid paraffin and palm–olein (0−100%) did not produce semisolid lipogels. Either unstable (syneretic) systems or solid lipogels unsuitable for dermatological use were formed. The work described in this chapter investigates whether the two methods, method 1 (addition of 0%, 1%, 2%, 3% and 4% water upon cooling) and method 2 (homogenisation upon cooling without water) developed in chapter V adapted from Scric's original method using liquid paraffin would also provide semisolid lipogels with palm–olein. To do this, 12.5% MgSt and a 70:30 ratio of liquid paraffin and palm–olein was used as this had given the best systems with Scric's original method (not shown).

6.1.1 Aims of the chapter

This chapter explores whether liquid paraffin could either be replaced by palm–olein or used in combination with palm–olein to provide semisolid lipogels of MgSt suitable for dermatological use. The overall aims include:

1. To prepare semisolid, stable lipogels of magnesium stearate with palm−olein using two methods, method 1 (addition of water upon cooling) and method 2 (homogenisation upon cooling) adapted from Scric's original method,

2. To prepare semisolid, stable lipogels of magnesium stearate in liquid paraffin and palm olein with a fixed ratio (70:30) of liquid paraffin: palm−olein respectively using method 1 and method 2.

6.2 Methods

6.2.1. Preparation of lipogels using methods 1 and 2

The fixed amount (12.5%) of mixed homologue MgSt (dihydrate, batch 3) was dispersed in the palm−olein alone and in a fixed ratio (70:30) of liquid paraffin and palm olein using a glass rod in a beaker. Dispersions were then heated and cooled using the adapted method developed in the previous chapter from Scric's original method (Chapter V, section 5.2.2), which involves heating dispersions at ~5–10°C/min to 110°C, holding at 110°C for 1–2 hrs, cooling dispersions naturally in the oil bath (~0.1–0.2°C/min). Upon cooling to just below 100°C, 0–4% water was added with continuous stirring to dispersions (method 1) or alternatively cooled dispersions were homogenised without water (method 2).

6.2.2 Polarised light microscopy

The lipogels in addition to the palm−olein raw material were studied by polarised light microscopy using a Polyvar compound microscope (Reichert−Jung, Ansberg, Germany).

6.2.3 Hot stage microscopy

A TMS 91 hot stage (Linkam Scientific Instruments, UK) attached to the Polyvar microscope was used to study the melting behaviour of the palm−olein raw material.

6.2.4 Differential scanning calorimetry (DSC)

A DSC 822^e (Mettler Toledo, Leicester, UK) was used for the analysis of the lipogels and the palm–olein raw material.

6.2.5 Thermogravimetric analysis (TGA)

The TGA/SDTA851^e (Mettler Toledo, Leicester, UK) was used for the analysis of the palm–olein and the lipogels.

6.2.6 Rheology

A cone and plate CSL 100 Carri–med rheometer (TA Instruments, UK) was used to investigate the rheological properties of the lipogels. Flow curves were obtained using up and down curves with minimum shear rate of 0.5 (s^{-1}) and maximum of 500 (s^{-1}).

6.2.7 Accelerated stability centrifuge test

Due to instrument availability only lipogels containing 70:30 ratio of liquid paraffin and palm–olein with 1–4% water were analysed for the long–term stability using LumiFuge stability analyser (*c.f. Chapter II*).

6.3 Results

6.3.1 Visual appearance of the lipogels

The lipogels were prepared using 12.5% mixed homologue dihydrate MgSt in palm–olein alone and 70:30 ratio of liquid paraffin and palm–olein by the two methods. Heating of dispersions to 110°C and holding for 1–2 hrs produced foam–free translucent yellow dispersions.

Method 1 produced stable semisolid light yellow (for palm–olein) or off white (for 70:30 ratio of liquid paraffin and palm–olein) lipogels. However, the lipogels containing 1–2% water appeared to be more viscous than the lipogels containing 3–4% water *(c.f. results Rheology Fig.6.8).*Upon storage for two years (to date) at

ambient temperature no changes were observed in all lipogels. In contrast, the systems prepared by method 2 were semisolid lipogels on the day of preparation, which showed significant thickening after two days storage to form solids, unsuitable for dermatological use.

6.3.2 Polarised light microscopy

The palm–olein raw material and the lipogels were studied by polarised light microscopy.

Figure 6.1 shows photomicrographs of palm–olein raw material. Palm–olein showed numerous long and a few small needle–like crystals with dark background. Many star like crystalline masses were also observed. The long needle–like crystals were not seen in any other sample.
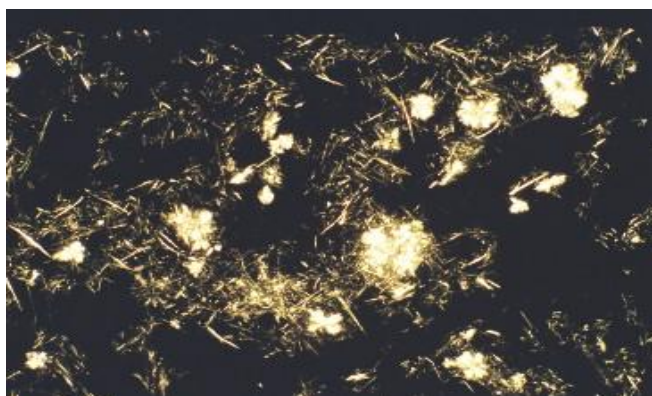
Figure 6.1: Photomicrographs of Palm–olein raw material (Scale: 1cm= 100μm).

Figure 6.2 shows photomicrographs of the lipogels prepared by method 1 (with 0−4% water added upon cooling) using 12.5% MgSt and palm–olein. There appeared to be an increase in structure with an increase in water content. All lipogels showed needle–like crystals. A large number of needle–like crystals with few clusters were observed in the lipogels containing 1% water with dark background (Fig. 6.2a). In contrast, lipogel containing 4% water showed numerous small needle–like crystals with intense glowing background (Fig. 6.2b).

(a)   (b)
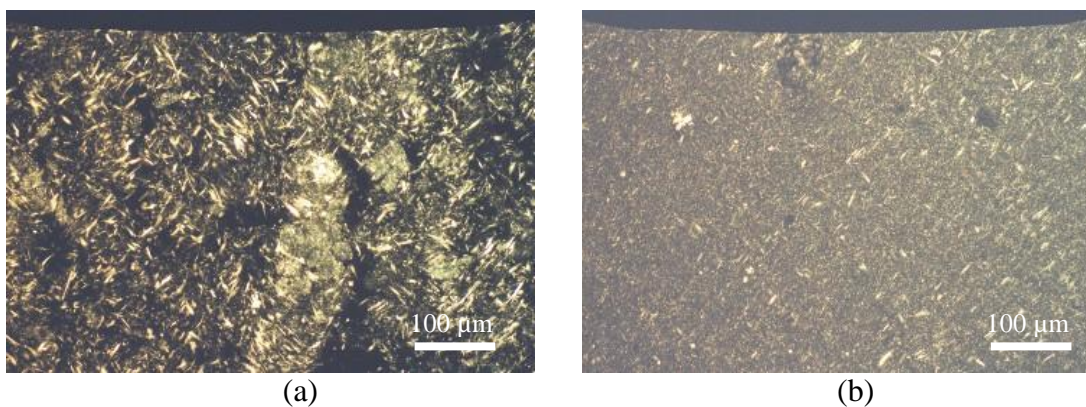
Figure 6.2: Photomicrographs of the lipogels prepared by method 1 using palm–olein and 12.5% MgSt with (a) 1% water and (b) 4% water.

Figure 6.3 shows photomicrographs of lipogels prepared by method 1 using 12.5% MgSt in a fixed ratio (70:30) of liquid paraffin and palm–olein. All formulations showed three types of anisotropic structures *i.e.* wavy crystals, clusters of crystals and star–shaped crystals. There appeared to be a discernible pattern of increase in wavy crystals with an increase in water content. Furthermore, all formulations showed dark background. The lipogel containing 4% water showed numerous star–shaped crystals (Fig. 6.3b). In contrast, few star–shaped crystals were seen in lipogel containing 1% water (Fig. 6.3a).

(a)   (b)
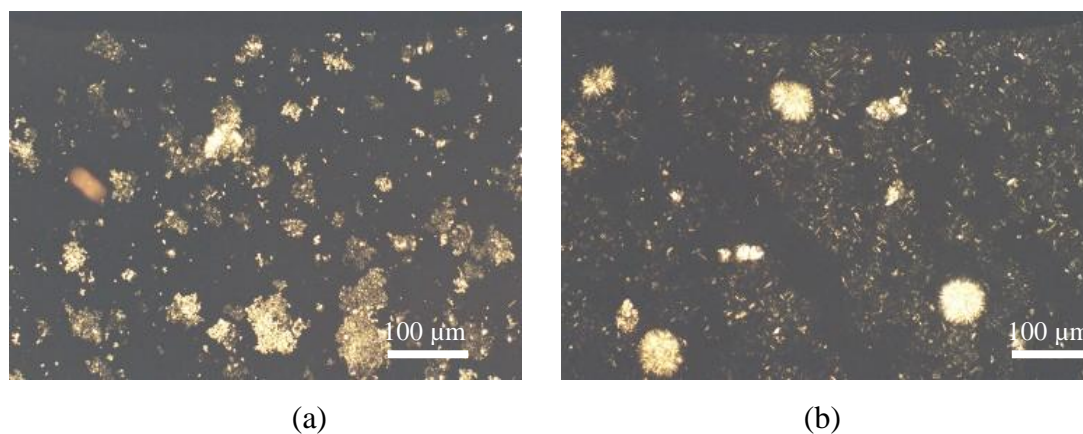
Figure 6.3: Photomicrographs of lipogels prepared by method 1 using 12.5% MgSt with a fixed ratio (70:30) of liquid paraffin and palm–olein containing (a) 1% water and (b) 4% water.

168

6.3.3 Hot stage microscopy

Figure 6.4 shows hot stage photomicrographs of the palm–olein raw material which showed two different phase transition temperatures involving melting of needle–like and star–shaped crystals. The 1st phase transition between 28–35°C was due to the melting of the needle–like crystals (Fig. 6.4a and b). The 2nd phase transition (44–65°C) involved melting of star–shaped crystals.

| (a) | (b) |
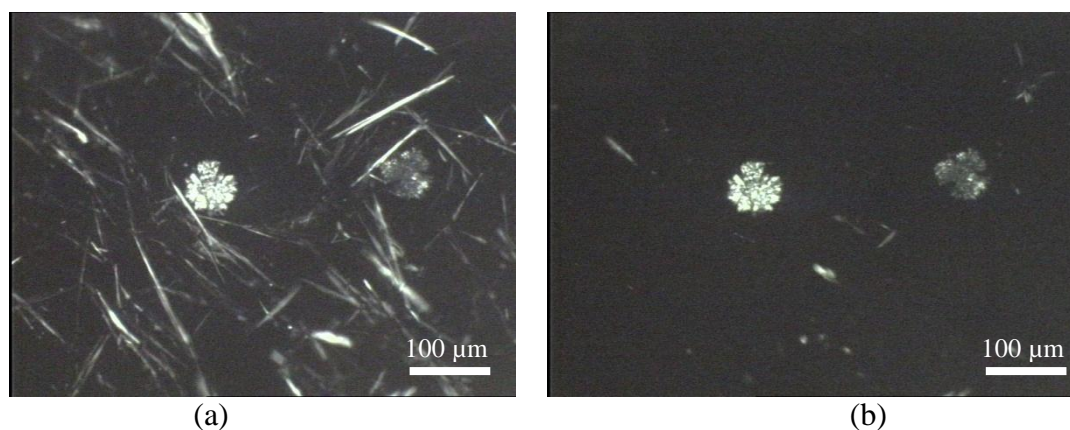
Figure 6.4: Hot stage photomicrographs of palm–olein raw material (a) at 25°C and (b) at 35°C.

6.3.4 Differential scanning calorimetry (DSC)

Figure 6.5 shows DSC spectra of palm–olein, which showed only one low temperature sharp endotherm peaking at 32°C with a shoulder at 35°C. No other thermal event was observed.

Figure 6.6 shows the DSC spectra of lipogels prepared using 12.5% MgSt in palm–olein by methods 1 and 2.

All lipogels showed two endotherms each peaking between 70°C and 120°C. The thermograms of lipogels prepared using two adapted methods were similar to each other, but different from unhomogenised lipogels, showing endotherms peaking at different temperatures (Fig. 6.6). The lipogels prepared using both methods (methods 1 and 2) showed significantly higher enthalpy values compared to unhomogenised lipogels prepared using Scric's original method (Table 6.1).

169
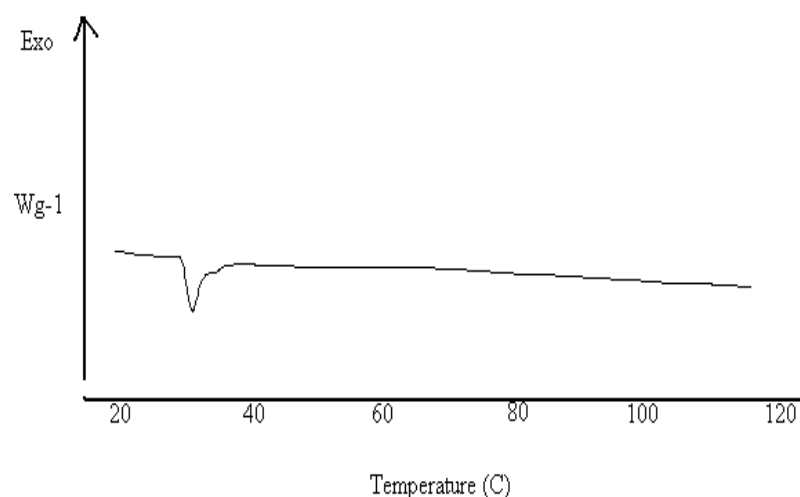
Figure 6.5: DSC (822^e) thermogram of palm–olein raw material using a heating cycle of 15°C–140°C at a rate of 10°C/min.
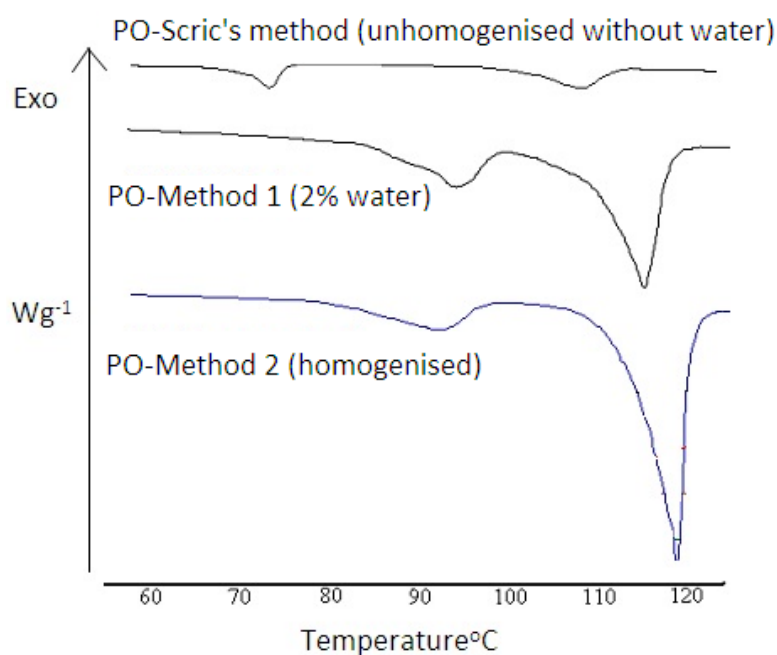
Figure 6.6: DSC (823^e) thermograms of the lipogels prepared using 12.5% magnesium stearate and palm–olein by methods 1, 2 and Scric's method (unhomogenised) using a heating cycle of 25°C–150°C at a rate of 10°C/min.

The unhomogenised lipogel without water (Scric's method) showed a low temperature endotherm peaking at 75°C, which was not seen in the lipogel prepared using improved method. The second high temperature endotherm peaked at 110°C.

In contrast, both lipogels prepared using methods 1 and 2 showed two broad endotherms peaking between 95°C and 120°C. The first endotherm appeared at 95°C in both lipogels (Fig. 6.6). However, second endotherm peaked at slightly higher temperature (120°C) in lipogel prepared using method 2 compared to the lipogel prepared using method 1 (116°C).

Figure 6.7 shows thermograms of lipogels prepared using 12.5% MgSt in a fixed ratio (70:30) of liquid paraffin and palm–olein using improved and Scric's methods.

All lipogels showed one or two broad endotherms peaking between 80°C and 120°C. The lipogels of methods 1 and 2 were different from lipogels prepared using Scric's method. The lipogels of methods 1 and 2 showed a low temperature endotherm peaking at 80°C in addition to a very broad endotherm peaking at 120°C. In contrast, lipogels prepared using Scric's method showed only one very broad endotherm peaking at 103°C (Fig. 6.7).
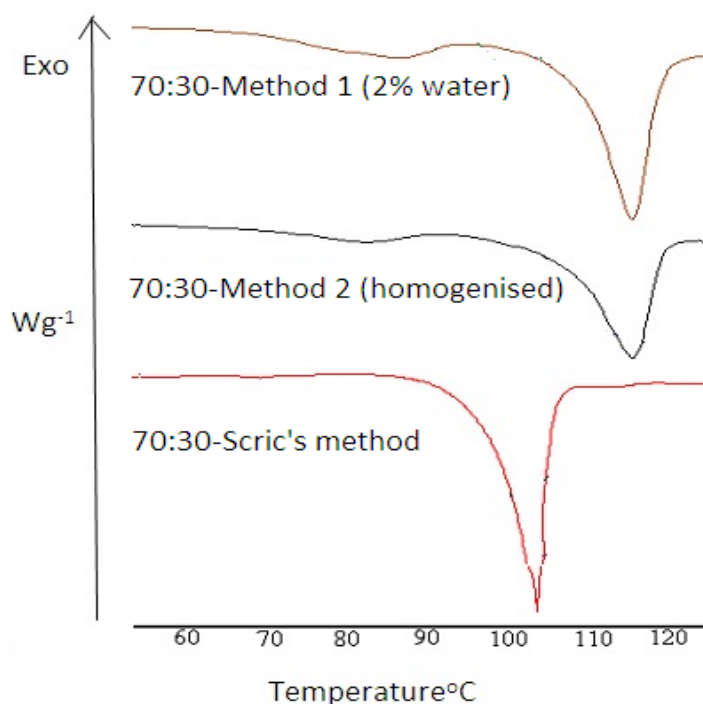
Figure 6.7: DSC (823[e]) thermograms of the lipogels prepared using 12.5% magnesium stearate and a fixed ratio (70:30) of liquid paraffin and palm–olein by methods 1, 2 and Scric's method using a heating cycle of 25°C–150°C at a rate of 10°C/min.

Table 6.1: DSC data showing peak temperatures and enthalpy values for lipogels prepared using method 1 (addition of water), method 2 (homogenised without water) and Scric's method (unhomogenised without water).

Type of Lipogels	T (^{o}C)	ΔH (J/g)
Palm−olein	32.0	-75.4
L-PO (method 1-1% water)	95.0, 115.0	-24.3
L- PO (method 1-2% water)	95.0, 116.0	-22.1
L- PO (method 1-3% water)	98.1, 119.0	-25.1
L- PO (method 1-4% water)	100.0, 120.3	-20.1
L- PO (method 2-homogenised)	95.0, 120.0	-30.2
L-PO Scric's method (unhomogenised)	75.0, 110.0	-10.2
L-70:30 (method 1-1% water)	80.0, 117.1	-22.2
L-70:30 (method 1-2% water)	80.0, 120.0	-24.5
L-70:30 (method 1-3% water)	83.2, 120.2	-26.1
L-70:30 (method 1-4% water)	83.1, 120.3	-21.2
L-70:30 method 2-(homogenised)	82.1, 116.0	-30.0
L-70:30 Scric's method (unhomogenised)	103.0	-8.5

6.3.5 Thermogravimetric analysis (TGA)

TGA was used for the analysis of the palm−olein in addition to the lipogels prepared by methods 1 and 2. Palm−olein showed very little weight loss *i.e.* 0.26% (Table 6.2). Lipogels of palm−olein prepared with addition of 2% water showed higher water loss than homogenised and unhomogenised lipogels (Table 6.2).

Table 6.2: TGA data showing weight loss from various lipogels prepared using magnesium stearate.

Type of sample	Weight loss (%)
Palm−olein raw material	0.260
PO-Method 2 (homogenised)	0.240
PO-Method 1 (2% water)	0.840
PO-Scric's method (unhomogenised)	0.035
70:30-Method 2 (homogenised)	0.120
70:30-Method 1 (2% water)	0.820
70:30-Scric's method (unhomogenised)	0.070

6.3.6 Rheology

Figure 6.8 shows flow curves of the lipogels prepared by methods 1 and 2 on preparation day.

All lipogels showed complex non–Newtonian behaviour. The flow curves were in the form of anti clock wise hysteresis loops. There is a discernible pattern of an increase in the area of hysteresis loops with a decrease in water content of the lipogels. Visual inspection of rheograms showed that all lipogels presented varying amounts of yield values (not calculated). There appeared to be a decrease in the yield value with increase in water content.

All lipogels showed different apparent viscosities, which were calculated from the apex of the loop ($500s^{-1}$). There appeared to be a discernible pattern of decrease in apparent viscosity with an increase in water content from 1–4% in the lipogels of palm–olein alone and the lipogels containing combination of liquid paraffin and palm olein (Table 6.3). The lipogel containing 1% water showed maximum viscosity. In contrast, the lipogel with 4% water showed minimum viscosity (Fig. 6.8a and 6.8b). The viscosity of homogenised lipogels was similar to the lipogel containing 1% water on day of preparation (Table 6.3). The viscosity of lipogels prepared using 70:30 ratio of liquid paraffin and palm–olein containing 1% water or homogenised was significantly higher than the lipogels prepared using palm–olein alone with same water content (Fig. 6.8a and 6.8b).

Table 6.3: Apparent viscosity of various lipogels prepared using methods 1 and 2.

Sample type	Viscosity (Pa.s)
PO-Method 1 (1% water)	0.28
PO-Method 1 (2% water)	0.20
PO-Method 1 (3% water)	0.10
PO-Method 1 (4% water)	0.05
PO-Method 2 (homogenised)	0.29
70:30- Method 1 (1% water)	0.40
70:30- Method 1 (2% water)	0.16
70:30- Method 1 (3% water)	0.09
70:30- Method 1 (4% water)	0.05
70:30- Method 2 (homogenised)	0.47
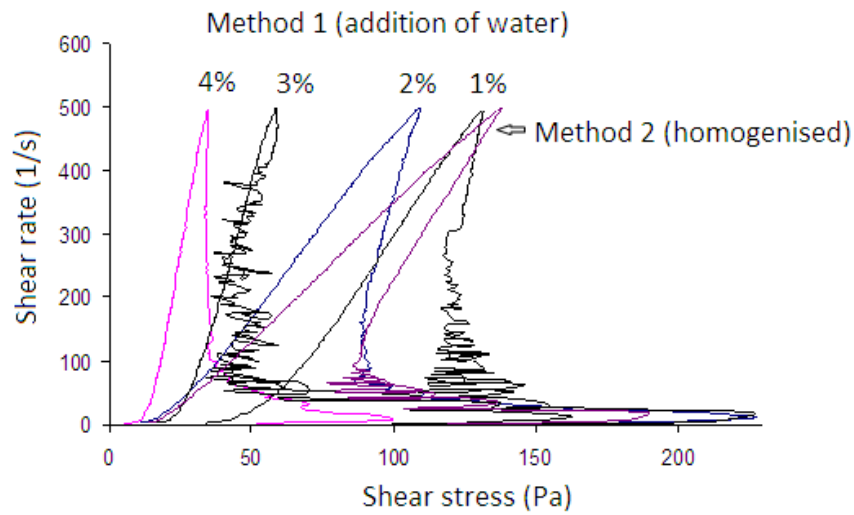
(a)
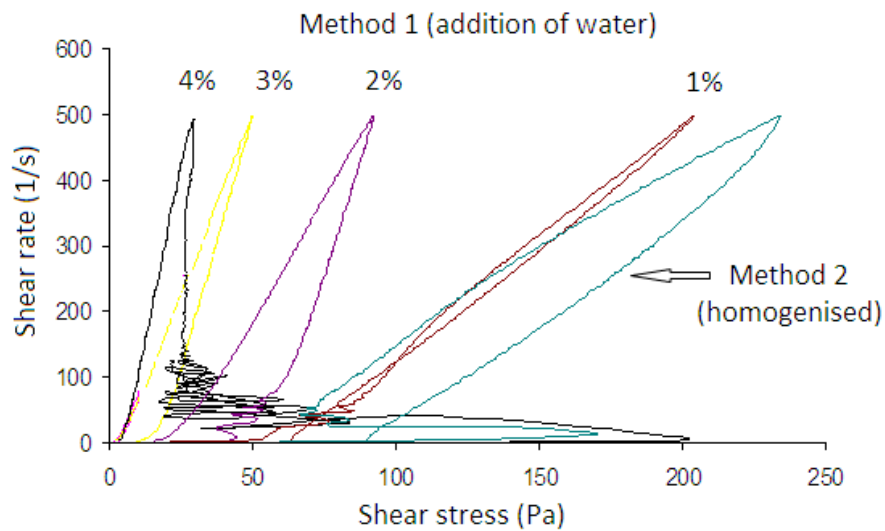
(b)

Figure 6.8: Flow curves of the lipogels prepared by methods 1 (added with 1−4% water) and 2 (homogenised) using (a) palm–olein and (b) a fixed ratio (70:30) of liquid paraffin and palm–olein. All experiments were conducted on day 1.

6.3.7 Accelerated stability centrifuge test

Figures 6.9–6.11 show accelerated stability of the lipogels as a function of centrifuge speed and time of the lipogels prepared using 12.5% MgSt with fixed ratio (70:30) of liquid paraffin and palm–olein containing various amounts (1–4%) of water.

The behaviour and movement of separated oil under high shear was investigated. In addition, slope of time (s) versus oil separated (mm) was calculated which provided information about the stability of the lipogel. In general, the lipogel containing 1% water was most stable.

The lipogels containing 1–2% water showed very little separation when examined at 1500 or 4000 rpm (Fig. 6.9a) as the slope values were very low (0.057 μm/sec). In contrast, the lipogels containing higher amounts of water (4%) showed significantly higher separation (Fig.6.9b) evident from higher slope value (0.4 μm/sec). There appeared to be an increase in separation rate with an increase in amount of water beyond 2%. However, separation rates were significantly different at varying centrifuge speed. In addition, all systems showed reasonably good stability at the ground state with no separation seen below 1000 rpm.

The lipogels injected in to the machine at varying speed showed differences in the slopes. At each time point, the slope of fast injected lipogel was higher than the slowly injected lipogel (Fig. 6.10).

(a)   (b)
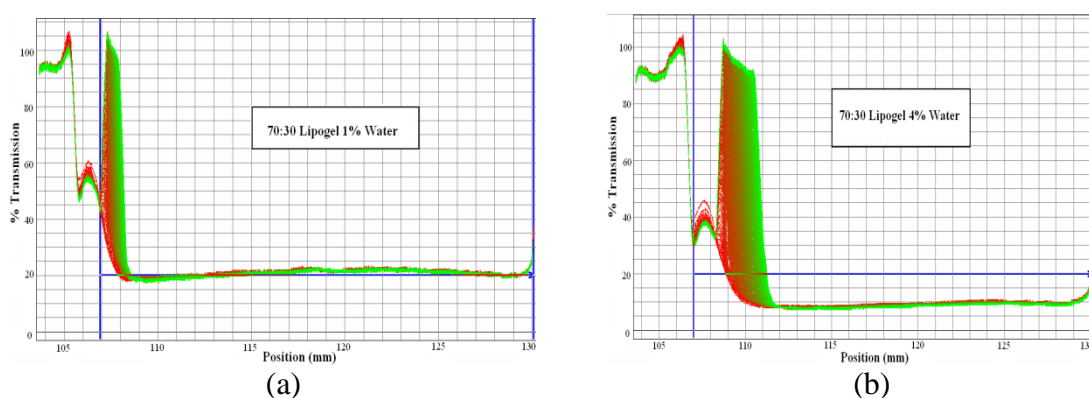
Figure 6.9: Accelerated stability analyses of the lipogels of magnesium stearate and fixed ratio (70:30) of liquid paraffin and palm–olein prepared by method 1 added with (a) 1% and (b) 4% water.
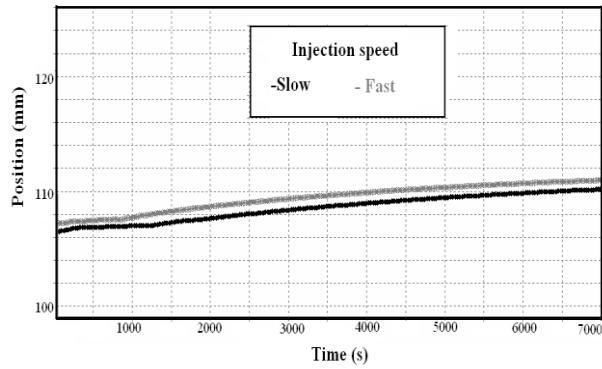
Figure 6.10: Effect of varying injection speed (slow and fast) of the sample into the sample container on the separation behaviour (slope) of the lipogel prepared by method 1 (2% water).

Figure 6.11 shows the % normalised light transmission as a function of phase behaviour. The lipogels containing 1% water showed similar distance between the lines from first profile to last profile (Fig. 6.11a) whereas other lipogels containing 2–4% water showed wider gap between the lines from position 107mm to 110mm (Fig. 6.11b). All samples showed shear thinning behaviour as the separation factor was more than seven (7) in all lipogels.

(a) **(b)**
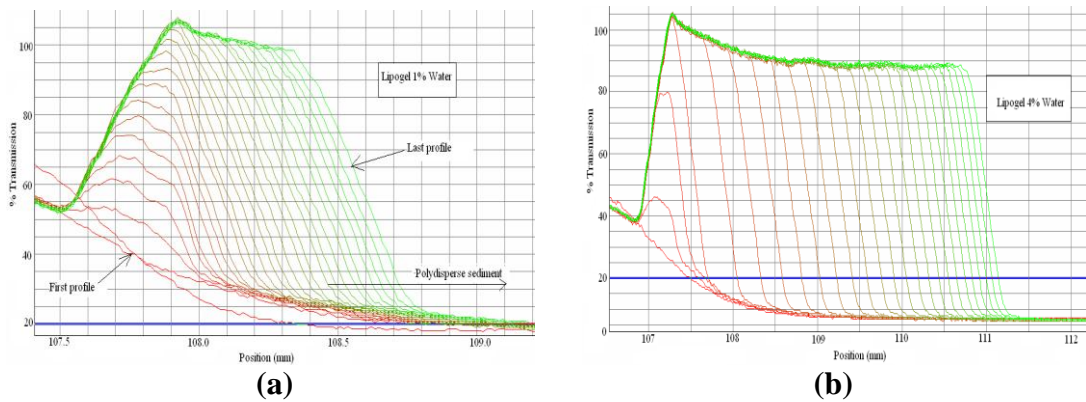
Figure 6.11: Separation kinetics of the lipogels containing 12.5% magnesium stearate with fixed ratio (70:30) of liquid paraffin and palm–olein prepared by method 1 containing various amounts of water (a) 1% and (b) 4%.

6.4 Discussion

Semisolid lipogels of 12.5% mixed homologue MgSt (dihydrate, chapter III) in palm–olein alone and in fixed ratio (70:30) of liquid paraffin and palm–olein were prepared using the two methods developed in chapter V, adapted from Scric's

176

original method. Method 1 involves addition of 1−4% water upon cooling and method 2 involves homogenisation upon cooling without addition of water.

The lipogels of palm–olein prepared by methods 1 and 2 were yellow, non–syneretic semisolids whereas the lipogels of 70:30 ratio of liquid paraffin and palm–olein were off–white, non–syneretic semisolids immediately after preparation. Upon ageing all lipogels prepared by method 2 (homogenised) were solids, not suitable for dermatological use. In contrast, the lipogels prepared by method 1 (added with 1−2% water) were non–syneretic semisolid which showed little change on ageing for two years (to date) suggesting that only method 1 is suitable for the preparation of semisolid, non-syneretic lipogels suitable for dermatological use.

In chapter V we hypothesized formation of reverse lamellar phases in the non-syneretic, semisolid lipogels of liquid paraffin and magnesium stearate in the presence of small amounts (1-2%) of water. The reverse lamellar structures were affected by the pseudopolymorphic changes in the magnesium stearate. The pseudopolymorph containing mixture of crystalline and anhydrous forms produced reverse lamellar phases. In contrast, pure anhydrous or pure crystalline forms did not produce reverse liquid crystalline phases (Fig. 5.13).

Frieberg (1966) demonstrated existence of lamellar liquid crystalline structures in the non-aqueous systems containing sodium stearate and n-hexadecane. In addition, Kon-No and Kitahara (1971) showed formation of reverse micelles of cationic (quaternary ammonium chloride) and anionic (sodium sulfosuccinate) surfactants in non-polar solvents like benzene and cyclohexane. Fukasawa and Tsutsumi (1991) showed presence of fibrous structure due to formation of reverse micelles in the aluminium salt of hexadecyl phosphate/n-hexadecane systems. Similarly, Murdan *et al*., (1999) attributed existence of tubular structures of span 80 in sorbitan mono−oleate to the formation of reverse lamellar phases. Terech and Weiss, (1997) also proposed formation of reverse lamellar phases in the organogels containing long chain fatty acid gelling agents.

We also observed similar tubular structures to Murdan *et al*., (1999) in the lipogels containing magnesium stearate and liquid paraffin alone and a fixed ratio (70:30) of

liquid paraffin and palm–olein in the presence and absence of ibuprofen (Chapter VII). Therefore, formation of tubules in lipogels can be attributed to the reverse lamellar phases, giving semisolid nature to the lipogels. This view was supported by the presence of numerous Maltese crosses in lipogels.

The viscosity measures the ability of any system to resist the structural breakdown during a shearing process (Ribeiro *et al*., 2004). The lipogels of palm–olein alone and in combination with liquid paraffin (30:70 ratio) showed maximum viscosity containing 1% water. However, there was a decrease in viscosity with an increase in water content from 1% to 4% (Fig. 6.8a) suggesting decreased resistance of lipogels to the shear with increasing water content. As discussed earlier formation of semisolid lipogels is attributed to the existence of reverse micelles. However, it has been reported that some non-ionic surfactants do not produce micelles in non-polar solvents but addition of traces of water significantly enhances micelle formation (Kon-No and Kitahara 1971). They proposed that driving and inhibiting force for micelle formation in non-polar solvents is the attraction between the polar groups and stearic hindrance of the hydrocarbon chain of surfactants respectively.

In the previous chapter (Chapter V) we have shown that MgSt in the lipogels of liquid paraffin can exist either in pure amorphous, pure crystalline states or mixture of two affecting properties of the lipogels. The amorphous state was related to solid lipogels whereas the crystalline state formed inverse lamellar phases producing semisolid lipogels (Fig.5.13). In the present chapter, TGA of semisolid lipogels of palm–olein containing 1−2% water showed more water loss than unhomogenised lipogels (Table 6.1). Therefore, it is suggested that the semisolid lipogels containing 1−2% water possess more crystalline component of MgSt, which may increase attraction between the polar groups producing inverse lamellar structures. In contrast, solid lipogels may contain pure amorphous MgSt, which inhibits polar group attraction and micelle formation. Therefore, addition of traces of water (1%) to the lipogels upon cooling may have changed pure anhydrous MgSt to more crystalline form, increasing attractive forces between polar groups to form reverse micelles. In contrast, additional water produces pure crystalline pseudopolymorph, which increases stearic hindrance of the hydrocarbon chains, reducing micelle formation

leading to mobile dispersions.

DSC results also supported this view as there was a decrease in enthalpy values with increasing water content. Semisolid lipogels prepared by method 1 (1% and 2% water) showed a broad endotherm peaking between 80 and 120°C, which was not seen in the lipogels prepared by method 2 (homogenised without water) or Scric's method (unhomogenised without water). Microscopic observations of semisolid lipogels containing 1% and 2% water showed presence of star–shaped crystals, which were not seen in any other unhomogenised or homogenised lipogels, suggesting that certain amount of water (1–2%) is required to produce semisolid lipogels. This observation confirms that this endotherm belongs to the star–shaped crystals produced by addition of traces of water upon cooling, showing high enthalpy values compared to unhomogenised lipogels (Table 6.3).

Long–term stability of the lipogels was confirmed by the results of accelerated stability centrifuge experiment as the lipogels containing 1–2% water showed minimum separation. In addition, all samples were sensitive to the applied shear. This view was supported by the results of accelerated stability centrifuge experiment where speed of the lipogel injection to the sample holder caused significant changes in the separation behaviour. The same lipogel injected at different speed showed slightly different slopes (Fig. 6.10) confirming that these systems are affected by the shear.

6.5. Conclusions

1. Semisolid, non–syneretic lipogels of palm−olein and MgSt alone and in a fixed ratio (70:30) of liquid paraffin and palm–olein were prepared by adding an optimum amount of water (1–2%) to the cooling dispersions (method 1). Therefore, palm–olein can be used alone or in combination with liquid paraffin as a vehicle for the preparation of semisolid, stable lipogels of MgSt suitable for dermatological use. In contrast, lipogels prepared by method 2 (homogenisation) or Scric's method were unstable solids unsuitable for dermatological use.

2. The semisolid appearance of lipogels in the presence of water may be attributed to

the pseudopolymorphic modification in MgSt. The amorphous MgSt in the solid lipogels changes to crystalline form upon addition of water. This was evident from the increased water loss from semisolid lipogels than unhomogenised ones in the TGA experiments.

3. Long–term stability of the lipogels can be predicted by the accelerated stability centrifuge testing, which provides information about the separation rate and particle movement behaviour under high shear rate (4000rpm). The lipogels showed polydispersed, non–flocculated behaviour of system resembling w/o emulsions.

4. The lipogels showed sensitivity to stress evident from the changes in the slopes of the same lipogel when injected into the centrifuge vial at different speed. Slow speed showing low slope whereas fast injection showed slightly higher slope.

CHAPTER VII

INCORPORATION OF IBUPROFEN INTO THE LIPOGELS

7.1 Introduction

The addition of a drug to a formulation may affect its rheological properties (*i.e.* consistency), stability and drug release (Hsu, *et al*.1993; El Gendy *et al*., 2002; Vintiloiu *et al*., 2007). The incorporated drug may participate in the structure of the carrier system by molecular interactions with other constituents of the dosage form (El–Laithy and El–Shaboury, 2002; Mueller–Goymann, 2004). Many drugs show these properties especially if they are also surface active. Ibuprofen (IBP) shows amphiphilic activity and may be expected to affect the physicochemical properties of the dosage forms such as the lipogels. This chapter explores the effect of incorporation of ibuprofen on the microstructure and physicochemical properties of lipogels prepared using mixed homologue magnesium stearate (MgSt) (dihydrate, chapter III) in liquid paraffin, palm−olein and their combination (70:30 ratio respectively) (*c.f.* Chapter VI).

7.1.1 Aims of the chapter

i. To determine the saturated solubility of ibuprofen (IBP) in oils (liquid paraffin, palm−olein and their combination (70:30 ratio respectively)) and in aqueous 0.1M NaOH solution.

ii. To investigate the influence of ibuprofen at its saturation concentration in the oils on the physicochemical properties of lipogels of MgSt (12.5%, 15% and 20%) prepared using the oils (liquid paraffin, palm−olein and their combination (70:30 ratio respectively).

iii. To investigate the effect of ibuprofen (1−5%) on the physical appearance of lipogels prepared with 12.5% magnesium stearate, liquid paraffin and 1−4% Water (*c.f.* method 1, Chapter V).

iv. To investigate the effect of pH adjustment on the physical properties of systems

containing MgSt (12.5%) in liquid paraffin with and without ibuprofen (~5%) formed by the addition of phosphate buffer solutions upon cooling.

7.2 Methods

7.2.1 Determination of saturated concentration of ibuprofen in the oils *i.e.* liquid paraffin, palm−olein and their combination and in 0.1M NaOH solution

The method for the preparation of saturated solutions of ibuprofen in the oils and NaOH solution was adapted from Ng. (2007). Excess (approximately 1.5g) ibuprofen was weighed and mixed separately with 20mL of each oil or 0.1M NaOH (20mL) solution to achieve a homogenous dispersion by stirring with a glass rod in a 100mL conical flask. Additional oil or NaOH solution was added to the mixture to make up the volume to 50mL. The resultant suspension was then transferred to LM−510 Orbital Shaker (Yih Der, Korea) and agitated at $60^{o}C$ for 2 hours at 150rpm. The suspension was then filtered at the same temperature. The filtrate was placed on the bench and allowed to cool to room temperature overnight and filtered again using vacuum filtration with a 0.22μm filter paper. The crystals accumulated on the filter paper after vacuum filtration, were air−dried and stored in a well closed container for future drug release experiments (Chapter VIII). The clear filtrate after appropriate dilution was analysed using UV spectrophotometer at 272nm and the saturation concentration calculated from the standard curve prepared using ibuprofen in the respective oils and NaOH solution and compared with the literature values.

7.2.2 Incorporation of ibuprofen into lipogels

i. Lipogels of MgSt (12.5%) and liquid paraffin containing either 1%, 2%, 3% or 4% water (added at $90^{o}C−$ *c.f.* method 1) were prepared. Molten ibuprofen (1%, 2%, 3%, 4% or 5%) was added at ~$75^{o}C$ during the cooling cycle of preparation *i.e.* just below the melting point ($78^{o}C$) of ibuprofen.

ii. Lipogels with three different concentrations of MgSt (12.5%, 15% and 20%) were prepared in the oils *i.e.* liquid paraffin, palm−olein and their combination (70:30 ratio respectively). For 12.5% MgSt, molten ibuprofen (1%, 1.5%, 2%, 2.5%, 3%, 4%,

4.5% and 5%) was added at ~75°C during the cooling cycle of preparation as above. For the lipogels containing higher amounts of MgSt (15% and 20%) only 3%, 4% and 5% molten ibuprofen was added as above. (Note: these samples did not contain water).

7.2.3 Influence of pH on properties of systems formed by addition of phosphate buffer solution

The effect of pH on systems formed from lipogels of magnesium stearate and liquid paraffin by the addition of phosphate buffer solution was investigated. Two series of experiments were performed. In the first series, phosphate buffer solution of pH 4.1 (~1−4%) was added to the systems whereas in the second series phosphate buffer solution of pH 9.25 (~1−10%) was added. The second series also contained 5% ibuprofen.

Series I: Systems were prepared by method 1 but 1%, 2%, 3% and 4% phosphate buffer solutions of pH 4.1 were added rather than water (Sample 1). A control, containing 2% water was also prepared by method 1 (*c.f.* method 1, Chapter V) (Sample 2).

Series II: Ibuprofen (5%) was added to the systems at 75°C during the cooling cycle of preparation. Upon cooling to room temperature, phosphate buffer solution of pH 9.25 (~1−10%) was added. The systems were investigated visually but only 10% PBS was used for further experiments (Sample 3). Due to time constraints, systems containing PBS of pH 9.25 without ibuprofen were not investigated.

Another system was also prepared by adding 5% ibuprofen at ~75°C as above but no PBS solution was added (Sample 4).

7.2.4 Polarised light microscopy

Leica microscope (Histocentre, Malaysia) was used to investigate the microstructure of ibuprofen raw material and the lipogels prepared using MgSt (12.5%) in liquid paraffin containing 1−4.5% ibuprofen.

7.2.5 Scanning electron microscopy (SEM)

A Leo 1450VP electron Microscope (Oxford Instruments, UK) was used to study structure of the selected lipogels prepared using 12.5% MgSt with liquid paraffin containing 1% and 4% ibuprofen. The lipogels were studied directly without gold coating, by placing a small sample on the stub using cold plate under low vacuum. Each sample was studied at powers between x 15 and x 5000, and photographed at appropriate magnifications.

7.2.6 Differential Scanning Calorimetry (DSC)

A DSC 823^e (Mettler Toledo, Switzerland) was used for the analysis of the selected lipogels containing 1.5−4.5% ibuprofen (*c.f.* section 7.2.2.ii)) in addition to the ibuprofen raw material using a standard heating cycle of $25^oC–150^oC$ at a rate of 10^oC/min to observe thermal changes in the samples. The samples did not contain water.

7.2.7 Rheology

A cone and plate Physica MCR 301, air–bearing Pelletier rheometer (Anton Paar, Germany) with parallel plates (5cm diameter) and zero gap (1mm) was used to investigate the rheology of four samples (section 7.2.3). The lipogels were characterised by flow curves and oscillation sweep studies. All experiments were conducted at room temperature (~28^oC).

Flow curves were derived using standard shearing cycle ($10^{-3}s^{-1}$ –$100s^{-1}$) with a 5 minute sweep time to investigate the zero shear and apparent viscosities (obtained from the apex of the up and down flow curve) of four samples.

Oscillation experiments were conducted using amplitude and frequency sweeps to investigate the effect of low shear on the selected formulations (samples 1−3). The storage or elastic (G′) and loss or viscous (G′′) moduli, complex viscosity and phase angle were investigated.

A standard amplitude sweep of strain (γ) =0.01−100% and constant frequency (ω) =10 1/s was chosen to investigate G′ and G″ in addition to the flow point and deflection angle for four samples.

Typical frequency sweep setting of ω=100−0.1 (1/s) and γ=5% were chosen to obtain G′, G″ and complex viscosity in addition to the deflection angle (delta) of the selected samples (samples 1 and 2). The linear viscoelastic (LVE) region was determined prior to the frequency sweep test.

7.2.8 X-ray diffraction (XRD)

A powder X–ray diffractometer (Bruker 8 Advances, Germany) was used for the analysis of the selected samples (section 7.2.2.ii).

7.3 Results

7.3.1 Appearance of saturated solutions of ibuprofen in the oils and in aqueous 0.1M NaOH solution

Approximately 1.5g of ibuprofen was dissolved in 50mL of each of the oils and aqueous 0.1M NaOH solution and shaken at $60^{o}C$ for 2 hours before it was filtered at the same temperature. The filtrate was cooled to room temperature and filtered using a membrane filter (0.22μ).

Upon mixing, ibuprofen in each of the oils and in NaOH solution produced a homogenous suspension, white for liquid paraffin and NaOH, off−white for the combination of liquid paraffin and palm−olein (70:30 ratio respectively) and pale yellow for palm−olein. Upon heating with continuous shaking at $60^{o}C$ for 2 hours, all ibuprofen dissolved in the respective oils producing a clear solution. Upon cooling to $37^{o}C$, the clear solution showed no change in the appearance. Further cooling to room temperature (~$28^{o}C$) produced short and long needle–like white crystals in each solution. The long crystals appeared at the bottom of the solution. In contrast, short crystals were floating on top of the solution. Upon filtration at room temperature, a clear filtrate was obtained.

The saturated concentration of ibuprofen was determined from the calibration curves constructed separately using the oils and the aqueous 0.1M NaOH. The saturated concentration of ibuprofen in the oils was in the range of 4.2–5g/100mL whereas it was 3.9g/100mL in aqueous 0.1M NaOH solution as shown in Table 7.1.

Table 7.1: Saturated concentrations of ibuprofen in the oils (palm–olein, liquid paraffin and their combination (70:30 ratio respectively) and in aqueous 0.1M NaOH solution at 33°C.

Sample type	Ibuprofen concentration (g/100mL) (Experimental data)	Ibuprofen concentration (g/100mL) (Literature values)
Water	0.00	0.01*
Liquid paraffin	4.20	4.10*
Palm–olein	5.00	−
Combination (70:30 ratio)	4.50	−
Aqueous 0.1M NaOH solution	3.90	4.00**

*Kulichenko and Fessenko (2003); ** Ng (2007)

7.3.2 Appearance of lipogels after incorporation of ibuprofen into lipogels

The lipogels were prepared using 12.5%, 15% and 20% MgSt in the oils (liquid paraffin, palm–olein and their combination (70:30 ratio respectively). Molten ibuprofen (1−5%) was added at ~75°C during cooling cycle (section 7.2.2(ii)).

Upon cooling to room temperature (~28°C), formulations of varying consistency from mobile fluids to semisolid lipogels were obtained depending on the amount of ibuprofen and magnesium stearate.

All systems containing 12.5% MgSt and 1–2.5% ibuprofen were semisolids. The liquid paraffin systems containing oil saturation concentration (~4.2%) of ibuprofen were mobile fluids whereas systems containing palm–olein or combination of liquid paraffin and palm–olein having oil saturation concentration (~5 and 4.5% respectively) were semisolids.

The systems prepared using liquid paraffin containing higher concentrations (15% and 20%) of MgSt and saturation concentration (~4.2%) appeared to be thick

structured fluids and did not change to semisolid lipogels. In contrast, the systems prepared using 12.5–20% MgSt with palm–olein or combination of liquid paraffin and palm–olein (70:30 ratio respectively) containing oil saturation concentration (~5% and 4.5% respectively) of ibuprofen were similar and appeared as semisolid lipogels (Fig. 7.1). Upon storage for two years, no significant changes were observed in all samples.

The systems containing MgSt (12.5%) and liquid paraffin prepared by method 1 (0%, 1%, 2%, 3% and 4% water) containing 0%, 1%, 2%, 3%, 4% and 5% ibuprofen (section 7.2.2(i)) also showed varying consistencies from mobile structured fluids to semisolids as summarised in Figure. 7.2.
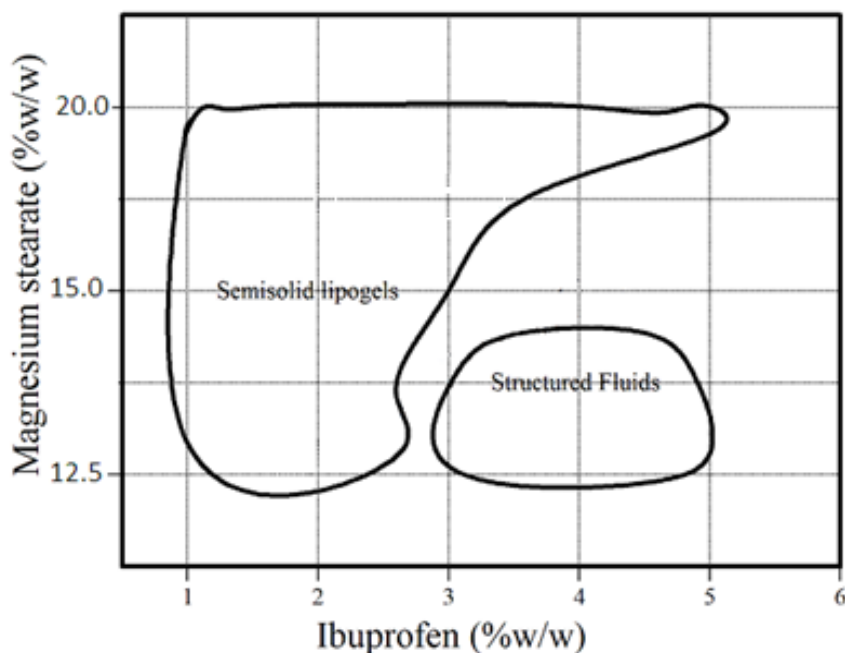
Figure 7.1: Schematic diagram showing summary of physical appearance of selected systems prepared using magnesium stearate (12.5%, 15% and 20%) in palm−olein containing 1−5% ibuprofen (*c.f.* section 7.2.2(ii)).
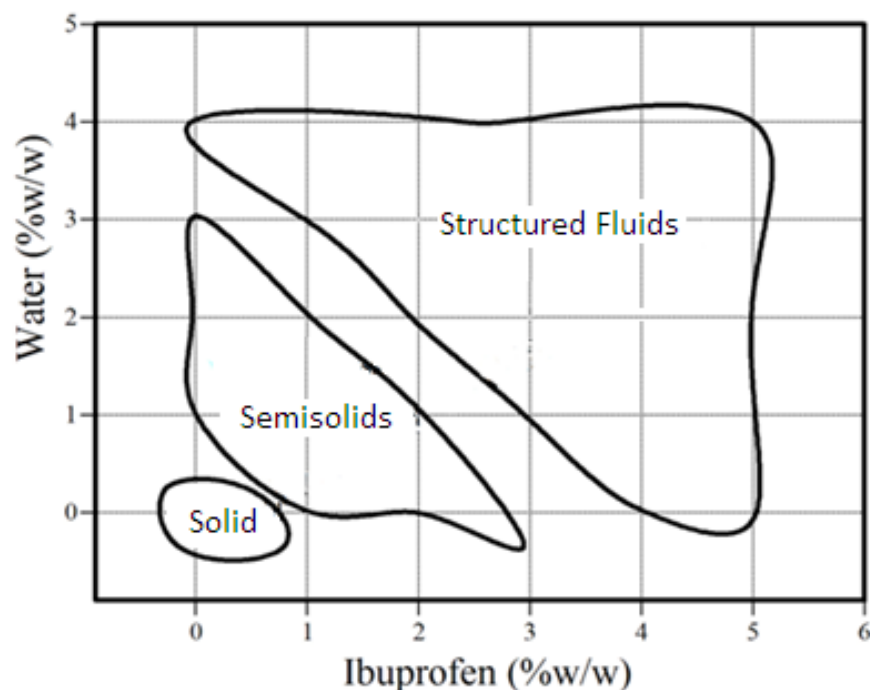
Figure 7.2: Schematic diagram showing effect of ibuprofen (0−5%) on physical appearance of the lipogels prepared using magnesium stearate (12.5%) in liquid paraffin by method 1 (0−4% water-(section 7.2.2 (i)).

7.3.3 Influence of pH on properties of systems formed by addition of phosphate buffer solution

Lipogels prepared by method 1 but using 1–4% phosphate buffer solution (PBS) of pH 4.1 instead of water upon cooling (Sample 1) varied from semisolid to solids depending on the amount of PBS (section 7.2.3). Preparations containing 1–3% PBS appeared to be solids whereas formulation containing 4% PBS was white stable semisolid (no syneresis) lipogels of neutral pH similar to Sample 2 (method 1, Chapter V).

The systems containing 5% ibuprofen, and after addition of ~1−10% PBS of pH 9.25 (section 7.2.3) were liquids to semisolids depending on the amount of PBS *i.e.* systems containing ~1−9% PBS were liquids whereas preparation containing ~10% PBS was semisolid showing neutral pH (Sample 3). In contrast, sample 4 appeared as a white fluid showing acidic (5.5) pH.

7.3.4 Polarised light microscopy

The influence of ibuprofen (1–4.5%) on the lipogels prepared using magnesium stearate (12.5%) in liquid paraffin (section 7.2.2(ii)) was investigated. Addition of ibuprofen (1–4.5%) significantly affected the appearance of the lipogels.

Figure 7.3 shows the photomicrograph of ibuprofen raw material. Anisotropic structures with needle–like crystals were observed against the dark background. Two populations of short and long needle–like crystals were observed.
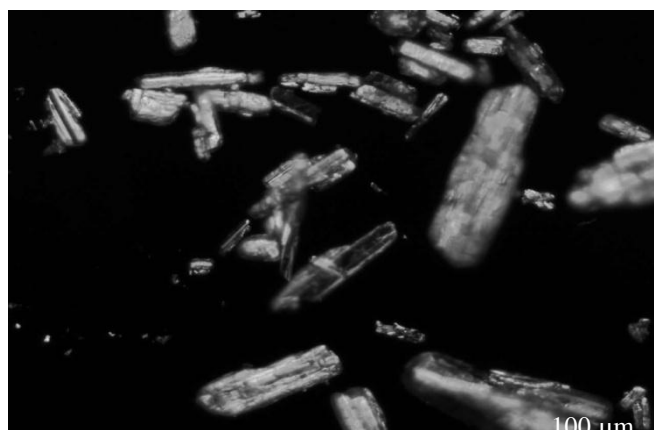
Figure 7.3: Photomicrograph of ibuprofen raw material showing needle–like crystals between cross polars. (Scale: 1cm= 100µm).

Figure 7.4 shows photomicrographs of selected lipogels prepared using magnesium stearate (12.5%) and liquid paraffin containing 1–4.5% ibuprofen (section 7.2.2(ii)). All lipogels showed anisotropic structures with various types of crystals. The lipogels containing low quantity of ibuprofen (1–1.5%) were different from the lipogels containing higher concentration of ibuprofen (2–4.5%). The lipogels containing 1% ibuprofen showed numerous small crystals (Fig. 7.4a) with occasional "Maltese crosses" (not seen). In contrast, the lipogel containing 1.5% IBP showed numerous typical fan–shaped crystals in addition to Maltese crosses (Fig. 7.4b). The lipogel containing 1% IBP showed relatively more structure compared to the lipogels containing 1.5–2.5% IBP. The lipogel containing 1.5% IBP showed three types of anisotropic structures against dark background *i.e.* Maltese crosses, fan–shaped and small crystals (Fig. 7.4b). The lipogels containing 2.5–4.5% IBP showed clusters of flower–shaped crystals. There was a discernible pattern of increase in clusters with

an increase in concentration of ibuprofen (Fig. 7.4b–7.4d). The maximum clusters were observed in the lipogel containing 4.5% ibuprofen (Fig. 7.4d).

(a)

(b)

(c)

(d)
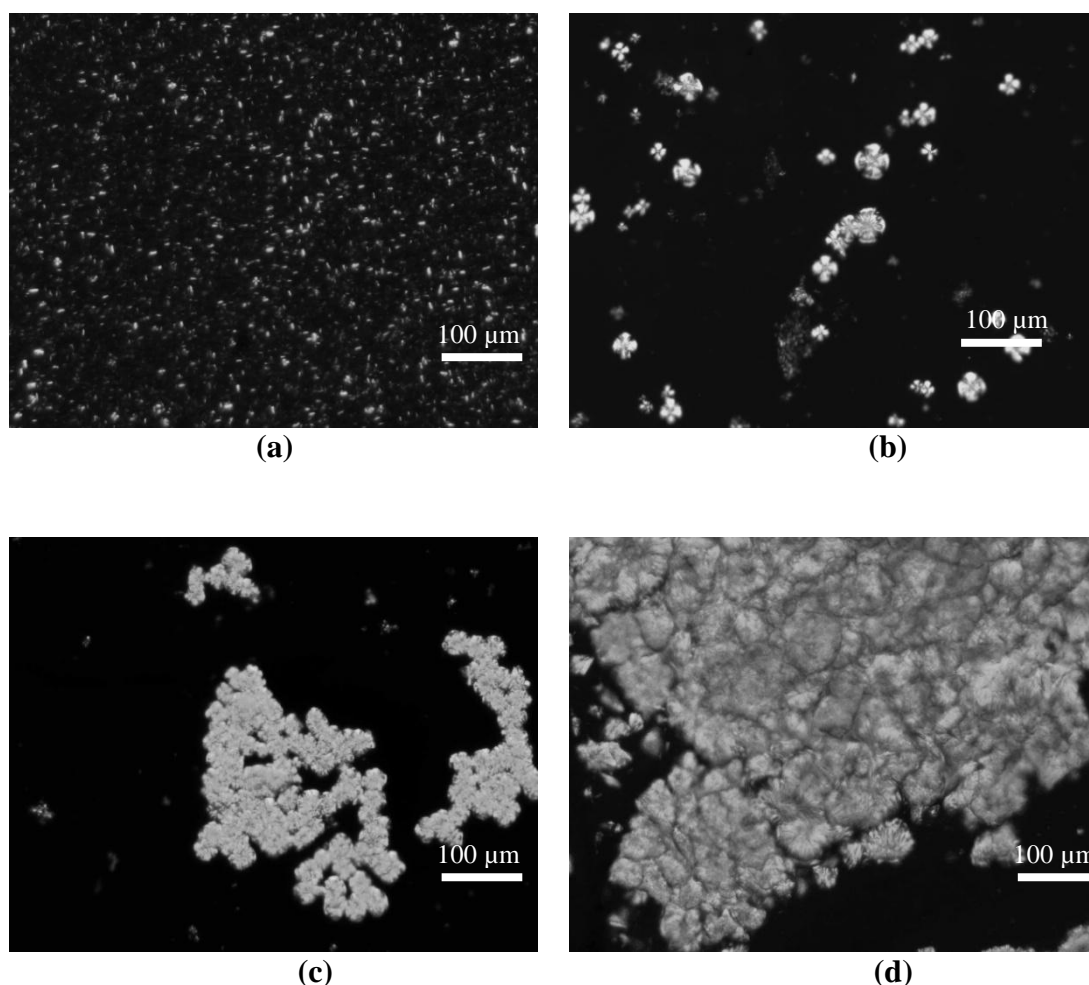
Figure 7.4: Photomicrographs of the selected lipogels prepared using 12.5% MgSt and liquid paraffin containing ibuprofen (a) 1%, (b) 1.5%, (c) 2.5% and (d) 4.5%.

7.3.5 Scanning electron microscopy (SEM)

Lipogels were prepared using MgSt (12.5%) in liquid paraffin containing 1−4% ibuprofen (section 7.2.2(ii)). Figure 7.5 shows electron photomicrographs of the selected lipogels containing 1% and 4% ibuprofen. All lipogels showed numerous needle–like crystals. However, more needle–like crystals were observed in the lipogel containing 1% ibuprofen. The lipogels containing 2–4% ibuprofen showed various plate–like crystals and the number of plate–like crystals increased with an increase in ibuprofen concentration (not shown). The lipogel containing 4%

ibuprofen showed maximum plate–like crystals (Fig. 7.5b). In contrast, occasional plate–like crystals were observed in the lipogel containing 1% ibuprofen (Fig.7.5a).
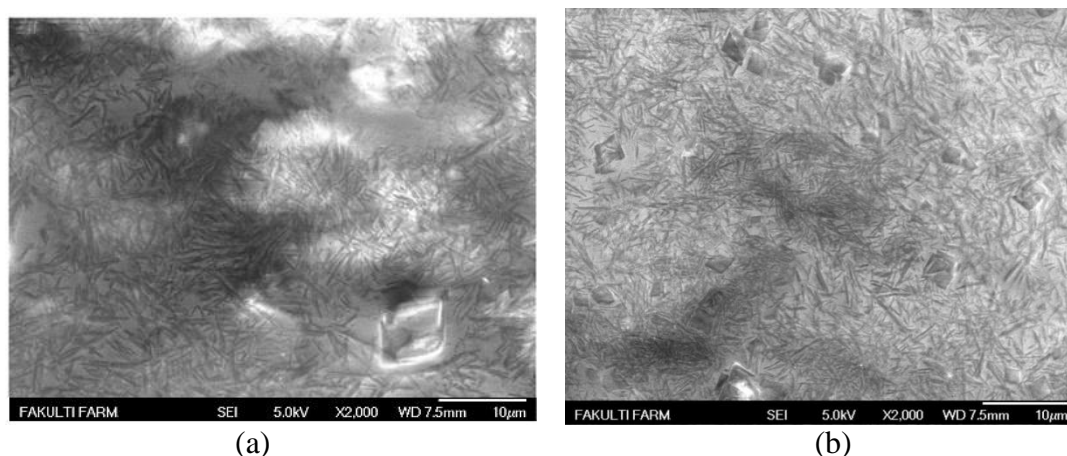
Figure 7.5: SEM photomicrographs of selected lipogels prepared using 12.5% MgSt in liquid paraffin containing ibuprofen (a) 1% and (b) 4%.

7.3.6 Differential Scanning Calorimetry (DSC)

The lipogels prepared using 12.5% MgSt in oils (liquid paraffin, palm–olein and their combination (70:30 ratio respectively) containing 1−4.5% ibuprofen (section 7.2.2(ii)) were analysed using a standard heating cycle of $25^{o}C–150^{o}C$ at a rate of $10^{o}C/min$ to observe thermal changes in the samples.

Figure 7.6 shows the DSC thermogram of ibuprofen raw material. A sharp endotherm was observed, peaking at $~78^{o}C$. Figure 7.7 shows DSC spectra of selected lipogels prepared using magnesium stearate (12.5%) in liquid paraffin containing ibuprofen (1.5–4.5%). Each lipogel showed one to two broad endotherms peaking between 83 and $110^{o}C$. The lipogels containing 1.5−3% ibuprofen showed a low temperature broad endotherm between 83 and $88^{o}C$ and a high temperature small endotherm peaking between 100 and $110^{o}C$. In contrast, the lipogel containing 4.5% ibuprofen showed only one high temperature broad endotherm peaking at $~98^{o}C$. In addition, lipogels containing 1.5%, 3% and 4.5% ibuprofen showed doublets. There appeared to be a discernible pattern of shift to the left in the low temperature endotherm with an increase in ibuprofen concentration.
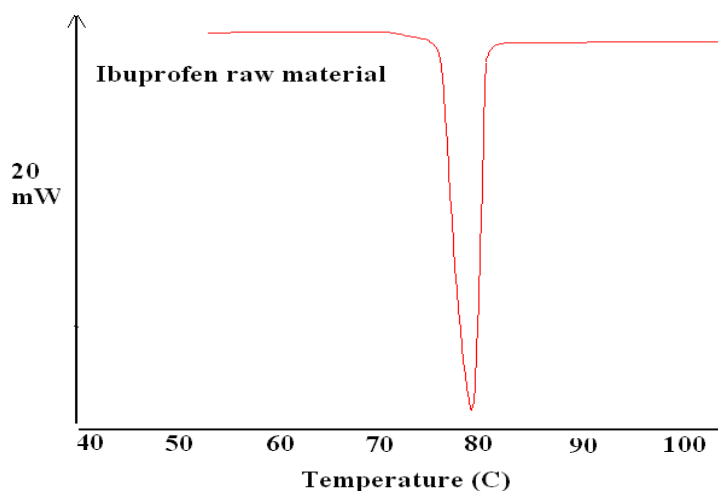
Figure 7.6: DSC 823^e spectrum of ibuprofen raw material conducted using a heating cycle of 25°C–150°C at a rate of 10°C/min.

The lipogel containing 1.5% ibuprofen showed a broad endotherm peaking at 85°C in addition to a high temperature doublet peaking between 100 and 110°C (Fig. 7.7). The lipogel containing 2.5% ibuprofen also showed a broad endotherm peaking at 88°C in addition to a small endotherm peaking at 100°C. The lipogels containing 3% and 4.5% ibuprofen showed doublets between 83 and 98°C. The doublet of lipogel containing 3% peaked between 83 and 88°C in addition to a small endotherm peaking at 100°C. In contrast, the lipogel containing 4.5% ibuprofen showed only a doublet peaking at 98°C (Fig. 7.7).
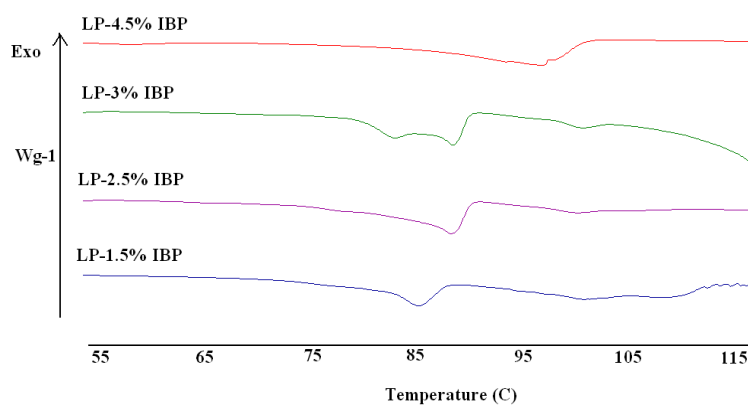
Figure 7.7: DSC 823^e spectra of selected lipogels prepared using magnesium stearate (12.5%) in liquid paraffin containing 1.5–4.5% ibuprofen (section 7.2.2(ii)).

192

Figure 7.8 shows DSC spectra of four samples prepared using magnesium stearate (12.5%) and liquid paraffin containing phosphate buffer solution (section 7.2.3) in addition to the selected lipogels containing higher concentrations (12.5% and 20%) of MgSt in palm−olein and combination of liquid paraffin and palm−olein containing 5% ibuprofen (section 7.2.2(ii)). All lipogels showed one to two distinct endotherms peaking between 50°C and 116°C.

Sample 1 showed a very broad endotherm peaking at 110°C in addition to a small thermal event at 101°C without any peak (Fig. 7.8a). Sample 2 showed two distinct high temperature broad endotherms. The first broad endotherm peaked at 90°C and a second very broad high temperature endotherm peaking at 108°C (Fig. 7.8a). Sample 3 showed two distinct broad endotherms peaking between 87 and 115°C. The first low temperature broad endotherm peaked at 87°C whereas the second extremely broad endotherm peaked at 115°C with a shoulder at 105°C (Fig. 7.8a). In contrast, sample 4 showed a doublet at ~97°C.

The lipogels of higher concentrations (12.5% and 20%) of MgSt in palm−olein and combination of liquid paraffin and palm−olein (70:30 ratio respectively) showed similar thermal events (Fig. 7.8b). Two extremely broad endotherms were observed peaking between 52°C and 80°C.

193
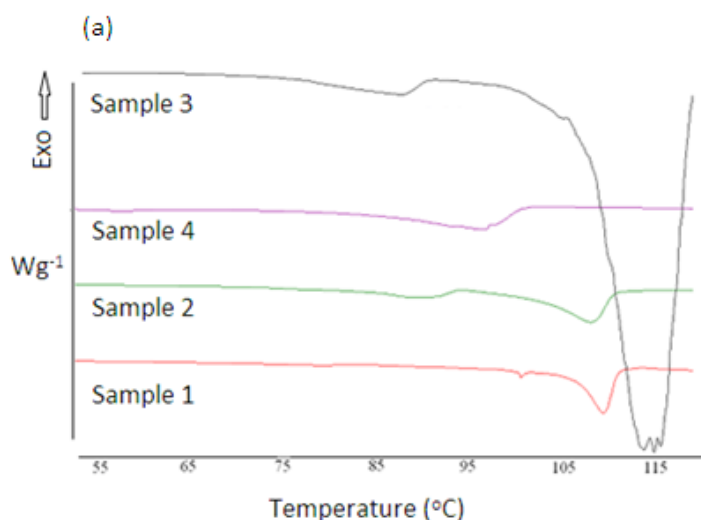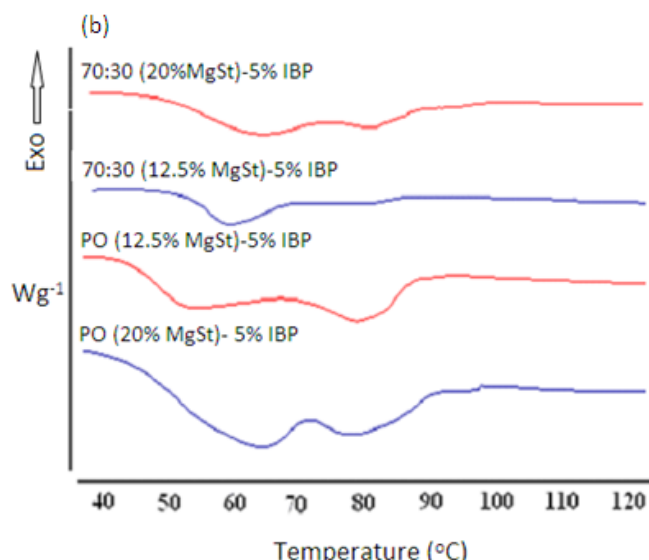
Figure 7.8: Effect of pH. DSC 823^e spectra of (a) four samples prepared using 12.5% MgSt in liquid paraffin containing PBS (section 7.2.3) and (b) selected lipogels containing 12.5% and 20% MgSt in palm–olein and combination of liquid paraffin and palm–olein (70:30 ratio respectively) containing 5% ibuprofen (section 7.2.2(ii)).

There appeared to be a decrease in enthalpy values with an increase in ibuprofen concentration in all lipogels (Table 7.2). Sample 3 showed highest (-40.85J/g) enthalpy values. In contrast, sample 4 showed lowest enthalpy (-1.39J/g) values. The enthalpy values and peak temperatures of all lipogels are summarised in Table 7.2.

Table 7.2: Effect of pH. DSC results showing peak temperatures and enthalpy values of lipogels prepared using MgSt in the oils containing ibuprofen (1−5%) with and without addition of PBS.

Sample Type	Peak Temperature (^{o}C)	Enthalpy (J/g)
LP–1.5%IBP (Fig. 7.7)	84.87, 108.46	-18.75
LP–2.5%IBP (Fig. 7.7)	88.01,99.77	-16.24
LP–3%IBP (Fig. 7.7)	88.16, 100.18	-13.71
LP–4.5%IBP (Fig. 7.7)	96.75	-13.14
Sample 1 (Fig. 7.8a)	101.01. 110.23	-13.21
Sample 2 (Fig. 7.8a)	90.01, 108.10	-18.64
Sample 3 (Fig. 7.8a)	88.27, 115.01	-40.85
Sample 4 (Fig. 7.8a)	99.01	-1.39
PO (12.5%MgSt) –5%IBP (Fig. 7.8b)	50.00, 80.00	-4.07
PO (20%MgSt) –5%IBP (Fig. 7.8b)	55.00, 84.00	-5.04
70:30 (12.5% MgSt) –5%IBP (Fig. 7.8b)	55.05	-4.34
70:30 (20% MgSt) –5%IBP (Fig. 7.8b)	55.01, 78.05	-5.47

7.3.7 Rheology

Figures 7.9 and 7.10 show flow curves and effect of increase in shear rate on apparent viscosity respectively of the four samples prepared using magnesium stearate (12.5%) in liquid paraffin containing PBS (section 7.2.3).

All samples showed non–Newtonian behaviour with flow curves in the form of anti−clock−wise hysteresis loops. Rheograms of all four samples were different from each other showing varying hysteresis loops *i.e.* sample 2 showing the broadest loop and sample 4 the smallest (Fig. 7.9). There appeared to be an increase in the area of hysteresis loop with addition of PBS to the lipogels. In addition, samples 1, 2 and 3 also showed certain amount of yield values.
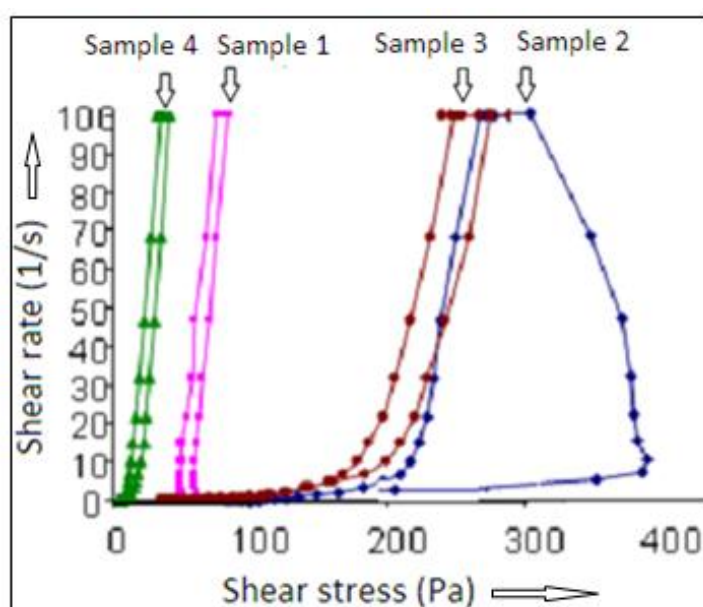
Figure 7.9: Effect of pH. Flow curves of four samples prepared using MgSt (12.5%) in liquid paraffin containing phosphate buffer solutions with or without ibuprofen (section 7.2.3). A standard shearing cycle ($10^{-1}s^{-1}$–$100s^{-1}$) was used.
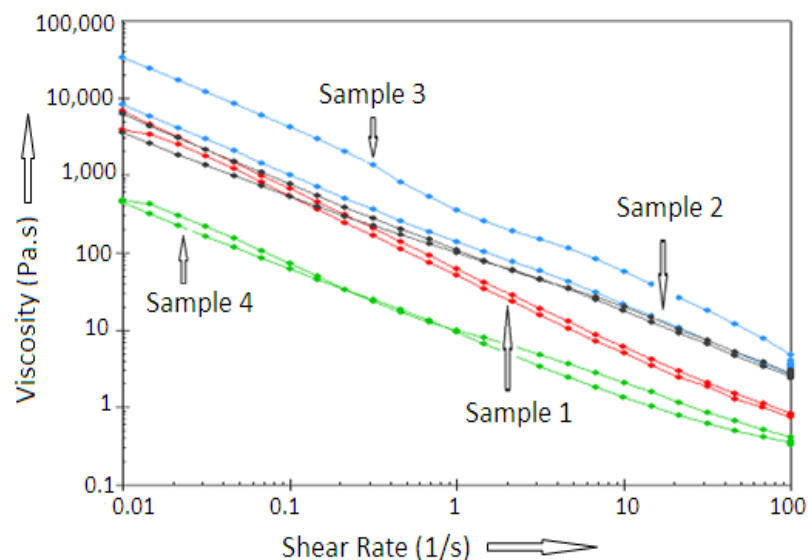
Figure 7.10: Effect of increase in shear rate on the apparent viscosities of four samples prepared using MgSt (12.5%) in liquid paraffin containing phosphate buffer solutions with or without ibuprofen. A repeat cycle (0.01 to 100 to 0.01) was used.

There appeared to be marked differences in the apparent viscosities of all samples. Sample 2 showed maximum viscosity and sample 4 the minimum (Table 7.3). The corresponding apparent viscosities of samples 1, 2, 3 and 4 were 0.50, 0.86, 0.76 and 0.37 Pa.s respectively (Table 7.3). Upon increasing shear rate to 100/s, there was a marked decrease in the apparent viscosity of all samples. Samples 1, 2 and 3 were semisolid and showed yield values of 38.7, 134 and 62.5 Pa respectively. In contrast, sample 4 was liquid and did not show any yield value. Upon storage for 3 months, sample 2 showed significant increase in apparent viscosity. In contrast, other samples showed little change in apparent viscosity with time (Table 7.3).

Table 7.3: Effect of pH. Rheological data of four samples prepared using MgSt (12.5%) in liquid paraffin containing phosphate buffer solutions with or without ibuprofen (section 7.2.3).

Sample	Apparent viscosity day zero (Pa.s)	Apparent viscosity 3 months (Pa.s)	Yield value (Pa)
Sample 1	0.50	0.67	38.7
Sample 2	0.86	0.90	314
Sample 3	0.76	0.80	62.5
Sample 4	0.37	0.40	–

196

Figures 7.11 and 7.12 show the oscillation amplitude sweep experiments of selected formulations (samples 1, 2 and 3). The storage (G′) and loss (G″) moduli in addition to the deflection angle and flow point were investigated using an increasing strain from 0.01–100% at a fixed frequency (10s^{-1}). Figure 7.11 shows storage and loss moduli in addition to the flow point for all the three samples. In contrast, Figure 7.12 shows the deflection angles.

All three samples showed storage moduli (G′) to be higher than the loss moduli (G″) in the viscoelastic region (VER) and the opposite trend was observed after the flow point *i.e.* cross–over point for the two moduli (Fig. 7.11). Each sample showed distinct flow point at different strain values.

Samples 2 and 3 showed rather similar storage (G′ ~10^5 Pa) and loss moduli (G″ 10^4 Pa) values. In contrast, G′ and G″ for sample 1 were significantly lower *i.e.* ~10^4 and 10^3 Pa respectively (Fig. 7.11). Further increase in strain up to 100% caused a sharp decrease in G′ of sample 3 and it reached almost the same value as sample 1 *i.e.* 10^2. In contrast, sample 2 showed higher G′ values *i.e.* 10^3. Flow point of samples 1 and 2 were rather similar *i.e.* ~20% strain. In contrast, sample 3 showed lower flow point (~1% strain).
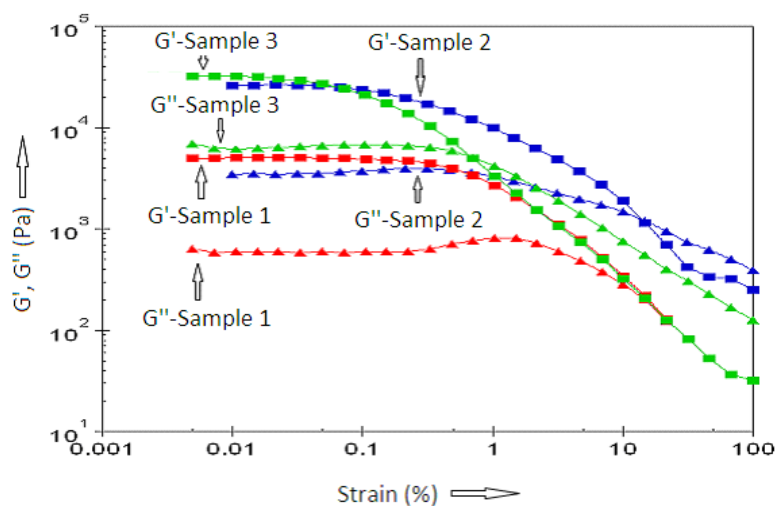
Figure 7.11: Effect of pH. Oscillation amplitude sweep experiments showing effect of increasing strain on the storage and loss moduli and flow points of selected samples 1, 2 and 3 (section 7.2.3). A standard strain sweep cycle (0.001 to 100%) was used.

Figure 7.12 shows deflection angle for samples 1, 2 and 3. An increase in strain showed an increase in deflection angle (δ) for all three samples. Sample 3 showed highest increase in δ *i.e.* 80° and sample 2 the lowest *i.e.* 40° at 100% strain.
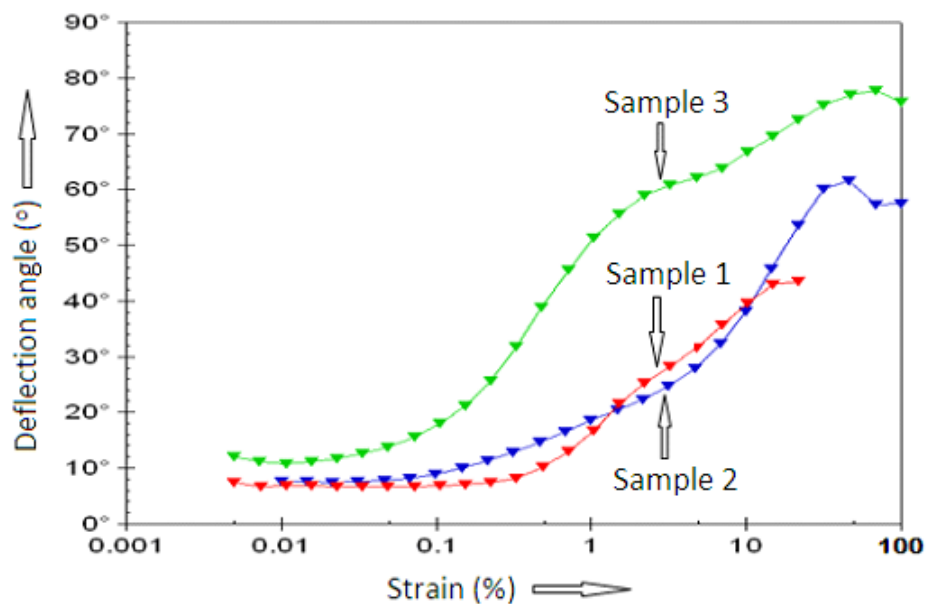
Figure 7.12: Effect of pH. Oscillation amplitude sweep experiments showing effect of increase in strain on the deflection angle of selected samples 1, 2 and 3 (section 7.2.3). A standard strain sweep cycle (0.001 to 100%) was used.

Figures 7.13–7.15 show rheograms of the frequency sweep experiments conducted using a setting of ω=100–0.1 (1/s) and γ=5% to investigate G′, G″ and complex viscosity in addition to the deflection angle (delta) for samples 1 and 2 (section 7.2.3). The G′ for sample 2 was significantly higher (4E+4 Pa) than sample 1 (5E+3 Pa) at higher frequency (Fig. 7.13). An increase in frequency showed an increase in the storage modulus of sample 2. In contrast, increase in frequency did not change G′ for sample 1. In addition, loss modulus (G″) for sample 2 appeared to be similar to the storage modulus (G′) for sample 1.
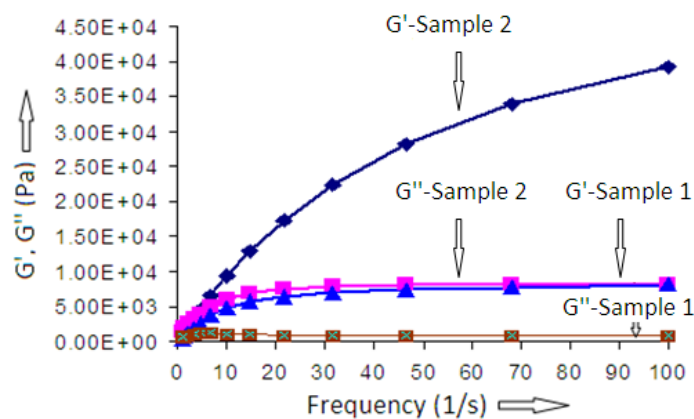
Figure 7.13: Effect of pH. Oscillatory frequency sweep experiments showing effect of increase in frequency on the storage and loss moduli of selected samples 1 and 2 (section 7.2.3). A standard frequency sweep cycle (0 to 100 (1/s)) was used.

Figures 7.14 and 7.15 show the effect of increase in frequency on the deflection angle and the complex viscosity of samples 1 and 2 respectively. The deflection angle and complex viscosity of sample 2 appeared to be higher than sample 1. An increase in frequency showed no effect on the deflection angle of both samples (Fig. 7.14). However, an increase in frequency (0–10 1/s) markedly decreased complex viscosity of both samples after which there was no effect of frequency increase on the viscosity (Fig. 7.15). This region of frequency (0–10) is considered as the linear viscoelastic (LVE) region.
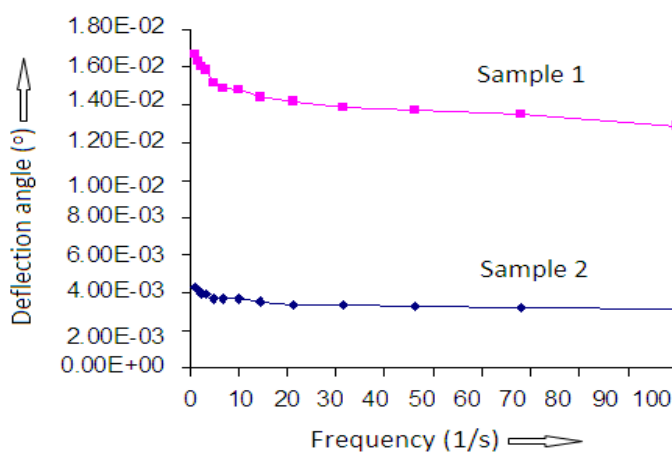
Figure 7.14: Effect of pH. Oscillatory frequency sweep experiments showing effect of increase in frequency on the defection angles of selected samples 1 and 2 (section 7.2.3). A standard frequency sweep cycle (0 to 100 (1/s)) was used.

199
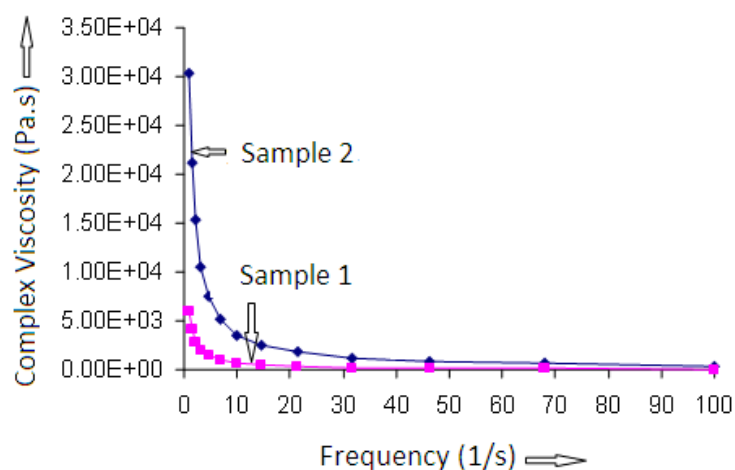
Figure 7.15: Effect of pH. Oscillatory frequency sweep experiments showing effect of increase in frequency on the complex viscosity of selected samples 1 and 2 (section 7.2.3). A standard frequency sweep cycle (0 to 100 (1/s)) was used.

7.3.8 X-ray diffraction (XRD)

Figure 7.16 shows the XRD spectra of the selected lipogels prepared using MgSt (12.5%) in liquid paraffin containing 1%, 3% and 5% ibuprofen (section 7.2.2(ii)). All lipogels showed numerous peaks of varying intensity at 2θ between 5 and 25°. There appeared to be an increase in peak intensity with an increase in ibuprofen concentration from 1−5% at 2θ between 20 and 24° (Fig. 7.16a). The lipogel containing 3% and 5% ibuprofen showed three distinct sharp peaks at 2θ= 20, 22 and 24°. In contrast, lipogel containing 1% ibuprofen showed only two peaks *i.e.* at 2θ=20 and 24° of relatively low intensity.

All lipogels also showed a sharp peak of varying intensity at low 2θ=5° (Fig. 7.16b). The lipogels containing 1% and 3% ibuprofen showed similar intensity. In contrast, lipogel containing 5% ibuprofen showed significantly low intensity. Several small peaks of similar intensity were also seen in all preparations at 2θ between 8 and 10° with no significant differences.

200
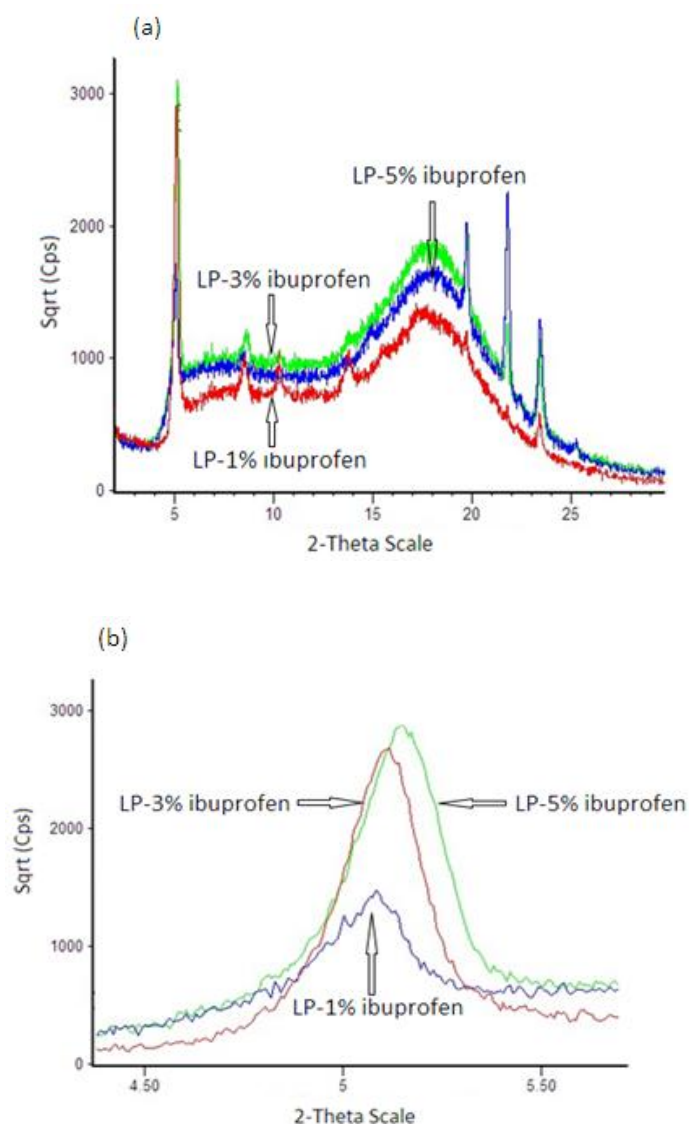
Figure 7.16: XRD diffractograms of the lipogels prepared using 12.5% magnesium stearate in liquid paraffin containing 1%, 3% and 5% ibuprofen (section 7.2.2.(ii)) showing peaks at (a) full scale ($2\theta=3-40^{\circ}$) and (b) specified 2θ scale between $4.5-5.5^{\circ}$.

7.4 Discussion

Lipogels of MgSt (12.5%, 15% and 20%) were prepared in the oils *i.e.* liquid paraffin, palm−olein and their combination (70:30 ratio respectively). For 12.5% MgSt, molten ibuprofen (1%, 1.5%, 2%, 2.5%, 3%, 4%, 4.5% and 5%) was added upon cooling at 75°C whereas only 3%, 4% and 5% molten ibuprofen was added to lipogels with 15% and 20% MgSt (section 7.2.2.(ii)). These systems did not contain

water. In addition, effect of incorporation of ibuprofen (1−5%) was also investigated on the lipogels prepared by method 1 *i.e.* 1−4% water- Chapter V (section 7.2.2(i). The effect of pH was investigated on properties of the lipogels by adding phosphate buffer solutions upon cooling (section 7.2.3).

Lipogels prepared using MgSt (12.5%) in liquid paraffin containing ibuprofen (1−4.5%) showed liquids to semisolid appearance depending on the quantity of ibuprofen. Lipogels with lower concentrations (1−2.5%) of ibuprofen showed semisolid appearance with higher viscosity than the structured fluids obtained with higher amounts (3−4.5%) of ibuprofen (IBP). This implies that ibuprofen destroys structure.

Lipogels containing 15% and 20% MgSt in palm−olein and combination of liquid paraffin and palm−olein (70:30 ratio respectively) containing 5% ibuprofen resulted in semisolid lipogels. In contrast, the lipogels of liquid paraffin with 20% MgSt produced thick structured fluids suggesting significant differences in the structure of various lipogels.

The literature on microstructure of semisolids is confused as researchers do not distinguish between liquid crystalline (micelles, tubules, liposomes) and α-crystalline structures. α-crystalline lamellar structures have been attributed to the swelling and stability of aqueous semisolid systems. However, rheological properties of the systems showing α-crystalline or liquid crystalline phases are significantly different. The liquid crystals can entrap very small amount of water showing limited swelling of the systems. In contrast, α-crystalline lamellar gel phases can accommodate significant amount of water showing enormous swelling of the aqueous systems (Eccleston, 1986; 1997).

Mueller–Goymann (2004) in her review of colloidal delivery systems described that drugs possessing surfactant–like activity can affect the microstructure of the dosage form by molecular interactions with other components of the dosage form, changing physicochemical properties of the drug delivery system. Stability of colloidal dispersions may be associated with the formation of mesomorphic lamellar structures

such as micelles, vesicles, liquid crystals, hexagonal or nanoparticle (Rao et al., (1992); Kriwet and Mueller–Goymann, (1993). Therefore, addition of amphiphilic drug may disrupt these microstructures causing changes in the rheological properties of the dosage form. Vintiloiu *et al*., 2007 also observed decrease in gel–sol temperature in the oleogel containing Safflower oil and an organogelator upon incorporation of increasing amounts (4–40%) of rivastigmine and correlated these changes to the weakening of the interactions between organogelator and the oil phase. Therefore, the same analogy can be used to explain a decrease in enthalpies and viscosities of the lipogels containing magnesium stearate in the oils with an increase in ibuprofen from 1–5% and may be related to the weakening of the MgSt–liquid paraffin interactions, leading to the breakdown of the gel structure producing structured fluids.

Apparent viscosity values measure the ability of any system to resist the structural breakdown during a shearing process (Realdon *et al*., 2001; Ribeiro *et al*., 2004; Tadros, 2004). Furthermore, viscosity determinations provide information about the structural organisation of the formulation *i.e.* there is an increased organisation of the lamellar structure with an increase in the viscosity. Generally, viscosity of the aqueous cubic and hexagonal mesophases is higher than the lamellar mesophases which is associated to the three–, two– and one–dimensional structure respectively (Kohler and Strand, 1990; Mueller–Goymann, 2004). The lipogels without ibuprofen showed a good structural network with significantly higher apparent viscosities compared to the lipogels containing various amounts of ibuprofen (1−5%). It can be postulated that a decrease in viscosity with an increase in ibuprofen concentration causes structural breakdown mainly due to disruption of lamellar structure. These observations were further confirmed by the DSC and microscopy data. The lipogels with and without ibuprofen showed significantly different thermal events *i.e.* enthalpy values for the lipogels containing ibuprofen (~5%) was 5 fold lower than the lipogels prepared by method 1 (2% water) instead of ibuprofen (Table 7.3), suggesting that ibuprofen causes significant reduction in the thermodynamic activity of the lipogels.

Microscopic investigations also support this view as the lipogels without ibuprofen showed numerous "Maltese crosses" suggesting the existence of hexagonal lamellar structures (Fig. 7.4a). Furthermore, some lipogels showed typical fan–shaped anisotropic structures (Fig. 7.4b) providing strong evidence of existence of hexagonal arrangement of reverse lamellar phases. This observation is consistent with the previous knowledge of the lipogels containing magnesium stearate and liquid paraffin (Scric *et al.* 1988), which suggested that unstable gels showed isotropic structure in contrast to the anisotropic micellar structure of stable gels between cross polars.

All lipogels contained needle–like crystals. Murdan *et al.*, (1999) showed presence of needle–like crystals in the organogels and described them as tubules. Therefore, same analogy can be used in the present work and the needle–like crystals (tubules) in lipogels may represent α−crystalline lamellar structures.

An increase in ibuprofen concentration from 1% to 4.5% caused significant change in the structure of the semisolid lipogels producing structured fluids. This observation was supported by electron photomicrographs of the lipogels containing ibuprofen (1–4.5%). Lipogels containing 1% ibuprofen showed needle–like crystals, with occasional plate–like crystals (Fig. 7.5a). In contrast, lipogels with higher concentration (~4.5%) of ibuprofen showed numerous plate–like crystals (Fig. 7.5b). Presence of plate–like crystals in semisolid aqueous systems has been related to the unstable systems (Eccleston, 1986). Therefore, fluid nature of preparations containing 3–4.5% ibuprofen may be attributed to the presence of plate–like crystals rather than inverse lamellar phases. It is suggested that ibuprofen at lower concentration (1–2.5%) fixes itself in between the fatty acid voids reducing viscosity of solids (prepared without ibuprofen or water) forming lamellar structure, showing semisolid consistency. This hypothesis was supported by increased d spacing, evident by a left shift of the peaks at $2\theta=21–24^{o}$ in the lipogels containing lower amount of ibuprofen. However, further addition of ibuprofen (3–5%) caused disruption of the liquid crystalline lamellar structure developed due to interaction of magnesium stearate and the liquid paraffin. This view was supported by the

microscopic results where flower–like crystals were observed in the lipogels containing ibuprofen which increased in number with an increasing amount of ibuprofen (Fig. 7.4c–d).

Ibuprofen is an aryl propionic acid derivative and forms thermotropic mesophases alone or lyotropic liquid crystalline mesophases with the solvents (Westensen *et al*., 2001). The thermotropic mesophases of the drug may interact with mesomorphic vehicles in addition to the liquid crystalline and lamellar structures (Mlodozeniec, 1978). Therefore, lower enthalpies and decreased viscosity of the lipogels with increasing amount of ibuprofen can be attributed to its molecular interactions with the aggregates formed by liquid paraffin and MgSt causing disruption of lamellar structures forming clusters of flower–like crystals. Ibuprofen is known to act as a surfactant. Al–Saidan, (2004) suggested that ibuprofen interacts with stratum corneum (SC), partially extracts lipids from the SC causing hydration. As discussed above, there appeared to be interaction of ibuprofen with the components of lipogels *i.e.* magnesium stearate and/or liquid paraffin depending on the amount of ibuprofen. Therefore, at higher concentration (2.5–4.5%), ibuprofen due to surface activity may have extracted magnesium stearate from the lipogels, forming flower–like crystals.

Effect of ibuprofen on the modification of lamellar structure of lipogels can also be explained in terms of pseudopolymorphic modification of MgSt from partially crystalline to fully crystalline material producing structured fluids. This view was supported by the XRD results. An increase in ibuprofen concentration from 1−5% showed significant increase in intensity of peaks at 2θ=5, 20 and 24$^\mathrm{o}$, suggesting an increase in crystalline nature of MgSt, disrupting lamellar structures and producing structured liquids. Ibuprofen having acidic properties at lower pH, may dissociate (ionise) upon dissolution in water (neutral to basic pH) to form salts with amphiphilic properties and together with appropriate counter ions may form lyotropic mesophases (micelles) with water giving structure to the dosage form as described by Mueller–Goymann, (2004).

Similar results were obtained in the present work where liquid formulations containing higher quantities of ibuprofen (~4.5%) added with PBS (water) produced

semisolid lipogels showing lamellar structures. Formulations were liquids at slightly acidic pH (5–6). In contrast, semisolid lipogels were obtained at neutral to slightly basic pH. Ibuprofen is a hydrophobic material at low pH and its hydrophilicity increases with an increase in pH as the unionised carboxylic acid changes to an ionised form (Sarveiya *et al*. 2004). However, in lipophilic medium ibuprofen may form neutral ion–pairs with counter–ions at higher pH increasing its lipophilicity by binding to the medium (Comer, 2005). Therefore, ibuprofen may be present in unionised form at low pH producing liquid formulations. Nevertheless, addition of PBS (water) of higher pH, may have converted unionised ibuprofen to neutral ion–pairs, leading to increased lipophilicity forming new aggregates composed of IBP–MgSt–liquid paraffin–water producing semisolid lipogels.

This above view was supported by microscopic observations as none of the lipogels containing phosphate buffer solutions showed flower–like crystals, which were observed in abundance in the liquid formulations. However, no Maltese crosses were observed. In addition, fan–shaped crystalline structures suggesting hexagonal crystalline phases in the lipogels after addition of phosphate buffer solutions were also different from the lamellar structures observed in the semisolid lipogels of liquid paraffin, MgSt and water without ibuprofen. This observation suggests that the aggregates formed after pH adjustment are due to entrapment of water in the lipogel structure forming a bridge between ibuprofen and MgSt–liquid paraffin aggregates, significantly increasing viscosity, evident from increased interlamellar distance. DSC data also supported the view as the enthalpies of the lipogel containing 5% ibuprofen with phosphate buffer solution (sample 3) was significantly higher than the liquid formulations containing ibuprofen (5%) but without pH adjustment (sample 4) (Table 7.3).

Rheological data of all the three semisolid formulations (samples 1, 2, and 3) showed G′ to be higher than G″ at lower shear stress suggesting elastic nature of these lipogels at rest and deformation of structure at higher stress (Fig. 7.10). Deflection angle of $8–12^{o}$ at low strain also suggested elastic nature of these lipogels (Fig. 7.12). Although, apparent viscosity of sample 3 was rather similar to sample 2 but flow point of samples 1 and 2 (no ibuprofen) was higher than sample 3 (containing 5%

ibuprofen and pH adjusted with ~10% PBS of pH 9.25) suggesting that lipogels without ibuprofen are more resistant to stress compared to the semisolid lipogel containing 5% IBP and pH adjusted with PBS (sample 3). Furthermore, sample 3 (semisolid lipogel) showed higher apparent viscosity compared to sample 4 (5% IBP but no pH adjustment with PBS). DSC results also showed higher enthalpies for sample 3 than sample 4 suggesting that sample 3 was more stable than the formulation containing same amount of ibuprofen without pH adjustment (sample 4). These observations again support the view that pH adjustment (addition of water) provides rheological strength to the formulation containing magnesium stearate, liquid paraffin and ibuprofen due to formation of mesomorphic liquid crystalline structures related to pseudopolymorphic changes in MgSt from fully crystalline to partial crystalline material.

7.5 Conclusions

i. Incorporation of saturated amount (4.5–5%) of ibuprofen in the lipogels containing magnesium stearate and the oils (liquid paraffin, palm−olein and their combination (70:30 ratio respectively) produced structured fluids of low enthalpy and viscosity with numerous clusters of flower–like crystals causing disruption of the lamellar structures formed in the absence of ibuprofen in the lipogels.

ii. However, addition of ~10% phosphate buffer solution of pH 9.25 converted structured fluids of low enthalpy and apparent viscosity to stable semisolid lipogels (no syneresis) of significantly higher enthalpy and apparent viscosities.

iii. Stability (no syneresis) of semisolid lipogels containing saturated amounts of ibuprofen can be attributed to the added buffer (PBS), which bridges between ibuprofen and MgSt–liquid paraffin aggregates forming hexagonal lamellar structures evident from the presence of Maltese crosses and fan–like structures.

iv. The changes in physical and microscopic appearance may also be related to the surface activity, presence of counter ions of ibuprofen and pseudopolymorphic change in magnesium stearate from fully crystalline material to mixture of crystalline and amorphous material.

CHAPTER VIII

IN VITRO DRUG RELEASE STUDIES

8.1 Introduction

Saturated oil concentrations of ibuprofen (~5%) in lipogels containing magnesium stearate (12.5% and 20%) in the oils *i.e.* liquid paraffin, palm−olein and their combination (70:30 ratio respectively) produced either structured fluids or semisolid lipogels depending on concentration of magnesium stearate and the type of the oil (*c.f.* Chapter VII). The present chapter explores diffusion of oil saturated concentrations of Ibuprofen from lipogels and structured fluids using Franz diffusion cells.

Due to large variations in drug release profile, validation of Franz diffusion cells prior to actual drug release experiments has become integral part of drug release studies. Generally, the one factor at a time (OFAT) approach is used for the method validation, which uses trial and error methods requiring significantly long experimentation times. Ng, (2007) performed detailed investigation of factors affecting validation of tailor-made static Franz diffusion cells. This chapter explores critical factors, based on Ng, (2007) experimental approach but with different set (PermGear) of Franz diffusion cells by a systematic Design of Experiment approach (discussed in Chapter II) using a commercial 5% ibuprofen hydrogel. The validated Franz cells were then used to investigate the release of ibuprofen from lipogels containing magnesium stearate in the oils.

8.2. Aims of the chapter

The aim of the present chapter is to investigate the diffusion of Ibuprofen from the lipogels prepared from magnesium stearate and the oils (liquid paraffin, palm−olein and the combination of liquid paraffin and palm−olein (70:30 ratio respectively) using Franz diffusion cells. The overall aims include:

i. An investigation of the critical factors causing variations in drug release by validation of Franz diffusion cells using a systematic design of experiment (DoE) approach.

ii. An investigation into the drug release of an oil saturated concentration (~5%) of ibuprofen from lipogels prepared using magnesium stearate (12.5% and 20%) and the oils (liquid paraffin, palm−olein and the combination of liquid paraffin and palm−olein (70:30 ratio respectively)

8.3. Methods

8.3.1 Preliminary studies to validate Franz Cells

Validation of Franz diffusion cells experiments involves investigation of numerous factors related to dimension of the donor and the receptor, temperature and stirring, membrane type and its quality, membrane soaking time, closure of all openings of the donor and the receptor, sampling frequency, sampling site and degassing of the receptor medium. Hence it was not possible to study all factors using DoE. Therefore, the factors such as closing of all openings, degassing of the receptor dissolution medium, membrane soaking and matching of the donor and the receptor were investigated using preliminary studies prior to investigation of the critical factors using DoE.

8.3.1.1 Investigation into the dimensions of Franz cells

Franz cell apparatus including donor, receptor (with two sampling arms), stirrer (PermGear, Bethlehem, USA) and a thermostatic water pump (Huber, Germany) were used for the drug release experiments (*cf.* Chapter II). The height, internal diameter of the donor and the receptor were measured using a pair of digital caliper. Effective diffusion area (E.D.A.) was calculated with the help of formula πr^2, where r is the radius of the donor and the receptor. The angles of the two arms of receptor were measured using a protractor.

The volume of the receptor was measured by filling the receptor to its brim with distilled water. To determine the volume of the donor, it was placed on a flat surface and the bottom side of the donor sealed with double layer of parafilm and then water added to measure the volume. Matching of the donors and the receptors was carried out on the basis of appropriate E.D.A. *i.e.* the donor with the lowest E.D.A was matched with the receptor having the lowest E.D.A. and vice versa.

8.3.1.2 Influence of Stirring

The efficiency of receptor stirring was observed using potassium permanganate dye ($KMnO_4$), which has low molecular weight (158.0) rather similar to the drug studied *i.e.* ibuprofen (206.3). Two receptors were filled with water up to their brims, and the matched donor placed on top of each receptor, clamped and placed inside glass holder of the receptor, which was located on the top of the stirring device. A small stirrer bar (12.5 x 3.2 mm) was placed in one of the receptors while the other receptor was left without the stirrer bar. A few crystals of $KMnO_4$ dye were added into the donor of each Franz cell and the time taken for the dye to distribute throughout the receptor (including the two arms) was recorded. The stirrer was fixed at a constant speed *i.e.* 500rpm by the manufacturer and therefore it was not possible to change the stirrer speed.

In a separate experiment the three receptors of Franz cells were used, each containing stirrer bar of different dimensions *i.e.* 12.5 x 3.2mm, 15.44 x 5.15mm and 12.48 x 4.6mm. A few crystals of $KMNO_4$ were added to each receptor containing water maintained at 37°C and time required for dye to distribute through entire cell was recorded for each stirrer bar. The experiment was performed three times.

Another experiment was conducted by adding 1mg, 5mg and 10mg of $KMNO_4$ dye to receptors containing water and the time required for the dye to distribute through the entire cell was recorded using the stirrer bar (12.48x4.6mm).

All stirring factors investigated showed long stirring times to achieve homogenous mixing including the two sampling arms (*c.f. results 8.4.1.2*). The manufacturer recommended use of a peristaltic pump, However, due to the unavailability of a

peristaltic pump, the influence of mixing the receptor contents through the sampling arm was investigated using a latex tubing attached to plastic syringe (Fig. 8.1), immediately after adding the dye into the receptor and just before each sampling *(premix)* to achieve a homogenous solution throughout the receptor (including the two sampling arms) to reduce the waiting time.

Figure 8.1: Plastic syringe with latex tubing used for sampling

8.3.1.3 Influence of temperature variation

The temperature of the Franz cell apparatus (donor and receptor) was maintained at 33^oC throughout the experiment by an external circulating water bath maintained at 37^oC. The receptor was filled with water and the temperature of the water in the receptor was recorded using a digital thermometer containing a long metal sensor. A Cellulose acetate membrane was placed on top of the receptor, the donor placed on top of membrane and 1mL water transferred to the donor. All openings *i.e.* the top of the donor and the two arms of the receptor were covered with a double layer of parafilm. The temperatures were recorded after equilibration for half an hour. The metal sensor of the digital thermometer was straight. In contrast, the two sampling arms of the receptor cell were curved (Fig.1.14−Chapter I) and therefore, it was not possible for the metal sensor to reach the centre or bottom of the receptor cell and measure the temperature of the receptor medium during experiment.

8.3.2 Preliminary experiments to investigate drug release

After investigating factors related to stirring and heating, four preliminary drug release experiments were conducted to analyse the effect of selected factors as follows:

All openings including top of the donor, sampling arms of the receptor and junction between the donor and the receptor hosting the membrane were closed using parafilm.

The donors and the receptor were either matched or not based on effective diffusion area (EDA) and the donors and receptors showing similar dimensions were used together.

The Cellulose acetate membranes (pore size 0.22µm) were soaked in the receptor dissolution medium (0.1M NaOH) for 24 hours prior to experiments and again rinsed in fresh dissolution medium couple of times before starting experiment.

The receptor dissolution medium was degassed for 20 minutes using sonicator immediately prior to the experiment.

All factors were then investigated in the following four combinations of experiments using Franz diffusion cells in six replicates.

8.3.2.1 Preliminary experiment 1

All openings involving the donor and the receptor were left open, the donor and the receptor were not matched, membranes were not soaked in the dissolution medium and used as it is and the degassing of the dissolution medium was not carried out (experiment no. 1, Table 8.1).

8.3.2.2 Preliminary experiment 2

All openings involving the donor and the receptor were closed, the donor and the receptor were not matched, membranes were soaked in the dissolution medium for

24 hours and the degassing of the dissolution medium was not carried out (experiment no. 2, Table 8.1).

8.3.2.3 Preliminary experiment 3

All openings involving the donor and the receptor were closed, the donor and the receptor were not matched, membranes were soaked in the dissolution medium for 24 hours and the degassing of the dissolution medium was carried out (experiment no. 3, Table 8.1).

8.3.2.4 Preliminary experiment 4

All openings involving the donor and the receptor were closed, the donor and the receptor were matched, membranes were soaked in the dissolution medium for 24 hours and the degassing of the dissolution medium was carried out (experiment no. 4, Table 8.1).

The factors which were kept constant included membrane type: Cellulose acetate (0.22µm pore size), sampling frequency: frequent (*c.f.* 8.3.3), sampling site: centre of the receptor, stirrer bar: 12.50 x 3.2mm and premix: yes.

Table 8.1: Factors investigated in the preliminary drug release studies.

Experiment no.	All openings closed (yes/no)	Membrane soaking (yes/no)	Matching of donor and receptor	Degassing (yes/no)
1.	no	no	no	no
2.	yes	no	yes	no
3.	yes	no	yes	yes
4.	yes	yes	yes	yes

A separate experiment was also performed in triplicate using cellulose acetate membranes with pore sizes 0.22µm and 0.45µm to investigate the effect of membrane pore size on drug release using commercial ibuprofen (5%) hydrogel with all other factors being constant. Membranes with different pore sizes (0.22µm or

0.45µm) showed rather similar (*c.f. 8.4.2*) drug release and hence the cellulose acetate membrane (pore size 0.22µm) was used for further validation work.

The effective diffusion area of the tailor–made Franz cell is reported (Ng, 2007) to vary between 15–20%, which has significantly affected the drug release. However, the dimensions of the donors and receptors of the three commercial (PermGear) Franz cells were found to be only slightly different from each other. Therefore, the effect of matching of the donor and the receptor on drug release was investigated.

It has been reported that the presence of air bubble in dissolution medium also hinders the permeation of drug (Hauck *et al*., 2007). Therefore, the effect of degassing of 0.1M NaOH on drug release was also studied using following experimental methodology:

The experiments were conducted with six (6) replicates using Franz cells. The receptors were placed in the stirrer block, filled with the receptor fluid (0.1M NaOH), stirrer bars (12.50x3.2mm) placed in the receptors, cellulose membranes (0.22µ pore size) placed on top of the receptors and then the donors placed on the membranes. The receptor and donor with the membrane in between then tightly secured using a metal screw–type clamp. The flat flange joint (between donor and receptor) was then covered with the double layer of parafilm to avoid evaporation. The temperature of the receptor medium was regulated at 33°C using a circulating water bath (Huber, Germany) linked to the receptor ports through latex tubing. The air bubbles (if any) in the receptor cells were removed by taking the cell out from the stirrer device and tilting the whole cell until the bubbles escaped through the upper sampling port. The stirrer was switched on (a fixed speed of 500rpm) and the whole system was left for temperature equilibration for 15 minutes prior to drug release experiments.

A commercial ibuprofen 5% hydrogel (Mentholatum, UK) was used as a control for the experiments. Approximately 0.5–1g gel was transferred to each donor using a plastic syringe. The top of the donor was then covered with the parafilm.

A plastic syringe (5mL capacity) with latex tubing (Fig. 8.1) was used to draw sample from the receptor medium. The latex tubing was immersed in the centre of the receptor from the upper arm. ~1.5mL of the receptor fluid was drawn at specified time intervals including at zero time. Each time the sample was directly transferred to the quartz cuvette (1mm in thickness and ~1.5mL capacity) and the absorbance was recorded at 272nm using double beam UV spectrophotometer (Shimadzu, Japan) immediately after replenishing the solvent. The time required for entire sampling (withdrawal and replenishing) was maintained at approximately 40 seconds. The experiments were conducted for a maximum of seven (7) hours and the samples taken at 0.5, 1, 1.5, 2, 3, 4, 5, 6 and 7 hours.

8.3.3 Validation of Franz cells using Design of Experiment

Initial screening of the factors discussed above i.e. closure of all openings, matching of the donor and the receptor, soaking of membranes, and degassing of the receptor fluid helped to narrow down the number of variables to be studied by the DoE. The factors investigated by DoE included membrane type (Visking and Cellulose acetate), appropriate membrane soaking time (0.5 or 24 hours), sampling site (centre or bottom of the receptor cell), sampling intervals (frequent (every 15 minutes for the first one and half hour) or infrequent (every 30 minutes for the first one and half hour)), appropriate stirrer bar with dimensions (12.50 x 3.2mm or 12.48 x 4.6mm) and need for premixing of the receptor solution prior to sampling (yes or no). The information is fed into the software, which assigns a designation to each factor and the levels (Table 8.2).

Table 8.2: Factors studied in the validation of Franz cell using DoE.

Factors	Designation of factors	Levels
Membrane type	A.	Cellulose acetate (A-), Visking (A+)
Membrane soaking time	B.	0.5 hr (B-) and 24 hrs (B+)
Sampling site	C.	Centre (C-) and bottom (C+) of the receptor
Sampling intervals	D.	Frequent (D-) and infrequent (D+)
Stirrer bar type	E.	12.50x3.2mm (E-) and 12.48x4.6mm (E+)
Premixing	F.	"Yes" (F-) and "no" (F+)

8.3.3.1 Membrane type

Two different membranes were studied for these experiments *i.e.* Cellulose acetate (pore size–0.22µm) and degenerated cellulose (Visking) membranes.

8.3.3.2 Membrane soaking time

Soaking of both membranes prior to use was carried out as follows:

0.1M NaOH was freshly prepared for each experiment, degassed by sonication for 20 minutes and stored at 37°C. Cellulose acetate and Visking membranes were placed in the Petri dish containing 0.1M NaOH and placed in the oven maintained at 37°C for either 0.5 hour or 24 hours. Finally, membranes were rinsed couple of times with the fresh solvent to completely remove the impurities.

8.3.3.3 Sampling site

Static diffusion cells normally have only one arm for sampling. However, the receptor of the commercial Franz cell (PermGear) used in the present study had two arms of varying lengths and angles. Therefore, the samples were taken from both arms to investigate whether or not varying the sampling site produces any variation in amount of drug permeated. The sampling from the upper arm was considered as centre of the receptor and the sampling from the lower arm was categorised as the bottom of the receptor.

8.3.3.4 Sampling Frequency

The effect of frequent (15, 30, 45, 60, 75, 90, 120, 150, 180, 240, 300, 360 and 420min) and infrequent (30, 60, 90, 120, 180, 240, 300, 360 and 420min) sampling intervals on drug release and %CV was also investigated.

8.3.3.5 Stirrer bar type

Two stirrer bars (12.50 x 3.2mm and 12.48 x 4.6mm) were investigated for their stirring efficiency for the validation experiments.

8.3.3.6 Premixing

In preliminary studies long waiting periods were observed for $KMNO_4$ dye to homogenously disperse throughout the receptor fluid including the two arms with all three stirrer bars investigated. Therefore, it was decided to premix by rinsing the receptor fluid couple of times using the plastic syringe having the latex tubing prior to sampling. In preliminary experiments it took less than a minute to achieve homogeneous sample after rinsing with the syringe. Therefore, need of premixing (yes or no) was selected as one of the variable in the validation of Franz cells experiments using DoE.

After selection of factors (each at two levels), a layout (matrix) for the experimental conditions (Table 8.3) was generated for 6 factors by the DoE (DX® 7.1.5). A factorial design with minimum experimental runs resolution 5 (Minimum Run Res 5) without centre points was selected to investigate the effect of all factors and the interactions between the factors. A matrix of 22 experiments was generated by the software (Table 8.3).

Based on the generated matrix, the real experiments were carried out using the same experimental methodology as for the prelminary drug release studies to capture the effect of various factors on the drug release using the Franz cell. Experiments were carried out in triplicate on the same day and cumulative drug release and CVs values at each time interval were calculated using PCP DISSO vol.3 software which uses standard equations related to drug release as described earlier (Chapter II).

The data were visualised by graphical display using Microsoft Excel® 2003. To determine the best combination of the factors studied, the data obtained on drug release and CVs were entered in the matrix obtained from the DX® and analysed using appropriate model suggested by the DoE. The data for all responses were randomised and evaluated by Box Cox plot, which helps to analyse whether any transformation of data is required before the final analysis.

Table 8.3: Matrix of experimental factors generated by DX® 7.1.5 for the validation of Franz cells.

Experiment no.	Membrane Type	Membrane soaking time (hours)	Sampling Frequency	Sampling Site (Receptor)	Stirrer Bar type	Need for Premix
1	Cellulose	0.5	Infrequent	Bottom	12.48x4.6	Yes
2	Cellulose	24	Infrequent	Centre	12.5x3.2	Yes
3	Cellulose	24	Frequent	Bottom	12.48x4.6	No
4	Visking	0.5	Frequent	Bottom	12.48x4.6	No
5	Cellulose	24	Frequent	Centre	12.48x4.6	Yes
6	Visking	24	Frequent	Bottom	12.48x4.6	No
7	Cellulose	0.5	Infrequent	Centre	12.5x3.2	No
8	Cellulose	0.5	Frequent	Centre	12.5x3.2	No
9	Visking	0.5	Infrequent	Bottom	12.48x4.6	Yes
10	Cellulose	0.5	Frequent	Bottom	12.48x4.6	Yes
11	Visking	24	Infrequent	Centre	12.5x3.2	Yes
12	Cellulose	24	Infrequent	Centre	12.5x3.2	No
13	Visking	24	Frequent	Bottom	12.5x3.2	No
14	Cellulose	0.5	Infrequent	Bottom	12.48x4.6	No
15	Visking	24	Frequent	Centre	12.5x3.2	No
16	Visking	0.5	Infrequent	Centre	12.5x3.2	No
17	Visking	0.5	Frequent	Centre	12.48x4.6	Yes
18	Cellulose	0.5	Frequent	Centre	12.5x3.2	Yes
19	Visking	0.5	Infrequent	Centre	12.5x3.2	Yes
20	Visking	24	Infrequent	Bottom	12.5x3.2	No
21	Cellulose	24	Infrequent	Bottom	12.48x4.6	Yes
22	Visking	24	Frequent	Bottom	12.48x4.6	Yes

The DX® suggested a provisional model for drug release and CVs for each time interval. The model with a probability (p) value <0.05 was considered significantly powerful to analyse the results. Based on the significance level of p value, the factors were included in or excluded from the model. The non–significant factors were excluded from the model using backward elimination with alpha to exit set at 0.1, implemented in DX® 7.1.5, the model was re–fitted with only significant factors and selected based on the goodness–of–fit statistical criteria (Khuri and Cornell, 1987). The optimisation criteria were the maximum drug release and minimum CVs at each time interval. The desired level of CVs was set to be equal or less than 5%.

The DX® 7.1.5, on the basis of the contribution of the individual factors in addition to the interactions between the factors predicted experiments with various combinations of the variables producing maximum (100%) desirability to minimum

(30%) desirability. The experiment with 100% desirability predicted maximum drug release whereas the experiment with 30% desirability showed minimum drug release.

The confirmatory experiments were conducted in six (6) replicates to access the accuracy of the prediction of DX® 7.1.5 using the maximum desirability conditions (100%). The agreement of predicted and experimental responses was evaluated by observing response values within prediction at 95% confidence interval. An outcome within this interval validated the model (Weisberg, 1985).

8.3.4 Drug release from lipogels using validated Franz Cell

The validated Franz cells were used to study the release of ibuprofen from the lipogels containing MgSt (12.5% and 20%) in liquid paraffin, palm−olein and the combination of liquid paraffin and palm−olein (70:30 ratio respectively) (section 7.2.2(ii)) using the standard experimental methodology as described in section 8.3.2. The validation experiments showed that drug release from commercial ibuprofen hydrogel was significantly different when investigated using Visking and Cellulose acetate membranes. Therefore, these two membranes were also used to investigate whether drug release from lipogels is also affected by the membrane type. The amount of MgSt in the formulations influences the consistency of the lipogels. Therefore, the effect of MgSt (12.5% and 20%) in the lipogels on drug release was also investigated.

8.4 Results

8.4.1 Preliminary studies for validation of the Franz Cell

8.4.1.1 Franz cell dimension

Dimensions of the donors of the three Franz cells (FC) were compared with each other in addition to the comparison of dimensions of the receptors. Statistically, there appeared to be no significant difference between the dimensions of the donors as well as receptors (Table 8.4). However, donors and receptors were matched based on their mean diameters in all release experiments. The mean diameter of the Franz cell

3 was observed to be biggest. In contrast, the mean diameter of the Franz cell 3 was the smallest.

Table 8.4: Dimensions of the three commercial Franz cell (PermGear).

Dimensions	Franz cell 1 (mean±s.d.)	Franz cell 2 (mean±s.d.)	Franz cell 3 (mean±s.d.)
Donor compartment			
–Height (cm)	1.79 ± 0.20	1.81 ± 0.04	1.80 ± 0.03
–Volume (mL)	3.23 ± 0.20	3.23 ± 0.02	3.20 ± 0.04
–Internal diameter (cm)	1.50 ± 0.01	1.51 ± 0.01	1.50 ± 0.02
–External diameter (cm)	1.51 ± 0.01	1.50 ± 0.01	1.53 ± 0.03
–Mean diameter (cm)	1.50	1.50	1.52
Effective diffusion area (EDA cm^2)	1.77	1.77	1.81
Receptor compartment			
–Height (cm)	6.22 ± 0.01	6.42 ± 0.10	6.23 ± 0.16
–Volume (mL)	13.60 ± 0.10	13.80 ± 0.10	13.78 ± 0.13
–Internal diameter (cm)	1.50 ± 0.01	1.50 ± 0.02	1.51 ± 0.02
–External diameter (cm)	1.50 ± 0.02	1.52 ± 0.02	1.53 ± 0.02
– Mean diameter (cm)	1.50	1.51	1.52
Effective diffusion area (EDA cm^2)	1.77	1.79	1.81
–Length of the upper arm (mm)	60.58 ± 1.70	58.69 ± 0.94	55.90 ± 0.05
–Length of the lower arm (mm)	89.98 ± 1.06	90.21 ± 0.60	87.34 ± 0.11

8.4.1.2 Influence of Stirring

Two Franz cells were used to investigate the effect of stirring (~500rpm) on the distribution of the dye ($KMnO_4$). Figure 8.2 shows the effect of stirring on the diffusion of $KMNO_4$ dye into the receptors of the FC. The FC without stirrer bar showed that the dye accumulated at the base of the receptor and diffused very little into the arms after one hour. In contrast, The FC with stirring showed homogeneous diffusion of the dye throughout the receptor except the two arms (Fig. 8.2). Although the dye did not accumulate at the bottom, however, it took a long time (~1-2 hours) to homogenously diffuse into both arms.

In the second experiment, the effect of stirrer bar type on the mixing of dye was observed. Figure 8.3 shows the effect of stirrer bar type on the diffusion of the dye throughout the receptor medium including the two arms. All three (3) stirrer bars

required varying amount of time for the complete diffusion of dye. The stirrer bar with dimensions 15.44 x 5.15mm showed the shortest diffusion time *i.e.* one hour. In contrast, the stirrer bar with dimensions 12.5 x 3.2mm showed the longest time for complete diffusion *i.e.* three hours. Although, the stirrer bar with dimensions 15.44 x 5.15mm showed shortest time for complete diffusion, it consistently touched the receptor walls during stirring. In contrast, the stirrer bar with dimensions 12.48 x 4.6mm took one and half hour to achieve homogenous mixing.

In the third experiment, effect of the mass of the dye on the diffusion time was observed (Figure 8.4) using the same stirrer bar (12.48 x 4.6mm). The FC containing maximum amount of dye (10mg) took longest time (2.5 hrs) to achieve homogeneous mixing. In contrast, the smallest amount (1mg) of the dye took shortest time (22 minutes) for complete diffusion. The FC with 5mg dye took 30 minutes to achieve homogeneity. However, premixing with the latex tubing resulted in immediate homogenous mixing throughout the receptor including the two sampling arms.

Figure 8.2: Effect of stirring factors on the mixing of $KMNO_4$ dye in the receptor cell (left) no stirring and (right) stirring using stirrer bar (12.5 x 3.2 mm).
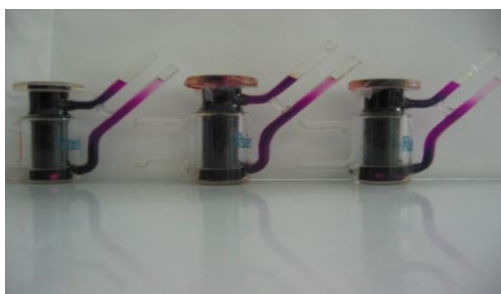
Figure 8.3: Effect of various magnetic bars on the distribution of $KMnO_4$ dye. Left (15.44 x 5.15mm– after 1 hour), centre (12.5 x 3.2mm– after 3 hours) and right (12.48 x 4.6mm– after 1.5 hours).

Figure 8.4: Effect of weight of the dye on the time required to distribute throughout the receptor cell including the two arms (left) 10mg– time taken 2.5 hours (centre) 5mg– time taken 30 minutes and (right) 1mg– time taken 22 minutes.

8.4.1.3 Influence of Temperature variation

The Franz cell was equilibrated for half an hour prior to investigation of temperature. The temperature of the donor and the receptor medium was 33°C, achieved by maintaining circulating water in the surrounding water jacket at 37°C without placing membrane in between the donor and the receptor. It was not possible to check the temperature below membrane before or after sampling as the metal sensor of the digital thermometer was straight whereas the two sampling arms of the Franz cell were curved and it was not possible for the metal sensor to reach the centre of the receptor. In addition, the thermocouples were not available.

8.4.2 Cumulative drug release for preliminary drug release studies

PCP DISSO v.3 software was used to investigate drug release and %CVs of the four preliminary validation experiments (closing all openings (yes/no), membrane soaking (yes/no), degassing of receptor medium (yes/no), and matching of the donors and the receptors (yes/no). All preliminary experiments showed rather similar cumulative drug release *i.e.* between 17–20% after 420 minutes (Fig. 8.5). However, experiment 1 showed rather higher drug release at each time interval compared to other preliminary experiments, which showed rather similar drug release. The CVs for all experiments appeared to be significantly different from each other and there appeared to be a gradual decrease in CVs from experiment 1 through experiment 4

i.e. experiment 1 showed highest CVs. In contrast, the fourth experiment showed lowest CVs (Fig. 8.5).

8.4.2.1 Preliminary Experiment 1

All factors were uncontrolled in this experiment as they were set as **no** (experiment no.1, Table 8.1). All replicates showed rather similar cumulative drug release (~20%) after 420 minutes. However, large variation was observed in the CVs amongst the six replicates (Fig. 8.5a).

8.4.2.2 Preliminary Experiment 2

The factors for this experiment were as follows: openings closed (yes), membrane soaking (no), matching of the donor and the receptor (yes) and degassing (no). The cumulative drug release was equivalent to the experiment 1 (~19%) but the CVs were relatively lower than the experiment 1 (Fig. 8.5b) but were higher than the CVs of experiment 3.

8.4.2.3 Preliminary Experiment 3

The factors for this experiment were as follows: openings closed (yes), membrane soaking (no), matching of the donor and the receptor (yes) and degassing (yes). A significant reduction in the CVs was observed amongst the replicates compared to the CVs of experiments 1 and 2 (Fig. 8.5b). However, the cumulative drug release was rather similar (~17%).

8.4.2.4 Preliminary Experiment 4

The factors for this experiment were as follows: openings closed (yes), membrane soaking (yes), matching of the donor and the receptor (yes) and degassing (yes). The lowest CVs amongst all the four experiments were observed in the experiment no.4 (Fig. 8.5b). However, the cumulative drug release was rather similar (~18%).
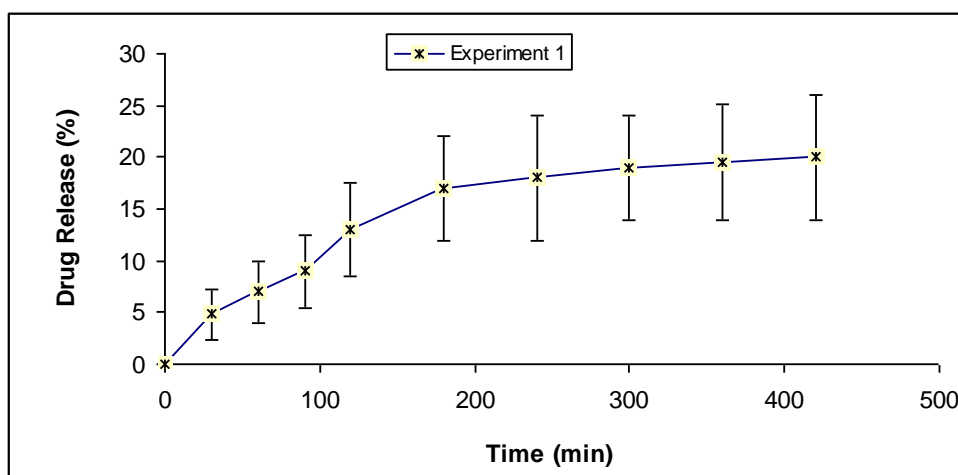
(a)
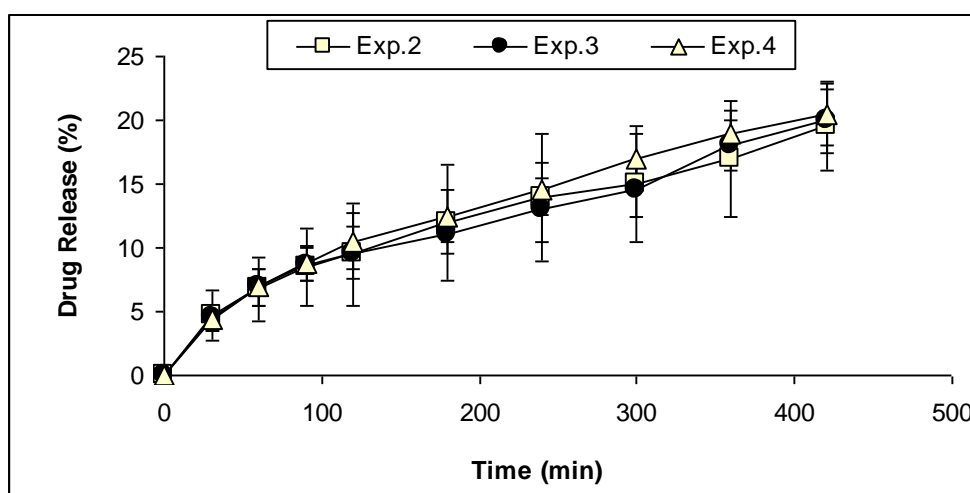
(b)

Figure 8.5: Ibuprofen hydrogel. Release data for four preliminary experiments prior to validation by DoE at intervals from 0−420 minutes (a) *preliminary experiment 1 and (b) preliminary experiments 2, 3, and 4. The Y−error bars showing CVs amongst the six replicates of each experiment.

*Experiment 1: all factors set as **no;** experiments 2 and 3: opening closed (yes), membrane soaking (no), matching of the donor and the receptor (yes) and degassing no and yes respectively; Experiment 4: all factors set as **yes** *(c.f. Table 8.1).*

In a separate experiment the Cellulose acetate membrane (pore size 0.22µm or 0.45µm) was used to investigate the effect of pore size on the drug release and the CVs. There appeared to be rather similar drug release (~20%) after 420 minutes (not shown). Therefore, the Cellulose acetate membrane with pore size (0.22µm) was selected for further validation experiments.

8.4.3 Validation of Franz cell experiments using Design of Experiment

Franz cell validation using DoE was carried out by conducting 22 experiments (each in triplicate) provided by the matrix generated by DX® 7.1.5 as described in the Table 8.3. The data for cummulative drug relase and CVs generated for each time interval by PCP DISSO v.3 are listed in Tables 8.5 and 8.6 reespectively. All experiments showed varying amount of cumulative drug release and CVs. The software also predicted optimised drug release at lowest CVs (Fig. 8.6).

Table 8.5: Ibuprofen hydrogel. Cummulative %drug release obtained for 22 experiments performed using the matrix provided by DX® 7.1.5 (*c.f.* Table 8.3). The %R30–420 represent %drug releae at the corresponding time interval in minutes. The DoE compares the effect of common time intervals of the factor (Sampling frequency). Each experiment was conducted in triplicate.

Exp.no	%R30	%R60	%R90	%R120	%R180	%R240	%R300	%R360	%R420
1	2.265	4.079	5.268	6.967	8.973	11.009	12.762	13.815	15.309
2	2.085	3.479	4.235	5.389	6.706	7.999	9.305	10.469	11.486
3	2.424	3.934	5.267	6.333	8.434	10.127	11.825	13.288	14.651
4	1.899	2.846	4.027	4.970	6.758	8.237	9.512	10.721	11.784
5	1.858	3.267	4.397	5.313	7.040	8.477	9.969	11.047	12.032
6	2.359	4.007	5.363	6.654	8.718	10.862	12.266	13.784	15.205
7	2.002	3.393	4.584	5.761	7.522	9.338	10.705	12.071	13.800
8	1.986	3.308	4.398	5.260	6.991	8.378	9.666	10.886	11.838
9	2.676	4.332	5.764	7.032	9.299	11.160	12.784	14.497	15.920
10	1.942	3.293	4.533	5.534	7.419	8.848	10.260	11.573	12.738
11	2.075	3.526	4.723	5.780	7.321	8.859	10.503	11.763	12.901
12	2.109	3.281	4.340	5.249	7.000	8.474	9.805	11.598	13.044
13	3.083	5.045	6.646	8.095	10.552	12.627	14.543	16.226	17.706
14	1.753	3.162	4.226	5.500	6.734	8.214	9.568	10.777	11.851
15	4.971	8.065	10.954	13.665	18.018	22.265	26.524	30.371	33.876
16	4.159	7.197	9.754	11.952	15.874	19.548	22.835	25.890	28.932
17	3.871	6.571	8.972	11.047	14.699	17.913	20.986	23.823	26.319
18	1.842	3.130	4.065	4.915	6.482	7.774	9.086	10.122	11.177
19	4.260	7.303	9.702	12.008	15.917	19.442	22.732	25.893	28.957
20	4.019	7.209	9.964	11.905	14.591	17.273	19.670	22.417	25.100
21	3.404	6.480	9.082	11.208	15.072	18.511	21.659	24.662	27.241
22	4.173	7.062	9.481	11.379	15.591	18.844	22.160	25.116	27.944

Table 8.6: Ibuprofen hydrogel. % CVs obtained for 22 experiments using the matrix (*c.f.* Table 8.3) provided by DX® 7.1. The CV30–420 represent time interval in minutes and CV represents % coefficient of variance (the DoE compares the effect of common time intervals of the factor (Sampling frequency)). Each experiment was conducted in triplicate.

Exp. no	CV30	CV60	CV90	CV120	CV180	CV240	CV300	CV360	CV420
1	12.43	9.66	13.71	17.88	5.93	3.74	3.48	3.45	2.89
2	9.46	11.85	4.83	6.45	6.00	5.87	7.67	9.70	8.91
3	9.55	11.79	16.65	14.83	14.77	15.76	17.51	17.20	18.33
4	22.21	14.64	10.35	10.89	11.96	10.75	10.21	10.92	10.41
5	7.26	6.30	6.22	6.34	6.14	6.33	5.10	5.09	4.70
6	9.67	3.18	3.31	1.79	0.93	8.09	2.44	2.62	1.31
7	26.83	23.28	21.87	24.67	24.77	22.37	24.45	25.56	21.74
8	0.91	4.53	4.97	5.63	5.89	6.03	5.84	4.99	5.72
9	8.17	4.55	4.98	4.94	4.69	4.84	4.57	4.47	4.49
10	3.79	2.27	3.93	3.55	7.25	4.69	4.44	5.52	5.85
11	11.39	11.94	14.02	13.24	11.97	13.11	13.92	13.87	13.84
12	21.23	14.19	6.64	5.42	2.24	5.24	5.41	3.22	7.54
13	5.17	4.88	4.34	4.99	4.64	4.94	5.27	4.95	4.74
14	8.54	2.99	3.97	6.47	5.47	4.23	5.65	4.44	4.74
15	11.00	9.03	10.67	11.04	11.95	12.60	13.19	12.81	14.24
16	17.06	14.48	14.37	13.28	13.13	13.37	14.83	15.47	16.02
17	3.69	5.76	7.28	7.50	9.08	8.94	9.49	9.20	9.79
18	7.30	4.11	2.57	2.95	2.69	0.89	1.24	1.61	1.35
19	12.90	15.62	13.89	15.94	16.60	17.76	18.70	19.41	19.64
20	8.53	5.14	5.13	6.74	4.74	4.70	5.38	4.03	3.88
21	4.93	8.29	8.88	9.96	11.52	10.52	10.60	11.18	12.59
22	16.82	18.81	18.83	19.05	18.19	19.01	18.55	19.73	18.89
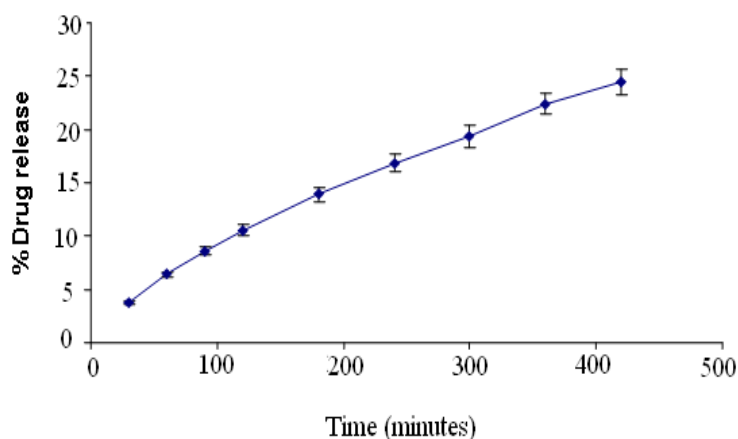
Figure 8.6: Ibuprofen hydrogel. Release data for validation experiment predicted by DoE with 100% desirability from zero through 420 minutes time interval. The CVs were ~5%.

The data from Tables 8.5 and 8.6 was fed in the DX® 7.1.5 and analysed using "Factorial desing" model for each time point. The software randomised and evaluated the need for data transformation for all responses by Box Cox plot and no data transformation was required, as the lambda was equal to 1 (best lambda= 1.48) (Fig. 8.7). The data was analysed by ANOVA, which categorised the factors into significant, critical and non-significant, depending on the p value (Table 8.7).
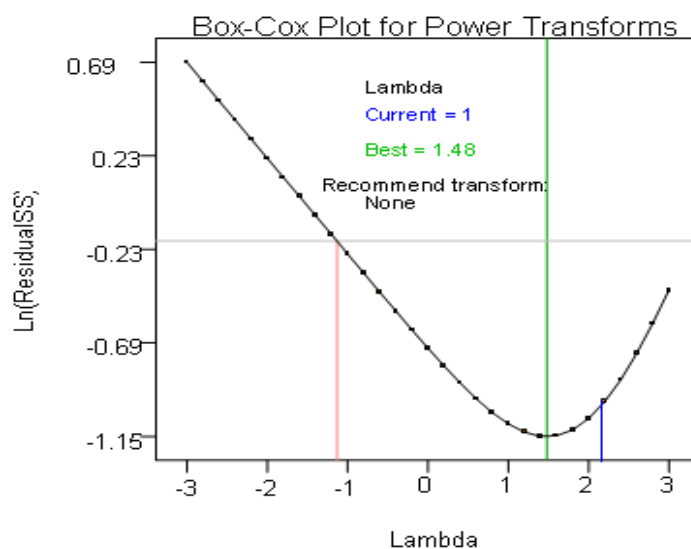
Figure 8.7: Box–Cox plot for power transforms showing lambda value which affect the need for data transformation (lambda equal to 1 does not require data transformation).

The Pareto chart demonstrates influence of various experimental factors and interactions between the factors on the overall outcome (Fig. 8.8). The factors showing t–value more than the lower limit (2.77645) are considered as significant factors whereas the factors with t-value above Bonferroni value (6.84714) are considered as critical factors (Fig. 8.8).

8.4.3.1 Membrane type

The Cellulose acetate (A-) and Visking (A+) membranes were used. The influence of membrane type and its interactions with other factors can be explained by the Pareto chart (Fig. 8.8) as well as ANOVA statistics (Table 8.7). Membrane type showed a significant effect on the overall outcome of the experiment (P<0.0002) showing

227

positive effect (represented by the orange colour) as the t-value was above the lower line (Fig. 8.8) but it failed to reach the Bonferroni limit (a measure of critical effect). However, its interactions with sampling intervals (AD) and membrane soaking time (AB) appeared as critical factors (above Bonferroni limit). The factor AD showed positive effect. In contrast, factor AB showed negative influence.
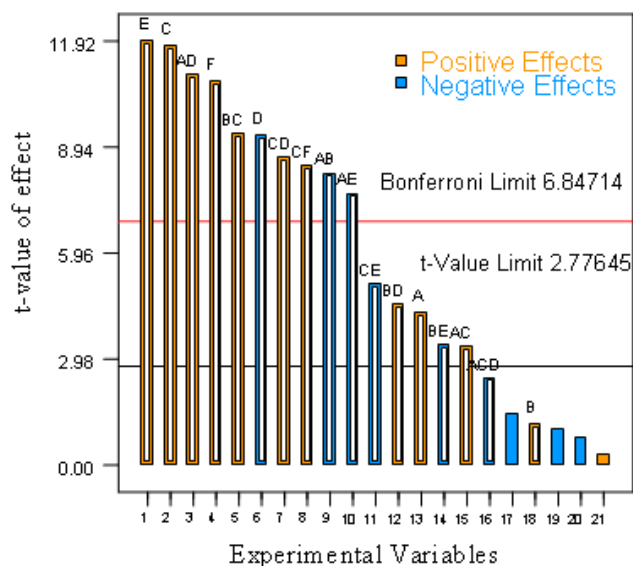
Figure 8.8: Significance of the factors and their combinations on Ibuprofen hydrogel release and %CVs explained by Pareto chart.

Table 8.7: ANOVA showing contribution of various factors on Ibuprofen hydrogel release.

Parameters	Source	Sum of Squares	Mean Square	F Value	p–value Prob > F
	Model	55.50	6.17	19.53	< 0.0001
	A–Memb Type	11.83	11.83	37.47	< 0.0002
	B–Visk Time	4.08	4.08	12.92	0.0670
Drug release after 420 minutes	C–Samp Freq	7.31	7.31	23.16	0.0004
	D–Samp Site	2.34	2.34	7.41	0.0185
	E–Sir Bar	5.22	5.22	40.55	0.0001
	F–Premix	4.95	4.81	13.73	0.0015
	AD	5.60	5.60	14.74	0.0012
	BD	2.91	2.91	9.23	0.0103
	BC	8.54	8.54	23.04	0.0005

8.4.3.2 Membrane soaking time

Membrane soaking time was selected as either 0.5 hr (B-) or 24 hrs (B+). Membane Soaking time appeared to be insignificant variable (P value 0.067 (Table 8.7)) and the t-value was below the lower line in the Pareto chart (Fig. 8.8). However, it showed significant interactions with other experimental factors to produce critical effect especially with the sampling frequency (BC) and produced a positive effect (Fig. 8.8).

8.4.3.3 Sampling site

The centre (C-) and the bottom (C+) of the receptor cell were selected as two sampling sites. The sampling site alone (C) and its interactions with other factors (BC, CD and CF) showed highly critical (positive) effect on overall results as all of these factors were above the Bonferroni limit (Fig. 8.8).

8.4.3.4 Sampling Frequency

Frequent (D-) and infrequent (D+) intervals were selected as sampling frequencies. Sampling site alone had a critical (Bonferroni value 8.94) but negative influence (Blue colour) on the overall results. However, it showed significant interactions with other factors such as membrane type (AD) and sampling site (CD) to produce positive effect (orange colour) (Fig. 8.8).

8.4.3.5 Stirrer bar type

Two stirrer bars with dimensions (12.50 x 3.2mm (E-) and 12.48 x 4.6mm (E+)) were used for the studies. The stirrer bar dimension appeared to be the most critical factor (Bonferroni value 11.92) showing positive effect when used individually. However, its interaction with membrane type produced critically negative effect (AE). Other interactions such as (BE and CE) also showed significantly negative influence (Fig. 8.8).

8.4.3.6 Premixing

The final factor was premixing of the dissolution medium couple of times prior to sampling and was represented by Yes (F-) or no (F+). It showed critical effect on the overall results (Bonferroni value 10.5). It was the only factor which did not show interaction with any other factor (Fig. 8.8).

The overall influence of all factors and the interactions between the factors on the drug release at 420 minutes time interval is summarised by the equation 8.1:

Drug release after 420 minutes = 4.28 + 0.21A + 0.09B + 0.71C - 0.34 D + 0.89 E + 0.61F + 0.65 A D + 0.39BC - 0.17 BE   (Equation 8.1)

Order of effect of factors and interactions between the factors was as follows:

$$E > C > AD > F > BC > D > A > BE > B$$

The interactions between various factors at each time interval provided significant amount of data and it is not possible to show all data here therefore typical interaction plots showing effect of various factors as a function of cummulative drug release at 420 minutes are shown in Figure 8.9 whereas cube plot demonstrates influence of factors and the interactions between the factors on the CVs at 420 minutes time interval in Figure. 8.10.

Figure 8.9 shows the influence of interactions between various factors on the cummulative drug release. The investigation of the interactions of various factors showed that when Visking membrane (A+) and stirrer–bar (12.50 x 3.2mm (E+)) with samplig site (D)= centre are used, changing the membrane soaking time (B- or B+) have insignificant effect on the drug release as both soaking times produced rather similar drug release (Fig. 8.9a). However, Cellulose acetate membrane (A-) with same variables showed significant contribution of the change in the membrane soaking time on the drug release *i.e.* membrane soaking time for 0.5 hr (B-) or 24 hrs (B+) showed differnet drug relase (~13.5% and 28.0% respectively). In contrast, when the stirrer–bar with dimensions 12.48 x 4.6mm (E-) was selected, there was a significant effect of change in the membrane soaking time for both membranes *i.e.*

B- showing lower drug release whereas B+ predicting significantly higher drug release for both membranes (Fig. 8.9b).

(a)

(b)
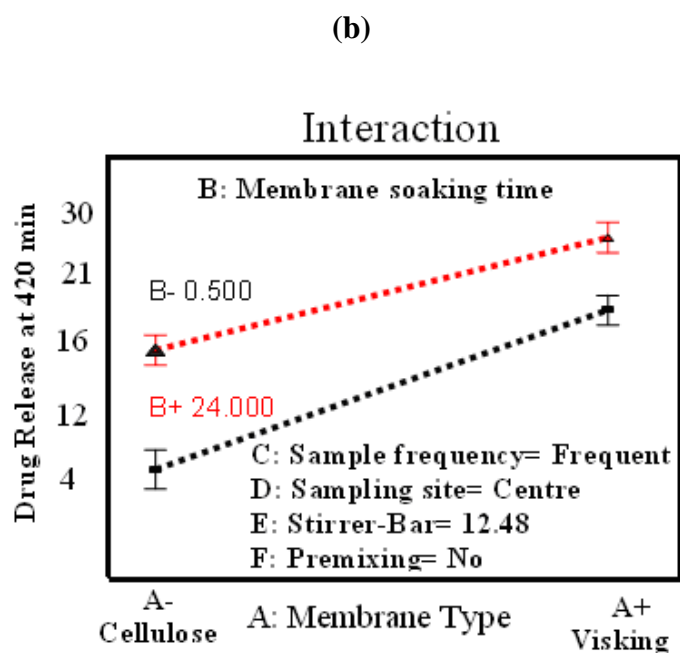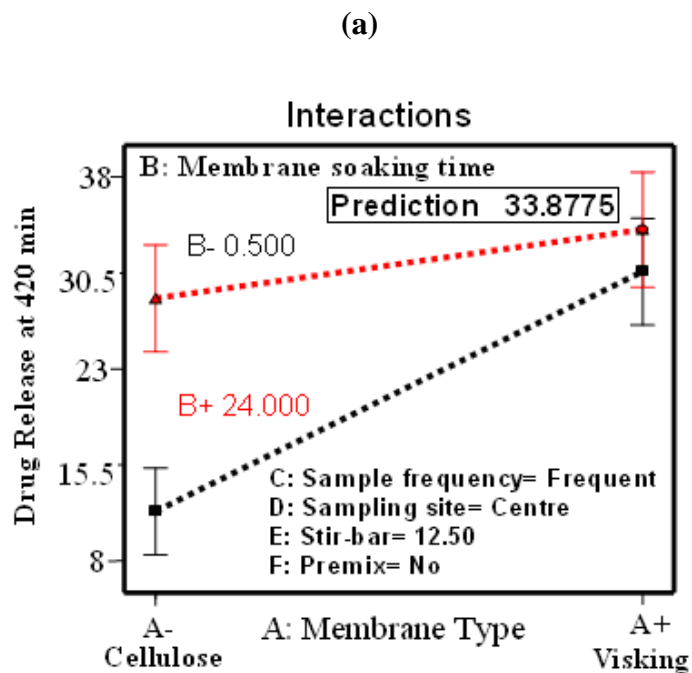
Figure 8.9: Ibuprofen hydrogel. Effect of sampling site and the stirrer bar dimension on the cumulative drug release as predicted by DoE (a) 12.50 x 3.2mm and (b) 12.48 x 4.6mm. *Visking time= Membrane soaking time.

Figure 8.10 (cube plot) shows the influence of interactions of various factors on the %CVs at 420 minutes time interval when sampling site is the centre of the receptor. %CVs are significantly affected by changing the factors *i.e.* when membrane type is Visking (A+), sampling inervals are infrequent (C-) and the membrane soaking time is 0.5 hr (B-) the overall %CVs are 15.8967 (Fig. 8.10). However, when the membrane soaking time is changed to 24 hrs (B+), keeping other variables constant, the %CVs significantly reduces to 5.99058. Similar %CVs (5.59693) can also be obtained by using Cellulose membrane (A-), membrane soaking time 0.5hr (B-) and sampling intervals to be frequent (C+), by keeping the same sampling site as the centre of the receptor (D-) (Fig. 8.10). Therefore, with the knowledge of critical factors obtained by DoE, the outcome was optimised.
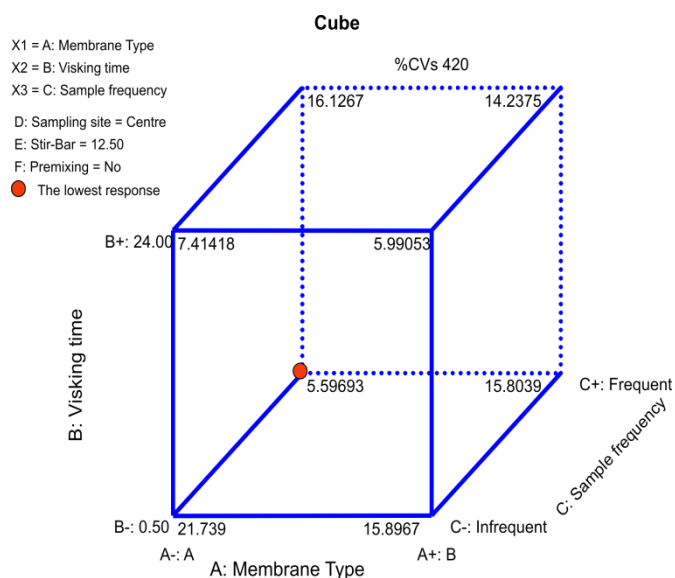
Figure 8.10: Cube plot showing the combined effect of membrane, visking time (Membrane soaking time) and sample frequency %CV.

DoE produced an experiment with combination of experimental factors to achieve the optimized ibuprofen release and reasonably low %CV for all time points (Experiment no. 20, Table 8.3). The confirmatory experiment was performed using the predicted experimental conditions (factors). The results of confirmatory experiment were rather similar to the predicted values (P<0.05), suggesting appropriateness of the selected model and the combination of factors. In addition, these results were comparable to the Ng (2007) results for drug release and CVs (Fig.

8.11). Therefore, optimised critical factors were selected as predicted by DoE for the drug release studies on the lipogels of various vehicles containing saturated amount of ibuprofen.
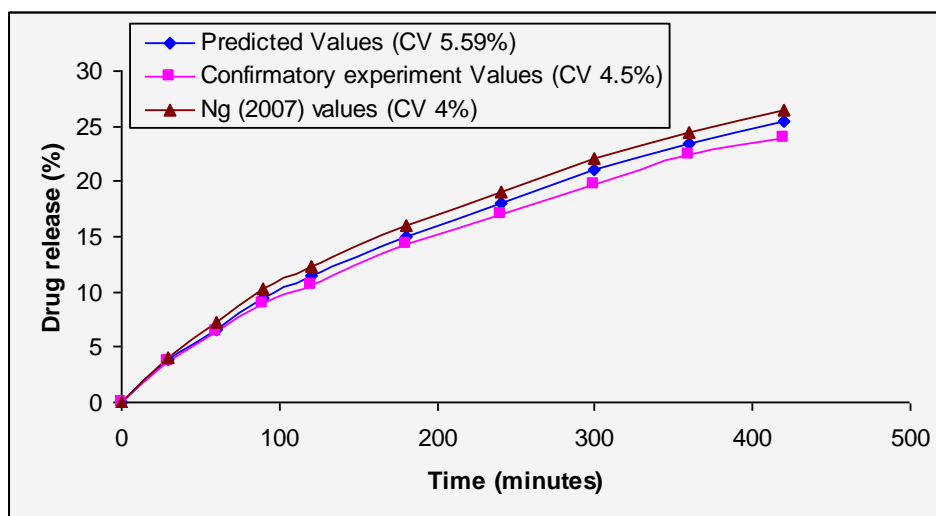
Figure 8.11: Ibuprofen hydrogel. Comparison of predicted, confirmatory and Ng (2007) experimental results for drug release and CVs.

8.4.4 Drug release from lipogels using validated Franz Cell

The ibuprofen release from the lipogels of liquid paraffin, palm−olein and their combination (70:30 ratio respectively) containing MgSt (12.5% and 20%) appeared to be significantly different from each other and from the commercial ibuprofen hydrogel depending on the amount of MgSt, type of membrane used and the consistency of the formulations *i.e.* semisolid or structured fluid.

Figure 8.12 shows the cumulative % drug release for the lipogels of palm−olein, liquid paraffin, mixture of liquid paraffin and palm−olein in addition to the commercial ibuprofen hydrogel diffused through Cellulose acetate membranes of 0.22μm pore size. The lipogels of palm−olein showed the highest amount of drug release whereas liquid paraffin alone or in combination with palm−olein showed significantly lower drug release values. In contrast, commercial hydrogels showed relatively lower drug release than palm−olein lipogels but significantly higher than the lipogels of liquid paraffin alone or in combination with palm−olein (Fig. 8.12).
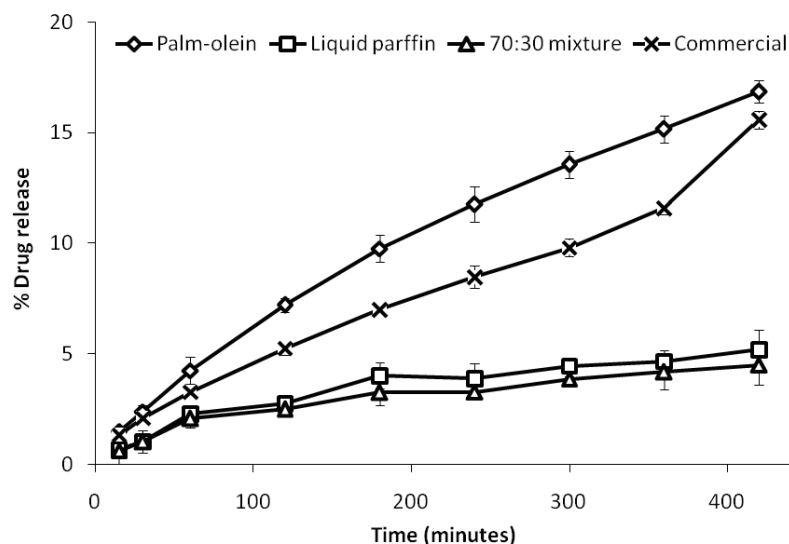
Figure 8.12: Cumulative drug release of various formulations using Cellulose acetate membranes. All experiments were performed in six replicates.

Figure 8.13 shows the effect of membrane type (Visking or Cellulose acetate) and the amount of MgSt on the drug release from the lipogels of the oils *i.e.* liquid paraffin, palm−olein, mixture of liquid paraffin and palm−olein and commercial ibuprofen hydrogels.
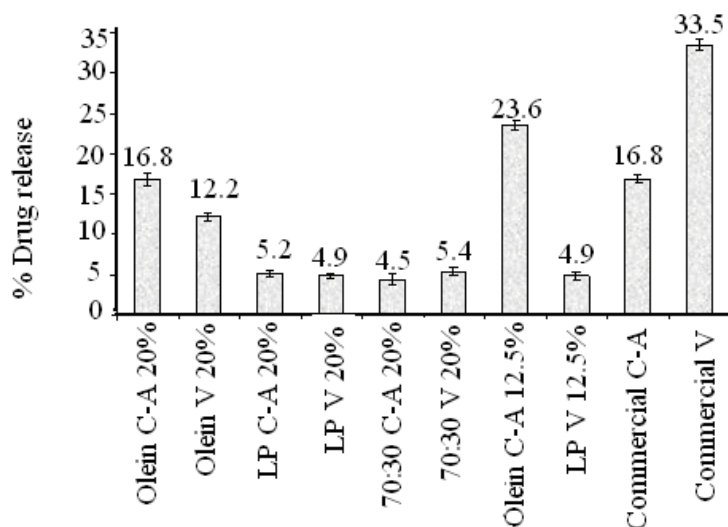
Figure 8.13: Effect of membrane type and amount of MgSt on the cumulative drug release from various formulations. C–A; Cellulose acetate membrane, V; Visking membrane, 12.5% and 20% represent amount of MgSt, All experiments were conducted in six replicates.

Membrane type significantly affected the drug release from various formulations. The commercial ibuprofen hydrogel showed significantly higher drug diffusion from the Visking membranes compared to all lipogels. Among the lipogels, the palm−olein showed significantly higher drug release from both membranes. Furthermore, the lipogels of palm−olein showed slightly higher drug release from the Cellulose acetate membranes compared to the Visking membranes (Fig. 8.13). However, the lipogels of liquid paraffin and the mixture of liquid paraffin and palm−olein showed rather similar drug release both from Cellulose acetate and Visking membranes and appeared to be significantly lower than the lipogels of palm−olein and the commercial ibuprofen hydrogel.

The amount of MgSt in the lipogel of palm−olein also had a significant effect on the drug release. The lipogels of palm−olein containing 12.5% MgSt showed significantly higher drug release compared to the lipogels containing 20% MgSt, diffused through Cellulose acetate membranes and appeared to be even higher than the commercial ibuprofen hydrogel from Cellulose acetate membranes (Table 8.8). In contrast, the drug release from the lipogels of liquid paraffin or 70:30 ratios of liquid paraffin and palm−olein was not affected by the amount of MgSt.

Table 8.8: Drug release from lipogels of various vehicles prepared using 5% IBP using Cellulose acetate and Visking membranes. C−A represents Cellulose acetate membrane.

Time (min)	LP (20%MgSt)		Olein (20%)		LP: olein (20%)		LP(12.5%) Visking	Olein C−A (12.5%)
	C−A	Visking	C−A	Visking	C−A	Visking		
15	0.693	0.941	1.518	1.555	0.638	0.904	0.025	2.501
30	1.042	1.542	2.389	1.840	1.036	1.305	0.685	4.154
60	2.290	2.550	4.252	3.096	2.086	2.005	1.068	6.742
120	2.746	3.639	7.202	5.384	2.510	3.016	1.589	10.797
180	4.028	4.646	9.755	6.916	3.258	3.737	1.981	13.590
240	3.892	4.910	11.747	8.440	3.275	4.183	2.369	16.591
300	4.460	5.280	13.561	9.823	3.864	4.615	2.751	18.839
360	4.660	5.772	15.160	11.050	4.180	4.748	3.104	21.402
420	5.190	6.164	16.850	12.223	4.496	5.431	4.912	23.580

8.5. Discussion

Validation of the Franz diffusion cells was carried out using commercial gel containing 5% IBP using a statistical tool *i.e.* design of experiment (DoE). The factors studied included stirring variable (stirrer bar dimension), membrane type, sampling frequency, sampling site, premixing prior to sampling in addition to membrane soaking time. The validated Franz diffusion cells were then used to investigate the ibuprofen (IBP) release from the lipogels.

Although, FDA stipulated guidelines for the scale up and post–approval changes for the non–sterile semisolid dosage forms (SUPAC–SS) a decade ago, however, there are no proper Pharmacopeial specifications to govern the *in vitro* release of drugs from topical semisolid formulations to date (FDA SUPAC–SS 1997; Siewert *et al*., 2003; Hauck *et al*., 2007). Therefore, the *in vitro* drug release studies over the years have shown great variations in the results, not only inter–laboratories but also intra–laboratory (Chilcott *et al*., 2005) and many researchers have related these variations to the lack of proper validation of the equipment as well as the process (Shah *et al*., 1999; Qvist *et al*., 2000; Siewert *et al*., 2003). Therefore, the validation process has become an integral part of the *in vitro* drug release studies.

Validation of Franz diffusion cells involves investigation of various factors affecting drug release. In this context, almost all researchers have used one factor at a time approach (OFAT) in which one factor is studied at a time by keeping all the other factors constant. However, this approach has two limitations *i.e.* it is time intensive and no information is obtained about the interactions between the factors. Therefore, in the present study, a statistical tool *i.e.* design of experiment (DoE) was utilised, which tremendously reduces the time for experimentation and provides invaluable information about the statistical contribution of each factor in addition to the effect of interactions between various factors (Lewis *et al.* 1999; Anderson and Whitcomb, 2005) based on the experimental approach of Ng, (2007).

In the present study, the effect of six (6) factors (Table 8.2) was investigated on the drug release. In this context, using OFAT approach, 64 experiments need to be conducted to obtain a complete set of data for the investigation of the effect of 6

factors. However, with the use of DoE, the same information was obtained with just 22 experiments. In addition, the software predicted a set of parameters by investigating effects of all the factors and their combinations to obtain optimum drug release with lowest possible coefficient of variance (CVs), the objective of the present study. The DoE revealed that for the Franz cells containing two sampling arms used in the present study, membrane soaking time and the stirrer bar dimension were the most critical factors for the overall drug release and CVs. Although, other factors also contributed in obtaining the optimised drug release but statistically they appeared to be non–critical.

Stirring speed is reported to influence drug release using static Franz cells (Ng, 2007). However, the stirrer used in the present study has fixed speed (~500rpm), and required long waiting periods to achieve homogenous mixing throughout the receptor (including the two arms) and therefore it was not possible to investigate the influence of stirring speed. This problem was solved by premixing of receptor contents using latex tubing attached to a plastic syringe prior to sampling, which produced homogenous solution throughout the receptor (including the two arms). Therefore, it is recommended that a peristaltic pump or premixing should be used to achieve reproducible results using the Franz cells containing two sampling arms as in the present study.

In addition, interactions of various factors showed significant effects on drug release at specific time interval. For example, at 420 minutes time interval, sampling frequency, sampling site and membrane soaking time showed significant effect on drug release and CVs from a specific membrane (Fig. 8.9 and 8.10 respectively). However, no interaction showed a significant contribution on overall drug release and CVs. Furthermore, the confirmatory experiment performed by using the predicted parameters provided by DoE, showed rather similar drug release and CVs to the predicted values and the results of Ng (2007), suggesting a good prediction of the software.

Membrane type is considered as the leading contributing factor for the variation as the drug release through various membranes has shown significant variations in the

drug flux (Clement *et al.*, 2000; Thakker and Chern, 2003). In addition, inter–membrane variations have been reported as greater than inter–laboratory or inter–cell variability (Barry and Brace, 1977; William, 2006). The selected membrane should function merely as a support for the dosage form and not the barrier, there should be no physical or chemical interactions between the dosage form components and the membrane. Furthermore, the membrane should be compatible with the chosen dissolution medium (Zatz, 1995; Thakker and Chern, 2003).

Ideally, biological membranes should be used in the *in vitro* studies to simulate the skin and for the quality control purposes, however due to problems related to variations in the lipid contents of the biological membranes, synthetic membranes have gain tremendous use in the quality control of topical dosage forms (Guy and Hadgraft, 1990; Shah *et al.*, 1992; Haigh and Smith, 1994; Loftsson *et al.*, 2002; Ng, 2007). A variety of synthetic membranes, classified as high flux and low flux membranes, depending on their physical properties such as pore size, molecular weight cut off point (MWCO) and the investigated drug are found to be ideal for testing topical formulations in the absence of human or animal skin (Pellet *et al.*, 1977; Sang–Chul and Soo–Young, 1996; Fang *et al.*, 1999; Trotta *et al.*, 2003; Fiala *et al.*, 2008).

For example, Cellulose acetate membranes have shown good drug release of various concentrations of retinoic acid from creams (Thakker and Chern, 2003) but on the other hand these membranes showed limited drug release of ibuprofen from the topical semisolid dosage forms (Ng, 2007). However, we had no other choice but to use Cellulose–based membranes for ibuprofen drug release studies due to unavailability of other membranes. Therefore, in the present study two Cellulose–based membranes were investigated for their effect on the drug release of ibuprofen *i.e.* Cellulose acetate and Visking membranes. Cellulose acetate membranes are available with pore sizes of 0.22µm and 0.45µm (Craig and Konigsberg, 1961). In the present study, Cellulose acetate membranes with pore sizes of 0.22µm or 0.45µm showed rather similar ibuprofen release from the commercial hydrogel and therefore either one could be used. This observation was in agreement with the results of Ng,

(2007). In this context, both of these membranes may be considered as low flux membranes.

Visking membranes showed higher drug release than the Cellulose acetate membranes for ibuprofen hydrogel (Table 8.8). However, the CVs for Cellulose acetate membranes appeared to be lower than the Visking membranes irrespective of membrane soaking time (Table 8.6). Visking membranes' CVs were significantly affected by the membrane soaking time *i.e.* higher CVs with 0.5 hr and significantly lower CVs with 24 hrs soaking time (Fig. 8.10).

Cellulose acetate membranes are hydrophilic in nature and stable only in the range of acidic to neutral pH (3–8) and show loss of integrity at higher pH (12.0) (Fiala *et al*., 2008). In contrast, Visking membranes are obtained from regenerated cellulose, and are stable at various pH values.

The low drug release of Cellulose acetate membranes can be explained in terms of pH of the dissolution medium. 0.1M NaOH is a strong base (pH 12.5) and contact of the vehicle with the membrane may have weakened the membrane integrity, leading to lower drug release (Ng *et al*., 2005). The drug release from Cellulose acetate membranes were rather low (11–15%, Table 8.5) irrespective of membrane soaking time suggesting an interaction between membrane and the vehicle.

The Visking membranes showed higher CVs (10–15%) when soaked in the dissolution medium only for 0.5 hr. In contrast, significantly lower CVs (~4.5%) were achieved after soaking for 24 hrs, suggesting that membrane soaking time had significant effect on lowering the CVs for Visking membranes. The same results were observed in the preliminary studies, where higher CVs were obtained without soaking whereas soaking for 24 hrs reduced the CVs significantly (Fig. 8.5).

It is known that Visking membranes contain significant amount of lipids such as glycerine, which are known to affect the drug permeation and may explain high CVs at relatively short membrane soaking time (0.5 hr) from Visking membranes. However, soaking for 24 hrs effectively removes the glycerine and a further rinsing for couple of times after soaking increased the drug permeation and reduced the CVs.

It has been reported that in the low flux membranes, the drug permeation is hindered by back diffusion, leading to low flux (Thakker and Chern, 2003; Ng, 2007). Therefore, the low release from Cellulose acetate membranes may also be explained on the basis of back diffusion, where drug may have accumulated on the surface of the membrane as a cake.

Sampling site also contributed to the variations in the drug release from two membranes in addition to the membrane soaking time and the stirrer bar dimensions. Sampling from the centre of the receiver showed higher drug release than from the bottom in addition to lower CVs for both membranes (not shown). The reason for this effect is unknown as the receiver fluid solubilising the permeated drug was given enough time between sampling for homogenous mixing. However, these results suggested that no drug was accumulated at the bottom of the receiver, ensuring homogenous mixing. Further work needs to be done to explain the effect of sampling site.

The presence of air bubbles in the diffusion cell causes a negative effect on the drug release and the CVs. This effect was observed in the preliminary studies where the receiver solution, without degassing showed significantly higher CVs than the degassed solution. It has also been reported that incorporation of air bubble just below membrane due to sampling causes a decrease in temperature *i.e.* after removing the sample and just before replenishment of the receptor medium (Ng, 2007), which reduces the effective diffusion area, leading to reduced drug permeation. Therefore, it is important to keep the sampling time as low as possible. The Franz cells with automated sampling system effectively avoid this problem but the manual sampling needs to overcome this problem by some means. In the present study, we used manual sampling and the effect of sampling was reduced by significant amount of training and practice. We managed to complete the sampling within 40 seconds to keep the effect of lowering of temperature as low as possible, leading to consistently higher drug release and low CVs.

Saturated oil concentration of ibuprofen in the lipogels of various oils (liquid paraffin, palm−olein and the combination of liquid paraffin and palm−olein (70:30

ratio respectively) showed significantly different drug release profiles. The lipogels of liquid paraffin containing either 12.5% or 20% MgSt showed significantly lower amounts of drug released (~4 fold lower) compared to the commercial ibuprofen hydrogel. This reduced drug release from the lipogels may be attributed to the hydrophilic nature of the membranes. The Cellulose and Visking membranes are hydrophilic and may significantly swell by absorbing water from the receptor medium, creating a water barrier layer impermeable to the drug from a lipophilic vehicle (Segers *et al*., 1997; Rangarajan and Zatz, 2001; Fiala *et al*., 2008) such as lipogel. Therefore, the selected membranes appeared to be suitable only for the hydrophilic vehicles such as commercial ibuprofen hydrogel.

In contrast, the lipogels of palm−olein showed the highest drug release amongst all the lipogels and even higher than the commercial ibuprofen hydrogel when Cellulose acetate membranes were used for comparison. However, Visking membranes produced significantly higher drug levels for commercial hydrogel compared to the palm−olein lipogels (Fig. 8.13). Fatty acids have long been used as penetration enhancers for various drugs through the skin (Scheuplein and Blank, 1971; Kaiho *et al*., 1987; Green *et al*., 1988; Roberts, 1997; Clarys *et al*., 1998). Palm−olein contains significant amounts of various saturated and unsaturated fatty acids, which are known penetration enhancers and may form the basis of higher drug release from the palm−olein lipogels compared to liquid paraffin lipogels.

It is now generally accepted that viscosity of the formulations significantly affects the drug diffusion through skin (Ostrenga *et al*., 1971; Almedia and Bahia, 2006; Lee *et al*., 2007; Vintiloiu *et al*., 2007). An increase in viscosity causes a decrease in the overall drug release. Similar observations were made in the present work where viscosity of the palm−olein lipogels was affected by the amount of MgSt used *i.e.* 12.5% MgSt produced structured fluids whereas semisolid lipogels were obtained using 20% MgSt. These differences in the consistency also affected the drug release from the lipogels. The structured fluid containing 12.5% MgSt showed higher drug release compared to the lipogels having 20% MgSt (Fig. 8.13). Therefore, the higher drug release from structured fluids may be attributed to the low viscosity compared to the lipogels with significantly higher consistency.

8.6 Conclusions

i. Franz diffusion cells showed significant variations in the drug release before and after validation. Therefore, it is necessary to investigate the Franz cell–related factors before studying the drug release from a specific drug delivery system.

ii. The use of computer–aided software (DoE) helped significantly reduce the time required for the validation of the Franz diffusion cell compared to the one factor at a time approach. Furthermore, DoE also investigated the interactions between various factors, leading to optimised drug release.

iii. The commercial 5% ibuprofen hydrogel showed significantly higher drug release from Visking membranes compared to the Cellulose acetate membranes with higher CV prior to validation. Nevertheless, soaking of Visking membranes for 24 hrs prior to use produced significantly low CVs (Fig. 8.10). In contrast, the drug release from the lipogels of liquid paraffin showed little dependency on the type of membrane as there was statistically no difference in the drug release from either membrane.

iv. The lipogels of palm−olein showed significantly higher drug release compared to the lipogels of liquid paraffin alone or the lipogels containing 70:30 ratio of liquid paraffin and palm−olein respectively. The higher drug release from the lipogels of palm−olein may be attributed to the presence of various fatty acids in the palm−olein, which are known penetration enhancers and enhance drug release. In addition, the lipogels containing 12.5% MgSt compared to the lipogels containing 20% MgSt also showed higher drug release, which is attributed to the low viscosity (structured fluids) of the formulations.

CHAPTER IX

GENERAL DISCUSSION AND CONCLUSIONS

9.1 General Discussion

Lipogels, novel lipophilic semisolid vehicles prepared from magnesium stearate (MgSt) and liquid paraffin are non–greasy with an ointment–like consistency and may also be used as ointment bases. Drugs and excipients may show polymorphism. Transformation from one polymorphic form to another during processing can affect the physical chemical properties of the dosage form. MgSt exists as polymorphs and may be composed of either pure or mixed homologues.

The aim of this work was to investigate the influence of the crystal state and the homologue composition of MgSt on the physical chemical properties of liquid paraffin lipogels prepared from them using different methods of preparation. In addition, the effect of the processing variables such as type of mixing, heating, cooling and stirring was investigated. The suitability of palm–olein in replacing liquid paraffin as a vehicle for lipogels was also studied. Addition of drugs to the formulations has been reported to influence the physical chemical properties of the drug delivery systems (Vintiloiu *et al*., 2007). Therefore, the effect of incorporation of ibuprofen on the physical chemical properties of lipogels was studied. Finally, release of saturated oil concentrations of ibuprofen from the lipogels was studies in validated Franz diffusion cells, using Design of Experiment.

The first experiment (chapter III) involved preparation of five different pseudopolymorphic forms of MgSt. Pure anhydrous magnesium stearate was obtained by heating magnesium oxide in pure stearic acid (~97% C_{18}) (S1). On hydration S1 formed the trihydrate (S2). Commercial mixed homologue (60:40 C_{16}-C_{18}) MgSt was used as received (S3) and dried to form a mixed homologue anhydrate (S4), which was rehydrated to yield dihydrate (S5). XRD data confirmed that all five forms were different from each other showing amorphous to crystalline structures.

Pseudopolymorphic changes in MgSt may affect the physical chemical properties of dosage forms. Therefore, the influence of different pseudopolymorphic forms of mixed and pure homologue magnesium stearate prepared in chapter III was investigated on the physical chemical properties of lipogels (Chapter IV). Various concentrations of mixed homologue dihydrate MgSt (2.5%−20%) were dispersed in the liquid paraffin, heated to temperature range between 110−130°C, and cooled naturally (slow cooling). An optimum concentration (~12.5%) of MgSt produced least syneretic solid lipogels. Therefore, 12.5% MgSt was selected to study influence of process variables on the physical chemical properties of the liquid paraffin lipogels. The anhydrate and hydrates (~12.5%) prepared from pure and mixed homologue MgSt were used to prepare liquid paraffin lipogels.

The hydrates of pure and mixed homologue MgSt influenced lipogels differently. The pure homologue generally produced liquids. The exception was trihydrate homologue which produced semisolid lipogels, which reverted to fluids upon gentle stirring, implying pressure sensitivity. In contrast, both (anhydrate and dihydrate) mixed homologue MgSt produced syneretic solid lipogels. The XRD data suggested that MgSt was present in significantly more amorphous state in the unstable solid lipogels.

It was shown that the pseudopolymorphic forms of MgSt produced either solid lipogels unsuitable for dermatological use or formed fluids. Therefore, the influence of various preparation variables such as type of heating, cooling, stirring, addition of water and homogenisation on the physical chemical properties of lipogels was investigated (Chapter V). Slow cooling (0.1−0.2^{o}C/min), addition of water and homogenisation produced semisolid, non−syneretic lipogels using mixed homologue MgSt. However, pure homologue MgSt generally produced liquids. The exception was the trihydrate which produced unstable semisolid lipogels, which reverted to liquids upon stirring, implying pressure sensitivity. Semisolid lipogels showed "Maltese crosses" structures microscopically between crossed−polars, suggesting presence of inverse lamellar phases. The XRD data showed that MgSt in the semisolid lipogels was present mainly in crystalline form. The pressure sensitive

semisolid obtained from pure trihydrate MgSt contained both plate like crystals and lamellar structures; the latter only disappeared on stirring (Fig. 4.5b).

It was possible to prepare non−syneretic lipogels of MgSt in the synthetic liquid paraffin vehicle (Chapter V). Natural occurring vehicles such as vegetable oils are increasingly being used in the formulation of topical drug delivery systems (Vintiloiu *et al*., 2007). Therefore, palm−olein was investigated for its suitability to replace liquid paraffin as vehicle for MgSt lipogels (Chapter VI).

Various concentrations of MgSt (2.5%−20%) were dispersed in the palm−olein alone or the combination of the liquid paraffin and the palm−olein in a fixed ratio (70:30) heated and cooled in the same fashion as for the liquid paraffin lipogels. An optimum concentration (~12.5%) of MgSt produced least syneretic solid lipogels. Therefore, 12.5% MgSt was selected to study influence of process variables on the physical chemical properties of lipogels.

Semisolid lipogels were obtained with an optimum concentration (~12.5%) of the palm−olein alone and in combination with liquid paraffin in a fixed ratio (70:30) only when an optimum amount of water (~1−2%) was stirred into the dispersions during the cooling cycle (at just below 100$^{\mathrm{o}}$C), and then cooled without agitation. Solid lipogels unsuitable for dermatological use were obtained without addition of water with natural cooling, similar to the liquid paraffin lipogels. The homogenised lipogels appeared to be semisolid after preparation but changed to solids upon storage after one week. The results suggest that palm−olein used alone, or used in combination with the liquid paraffin forms semisolid lipogels suitable for dermatological use only when an optimum amount of water (~1−2%) is added during cooling cycle.

Incorporation of drugs in semisolid vehicles may affect the physicochemical properties of the vehicle, most importantly rheological properties. Incorporation of various amounts of rivastigmine drug in an oleogel (oily systems) containing vegetable oil (Safflower oil) and *N*-stearoyl l-alanine methyl ester (SAM) organogelator has shown significant changes in the sol−gel temperature leading to

decrease in the viscosity of the formulation (Vintiloiu *et al*., 2007). In present study, influence of incorporation of ibuprofen on the physical chemical properties of the stable semisolid and fluid lipogels was investigated (Chapter VII). The incorporation of ~5% ibuprofen in liquid paraffin dispersions upon cooling produced structured fluids due to disruption of lamellar phases which was confirmed microscopically by the loss of "Maltese crosses" between crossed–polars. However, after addition of optimum amount (~10%) of phosphate buffer solution of pH ~9.25 to the liquid paraffin structured fluids, semisolid, non–syneretic lipogels were obtained. In contrast, addition of saturated oil concentration (~5%) of ibuprofen in semisolid lipogels formulations of palm–olein containing 20% MgSt did not fluidise the semisolid lipogels.

Previous knowledge of aqueous stearate–based semisolids suggests that their physical appearance is significantly influenced by pH. Al–Saidan, (2004) reported that ibuprofen acts as a surfactant and interacts with stratum corneum (SC), partially extracting lipids from the SC causing hydration and reducing pH. Therefore, effect of ibuprofen on the conversion of semisolid lipogels to structured fluids can be explained in terms of pH. Ibuprofen, at an oil saturation concentration of ~4.5%, due to surface activity, may have caused separation of magnesium stearate from the lipogel, producing free fatty acids leading to lower pH. This view was supported by the microscopic examination. The clusters of flower–like crystals were observed in the structured fluids of low pH, which may have formed due to interaction of magnesium stearate and ibuprofen.

Finally, drug release of ibuprofen from lipogels was also investigated using Franz diffusion cells, validated by Design of Experiment (Chapter VIII). Most of the drug release studies involving the use of Franz cells report significant variations in the results including intra–laboratory variations. Therefore, validation of Franz cell experiments has become an integral part of the *in vitro* drug release testing of topical semisolid formulations (Qvist *et al*., 2000; Ng, 2007). In the present study, validation of the Franz diffusion cells was carried out using a commercial gel containing 5% Ibuprofen and a statistical tool, the Design of Experiment (DoE) to investigate the influence of various factors and the interactions between the factors with minimum

experiments. The objective of the validation experiment was to achieve optimum drug release with low CVs.

Franz cell validation using DoE was carried out by performing only 22 experiments compared to the 64 experiments needed for one factor at a time (OFAT) approach. Furthermore, DoE also investigated positive and negative interactions between factors, for example membrane type (A) showed critical interactions with membrane soaking time (B) and with the sampling intervals (D). The interaction between membrane type and the membrane soaking time (AB) showed negative effect whereas the interaction between membrane type and the sampling intervals (AD) showed positive effect. The study of the interactions between the factors is not possible with OFAT approach (Sheikh *et al*., 2009).

Validated Franz diffusion cells were then used for the investigation of drug release from the lipogels of MgSt in liquid paraffin, palm−olein and combination of the two vehicles. Ibuprofen release from the liquid paraffin lipogels appeared to be ~4 fold lower than the aqueous commercial gel containing 5% Ibuprofen. These results can be explained in terms of thermodynamic activity of the drug in the vehicle. It is known that when drug concentration is same in different vehicles, the drug flux will depend on the type of vehicle and the membrane. For example, an aqueous hydrogel will show higher flux through hydrophilic membranes compared to the lipophilic gel. Same analogy can be used to explain higher drug release from the aqueous commercial hydrogels in the present work.

On the other hand, palm−olein lipogels showed significantly higher drug release compared to the lipogels of liquid paraffin alone or in combination with the palm−olein (Fig. 8.13). The drug release from palm−olein lipogels is expected to be higher than the liquid paraffin lipogels mainly due to the presence of unique combination of saturated and unsaturated fatty acids, which are proven to be good chemical penetration enhancers as they cause skin hydration, disrupting the stratum corneum lipid organisation making it more permeable to the drugs (Cornwell and Barry, 1995; Barry, 2001). In addition, unsaturated fatty acids have shown better drug release enhancing activity compared to the saturated fatty acids. Therefore,

palm−olein having relatively high percentages of unsaturated fatty acids like oleic acid and linolenic acid may have provided higher drug release from the lipogels compared to the lipogels of liquid paraffin.

Although, use of palm−olein in combination with the liquid paraffin produced aesthetically stable semisolid lipogels however the drug release from these lipogels was not very different from the lipogels of liquid paraffin alone, suggesting that liquid paraffin interferes with the drug releasing properties of palm−olein constituents leading to non−productive combination. Therefore, it may be concluded that liquid paraffin provides aesthetically good semisolid lipogels whereas palm−olein yields reasonably acceptable pale yellow coloured semisolid lipogels in addition to a markedly enhanced drug release profile.

9.2 Conclusions

1. Anhydrous pure homologue magnesium stearate was prepared by the fusion of pure homologue stearic acid and magnesium oxide whereas anhydrous mixed homologue MgSt was obtained by drying commercial dihydrate at 110°C under vacuum. Both anhydrates were amorphous in nature. Various hydrates of pure and mixed homologue MgSt were prepared by treating anhydrate MgSt at 100% relative humidity for 6 weeks. Pure homologue anhydrate changed to trihydrate whereas mixed homologue anhydrate produced dihydrate instead. All hydrates were crystalline in nature.

2. Semisolid, non−syneretic lipogels of MgSt in liquid paraffin, palm−olein or a combination (70:30 ratio) of liquid paraffin and palm−olein respectively can be prepared by heating to 110°C, adding an optimum amount of water (~1−2%) upon cooling to just below 100°C (method 1) or by homogenisation (method 2) during the natural cooling (~0.1−0.2^{o}C) cycle (slow cooling).

3. Microscopy, DSC and XRD results revealed that the swelling of magnesium stearate in the vehicle can be explained on the basis of the presence of inverse lamellar structures, evident from the presence of the "Maltese crosses" structures. However, incorporation of oil saturated concentration of ibuprofen disrupted the

α−crystalline lamellar structure in the liquid paraffin lipogels, leading to reduced swelling and conversion into structured fluids. The semisolid lipogels of palm−olein were not affected by the oil saturation concentration of ibuprofen at 20% MgSt concentration.

4. Homologue composition and crystal state of the MgSt affected consistency and stability of the lipogels. Pure homologue MgSt generally produced structured fluids. The exception was trihydrate MgSt which produced pressure sensitive unstable semisolid lipogels. In contrast, mixed homologue MgSt in the presence of ~1−2% moisture produced semisolid, non−syneretic lipogels. The MgSt was present essentially in the amorphous form in the unstable solids whereas it was mainly in crystalline form in the semisolid lipogels.

5. Incorporation of saturation concentration of ibuprofen into the dispersions of MgSt in the liquid paraffin and the palm−olein during cooling cycle produced fluid lipogels and semisolid lipogels respectively. However, after addition of optimum amount of phosphate buffer solution of appropriate pH to the liquid paraffin fluid lipogels semisolid, non−syneretic lipogels were obtained which are suitable for dermatological use.

6. DoE helped optimizing the validation of Franz diffusion cell experiment in significantly short time compared to the conventional OFAT approach. In addition, investigation of interaction between the factors was also possible.

7. Drug release from the lipogels of liquid paraffin appeared to be significantly lower compared to the commercial hydrogel. However, palm−olein lipogels showed significantly higher drug release than the liquid paraffin lipogels and were comparable to the drug release from the commercial hydrogels. Therefore, palm−olein can replace liquid paraffin as vehicle for the formulation of stable semisolid lipogels.

9.3 Suggestions for future work

The semisolid lipogels of magnesium stearate in liquid paraffin, palm–olein and the combination of liquid paraffin and palm–olein (70:30 ratio) were prepared. The systems showed good stability at ambient temperature (no syneresis of oil) for more than two years, making lipogels promising hydrophobic drug delivery systems with good occlusive properties. The lipogels were also non-greasy after application to the skin and may replace the greasy ointment bases as hydrophobic bases for topical drug delivery systems. In addition, it was possible to incorporate saturated concentration (~5%) of ibuprofen in these systems. Palm–olein showed significantly higher drug release compared to liquid paraffin lipogels and hence is a good candidate for the dermal and transdermal delivery of hydrophobic drugs.

Liquid paraffin is stable at extreme environmental conditions (temperature and humidity) however palm–olein solidifies below 6^oC, showing polymorphism, which may cause changes in the physicochemical properties of the drug delivery systems. Therefore, future work should focus on:

i. Standardisation of the quality of palm–olein by identification of its metastable polymorphic forms and measures to convert them into stable polymorphs for wider temperature range (ongoing work at the Malaysian Palm oil board (MPOB)).

ii. Scale up of the current work to the commercial batch size (25-50Kg) and to explore areas for its commercialisation as replacement for the ointment bases.

iii. Incorporation of hydrophilic drugs into palm–olein to study their influence on the thermodynamic properties of the systems. It is expected that the occlusive effect caused by the lipogels would preserve skin moisture, providing ideal environment for the diffusion of hydrophilic drugs from lipogels to the skin.

iv. Various hydrates of magnesium stearate were prepared in present work but it was not possible to assign the exact hydration state of each hydrate (hemi, mono, di or tri). Therefore, we plan to conduct vapour sorption-desorption experiments at various % relative humidities (%RH) using Dynamic Vapour Sorption–Near Infra Red

(DVS-NIR) on various pseudopolymorphs of magnesium stearate in order to identify definite hydration state of each material.

References

Abraham M. H., (1993). Scales of solute hydrogen-bonding: their construction and application to physicochemical and biochemical processes. Chem Soc Rev, 22, 73-83.

Abraham M. H., Chadha H. S. Mitchell R. C., (1995). The factors that influence skin penetration of solutes. J Pharm Pharmacol, 47, 8-16.

Adami G., Larese F., Venier M., Barbieri B., Lo Coco F., Reisenhofer E., (2006). Penetration of benzene, toluene and xylenes contained in gasoline through human abdominal skin *in vitro*. Toxic in vitro, 20, 1321-1330.

Addicks W. J., Flynn G. L., Weiner N., (1987). Validation of a flow-through diffusion cell for use in transdermal research. Pharm Res, 4, 337-341.

Almeida I. F., Bahia M. F., (2006). Evaluation of the physical stability of two oleogels. Int J Pharm, 327, 73-77.

Al-Saidan S M., (2004). Transdermal self-permeation enhancement of ibuprofen. J Control release, 100, 199-209.

Anderson M. J., (2008). DOE FAQ alert (Newsletter by email circulation). 8(6): June issue.

Anderson M. J., Whitcomb P. J., (2005). Getting the most from the minimal-run designs. In: DOE simplified- practical tool for effective experimentation. 2nd edition. Anderson M. J., Whitcomb P. J., (Eds). John Wiley and Sons, New York. pp45-110.

Andres C., Bracconi P., Pourcelot Y., (2001). On the difficulty of assessing the specific surface area of magnesium stearate. Int J Pharm, 218, 153-163.

Anuer B. G., Valenta C., (2004). Influence of phloretin on the skin permeation of lidocaine from semisolid preparations. Eur J Pharm Biopharm, 57, 307-312.

Ashford M., (2002). Bioavailability- physicochemical and dosage form design. In: Pharmaceutics- The science of dosage form design. Aulton M. E., (Ed). Churchill Livingstone, London. 234-252.

Aungst B. J., Blake J. A., Hussain M. A., (1990). Contributions of drug solubilisation, partitioning, barrier disruption, and solvent permeation to the enhancement of skin permeation of various compounds with fatty acids and amines. Pharmaceutical Research, 7(7). 712-718.

Aungust B. J., Rogers N. J., Shefter E., (1986). Enhancement of naloxone penetration through human skin in vitro using fatty acid, fatty alcohol, surfactants, sulfoxides and amides. Int J Pharm, 33, 225-234.

Ayesha F., (1998). Formulation of multiple o/w/o emulsions. Thesis. University Science of Malaysia.

Baie S. H., Sheikh K. A., (1999). Effect of palm oil based haruan creams on the healing wounds in normal SD rats. In: Proceedings of the 18th European pharmaceutical technology conference. Utrecht, Netherlands.

Barra J., Somma R., (1996). Influence of the Physicochemical Variability of Magnesium Stearate on Its Lubricant Properties: Possible Solutions. Drug Dev Ind Pharm, 22(`11), 1105-1120.

Barrett J. S., (2004). Bioavailability and bioequivalance studies. In: Pharmacokinetics in drug development: Clinical study design and analysis. Bonate P. L., Howard D. R., (Eds). AAPS Press, Arlington. 91-121.

Barry B W., (2002). Drug delivery routes in skin: a novel approach. Adv Drug Del Rev, 54 (1). S31–S40.

Barry B. W., (1968). The self-bodying action of the mixed emulsifier sodium dodecyl sulphate/cetyl alcohol. J Colloid Interface Sci, 28, 82-91.

Barry B. W., (1974). Rheology of pharmaceutical and cosmetic semisolids. In: Beans H. S., Beckett A. H., Carless J. E., (Eds.). Advances in Pharmaceutical sciences, Vol.4, Academic Press, London, 1–72.

Barry B. W., (1983). Methods for studying percutaneous absorption. In: Dermatological formulations. Percutaneous absorption, Barry B. W., (Ed), New York, Marcel Dekker, Inc. 234-280.

Barry B. W., (1987). Mode of action of penetration enhancers in human skin. J Control Release. 6, 85–97.

Barry B. W., (2001). Review: Novel mechanism and devices to enable successful transdermal drug delivery. Eur J Pharm Sci, 14, 101-114.

Barry B. W., Brace A. R., (1977). Permeation of oestrone, oestradiol, oestrol and dexamethasone across cellulose acetate membrane. J Pharm Pharmacol, 29, 397-400.

Barry B. W., Eccleston G. M., (1973). Oscillatory testing of o/w emulsions containing mixed emulsifiers of the surfactant-long chain alcohol type: self-bodying action. J Pharm Pharmacol, 25, 244-253.

Burnett DJ, Thielmann F, Booth J (2004) Determining the critical relative humidity for moisture-induced phase transitions. Int J Pharm 287: 123-133.

Bekturov E. V., Bimendina L. A., (1981). Interpolymer complexes. Adv Polym Sci, 41, 99–147.

Block L. H., (2005). Medicated topicals. In: Remington: The science and practice of pharmacy (21st ed), Hendrickson R, Beringer P, DerMardrosian A., *et al*., (Ed). Philadelphia, Lippincott Williams and Wilkins, pp871-888.

Bolton S., Bon C., (2004). Pharmaceutical statistics- practical and clinical applications. 4th edition, Marcel Dekker, Inc.

Box G. E. P., Hunter W. G., Hunter J. S., (1978). Statistics of experiments. In: RSM simplified- optimizing processes using response surface methods for design of experiments. Anderson M. J., Whitcomb P. J., (Eds). John Wiley and Sons, New York. pp61.

Bozic M., Korbar-Smid. J., (1980). Structure. Cosmetics and Toiletries, 95, 29-31.

Bozic M., Korbar-Smid. J., Larvic J., (1980). Magnesium, Calcium, and Zinc stearate gels with liquid paraffin. 2. Evaluation of production conditions. Cosmetics and Toiletries, 95, 25-28.

Bracconi P., Andres C., N'diaye A., Pourcelot Y., (2005). Thermal analyses of commercial magnesium stearate pseudopolymorphs. Thermochimica Acta, 429, 43-51.

Bracconi P., Andres C., Ndiaye A., (2003). Structural properties of magnesium stearate pseudopolymorphs: effect of temperature. Int J Pharm, 262, 109–124.

Bragg W. H., Bragg W. L., (1913). "The structure of the diamond". Proceedings of the Royal Society (London) A89: 277–291.

Britain H. G., (1989). Raw materials. Drug Dev Ind Pharm, 15, 2083-2103.

Brown M. B., Hanpanitcharoen M., Martin G. P., (2000). An in vitro investigation into the effect of glycosaminoglyans on the skin partitioning and deposition of NSAIDs. Int J Pharm, 225, 113-121.

Bruggeller P., (1982). Freezing of water in w/o emulsions. J Disp Sci Technol, 3, 395–417.

Burnett D. J., Thielmann F., Booth J., (2004). Determining the critical relative humidity for moisture-induced phase transitions. Int J Pharm, 287, 123–133.

Butcher A. E., Jones T. M., (1972). Some physical characteristics of magnesium stearate. J Pharm Pharmacol, 24, 1P-9P.

Chapman D., (1957). The 720 cm^{-1} band in the infrared spectra of crystalline long-chain compounds. J Chem Soc, 4489-4491.

Chaudhary K. A., Singh G., Stephenson A. G., Ackermann L. B., (2005). Instrumental methods of analysis. In: Remington: The science and practice of pharmacy (21st ed), Hendrickson R., Beringer P., DerMardrosian A., et al., (Ed). Philadelphia, Lippincott Williams and Wilkins, 658-661.

Chiang C-M., Flynn G L., Weiner N D., Addicks W J., Szpunar G J., (1989). Bioavailability assessment of topical delivery systems: In vitro delivery of minoxidil from prototypical semi-solid formulations. Int J Pharm, 49, 109-114.

Chilcott R. P., Barai N., Beezer A. E., et al., (2005). Inter- and intralaboratory variation of in vitro diffusion cell measurements: An international multicenter study using quasi-standardized methods and materials. J Pharm Sci, 94(3), 632-638.

Cho Y. J., Choi H K., (1998). Enhancement of percutaneous absorptionof ketoprofen. Effect of vesicle and adhesive matrix. Int J Pharm, 169, 95-104.

Cilurzo F., Minghtti P., Sinico C., (2007). Newborn pig skin as model membrane in in vitro drug permeation studies: A technical note. AAPS PharmSciTech, 8(4) Article 94, E1-E4.

Cistola D. P., Atkinson D., Hamilton J. A., Small D. M., (1986). The Phase Behavior of Anhydrous and Hydrated 1:1 Fatty Acid-Soaps. Biochemistry, 25, 2804.

Clarys P., Alewasters K., Jadoul A., Brel A., Mandadas R O., Preat V., (1998). In vitro percutaneous penetration through hairless rat skin: influence of temperature, vehicle and penetration enhancers. Eur J Pharm Biopharm, 46, 279-283.

Clement P., Laugel C., Marty J P., (2000). Influence of three synthetic membranes on the release of caffeine from concentrated w/o emulsions. J Controlled Release, 66, 243-254.

Clowes H. M., Scott R. C., Richard H. J., (1994). Skin absorption: flow-through or static diffusion cells. Toxic in vitro, 8, 827-830.

Coates J., (2000). Interpretation of Infrared Spectra, A Practical Approach. In: Encyclopedia of Analytical Chemistry. Meyers, R. A., (Ed.). Chichester, John Wiley & Sons Ltd, 10815–10837.

Comer J., (2005). The relationships between lipophilicity, solubility and pKa for ionizable molecules. Sirius analytical instruments Ltd. Pesented at PhysChem Forum.

Cooper E., Iqbal A., Barlett C., Marriot C., Whitefield P. J., Brown M. B., (2004). A comparison of topical formulations for the prevention of human schistosomiasis. J Pharm Pharmacol, 56, 957-962.

Cordoba-Diaz M., Nova M., Elorza B., Cordoba-Diaz D., Chantres J. R., Cordoba-Borrego M., (2000). Validation protocol of an automated in-line flow-through diffusion equipment for in vitro permeation studies. J Controlled Release, 69(3), 357-368.

Cornwell P A., Barry B W., (1995). Effects of penetration enhancer treatment on the statistical distribution of human skin permeabilities. Int J Pharm, 117, 101-112.

Costa P., Lobo M S., (2001). Modeling and comparison of dissolution profiles. Eur J Pharm Sci, 13, 123-133.

Craig L. C., Konigsberg W., (1961). Dialysis studies. 3. Modification of pore size and shape in cellulose membranes. J Phy Chem, 65, 166–172.

Crowley M. M., (2005). Solutions, emulsions suspensions and extracts. In: Remington: The science and practice of pharmacy (21st ed), Hendrickson R., Beringer P., DerMardrosian A., *et al*., (Ed). Philadelphia, Lippincott Williams and Wilkins, 745-775.

Davis S. S., (1969). Viscoelastic properties of pharmaceutical semisolids. J Pharm Sci, 58(4), 418-421.

Dorset L. D., (1985). Electron crystal structure analysis of small organic molecules. J Electron Micro Tech, 2(2). 89-128.

Drozda T., Wick C., Benedict J. T., Veilleux F. R., (1983). Lubricating greases In: Tool and manufacturing engineers handbook. A reference book for manufacturing engineers, managers, and technicians (4th ed–online preview). Drozda T., Wick C., Benedict J. T., Veilleux F., (Ed). Dearborn, Mich.: Society of Manufacturing Engineers.

Eccleston G. M., (1977). Structure and rheology of cetomacrogol creams: the influence of alcohol chain length and homologue composition. J Pharm Pharmacol, 29, 157-162.

Eccleston, G. M., (1986). The microstructure of semisolid creams. Pharm Int, 7, 63–70.

Eccleston G. M., (1992). Emulsions. In: Swarbrick J., Boylan J. C., (Eds.). Encyclopedia of pharmaceutical technology, Vol.5, New York, Marcel Dekker, 137–188.

Eccleston G. M., (1997). Functions of mixed emulsifiers and emulsifying waxes in dermatological lotions and creams. Colloids Surf A Physicochem Eng Asp, 123-124, 169-182.

Eccleston G. M., Behan-Martin M. K., Jones G. R., Towns-Andrews E., (2000). Synchrotron X-ray investigation into lamellar gel phase formed in

pharmaceutical creams prepared with cetrimide and fatty alcohols. Int J Pharm, 203, 127-139.

El Gendy A. M., Jun H. W., Kassem A. A., (2002). In vitro release studies of flurbiprofen from different topical formulations. Drug Dev Ind Pharm, 28(7), 823-831.

El Laithy H. M., El-Shaboury K. M., (2002). The development of cutina lipogels and gel microemulsion for topical administration of fluconazole. AAPS PharmSciTech, 3(4), E35

Eros I, Soosne-Csanyi E., Selmeczi B., (1994). Influence of viscosity on drug release from ointments, creams, gels and emulsions. Acta Pharm Hung. 64(2), 57–61. (English abstract)

Ertel K. D., Carstensen J. T., (1988a). Chemical, physical, and lubricant properties of magnesium stearate. J Pharm Sci, 77(7), 625-629.

Ertel K. D., Carstensen J. T., (1988b). An examination of the physical properties of pure magnesium stearate. Int J Pharm, 42, 171-180.

Fang Y. J., Fang C. L., Sung K. C., Chen H. Y., (1999). Effect of low frequency ultrasound on the *in vitro* percutaneous absorption of Clobetasol 17–propionate. Int J Pharm, 191, 33–42.

FDA-SUPAC-SS, (1997). Guidance for industry. SUPAC-SS non-sterile semisolid dosage forms. Scale-up and post approval changes: Chemistry, manufacturing and controls. *In vitro* release testing and *in vivo* bioequivalence documentation.

Fiala S., Brown M. C., Jones S. A., (2008). An investigation into the influence of binary drug solutions upon diffusion and partition processes in model membranes. J Pharm Pharmacol, 60, 1615-1623.

Finnin B. C., Morgan T. M., (1999). Transdermal penetration enhancers: applications, limitations and potential. J Pharm Sci, 88, 955–958.

Florence A. T., Atwood D., (1988). Polymers and macromolecules. In: Physicochemical principles of pharmacy, 2nd edition, Florence A. T., Atwood D., (Ed), London, Pharmaceutical Press, 281-334.

Florence A. T., Atwood D., (2006). Drug absorption and routes of administration. In: Physicochemical principles of pharmacy, Florence A. T., Atwood D., (Ed), London, Pharmaceutical Press, 330-390.

Flynn G. L., (1989). Mechanism of percutaneous absorption from physicochemical evidence. In: Bronaugh R. L., Maibach H. I., (Eds), Percutaneous Absorption: Mechanism- Methodology -Drug Delivery, Dekker, New York, pp27-51.

Flynn G. L., (1993). General introduction and conceptual differentiation of topical and transdermal drug Delivery Systems. In: Topical drug bioavailability,

bioequivalence, and penetration. Shah V. P., Maibach H. I., (Eds.). Plnum Press, New York, 369-379.

Franz T. J., (1975). Percutaneous absorption. On the relevance of in vitro data. J Invest Dermatol, 64, 190-195.

Friberg S., (1965). Gelation of aluminium soaps in hydrocarbons. I. Infrared and rheological investigations. Acta Chem Scand, 19(4), 883-887.

Friberg S., (1966). Gelation of aluminium soaps in hydrocarbons. II. Relation with the temperature dependent transitions of soaps. Arkiv For Kemi Bad, 25(43), 475-483.

Friberg S., Mandell L., Larsson M., (1969). J Colloid Interface Sci, 20, 155.dddd

Gallagher S. J., Trottet L., Heard C. M., (2003). Ketoprofen: release from, permeation across and rheology of simple gel formulations that stimulate increasing dryness. Int J Pharm, 268, 37-45.

Garnier P., Gregoire P., Montmitonnet P., Delamare F., (1988). Polymorphism of crystalline phases of calcium stearate. J Mater Sci, 23, 3225- 3231.

Garti N., Wellner E., Saring S., (1982). Effect of surfactants on crystal structure modification of stearic acid. J Crystal Growth, 57(3), 577-584..

Gasperlin M., Kristl J., Smid– Korbar J., Kerc J., (1994). The structure elucidation of semisolid w/o emulsions systems containing silicone surfactant. Int J Pharm, 107, 51–56.

Genova C., Francesco B., Sandra G., (1997). Oil-based transparent gels. United States Patent. 5,597,576.

Green P. G., Guy R. H., Hadgraft J., (1988). In vitro and in vivo enhancement of skin permeation with oleic and lauric acids. Int J Pharm, 48, 103–111.

Gunstone F. D., (1967). An introduction to the chemistry and biochemistry of fatty acids and their glycerides. Chapman and Hall, London.

Guy R. H., Hadgraft J., (1990). On the determination of drug release rates from topical dosage forms. Int J Pharm, 60, 1–3.

Gwak H. S., Chun I. K., (2002). Effect of vehicles and penetration enhancers on the in vitro percutaneous absorption of tenoxicam through hairless mouse skin. Int J Pharm, 236, 57–64.

Hadgraft J., (2001). Skin, the final frontier. Int J Pharm, 224, 1-18.

Hadgraft J., Walters K. A., Wotton P. K., (1986). Facilitated percutaneous absorption: a comparison and evaluation of two *in vitro* methods. Int J Pharm, 32, 257-263.

Haigh J. M., Smith E. W., (1994). The selection and use of natural and synthehetic membranes for *in vitro* diffusion experiments. Eur J Pharm Sci, 2,311-330.

Hanssen E. V., Keksfabrik K. G., (1958). Die Veranderung der mikrostuktur von fett durch unterschieldliche kuhlung (translated in english by Dr. Jennifer Rouse, University of Strathclyde). Fette Seifen Anstrichmittel, 8, 658-660.

Hauck W W., Shah V P., Shaw W S., Ueda C T., (2007). Reliability and reproducibility of vertical diffusion cells for determining release rates from semisolid dosage forms. Pharm Res, 24(11), 2018-2023.

Higuchi T., (1960). Physical chemical analysis of percutaneous absorption from creams and ointments. J Soc Cosmet Chem, 11, 85−97.

Higuchi W. I., (1962). Analysis of data on the medicament release from ointments. J Pharm Sci, 51, 802-804.

Ho K. M., (2006). Proper choice of base of topical medicaments. Med Bulletin, 11(9), 7-8.

Hsu L. R., Huang Y. B., Wu P. C., Tsai Y. H., (1993). Studies on the optimization of the piroxicam FAPG ointment containing palmitic acid and oleic acid. Clin Pharm J, 45, 123-131.

Huang X. F., Tanojo H., Lenn J., Deng C., Krochmal L., (2005). A novel foam vehicle for dlivery of topical corticosteroids. J Am Acad Dermatol, 53, S26-S38.

Idson N., (1988). Pharmaceutical emulsions. In: Pharmaceutical dosage forms-disperse systems. Lieberman H. A., Rieger M. M., Banker G. S., (Eds). Marcel Dekker, Inc, New York. 199-243.

Jeong B., Kim S. W., Bae Y. H., (2002). Thermosensitive sol–gel reversible hydrogels. Adv Drug Deliv Rev, 54, 37−51.

Jibry N., Heenan R. K., Murdan S., (2004). Amphiphilogels for drug delivery: formulation and characterisation. Pharm. Res. 21, 1852–1861.

Jones D. S., Woolfson A. D., Djokic J., (1996). Texture profile analysis of bioadhesive polymeric semisolids: Mechanical characterization and investigation of interactions between formulation components. J Appl Poly Sci, 61, 2229–2234.

Jones D. S., Woolfson A. D., Brown A. F., (1997). Textural, viscoelastic and mucoadhesive properties of pharmaceutical gels composed of cellulose polymers. Int J Pharm, 151, 223–233.

Junginger H. E., Akkermans A. A. M. D., Heering W., (1984). The ratio of interlamellarly fixed water to bulk water in o/w creams. J Soc Cosmet Chem, 35, 45−57.

Kaiho F., Nomura H., Makabe E., Kato Y., (1987). Percutaneous absorption of indomethacin from mixtures of fatty alcohol and propylene glycol (FAPG base) through rat skin: effects of fatty acid added to FAPG base. Chem Pharm Bull, 35, 2928-2934.

Kantaria S., Rees G. D., Lawrence M. J., (1999). Gelatin–stabilized microemulsions–based organogels: rheology and application in iontophoretic transdermal drug delivery. J Control Release, 60 (2–3), 355–365.

Kaufman J., (2006). Multivariate calibration of mixtures of magnesium stearate hydrates. AAPS abstract, T3288.

Khan G M., Frum Y., Sarheed O, Eccleston G M., Midan V M., (2005). Assessment of drug permeability distributions in two different model skins. Int J Pharm, 303, 81-87.

Khuri A. I., Cornell J. A., (1987). Response surfaces- designs and analyses. In: RSM simplified- optimizing processes using response surface methods for design of experiments. Anderson M. J., Whitcomb P. J., (Eds). John Wiley and Sons, New York. pp123.

Kinget R., Kalala W., Vervoot L., Van der Mooter G., (1998). Colonic drug targeting. J Drug Target, 6, 129-149.

Kohler H., Strand J., (1990). Evaluation of viscosity measurements of dilute solutions of ionic surfactants forming rod–shaped micelles. J Phy Chem, 94, 7628–7634.

Koivisto M., Jalonen H., and Letho Vesa-Peka., (2004). Effect of temperature and humidity on vegetable grade magnesium stearate. Powder Tech, 147, 79-85.

Kon–No

Korbar-Smid J., Bozic M., (1978). Magnesium, calcium, and zinc stearate gels with liquid paraffin. Cosmetics and Toiletries, 93, 33-34.

Kriwet K., Mueller-Goymann C. C., (1993). Binary diclofenac diethylamine water systems: micelles, vesicles and lyotropic liquid crystals. Eur J Pharm Biopharm, 39, 234–238.

Lang J. C., Roehrs R. E., Jani R., (2005). Ophthalmic preparations. In: Remington: The science and practice of pharmacy (21st ed), Hendrickson R., Beringer P., DerMardrosian A., et al., (Ed). Philadelphia, Lippincott Williams and Wilkins, pp850.

Lashmar U. T., (1993). Correlation of rheological properties of an oil–in–water emulsion with manufacturing procedures and stability. Int J Pharm, 91, 59–67.

Lautenschlager., (2004). Oleogels-what non-aqueous products can accomplish. Kosmetiche Praxis, 4, 6-7.

Lee S., Lee J., Choi Y W., (2007). Skin permeation of ascorbyl palmitate by liposomal hydrogel (lipogel) formulation and electrical assistance. Biol Pharm Bull, 30(2), 393-396.

Leinonen U. I., Jalonen H. U., Viheravaara P. A., Laine E. S. U., (1992). Physical and lubrication properties of magnesium stearate. J Pharm Sci, 81(12), 1194-1198.

Lewis G. A., Mathieu D., Phan-Tan-Luu R., (1999). Pharmaceutical experimental design. In; Design of experiment. Phan-Tan-Luu R., (Ed). Marcel Dekker, New York.

Liebenberg W., Engelbrecht E., Wessels A., Devarakonda B., Yang W., De Villers M. M., (2004). A comparative study of the release of active ingredients from semisolid cosmeceutical measured with Franz, enhancer or flow-through cell diffusion apparatus. J Food Drug Anal, 12, 19-28.

Lin H. H., Huang Y. B., Hsu L. R., Tsai Y. H., (1994). The influence of process-induced variations on the nature of stearic acid incorporation into an FAPG base. Int J Pharm, 112, 165-171.

Lindenbaum S., Ratti E. S., Zuber G. E., Miller M. E., Ravin L. J., (1985). Polymorphism of auranofin. Int J Pharm, 26, 123-132.

Liu P., Nightingale J. A. S., Kurihara-Bergstrom T., (1993). Variation of human skin permeation *in vitro*: Ionic vs neutral compounds. Int J Pharm, 90, 171-176.

Loftsson T., Masson M., Sigurdsson H. H., (2002). Cyclodextrins and drug permeability through semi–permeable cellophane membranes. Int J Pharm, 232, 35–43.

Mahmoud M. N., Rady A. H., Faried A., El-Egieul A., (1996). Blending of palm olein with cottonseed oil. In: Proceedings of the 1996 PORIM international palm oil congress (chemistry and technology), 286-300.

Mamat H., Nor-Aini I., Said M, Jamaludin R., (2005). Physicochemical characteristics of palm oil and sunflower oil blends fractionated at different temperatures. Food Chem, 91, 731-736.

Marriott C., (2002). Rheology and the flow of fluids. In: Aulton's Pharmaceutics. The science and manufacture of medicines, Aulton M. E., (Ed), London, Churchill Livingstone, 41-58.

Marriott C., (2007). Rheology. In: Pharmaceutics. The science of dosage form design, Aulton M. E., (Ed), London, Churchill Livingstone, 17-37.

Marwaha S. B., Rubinstein M. H., (1988). Structure-lubricity evaluation of magnesium stearate. Int J Pharm, 43, 249-255.

McIntosh T. J., (2003). Organization of skin stratum corneum extracellular lamellae: Diffraction evidence for asymmetric distribution of cholesterol, Biophysical Journal 85, 1675-1681.

Megrab N A., Williams A C., Barry B W., (1995). Oestradiol permeation through human skin and silastic membrane: effect of propylene glycol and supersaturation. J Control Release, 36, 277-294.

Miller T. A., York P., (1985). Physical and chemical characteristics of some high purity magnesium stearate and palmitate powders. Int J Pharm 23, 55-67.

Miller T. A., York P., Jones, T. M., (1982). Manufacture and characterisation of magnesium stearate and palmitate powders of high purity. J Pharm Pharmacol, 34, 8P.

Miskandar M. S., Che-Man Y. B., Rahman R. A., Nor-Aini I., Yusoff M. S. A., (2005). Effects of emulsifiers on crystallization properties of low-melting blends of palm oil and olein. J Food Lipids, 13, 57-72.

Mlodozeniec A. R., (1978). Thermodynamics and physical properties of a lyotropic mesophases (liquid crystal) and micellar solution of an ionic amphiphile. J Soc Cosmet Chem, 28, 659–683.

Moghimi H. R., Williams A. C., Barry B. W., (1996). A lamellar matrix model for stratum corneum intercellular lipids. II. Effect of geometry of the stratum corneum on permeation of model drugs 5-fluorouracil and oestradiol. Int J Pharm, 131, 117-129.

Moody G., Rubinstein M. H., Fitzsimmons R. A., (1979). Lubricity measurement of magnesium stearate. J Pharm Pharmacol, 31, 71P.

Mortensen K., Perdersen S., (1993). Structural study on micelle formation of polyethylene oxide–polypropylene oxide–poly ethylene oxide triblock copolymer in aqueous solution. Macromolecules, 26, 805–812.

Mueller–Goymann C., (2004). Drug delivery-liquid crystals. In: Encyclopedia of Pharmaceutical technology, 2nd edition, Vol. 1, Swarbrick J., Boylan J. C., (eds.) Informa Health care, London, 834–849.

Müller A., (1923). The X-ray Investigation of Fatty Acids. J Chem Soci, 123: 2043–2047.

Muller V. B. W., (1976). Tribologische gesetzmabigkeiten und erkenntnisse in der tablettentechnologie. 2. Mitt: Untersuchungen uber den aufbau von schmirstoffschiichten. (English abstract). Pharm Ind, 38(4), 394-398.

Muller V. B. W., (1977). Polymorphism of magnesium stearate and the influence of the crystal structure on the lubricating behaviour of excipients. First international conference on pharmaceutical technology, Paris, 134-141.

Murdan S., Gregoriadis G., Florence A. T., (1999). Novel sorbitan monostearate organogels. J Pharm Sci, 88(6), 608-614.

Nakagaki M., Nishino M., (1963). Studies on the physicochemical properties of aluminium soaps. II. Structural viscosity of aluminum stearate in benzene. Jpn J Pharmacol, 83, 185-189.

Ng S. F., (2007). Investigation into the use of synthetic membranes for drug diffusion in Franz cells, PhD Thesis, University of Strathclyde, Glasgow.

Ng S. F., Rouse J. J., Sanderson F. D., Eccleston G. M., (2005a).Validation of Franz cell diffusion experiments and evaluation of drug release through various cellulose membranes. J Pharm Pharmacol, S53.

Ng S. F., Rouse J. J., Sanderson F. D., Eccleston G. M., (2005b). Investigation of drug diffusion through various synthetic membranes utilizing validated Franz cells. The AAPSPharmSci. 7, S2, R6078.

Nor-Aini I., Hanirah H., Tang T. S., (1996). Clarity and chemical composition of palm olein-sunflower and palm olein-sunflower oil blends. ELAEIS, 7(1), 64-86.

Nyqvist H., (1983). Saturated salt solutions for maintaining specified relative humidities. Int J Pharm Tech Prod Mfr. 4, 47-48.

Okoye P., Wu S. H., (2007). Lubrication of direct-compressible blends with magnesium stearate monohydrate and dihydrate. Pharmaceutical Technology Magazine. Sep. 2007: 1-24. PharmTech.com.

Ooi T. L., (1980). The pharmaceutical applications of palm oil. PhD thesis. University Science of Malaysia.

Ostrenga J., Steinmetz C., Poulsen B., (1971). Significance of vehicle composition I: relationship between topical vehicle composition, skin penetrability, and clinical efficacy. J Pharm Sci, 60, 1175-1179.

Pellet M. A., Watkinson A. C., Hadgraft J., Brian K. R., (1977). Comparison of permeability data from traditional diffusion cells and ATR−FTIR spectroscopy. Part I. Synthetic membranes. Int J Pharm, 154, 205−215.

Pellett M. A., Castellano S., Hadgraft J., Davis A. F., (1997). The penetration of supersaturated solutions of piroxicam across silicone membranes and human skin *in vitro* . J Control Release, 46, 205-214.

Pena L., (1990). Gel dosage forms: theory, formulations, and processing. Topical Drug Delivery Formulations. New York: Marcel Dekker, 381.

Pilpel N., (1963). Properties of organic solutions of heavy metal soaps. Chem Rev, 63, 221-233.

Pilpel N., (1971). Metal stearates in pharmaceuticals and cosmetics. Manuf Chem Aerosol News, 42, 37-40.

Pugh W. J., Roberts, M. S., Hadgraft J., (1996). Epidermal permeability penetrant structure relationships: 3. the effect of hydrogen bonding interactions and molecular size on diffusion across the stratum corneum. Int J Pharm, 138, 149-165.

Pugh W. J., Roberts, M. S., Hadgraft J., (1998). Physicochemical determinants of stratum corneum permeation. In: Drugs and the pharmaceutical sciences, dermal absorption and toxicity assessment (91st edition), Roberts M. S., Walters K. A., (Eds), New York, Marcel Dekker, 245-268.

Qvist M H., Hoeck U., Kreilgaard B., Madsen F., Frokjaer S., (2000). Evaluation of Gottingen minipig skin for transdermal *in vitro* permeation studies. Eur J Pharm Sci, 11, 59-68.

Rajala R., Laine E., (1995). The effect of moisture on the structure of magnesium stearate. Thermochemica Acta, 248, 177-188.

Rangarajan M., Zatz J. L., (2001). Effect of formulation on the delivery and metabolism of alpha-tocopheryl acetate. J Cosmet Sci, 52, 225-236.

Rao K. P., Chawla G., Kaushal A. M., Bansal A. K., (2005). Impact of solid-state properties on lubrication efficacy of magnesium stearate. Pharm Dev Technol, 10(3), 423-437.

Rao S. C., Schoenwald R. D., Barfknecht C. F., Laban S. L., (1992). Biopharmaceutical evaluation of ibufenac, ibuprofen, and their hydroxyethoxy analogs in the rabbit eye. J Pharmacokinet Biopharm, 20, 357-388.

Realdon N., Ragazzi E., Enrico R., (2001). Effect of gelling conditions and mechanical treatment on drug availability from a lipogel. Drug Dev Ind Pharm, 27(2), 165-170.

Reilly W. J., (2005). Pharmaceutical necessities. In: Remington, The science and practice of pharmacy. In: Remington: The science and practice of pharmacy, Hendrickson R., Beringer P., DerMardrosian A., *et al*., (Ed). Philadelphia, Lippincott Williams and Wilkins, 21[st]edition, 1077-1086.

Ribeiro H. M., Morais J. A., Eccleston G. M., (2004). Structure and rheology of semisolid o/w creams containing cetyl alcohol/non-ionic surfactant mixed emulsifier and different polymers. Int J Cosmet Sci, 26, 47–59.

Rieger M. M., (1988). Emulsions. In: Lachman L., Lieberman H. A., Kanig J. L., (Eds.). The theory and practice of industrial pharmacy. 3rd Edition, Philadelphia. Lea and Febriger, 502–532.

Roberts M. S., (1997). Targeted delivery to the skin and deeper tissues: role of physiology, solute structure and disease. Clin Exp Pharmacol Physiol, 24, 874-879.

Roberts M. S., Anderson R. A., Swarbrick J., (1977). Permeability of human epidermis to phenolic compounds. J Pharm Pharmacol, 29, 677-683.

Roberts M. S., Anderson R. A., Swarbrick J., Moore D. E., (1978). The percutaneous absorption of phenolic compounds: the mechanism of diffusion across the stratum corneum. J Pharm Pharmacol, 30(8), 486-490.

Roberts M. S., Walters K. A., (1998). The relationship between structure and barrier function of skin. In: Drugs and the pharmaceutical sciences, dermal absorption and toxicity assessment (91st edition), Roberts M. S, Walters K. A, (Eds), New York, Marcel Dekker, 1-42.

Rowe R. C., (1993). Formulating pharmaceuticals using expert systems. Pharm Tech Int, 5(8), 46-52.

Rowe R. C., (1997). Intelligent software systems for pharmaceutical product formulation. Pharm Tech Europe, 3, 36-43.

Rowe R. C., Roberts R. J., (1990). The mechanical properties of powders. Adv Pharm Sci, Academic Press.

Sang−Chul S., Soo−Young B., (1996). Controlled release of ehinylestradiol from ethylene−vinyl acetate membrane. Int J Pharm, 137, 95−102.

Sangkil L., Lee J., Choi Y. W., (2007). Skin permeation enhancement of ascorbyl palmitate by liposomal hydrogel (lipogel) formulation and electrical assistance. Biol Pharm Bull, 30(2), 393-396.

Sarveiya V., Templeton J F., Benson H A E., (2004). Ion-pairs of ibuprofen : increased membrane diffusion. J Pharm Pharmacol, 56, 717-724.

Savic S., Vuleta G., Daniels R., Muller-Goymann C. C., (2005). Colloidal microstructure of binary systems and model creams stabilized with an alkylpolyglucoside non-ionic emulsifier. Colloid and polymer science, 39-451.

Scheuplein R. J., Blank I. H., (1971). Permeability of the skin. Physiol. Rev, 51, 702-747.

Schnaare L. R., Block H. L., Rohan C. L., (2005). Rheology. In: Remington, The science and practice of pharmacy (21st edition). Hendrickson R., Beringer P., DerMardrosian A., et al., (Eds). Philadelphia, Lippincott, 338-357.

Schulman J. H., Cockbain E. G., (1940). Trans Faraday Soc, 36, 651.

Scric S., Korbar-Smid J., Bukovec P., Jezernik K., (1985). The structure investigation of magnesium soap-hydrocarbon system. Drug Dev Ind Pharm, 11(2&3), 281-298.

Scric S., Korbar-Smid J., Bukovec P., Jezernik K., (1988). Oleogels of magnesium stearate in liquid paraffin-Study of their stability and structure. Acta Pharm Jugosl, 38, 349-60.

Segers J. D., Zatz J. L., Shah V. P., (1997). *In vitro* Release of Phenol from Ointment Formulations. Pharm Tech, 21(1), 70-81.

Shah V P., (1994). Skin penetration enhancers: Scientific perspectives. In: Hsieh D. S., (Ed.), Drug Permeation Enhancement. Theory and Application. Marcel Dekker, New York, 19–23.

Shah V P., Elkins J., Williams R., (1999). Evaluation of the test system used for *in vitro* drug release for topical dermatological drug products. Pharm Dev techno, 4, 377-385.

Shah V. P., Elkins J. S., Lam S. Y., Skelly J. P., (1989). Determination of *in vitro* drug release from hydrocortisone creams. Int J Pharm, 53, 53-59.

Shah V. P., Elkins J., Skelly J. P., (1992). Relationship between *in vivo* skin blanching and *in vitro* release rate for Betamethasone valerate creams. J Pharm Sci, 81, 104–106.

Shah V. P., Polli J. E., (1996). Methods to compare dissolution profiles. Drug Inf J, 30, 1113-1120.

Sharpe S. A., Celik M., Newman A. W., Britain H. G., (1997). Physical characterisation of the polymorphic variations of magnesium stearate and magnesium palmitate hydrate species. Structural Chem, 8, 73-84.

Shigeyama M., Ohagaya T., Takeuchi H., Hino T., Kawashima Y., (2001). Formulation design of ointment base suitable for healing of lesions in treatment of bedsores. Chem Pharm Bull, 49(2), 129–133.

Siew W. L., Chong C. L., Nor-Aini I., *et al*. (1995). Composition of the oil in palm kernel from Elaeis guineensis. Journal of the American Oil Chemists' Society, 72(12), 1587–1589.

Siew W. L., Jaafar M. D. F., (2000). Compositional and differential scanning calorimetry (DSC) Studies of crystals of palm olein. J. Oil. Palm. Res. 12 (2), 1-13.

Siew W. L., Ng W. L., (1995). Diglyceride content and composition as indicators of palm oil quality. J food Sci Agric, 69, 73-79.

Siew W. L., Ng W. L., (2000). Influence of diglycerides on the crystallisation of palm oil. J Food Sci Agric, 79, 722–726.

Siewert M., Dressman J., Brown K C., Shah V P., (2003). FIP/AAPS guidelines for dissolution/*in vitro* release testing of novel/special dosage forms. Dissol Tech, 10(1),

Skoog, D. A., Holler J., Nieman T., (1998). Principles of Instrumental Analysis . 5th Edition. New York. 805-808.

Smith E. W., Haigh J. M., (1992). *In vitro* diffusion cell design and validation II. Temperature, agitation and membrane effects on betamethasone 17-valerate permeation. Acta Pharm Nord, 4, 171-178.

Smith G. H., (1947). The phase behaviour of soaps in organic solvents and its relation to lubricating greases. J Am Oil Chem Soc, 353-359.

Southwell D., Barry B. W., Woodford R., (1984). Variations in permeability of human skin within and between specimens. Int J Pharm, 18, 299-309.

Sriwirayanont P., (2001). A comparison of *in vivo* and *in vitro* penetration of all-trans retinol from facial skin care products. MSc Thesis, University of Cincinnati, USA.

Swaminathan V., Kildsig D. O., (2001). An examination of the moisture sorption characteristics of commercial magnesium stearate. AAPS PharmSciTech, 2(4), 28.

Swe P. Z., Che M. Y. B., Ghazali H. M., Wei L. S., (1994). Identification of major triglycerides causing clouding of palm olein. J Am Oil Chem Soc, 71, 1141-1144.

Sydow E. V., (1955a). On the structure of the crystal form C' of n-hendecanoic acid. Acta Cryst. 8, 810–813.

Sydow E. V., (1955b). On the structure of the crystal form A' of n-pentadecanoic acid. Acta Cryst. 8, 845–846.

Tadros T. F., Vincent B., (1983). Emulsion stability. In: Becher P., (Ed.). Encyclopedia of emulsions technology, vol 1, Dekker, New York, 129–285.

Tadros T., (2004). Application of rheology for assessment and prediction of the long-term physical stability of emulsions. Adv Coll Inter Sci, 108-109, 227-258.

Tadros T., Taelman M. C., Leonard S., (2005). Liquid crystalline phases in personal care emulsions: Their formation and benefits. J SOFW, 131(5), 2–9.

Terech P., (2002). Gels. In: Encyclopedia of surface and colloid science. London, Marcel Dekker Inc.

Terech P., Furman I., Weiss R. G., (1995). Structures of organogels based upon cholesteryl 4-(2-anthryloxy) butanoate, a highly efficient luminescing gelator:

Neutron and X-ray small-angle scattering investigations. J Phy Chem, 99, 9558-9566.

Terech P., Weiss R. G., (1997). Low molecular mass gelators of organic liquids and the properties of their gels. Chem Rev, 97, 3133-3159.

Thakker K. D., Chern W. H., (2003). Development and validation of *in vitro* release tests for semisolid dosage forms- case study. Dissol Tech, 10-15.

Timmins P., Browning I., Payne N. I., (1990). Differential scanning calorimetery characterisation of process-induced variations in an ointment base. J Pharm Pharmacol, 42, 583-585.

Trotta M., Ugazio E., Peira E., Pulitano C., (2003). Influence of ion pairing on topical delivery of retinoic acid from microemulsions. J Control Release, 86, 315–321.

Uwe A., Klaus S., Bruno K., (1992). Aluminum magnesium hydroxy fatty acid compounds and thermostable lipogels including same. United States Patent, 5169967.

Vaughn, N. A., (2007). Design-Expert software, Version 7.1. Stat-Ease, Inc. Minneapolis, MN.

Vintiloiu A., Lafleur M., Bastiat G., Leroux J. G., (2007). In situ-forming oleogel impant for rivastigmine delivery. Pharm Res, 25(4), 845–852.

Vintiloiu A., Leroux, J-C., (2008). Organogels and their use in drug delivery — A review, J Controlled Release, 125, 179–192.

Vold R. D., Mittal J., (1972). J Colloid Interface Sci, 38, 438.

Wada Y., Matsuhara T., (1994). Pseudopolymorphism and lubricating properties of magnesium stearate. Powder Tech, 78, 109–114.

Walters K. A., (1989). Electrically assisted transdermal and topical drug delivery. In: Hadgraft J., Guy R. H., (Eds). Transdermal drug delivery, Marell Dekker, New York, 197.

Walters K. A., Watkinson A., Brian K. R., (1998). *In vitro* skin permeation evaluation: the only realistic option. Int J Cosmet Sci, 20, 307–316.

Wayne W. D., (1991). Biostatistics: Analysis in the health sciences. 5th edition. Willey Science, New York.

Weisberg S., (1985). Applied linear regression. 2nd ed. John Wiley and Sons, New York, 16-73.

Wellner E., Garti N., Craig S., (2006). Stearic acid polymorphs in correlation with crystallization conditions and solvents, Cryst Res Technol, 15, 1303–1310.

Westensen K., Bunjes H., Hammer G., Siekmann B., (2001). Novel colloidal drug delivery systems. PDA. J Pharm Sci Technol, 55, 240–247.

William F M., (2006). *In vitro* studies–how good are they at replacing in vivo studies for measurement of skin absorption? Env Toxico Pharmacol, 21(2), 199–203.

Williams A. C., (2003). Structure and function of human skin. In: Transdermal and topical drug delivery, Williams A. C., (Ed), London, Pharmaceutical Press, 1–26.

Wu S., (2006). Effect of magnesium stearate hydrates on powder flowability. Tablet ease, and tablet quality. Technical report. Tyco healthcare-Mallinckrodt.

Young P. E., Coquilla V., Katz M., (1968). Effect of topical vehicle composition on the *in vitro* release of fluocinolone acetonide and its acetate ester. J Pharm Sci, 57, 921–933.

Yusuf B., Jalani B. S., Chan K. W., (eds.) (2000). In: Advances in oil palm research, vol.1. MPOB, Ministry of primary industries, Malaysia.

Zatz J. L., (1995a). Drug release from semisolids: Effect of membrane permeability on sensitivity to product parameters. Pharm Res, 12, 786–789.

Zatz J. L., (1995b). The Formulation of Dermatologic Vehicles. Cutis, 55(4S), 17–27.

Zettersten E. M., Ghadially K. R., Feingold D., Crumrine P. M., (1997). Optimum ratios of topical stratum corneum lipids improve barrier recovery in chronologically aged skin. J Am Acad Dermatol, 37, 403–408.

Conferences and Publications from this thesis

1. Sheikh KA, Bukhari NI, Ng SF, Rouse JJ, Kang YB, Eccleston GM (2009). Validation of Franz diffusion cell experiments: critical factor identification and analysis by factorial design. Poster Presentation at 2nd PharmSciFair, June 8–12, 2009, Nice, France.

2. Sheikh KA, Bukhari NI, Ng SF, Rouse JJ, Kang YB, Eccleston GM (2009). Influence of computer–based validation of Franz diffusion cell on the variation in drug release from topical dosage forms. Poster Presented at 36th Annual meeting and exposition of Controlled Release Society, July 18–22, 2009, Copenhagen, Denmark.

3. Sheikh KA, Rouse JJ, Kang YB, Eccleston GM (2010). The physical chemical properties of liquid paraffin lipogels prepared with different pseudopolymorphs of mixed and pure homologue magnesium stearate. Poster Presentation at 37th Annual meting of Controlled Release Society, 10–14 July 2010, Oregon, United States of America.

4. Sheikh KA, Rouse JJ, Kang YB, Eccleston GM (2010). Influence of hydration state and homologue composition of magnesium stearate on the properties of liquid paraffin lipogels. Poster presented at the UK–PharmSci conferene 2010, 1st–3rd September 2010, Nottingham, United Kingdom.

5. Sheikh KA, Rouse JJ, Kang YB, Eccleston GM (2010). Influence of hydration state and homologue composition of magnesium stearate on the properties of liquid paraffin lipogels. J Pharm Pharmacol 62(10), 1338-9.

6. Sheikh KA, Rouse JJ, Kang YB, Eccleston GM (2010). Influence of magnesium stearate concentration on the thermal and rheological properties of the lipogels containing liquid paraffin. Accepted for Poster Presentation at the PSWC-AAPS conference, 14–18 November 2010, New Orleans, United States of America.